

**MODELLING WAVE PROPAGATION IN
TWO-DIMENSIONAL
STRUCTURES USING A WAVE/FINITE
ELEMENT TECHNIQUE**

by

Elisabetta Manconi

Thesis submitted to the
Department of Industrial Engineering
in fulfilment of the requirements
for the degree of Doctor of Philosophy

Supervisors:
Prof. Brian R. Mace

Prof. Marco Amabili

University of Parma, Italy, March 2008

Il Coordinatore del Collegio dei Docenti
del Dottorato di Ricerca in
Ingegneria Industriale
Prof. Marco Spiga

Sommario

Lo studio della propagazione di onde elastiche è di interesse in molte applicazioni acustiche ed ingegneristiche. Alcuni esempi includono lo studio di vibrazioni libere e forzate ad alte frequenze, shock analysis [1], trasmissione del rumore [2, 3], tecniche non distruttive per il monitoraggio di danni nelle strutture [4], caratterizzazione delle proprietà elastiche dei materiali [5, 6], utilizzo di energy predictive tools [7]. Tra le principali caratteristiche di tali onde vi sono le curve di dispersione, che descrivono l’evoluzione dei numeri d’onda rispetto alle frequenze, ed i modi d’onda, che rappresentano le deformazioni della sezione normale alla direzione di propagazione dell’onda stessa. La conoscenza di tali caratteristiche consente di predire la propagazione dei disturbi nelle strutture, il trasporto di energia e la velocità di gruppo e la distribuzione dello stato di tensione e deformazione nelle strutture, specialmente ad alte frequenze. Tuttavia, i modelli analitici per la determinazione delle relazioni di dispersione sono risolvibili solo in pochi semplici casi, e.g. [2, 8]. In molti casi di interesse tecnico, la ricerca di soluzioni analitiche è estremamente difficoltosa. Ad alte frequenze, molte delle ipotesi e approssimazioni comunemente adottate sulla distribuzione dello stato di tensione e deformazione del solido non sono più valide e sono quindi necessarie teorie più dettagliate per ottenere modelli che predicono accuratamente il comportamento della struttura [8, 9]. Inoltre, le strutture spesso presentano sezioni con caratteristiche complicate. Uno dei metodi numerici piu’ utilizzati per l’analisi dinamica di strutture aventi geometrie complesse è il metodo agli elementi finiti, [10–12]. Tale metodo tuttavia è inadatto ad analisi dinamiche a medie–alte frequenze. Al fine di ottenere risultati accurati infatti, le dimensioni degli elementi finiti utilizzati nella discretizzazione devono essere comparabili con le lunghezze d’onda di interesse. Il costo computazionale a medie–alte frequenze risulta così proibitivo. In questi casi diviene quindi necessaria la ricerca di approcci numerici alternativi.

Lo scopo di questa tesi è stato lo sviluppo e l’applicazione di un metodo, Wave/Finite Element method (WFE), che fornisce un’alternativa numerica per la predizione delle caratteristiche di propagazione delle onde elastiche in strutture bi-dimensionali. Le strutture di interesse sono strutture uniformi in due dimensioni le cui caratteristiche possono però variare lungo la sezione, per esempio piastre o cilindri laminati, pannelli sandwich, strutture piane o curve trattate con layers di materiali polimerici etc. Tali strutture possono chiaramente essere

considerate strutture periodiche. Il metodo propone un approccio sistematico e diretto per correlare la teoria della propagazione ondosa in strutture periodiche, [13], con l’analisi agli elementi finiti risultando di particolare interesse nell’analisi dinamica ed acustica laddove le dimensioni della struttura sono comparabili alla lunghezza d’onda. Più in dettaglio, sfruttando le proprietà di periodicità della struttura, il metodo consiste nell’analisi di un solo segmento rettangolare della struttura, identificabile in un periodo della struttura stessa. Tale segmento è discretizzato tramite elementi finiti convenzionali. Questo implica tipicamente l’utilizzo di un solo elemento finito rettangolare di tipo shell o di un certo numero di elementi finiti di tipo brick, i cui “nodi” sono ottenuti concatenando tutti i nodi lungo la sezione del segmento. L’equazione del moto del modello discreto così definito è successivamente espressa in funzione degli spostamenti nodali di un unico “nodo” utilizzando relazioni tipiche della propagazione di disturbi armonici in strutture periodiche. Le curve di dispersione ed i modi d’onda si ottengono quindi da un problema di autovalori e autovettori che può assumere diverse forme, lineare, polinomiale o trascendentale, a seconda della natura della soluzione ricercata.

Uno dei vantaggi di questo metodo, rispetto ad altre tecniche recentemente proposte per analisi dinamica ed acustica, [14, 15], stà nella possibilità di interfacciarsi agevolmente con software commerciali agli elementi finiti. In questo lavoro ad esempio è stato utilizzato il software ANSYS. Sfruttando le capacità di mesh e le estese librerie dei codici commerciali basati sul metodo degli elementi finiti, è possibile ottenere l’equazione del moto di un periodo della struttura, e conseguentemente le sue matrici caratteristiche di massa, rigidezza ed eventualmente di smorzamento, in modo sistematico e veloce anche nel caso di strutture complicate. Altri vantaggi possono essere riassunti nei seguenti punti. Il costo computazionale è indipendente dalle dimensioni della struttura. Il metodo infatti richiede l’analisi di un piccolo modello agli elementi finiti le cui dimensioni sono legate alla dinamica della sezione nel campo di frequenze di interesse. Utilizzando il contenuto in frequenza relativo alla propagazione di onde piane, l’approccio consente di predire le caratteristiche ondose ad alte frequenze superando i limiti dell’analisi convenzionale agli elementi finiti. La formulazione è generale e può essere applicata, mantenendo lo stesso grado di semplicità, equivalentemente a strutture le cui caratteristiche di sezione sono semplici (ad esempio strutture isotropiche) o molto complicate (ad esempio strutture sandwich o honeycomb).

Nel corso di questa tesi il metodo è stato sviluppato e le implicazioni numeriche

sono state discusse. La prima parte della tesi è dedicata alla presentazione del metodo nella sua forma più generale, oltre che ad una breve introduzione ed ad una breve rivisitazione della recente letteratura collegata al presente lavoro. Nella seconda parte è mostrata una più specifica applicazione del metodo a tipiche strutture omogenee in 2 dimensioni. Gli esempi analizzati includono piastre e strutture cilindriche isotropiche, laminate e sandwich, cilindrici con fluido interno e piastre isotropiche o laminate trattate con layer di materiale viscoelastico. Una parte di questi esempi ha consentito di valutare l'accuratezza del metodo tramite il confronto con soluzioni analitiche o con soluzioni ottenute da altri autori tramite metodi diversi.

Il metodo ha dimostrato di fornire predizioni accurate ad un costo computazionale molto basso.

Abstract

This thesis presents a Wave/Finite element (WFE) method by which the wave characteristics for a 2-dimensional structure can be predicted from a finite element (FE) model.

The technique involves modelling a small segment of the structure using conventional FE methods. This is typically a 4-noded rectangular element or a stack of elements meshed through the cross-section. Periodicity conditions are applied to relate the nodal degrees of freedom and forces, resulting in various eigenproblems whose solution yields the wavenumbers and wavemodes. The form of the eigenproblem depends on the nature of the solution sought and may be a linear, quadratic, polynomial or transcendental eigenproblem. In this WFE method, commercial FE codes can be used to determine the mass and stiffness matrices of the segment of the structure. This is one of the main advantages of the technique since the full power of existing FE packages and their extensive element libraries can be exploited. Therefore a wide range of structural configurations can be analysed in a straightforward and systematic manner. Furthermore, making use of wave content, the WFE approach allows predictions to be made up to high frequencies. The formulation of the method is general and can be applied to any kind of homogeneous structures in 2 dimensions.

In the first part of the thesis the general method is outlined and numerical issues are discussed. The second part deals with application of the method to several examples. These include wave propagation in isotropic, orthotropic, laminated, laminated foam-cored sandwich plates and cylinders and fluid-filled cylindrical shells. Various interesting wave propagation phenomena are observed, particularly concerning cut-off and bifurcations between various wave modes. In the last chapter the WFE method is extended to account for viscoelastic material properties, enabling the prediction of dispersion, attenuation and damping behaviour when inherent damping is not negligible. Application to plates with constrained layer damping treatments is shown. The method is seen to give accurate predictions at very little computational cost.

Acknowledgements

I wish to express my sincere gratitude to Prof. B. R. Mace for giving all the possible guidance at all stages of this work. His stimulating suggestions and excellent advice helped me throughout my research and the writing of this thesis.

I also wish to express my appreciation and thanks to Prof. R. Garziera for many interesting and useful discussions.

I wish to particularly acknowledge Prof. M. Amabili for giving all the possible assistance.

I would like to thank all those people who made this thesis an enjoyable experience for me. A very special “thank you” to Alex. My loving thanks to Barbro and Simon; they welcomed me into a happy family in Southampton.

Part of this work was carried out while the author held a Fellowship funded by the European Doctorate in Sound and Vibration Studies. The author is grateful for the support provided.

Contents

Sommario	i
Abstract	iv
Acknowledgements	v
Contents	ix
1 Introduction	1
1.1 Scope of the dissertation	1
1.2 The Wave Finite Element approach	3
1.3 Thesis outline	4
2 Literature review	7
2.1 Dynamic Stiffness Method	8
2.2 Spectral Element Method	8
2.3 Transfer Matrix Method	10
2.4 Thin Layered Method	11
2.5 Spectral Finite Element Method	12
2.6 Methods for periodic structures	14
2.7 Transfer Matrix Method for periodic structures	14
2.8 Receptance Method	15
2.9 Wave Finite Element method	16
3 The Wave Finite Element method for 2-dimensional structures	19
3.1 Plane waves in 2-dimensional structures	19
3.2 The Wave Finite Element formulation for 2-dimensional uniform structures	22
3.2.1 Illustrative example	25
3.3 Application of WFE using other FE implementations	25

3.3.1	Mid-side nodes	25
3.3.2	Triangular elements	27
3.4	Forms of the eigenproblem	28
3.4.1	Linear algebraic eigenvalue problem for real propagation constants	29
3.4.2	Quadratic polynomial eigenvalue problem for complex propagation constant	29
3.4.3	Polynomial eigenvalue problem for complex propagation constants	30
3.4.4	Transcendental eigenvalue problem	32
3.4.5	Bounds of the eigenvalues: an algorithm for the distribution of the roots of the polynomial eigenvalue problem in the complex plane	35
3.5	Numerical issues	37
3.5.1	Periodicity effects	38
3.5.2	Numerical errors	39
3.5.3	Sensitivity analysis	40
	Figures	43
4	Wave Finite Element Method: application to plates	55
4.1	Introduction	55
4.2	Isotropic plate	56
4.2.1	Thin isotropic plate	57
4.2.2	Thick isotropic plate	58
4.3	Orthotropic plate	61
4.4	Sandwich and layered plates	62
4.4.1	Isotropic sandwich panel	64
4.4.2	Laminated plate	66
4.4.3	Antisymmetric cross-ply sandwich panel	66
	Figures	69
5	Wave Finite Element Method: application to cylinders	84
5.1	Introduction	84
5.2	WFE formulation for axisymmetric structures	85
5.2.1	The eigenvalue problem for closed axisymmetric structures	88
5.2.2	The ring frequency	89
5.3	Isotropic cylinders	91

5.3.1	Isotropic cylindrical shell, $h/R = 0.05$	92
5.3.2	Isotropic cylinder, $h/R = 0.1$	93
5.4	Orthotropic cylinder	94
5.5	Laminated sandwich cylinder	95
Figures		98
6	Wave Finite Element Method: application to fluid–filled elastic cylindrical shells	116
6.1	introducion	116
6.2	FE formulation for fluid–filled cylindrical shells	117
6.3	WFE formulation for fluid–filled cylindrical shells	118
6.4	Isotropic undamped steel cylindrical shell filled with water	119
Figures		123
7	Wave Finite Element Method: application to the estimation of loss factor	127
7.1	Introduction	127
7.2	Constrained layer damping	127
7.3	The loss factor	129
7.3.1	Definition of the loss factor	129
7.3.2	Definition of the loss factor for a structure including viscoelastic components	130
7.3.3	Modelling the loss factor using FEA	131
7.3.4	Estimation of the loss factor using WFE	133
7.3.5	Estimation of the loss factor using WFE: inclusion of frequency dependent material properties	134
7.4	Numerical examples	135
7.4.1	Aluminum beam with CLD treatment	135
7.4.2	Laminated plate with CLD treatment	137
7.4.3	Asymmetric angle-ply laminated sandwich plate	139
Figures		141
8	Concluding remarks	149
Appendix A		152
Appendix B		155

Appendix C	156
References	158

Chapter 1

Introduction

1.1 Scope of the dissertation

Vibrations can be described in terms of waves propagating through a structure. This approach is particularly appealing at high frequencies, when the size of the structure is large compared to the wavelength. Typical applications include free and forced vibration analysis, transmission of structure-borne sound, statistical energy analysis, shock response, non-destructive testing, acoustic emission and so on. In many cases, once the characteristics of wave propagation are known, the analysis becomes straightforward.

Theoretical understanding of wave propagation provides the background necessary for utilisation and better implementation of many techniques in science and industry. The analysis of wave propagation in beams, plates and shells is of importance in a number of non-destructive evaluations. Acoustic emission testing has been frequently employed as a technique for monitoring structural integrity. Discontinuities and cracks in structures subjected to stress and strain fields are accompanied by the emission of elastic waves which propagate within the material and can be recorded by sensors [4]. Within non-destructive evaluation techniques, acousto-ultrasonic techniques are also used [16]. These techniques combine some aspects of acoustic emission methodology with ultrasonic simulation of stress waves. In the context of material characterisation of anisotropic media, wave propagation in different directions are measured to determine the elastic constants [5, 6]. Owing to the increased use of laminate and sandwich panels, in particular in the transport engineering field, there is the need for methods to evaluate and optimise their vibroacoustic properties [3, 17]. The necessity to predict high frequency wave propagation is also typical in, for example, shock

analysis [1]. For high frequency vibrations and high modal density, statistical prediction methods can be used to evaluate the dynamic behaviour of complex structures. If energy predictive tools are considered (among which the prominent technique is Statistical Energy Analysis [7]) the main predictive analysis requires wave characteristics to be given. Indeed all these techniques would take advantage of improvements in the theoretical understanding of propagating waves.

The primary characteristics of these waves are the dispersion relations, which relate frequency and wave heading to the wavenumber, and wavemodes, which are related to the cross-section displacements. However, dispersion relations are frequently unavailable or treated in a simplified manner. In simple cases, analytical expressions for the dispersion equation can be found, e.g. [2, 8]. Examples include isotropic 1-dimensional structures such as rods and thin beams and 2-dimensional structures such as thin plates and cylinders. However at high frequencies the analysis becomes difficult also for these simple cases. The underlying assumptions and approximations concerning the stress-strain distribution in the solid break down and more complicated theories might be required to accurately model the behaviour as the frequency increases [8, 9]. Furthermore, the properties of the cross-section of a homogeneous solid might be complicated. Examples include rods of complicated cross-section geometry, layered media and laminated, fibre-reinforced, composite constructions. The equations of motion then become very complicated at best.

For the dynamic analysis of structures posed over complicated domains, the most commonly employed tool is the Finite Element Method (FEM) [10–12]. The FEM is a numerical method in which a structure is discretised into an assemblage of small finite elements interconnected by nodes. A convenient approximate solution, usually in the form of polynomial based shape functions, is assumed in each element. The compatibility of the displacements and equilibrium of the forces at the nodes is then required. However the method is inappropriate for large sized structures and high frequency analysis because the computational cost becomes prohibitive. In particular, in order to obtain accurate predictions at high frequencies, the size of the elements should be of the order of the wavelength, resulting in impossibly large computers models.

Thus in all such cases alternative semi-analytical and numerical methods are potentially of benefit for determining the dispersion properties, wavemodes, group and phase velocities and so on.

The aim of the present work is the development of a FE based approach, the

Wave Finite Element (WFE) method, by which the wave characteristics of a 2-dimensional structure can be predicted from a FE model. The method proposes a systematic and straightforward approach which combines the analytical theory for wave propagation in periodic structure with commercial FE tools. One of the main advantages of the WFE method is the fact that standard FE routines and commercial FE packages can be used. Hence the meshing capabilities and the wealth of existing element libraries of FE tools can be exploited. At the same time the method, making use of the wave content, enables the limitations of conventional FEA to be avoided.

1.2 The Wave Finite Element approach

The structures of interest for the method presented in this thesis are homogeneous 2-dimensional structures, whose properties can vary in an arbitrary manner through the thickness. It is clear that they can be considered as periodic structures in 2 dimensions. Examples include isotropic plates, sandwich plates, cylinders, fluid-filled pipes and so on. The method requires the analysis of just a small, generally rectangular, segment of the structure. The general displacements \mathbf{q}_L , \mathbf{q}_R , \mathbf{q}_B and \mathbf{q}_T and the generalised forces \mathbf{f}_L , \mathbf{f}_R , \mathbf{f}_B and \mathbf{f}_T at the left and right and at the bottom and top of this segment are related by the periodicity conditions

$$\begin{aligned}\mathbf{q}_R &= \lambda_x \mathbf{q}_L, & \mathbf{f}_R &= -\lambda_x \mathbf{f}_L, \\ \mathbf{q}_T &= \lambda_y \mathbf{q}_B, & \mathbf{f}_T &= -\lambda_y \mathbf{f}_B,\end{aligned}\tag{1.1}$$

where $\lambda_x = e^{-i\mu_x}$, $\lambda_y = e^{-i\mu_y}$ and μ_x , μ_y are the propagation constants of a plane harmonic wave in a 2-dimensional geometry.

The segment of the structure is discretised using conventional finite elements. This involves a low order FE model, commonly just a single rectangular finite element, or a stack of elements meshed through the cross-section. The mass and stiffness matrices, typically obtained using commercial FE packages, are subsequently post-processed using the periodicity conditions in order to obtain an eigenproblem whose solutions provide the frequency evolution of the wavenumber (dispersion curves) and the wavemodes. The form of the eigenproblem depends on the nature of the problem at hand. If μ_x and μ_y are real and assigned, the frequencies of the waves that propagate in the structure can be obtained from a standard eigenvalue problem while, if the frequency is prescribed, it yields a

polynomial or a transcendental eigenvalue problem. For the first two kinds of problem efficient algorithms, which include error and condition estimates, are well established while the last problem is less obvious and solutions can be found by a variety of methods.

1.3 Thesis outline

Chapter 2 is devoted to literature review. The aim of this chapter is to present a short summary of some of the recent semi-analytical and numerical methods for the computation of the dispersion curves in engineering structures.

Chapter 3 describes the WFE formulation for homogeneous structures in 2 dimensions. The various forms of the resulting eigenproblem are analysed. Numerical issues are also discussed and an illustrative example concerning the out-of-plane vibration of an isotropic plate is used to illustrate some considerations about general features of the method. In common with 1-dimensional WFE applications, significant issues arise because the original structure is continuous while the WFE model is a lumped, discrete, spring-mass structure which is spatially periodic. For wavelengths which are long compared to the size of the element there are no significant consequences of this and the WFE model predicts the wavenumbers with good accuracy. For shorter wavelength, i.e. higher frequencies, periodic structure effects occur.

Chapters 4, 5, 6 and 7 are devoted to the application of the method to several examples. One aim is to validate the approach in situations for which analytical solutions are well established. Another aim is to apply the method to situations where no immediate analytical solutions are available. In these examples the FE software ANSYS is used to obtain the mass and stiffness matrices of a small segment of the structure.

In Chapter 4 the method is applied to plate structures. Providing that the plate thickness remains small with respect to the bending wavelength, the WFE dispersion curves of an isotropic thin plate are compared with the one predicted by the Kirchoff theory. The dispersion curves of a thick plate are also shown up to high frequencies. An orthotropic plate made of fiber reinforced composite material is then analysed. More complicated examples concern composite sandwich and layered plates. The real dispersion curve for the transverse displacement of a three layered isotropic sandwich plate is compared with the one obtained by solving the sixth-order equation of motion originally proposed by Mead and Markus

in [18]. The complex dispersion curves and wavemodes of the sandwich plate are then given and analysed. An asymmetric [0/90] laminated plate is studied. For this example the dispersion curves obtained by the WFE method and the method proposed by Chackraborty and Gopalakrishnan in [19] are compared. The WFE approach can be applied equally to laminates of arbitrary complexity, with an arbitrary number of layers: the final example given in this chapter concerns an asymmetric, angle-ply laminated sandwich panel.

Chapter 5 shows the application of the WFE method to the analysis of wave propagation in uniform axisymmetric structures as a special case of WFE analysis of 2-dimensional structures. Two examples of isotropic cylindrical shells are analysed, for which the ratio of the thickness to mean radius is $h/R = 0.05$ and $h/R = 0.1$. In order to validate the method, the dispersion curves predicted by the WFE method for the first case are compared with the analytical results obtained by solving the Flügge equations of motion. The WFE method is also applied to predict the wave behaviour of a laminated sandwich cylindrical shell. A very similar construction was considered by Heron [20].

Chapter 6 addresses prediction of wave propagation in fluid-filled elastic cylindrical shells using the WFE method. The analysis exploits capability of an FE package to modelling acoustic fluid-structure coupling. The WFE formulation for fluid-filled cylindrical shells is presented and the method is applied to predict the complex dispersion curves of an isotropic undamped steel cylindrical shell filled with water.

In Chapter 7 the method is extended to account for viscoelastic materials, enabling the prediction of dispersion, attenuation and damping behaviour in composite materials when inherent damping is not negligible. The viscoelastic characteristics of the composites are taken into account by considering complex components in the material's stiffness matrix. This leads to dissipation in addition to dispersion. In the first part of the chapter definitions of the modal loss factor are given and the WFE approach for predicting propagating waves and the loss factor in viscoelastic structures is described. As a first example, the WFE results are compared with those obtained by Kerwin [21], and by Ghinet and Atalla [22], for the flexural loss factor of an aluminium beam with an attached constrained layer damping treatment. A laminated plate with constrained layer damping treatment is also analysed. In particular the effect of the viscoelastic material properties and the influence of the stacking sequence on the damping performance are discussed. The real and imaginary parts of the wavenumber ver-

sus the frequency for propagating waves in an asymmetric angle-ply laminated sandwich with viscoelastic material properties are also given. The loss factor for this last case is predicted as a function of the frequency and of the propagation direction.

Chapter 2

Literature review

Wave propagation in elastic solids has been the subject of many studies. For these waves, of primary importance are the dispersion relations and the wavemodes.

The existing literature on “exact” and approximate analytical theories to evaluate the dispersion relation is vast. In simple cases, analytical expressions for the dispersion equation can be found (e.g. [2, 8]). Examples include 1-dimensional structures such as rods and thin beams and 2-dimensional structures such as thin plates. For more complex structures or at higher frequencies the analysis becomes more difficult or even impossible, and the dispersion equation is often transcendental. At high frequencies the underlying assumptions and approximations break down - for example, for a plate, Mindlin [2, 8, 9] or Rayleigh-Lamb [8, 23] theories might be required to accurately model the behaviour as frequency increases. On the other hand, the algebra involved in the exact theory of linear elasticity is so complicated that the definition of the dispersion equation can be very difficult even for simple cases. Furthermore, the properties of the cross-section of a homogeneous solid might be complicated.

It is therefore not surprising that many authors have been interested in semi-analytical or numerical methods to predict wave motion. Many significant works have been published and it goes beyond the scope of this brief literature review to examine all of them. The aim of this chapter is to present a short summary of some of the recent methods for the computation of the dispersion curve in engineering structures.

2.1 Dynamic Stiffness Method

The first method considered is the Dynamic Stiffness Method, DSM. In the DSM the structure is divided into simple elements, whose degrees of freedom are defined at certain points called nodes. The key of the technique is the establishment of an element dynamic stiffness matrix in the frequency domain to relate nodal responses \mathbf{x} and forces \mathbf{F} , i.e.

$$\mathbf{D}(\omega)\mathbf{x} = \mathbf{F}, \quad (2.1)$$

where \mathbf{D} is dynamic stiffness matrix. The matrix \mathbf{D} is obtained from the analytical solutions of the element governing differential equations for harmonically varying displacements [24]. A global dynamic stiffness matrix at a specific frequency can be subsequently assembled as in standard FEM.

In contrast with the FEM, frequency-dependent shape functions, which are exact solutions to the local equations of motion for time harmonic motion, are adopted. As a consequence the computational cost is reduced significantly since there is no need of finer elements to improve the solution accuracy as the frequency increases. The method, given the assumption and approximation involved in deriving the equations of motion, can be considered as exact. Some applications of the method can be found in [25] where Lee and Thompson studied helical springs and in [26] where Langley applied the method to analyse free and forced vibrations of aircraft panels.

2.2 Spectral Element Method

The dynamic stiffness matrix can be obtained in a number of ways. In the Spectral Element Method (SEM), sometimes called the Analytical Spectral Element method (ASE), the dynamic stiffness matrix is formulated in the frequency domain from the general solution of the equation of motion represented by a spectral form. The solution is assumed to be a sum of simple harmonic waves at different frequencies. A Fast Fourier Transform (FFT) can be then performed to reconstruct the solution in the time domain [14]. The method is simple in the analysis of the behaviour of the waves but the frequencies and the mode-shapes are usually extracted using numerical approaches.

The works based on the SEM basically concern 1-dimensional waveguides, that is structures which are homogeneous in one direction, i.e. are uniform and extend to infinity along one direction, but which can have arbitrary cross-sectional

properties. A description of the method followed by a number of applications, including applications to isotropic plates and shells, can be found [14]. Mahapatra and Gopalakrishnan presented in [27] a spectral element for axial-flexural-shear coupled wave propagation in thick laminated composite beams with an arbitrary ply-stacking sequence. In [27] a first order shear deformation theory for the study of high order Lamb waves was considered. The effect of viscous damping on the wavemodes was also studied. Another spectral element for laminated composite beams can be found in [1]. The assumptions in [1] are similar to those in [27]. However the approach in [1] is focused on applications to pyroshock analysis and in particular the response of a sandwich beam subjected to a simulated pyroshock was determined. In [28] and [29] the free vibration problems of a twisted Timoshenko beam and of a doubly symmetric spinning beam respectively were addressed using the SEM. Spectral elements for asymmetric sandwich beam were also developed in [30] and in [31]. In [30] the governing differential equation for flexural vibration was obtained accepting the same basic assumptions that were adopted by Mead and Markus in [18] while in [31] a more complicated model for the displacement field was assumed: the outer layer behaves like a Rayleigh beam and the core behaves like a Timoshenko beam. In the latter, symbolic computation was required to make the analysis tractable. In [28–31] the eigenvalue problem was then solved using the Wittrick–William algorithm [32]. An elastic–piezoelectric two layer beam was studied by Lee and Kim in [33]. Lee and Kim also presented in [34] a spectrally formulated element for beams with active constrained layer damping in which the equations of motion were formulated within the Euler–Bernoulli theory assuming constant voltage along the length of the beam. The solutions were verified by comparison with FEA results. Wave propagation in a composite cylindrical shell was analysed in [35]. In [35] the spectral element was obtained considering three translational and three rotational degrees of freedoms at the cross section of the cylinder and involving a massive amount of algebra. An analytical solution for the impact–induced response of a semi–infinite membrane shell with unidirectional composite was presented to validate the SEM results. Numerical simulations for a clamped-free graphite/epoxy tubular element were also shown. The spectral element for thin–walled curved beams subjected to initial axial force was obtained by Kim et al. in [36]. The equations of motion, boundary conditions and force–deformations, rigorously obtained, gave a system of linear algebraic equations with non–symmetric matrices in 14 state variables and again involved a vast amount of algebra. Then the displacement parame-

ters were evaluated numerically. The accuracy of the method was validated by comparison with analytical and FE solutions for coupled natural frequencies of a non-symmetric thin curved beam subjected to compressive and tensile forces. Some other dynamic and acoustic applications of the SEM can be found in [37], in which the dynamics of a sandwich beam with honeycomb truss core was studied, in [38], where a spectral element model was developed for uniform straight pipelines conveying internal steady fluid and in [39], where a global-local hybrid spectral element (HSE) method was proposed to study wave propagation in beams containing damage in the form of transverse and lateral cracks. Applications of the method to 2-dimensional problems can be found for example in [40] and [41], where a harmonic dependence in one dimension was imposed, so that a 2-dimensional structure reduced to an ensemble of 1-dimensional waveguides. In [40] the dynamic stiffness matrix of a 2-dimensional Kirchhoff rectangular plate element with free edge boundary conditions was presented while in [41] Lamb wave propagation in angle-ply laminates were studied using a special spectral layer element.

In these papers generally the numerical verifications carried out to illustrate the effectiveness of the method have shown that the SEM provides accurate results over a wide frequency range. However, for complicated construction and in particular for 2-dimensional applications, the development of the spectral element becomes very difficult and the vast amount of algebra involved often necessitate the use of symbolic computation software. Moreover, since the method requires the exact solutions of the governing equation of motion, the formulation must be examined on a case by case basis. In any event the accuracy is limited by the given assumptions and approximations involved in deriving the equations of motion.

2.3 Transfer Matrix Method

A method for the analysis of wave propagation is the Transfer Matrix Method (TMM). The literature review and description of the Transfer Matrix Method for periodic structures is given in section 2.7.

The technique, originally proposed by Thompson in [42], basically consist in constructing a matrix that relates the displacements and the stress at the top and the bottom free surfaces of a waveguide, typically a plate. The plate is subdivided into a certain number of layers where the displacement field is in the

form of harmonic wave propagation. The stresses and displacements of one single layer interfaces are settled into a layer transfer matrix and a global global transfer matrix is obtained by multiplication of each layer transfer matrix in a recursive form. The plate dispersion equation results from imposing the general traction-free boundary conditions on the outer surfaces of the plate. The method has the advantage of obtaining exact analytical solutions and to allow one to calculate the dispersive characteristics in laminate with arbitrary stacking sequences. However the construction of the global transfer matrix for the whole structure is generally not straightforward.

Nayfeh [43] developed this method for studying the interaction of harmonic waves in n -layered plate. In [43] the dispersion curves for different representative cases of layered structures were shown. In [44] the method was modified in order to take into account acoustic field between the layer. Analytical expression for the transfer matrix and the interface matrix, which relate the acoustic field between one layer and another, have been provided for acoustic fluid, structural and porous layers. Uniform mean flow can also be included in the model. In [45] the TMM was applied to magneto-electro-elastic plate. The general displacements and stresses of the medium were divided into the “out-of-plane” variables and “in-plane-plane”. Then the transfer matrix was obtained connecting the “out-of-plane” variables at the top and the bottom of each layer. Due to the large number of variables involved, only the “out-of-plane” was considered. When the thickness of the layer increases, the transfer matrix becomes quasi singular leading to instability of the method. In order to solve this problem, instead of the layer transfer matrix a layer stiffness matrix was calculated in [46]. The layer stiffness matrix relates the stresses at the top and the bottom to the displacement at the top and the bottom of the layer. The global stiffness matrix is then obtained through a recursive algorithm. An alternative approach to a computationally stable solution is the Global Matrix method [47].

2.4 Thin Layered Method

The Thin Layered Method (TLM) [48] is an approach that combines the finite element method in the direction of the cross section with analytical solutions in the form of wave propagation in the remaining directions. In this method the plate is discretised in the direction of lamination. Every lamina of a cross section of the plate is subdivided into several thin sub-layers. The material properties

of every sub-layers are homogeneous while they can change for different layers. The upper and lower faces that bound the structure have prescribed stresses or displacements. The displacement field within the sub-layers is discretised in the finite element sense through interpolation functions, while the motion within each sub-layer is assumed in the form of harmonic wave propagation. The equilibrium within each lamina is preserved applying appropriate tractions, [48, 49]. After evaluating the mechanical energy expression by summation over all the laminae, a variational approach is generally used to obtain the governing equations for the cross section. Hence an eigenvalue problem is set which yields the wavenumbers for given frequency.

In [49] the TLM was applied to obtain complex dispersion curves for a plate with elastic modulus increasing with depth. Herein, a technique to obtain an algebraic eigenvalue equation instead of a transcendental one was proposed. Park and Kausel deeply investigated in [48] the numerical dispersion artifacts involved in the use of this technique. A similar approach to the TLM but termed discrete laminate method was used in [22] for modelling wave propagation in sandwich and laminate structures with viscoelastic layers.

2.5 Spectral Finite Element Method

Another method for structural dynamics and acoustic applications is the Spectral Finite Element Method (SFEM). In its standard formulation, the SFEM approach applies to 1-dimensional waveguides. In summary the cross-section of the elastic waveguide is discretised using a FE procedure. Assuming that the elastic wave travels along the waveguide with the wavenumber k , the characteristic finite element equation of motion for the cross-section becomes

$$(\mathbf{K}(k) - \omega^2 \mathbf{M})\mathbf{q} = \mathbf{0} \quad (2.2)$$

where \mathbf{q} defines the waveforms (i.e. \mathbf{q} is the vector of cross-section nodal displacements), \mathbf{M} is the mass matrix and

$$\mathbf{K}(k) = \sum_n (ik)^n \mathbf{K}_n. \quad (2.3)$$

Equation (2.2) results in an eigenvalue problem in either k or ω [15]. This formulation allows short wavelength propagation along the waveguide to be evaluated

since polynomial approximations of the displacement field in this direction are avoided. However, the matrices involved in the method are not conventional FE operators associated with the cross-section dimensions and must be determined using other approaches, typically using Hamiltonian approach, e.g. [50]. As a consequence, new elements and new spectral stiffness matrices \mathbf{K}_n must be determined case by case.

There have been various SFE studies. To the best of the author's knowledge, the method first appeared in [51] for the analysis of wave motion in prismatic waveguides of arbitrary cross section. More recently, application of the method for wave propagation in laminated composite panels was presented in [52]. In [52] a SFE was developed to obtain the dispersion curves of a four layered plate. Plane strain and anti-plane strain with respect to the section of lamination were both considered. The problem obtained seems tractable analytically only for propagation directions equal to 0° or 90° . Numerical results were compared for isotropic and orthotropic plates with the results obtained by Mindlin in [53], and with the results shown in [54] for a four-layers [0/90/0/90] plate. A generalisation of the approach in [52] was proposed by Mukdadi et al., [55, 56], to study dispersion of guided waves in anisotropic layered plates of rectangular cross section. Wave propagation in thin-walled beams and in railway tracks were described through the SFEM by Gavrić in [50, 57]. In [58] the method was used for studying propagating waves and wavemodes in a uniformly pretwisted beam. The SFE method was also applied to analyse wave propagation in a uniform circular duct with porous elastic noise control foam [59], in rib-stiffened plate structures [60] and fluid-filled pipes with flanges [61]. Prediction of turbulence-induced vibration in pipe structures was achieved in [62] by deriving the structural response to a travelling pressure wave. Wave propagation in laminated plates based on 1-dimensional SFE was studied by Tassoulas and Kausel [63] and by Shorter [64]. In particular, in [64] the dispersion properties of the first few wave types of a viscoelastic laminate plate were predicted considering a full 3-dimensional displacement field within the laminate. The strain energy distribution through the section was used to estimate the damping loss factor for each wave type. Recently a SFE for fluid and fluid-shell coupling have been presented in [65], where dispersion curves and some wave-shapes for a pipe and for a duct with nearly rectangular cross-section were shown.

As already pointed out, it can be noticed from these papers that the formulation of new spectral elements requires substantial effort. Especially for

complicated constructions, the technique necessitate a complicated treatments of coupling operators.

2.6 Methods for periodic structures

Other authors have proposed different approaches exploiting the properties of periodic structures to simplify the study of the dynamic behaviour of structures which exhibit characteristics that repeat periodically in either one, two or three dimensions. Periodic structures can be considered as an assemblage of identical elements, called cells or periods, which are coupled to each other on all sides and corners by identical junctions. This characteristic is indeed observable in many engineering real systems. Examples include railway tracks, flat or curved panels regularly supported, such as stringer stiffened panels, fluid filled pipes with regular flanges, acoustical ducts, rail structures, car tyres, composite plates or shells etc. For these structures the dynamic behaviour of the complete structure can be predicted through the analysis of a single period. One of the classical book where the mathematic of wave propagation in periodic structures has been discussed is that of Brillouin [13]. With his book, Brillouin, covering a wide range of problems that occur in solid state physic, optics and electrical engineering, traced the history of the subject.

The University of Southampton has contributed significantly to the analysis of free and forced wave motion in continuous periodic structures and an exhaustive literature review on methods developed was published by Mead in [66]. Many works in this context were carried out by Mead himself, who introduced significant investigations and characterisations of wave propagation in periodic structures. For the sake of brevity most are not cited here but the reader can find many references in [66].

2.7 Transfer Matrix Method for periodic structures

The Transfer Matrix Method for 1-dimensional periodic structures is based on the construction of a transfer matrix, which relates the displacements and the forces on both side of a periodic element of the structures. Consider the generalised displacements and forces at the left hand L of one period of the structures and

at the right end of next periodic element R . They are combined into the state vectors \mathbf{Q}_L and \mathbf{Q}_R and related by

$$\mathbf{Q}_R = \mathbf{T}_{L-R}\mathbf{Q}_L \quad (2.4)$$

where \mathbf{T}_{L-R} is the transfer matrix. Applying the Floquet's principle [67], the state vectors, in turn, are related by

$$\mathbf{Q}_R = \lambda_j \mathbf{Q}_L \quad (2.5)$$

where $\lambda_j = e^{i\mu_j}$ and μ_j is the propagation constant. Substituting equation (2.5) into (2.4), the eigenvalue problem

$$\mathbf{T}_{L-R}\mathbf{Q}_L = \lambda_j \mathbf{Q}_R. \quad (2.6)$$

is defined. Therefore λ_j , and consequently the propagation constant μ_j , is obtained as an eigenvalue of the transfer matrix \mathbf{T}_{A-B} . One of the first applications of this Transfer Matrix Method to 1-dimensional periodic structures can be found in [68]. Numerical problem are implicit in this approach since the eigenvalue problem (2.6) suffers from ill-conditioning. In [69], Zhong and Williams developed efficient and accurate computational procedures concerning the transfer matrix and the solutions of the eigenvalue problem (2.6). Wave motion energetics using transfer matrices were also analysed in [70]. As a complement of [70], a variety of results and properties concerning the transfer matrix were presented in [71].

2.8 Receptance Method

In this method a receptance matrix, which is the reciprocal of the dynamic stiffness matrix in equation (2.7), is considered to relate the displacements \mathbf{q} and the forces \mathbf{f} at the left and the right hand-side of a periodic element, i.e.

$$\mathbf{q} = \mathbf{R}\mathbf{f}. \quad (2.7)$$

\mathbf{q} and \mathbf{f} are then related by the propagation constant λ in the following way:

$$\mathbf{q}_R = \lambda \mathbf{q}_L; \quad \mathbf{f}_R = -\lambda \mathbf{f}_L, \quad (2.8)$$

where $\lambda = e^{-i\mu}$ and μ is the propagation constant. Substituting these periodicity conditions into the element equation of motion, an eigenvalue problem in the frequency ω and in the propagation constant μ is obtained.

Application of the method to beams with periodic supports can be seen [72]. Waves and wave vectors in mono-coupled periodic systems and multi-coupled periodic systems were analysed using the method by Mead in [73, 74]. In particular in [73, 74] a discussion about the relationships between the bounding frequencies of propagation zones and the natural frequencies of a period of the structures were discussed. The decay of forced harmonic motion for coupled flexural and axial wave motions in damped beams was studied in [75].

2.9 Wave Finite Element method

The Wave Finite Element method is a technique to investigate wave motion in periodic structures. In this method a period of the structure, that is for example a short section of a waveguide or a small segment of a 2-dimensional structure, is modelled using conventional FEs. The equation of motion for time-harmonic motion is therefore obtained from the FE model in terms of a discrete number of nodal DOFs and forces in the same form as the dynamic stiffness method, i.e. equation (2.7). Periodicity conditions are then applied and an eigenvalue problem is formulated whose solutions give the dispersion curves and wavemodes. In the WFE element formulation for waveguides, e.g. [76, 77], a transfer matrix as in equation (2.4) is formed from the FE dynamic stiffness matrix and then an eigenvalue problem is obtained applying periodicity condition.

Perhaps one of the first application of the method was the work of Orris and Petyt [78]. In [78] Orris and Petyt proposed a FE approach and applied a receptance method for evaluating the dispersion curves of periodic structures. In his PhD thesis, [79], Abdel-Rahman extended this FE approach to beams on periodic elastic supports, 2-dimensional flat plates with periodic flexible stiffeners and 3-dimensional periodic beam systems. Another early application of the method can be found in [80], where Thompson analysed the free wave propagation in railway tracks. The dynamic behaviour of railway track was also analysed by Gry in [81] using a similar approach. In the same way as the SFEM, the advantage of this strategy is that only one section of the structure has to be meshed and solved, reducing drastically the cost of calculation. However, unlike the SFEM, the numerical implementation of the technique is rather simple also

for complicated cross-sectional properties since conventional FE description of a period of the structure is used. This is a great advantage since no new elements have to be developed for each application. Mencik and Ichchou [82] applied the method to calculate wave transmission through a joint. Free wave propagation in simple waveguides were analysed by Mace et al. in [76]. In [76] the WFE approach was described and an estimation of energy, power and group velocity was given together with some illustrative numerical examples. In the approach proposed in [76] the high geometrical and material flexibility of standard commercial FE packages were exploited. In particular an application of the WFE method to wave propagation in a laminated plate using the FE software ANSYS was shown. In [77], after reformulating the dynamic stiffness matrix of one cell of a waveguide in terms of wave propagation, the dynamic stiffness matrix of the whole structure was then found using periodic structure theory. The response of the whole structure to force excitation was then evaluated. The two examples provided in [77] have shown that the accuracy of the method is good when common requirements for the accuracy of FE discretisation are satisfied. Waki et al. applied the method for predicting flexural wave propagation in a plate strip with free boundaries [83]. They also studied the example of forced vibration of a smooth tyre [84]. In [84] the tyre was considered as a uniform waveguide around the circumference with a geometrically complicated cross-section involving many different materials, including rubbers with frequency dependent properties. The FE software ANSYS was used to obtain the mass and stiffness matrices of a small segment of the waveguide. Despite the complicated geometry the size of the numerical model was only 324 degrees of freedom. It was shown that the WFE approach allows predictions to be made to 2kHz or more - the whole frequency range where tyre vibrations and radiated noise are important - at a very small computational cost. For 1-dimensional waveguides there have been applications of the WFE method to thin-walled structures [85], helical waveguides [86] and fluid-filled pipes [87, 88]. In [89] the WFE formulation for 2-dimensional periodic structures was applied for evaluating the propagation of elastic waves within cellular structures, such as a honeycomb plate. In [90], Duhamel applied the WFE approach as in [76, 77] to evaluate the Green's functions of a 2-dimensional structure. Harmonic dependence in one dimension was however imposed, so that a 2-dimensional structure reduces to an ensemble of 1-dimensional waveguides. The Green's functions were then found by evaluating an integral over the wavenumber k .

The method is extended in this thesis to 2-dimensional structures. Applications of the method for predicting free wave propagation in isotropic, orthotropic and composite laminated plates and cylinders and fluid filled-pipes were presented in [91, 92] and in the technical memorandum [93].

Chapter 3

The Wave Finite Element method for 2–dimensional structures

This chapter concerns the application of the WFE method to the analysis of wave propagation in uniform 2–dimensional structures. The structure is homogeneous in 2 dimensions but the properties might vary through the thickness. The method involves post–processing the mass and stiffness matrices, found using conventional FE methods, of a segment of the structure. This is typically a 4–noded rectangular segment, although other elements can be used. Periodicity conditions are applied to relate the nodal degrees of freedom and forces. The wavenumbers, which can be real, imaginary or complex, and the frequencies then follow from various resulting eigenproblems. The form of the eigenproblem depends on the nature of the solution sought and may be a linear, quadratic, polynomial or transcendental eigenproblem.

The different eigenproblem forms are examined and numerical issues are discussed. The example of a thin steel plate in bending vibration is used to illustrate the general behaviour of a 2–dimensional uniform structure studied using the WFE method.

3.1 Plane waves in 2–dimensional structures

This analysis considers time–harmonic waves propagating in a 2–dimensional structure as plane waves at frequency ω . A certain disturbance W_0 propagates as a plane wave if its magnitude is constant along planes perpendicular to the

direction of propagation. With reference to Figure 3.1, let $\mathbf{n} = \mathbf{e}_1 \cos \theta + \mathbf{e}_2 \sin \theta$ be the vector that represents the propagation direction. If the disturbance W_0 is travelling at a certain velocity \mathbf{c} , the equation of a plane perpendicular to \mathbf{n} at a distance $\mathbf{d} = \mathbf{ct}$ from the origin is

$$ct - \mathbf{n} \cdot \mathbf{r} = \text{constant}, \quad (3.1)$$

where $\mathbf{r} = x\mathbf{e}_1 + y\mathbf{e}_2$ is the position vector of an arbitrary point on the plane.

In order to satisfy equation (3.1), \mathbf{r} must increase in magnitude as the time increases. Suppose now that the disturbance is propagating with a harmonic pattern of wavelength λ , while k represents the number of complete harmonic oscillations per unit distance, i.e. the wavenumber, defined as $k = 2\pi/\lambda$. Under this circumstances

$$W(\mathbf{r}) = W_0 e^{ik(ct - \mathbf{n} \cdot \mathbf{r})}, \quad (3.2)$$

will represent a harmonic disturbance whose magnitude is the same for every plane defined by equation (3.1). Herein W_0 is the complex amplitude, $k(ct - \mathbf{n} \cdot \mathbf{r})$ is indicated as the *phase* while c , being the propagation velocity of the *constant phase*, i.e. $k\mathbf{n} \cdot \mathbf{r}$, is defined as the *phase velocity*. Equation (3.2) can be rewritten as

$$W(\mathbf{r}) = W_0 e^{i(\omega t - k_x x - k_y y)} \quad (3.3)$$

where ω is the angular frequency and $k_x = k \cos \theta$ and $k_y = k \sin \theta$ are the components of the wave vector $\mathbf{k} = k\mathbf{n}$ in the x and y direction.

When k_x and k_y are real valued, free waves can propagate without attenuation, i.e. *propagating waves*. Hence, k_x and k_y represent the change in phase of the oscillating particles per unit distance in the x and y directions respectively. On the other hand, if k_x and k_y are purely imaginary there is no propagation but oscillations of particles at the same phase with a spatial decaying amplitude. These waves are referred as *evanescent waves*. In general the wavenumber components k_x and k_y are complex quantities and these waves are referred to as *attenuating waves*. The real parts of $k_x x$ and $k_y y$ cause the change in phase with distance while their imaginary parts cause exponential decay of the wave amplitude. The global motion of the structure in a general case will be a superposition of different waves.

The relation between the wavenumber and the frequency

$$\omega = k c \quad (3.4)$$

is called the *dispersion relation* and basically governs the wave propagation. The nature of the propagating waves is said to be dispersionless if all wavelengths travel at the same speed, that is c is independent of k . It can be shown that if the propagation velocity of each harmonic is independent of k , a certain wave disturbance, which at the instant $t = 0$ is specified by a certain function, will travel with the velocity c without changing its shape [8]. If the wave is dispersive, c depends on k , thus each harmonic component will propagate at its own velocity. As a result, all the harmonic components will be superimposed at different moments with different phases, which leads to a change of shape compared to the original one. An analytical explanation of this phenomenon is evident when considering a disturbance whose spectrum differ from zero only in a small vicinity of a certain frequency $\bar{\omega}$ [8, 94]. Writing the disturbance in the form of a Fourier integral, it can be proved, see for example [8], that as this disturbance propagates it will resemble a modulated harmonic wave with the envelope propagating at the velocity

$$\mathbf{c}_g = \frac{d\omega}{dk}, \quad (3.5)$$

where \mathbf{c}_g is defined as the *group velocity*. This is the velocity at which energy propagates.

The *dispersion relation* is usually represented in a graphical form for easier interpretation. This graph is called the *dispersion curve*. As an example, flexural waves in a free thin plate are considered. The governing equation for the out-of-plane motion of the thin plate is [8]

$$D \left(\frac{\partial^4 w}{\partial x^4} + 2 \frac{\partial^4 w}{\partial x^2 \partial y^2} + \frac{\partial^4 w}{\partial y^4} \right) = -\rho h \frac{\partial^2 w}{\partial t^2}, \quad (3.6)$$

where

$$D = \frac{Eh^3}{12(1-\nu^2)},$$

is the flexural rigidity, $w(x, y, t)$ measures the deflection of the middle plane of the plate, h is the plate thickness and ρ is the material density [8]. Substituting (3.3) into equation (3.6), gives

$$D(k_x^2 + k_y^2)^2 = \rho h \omega^2. \quad (3.7)$$

Since $k_x = k \cos \theta$, $k_y = k \sin \theta$, and hence $k = k_x^2 + k_y^2$, the *dispersion relation* is

$$k = \sqrt{w} \sqrt[4]{\frac{\rho h}{D}}. \quad (3.8)$$

Figure 3.2 shows the *dispersion curve* for positive-going propagating flexural waves. From the dispersion curve it is possible to obtain information about the phase velocity and the group velocity. As an example, the slope of the segment OP in Figure 3.2 represents the phase velocity at point P , while the slope of the tangent to point P indicates the group velocity at that wavenumber.

3.2 The Wave Finite Element formulation for 2-dimensional uniform structures

Periodic structures can be considered as systems of identical segments each of which is coupled to its neighbours on all sides and corners. A famous example of periodic structure deals with crystal lattices [13]. Examples of engineering structures that can be treated as periodic structures are general waveguides with uniform cross-section, multi-span bridges, pipelines, stiffened plates and shells, multi-storeyed building, tyres and so on.

In particular this study considers uniform structures in 2 dimensions as a special case of periodic structures, that is structures homogeneous in both the x and y directions but whose properties may vary through its thickness in the z direction. These kinds of structures can be assumed to be an assembly of rectangular segments of length L_x and L_y arranged in a regular array as shown in Figure 3.3. Exploiting the periodicity of the structure, only one segment of the structure is taken and discretised using conventional FEM [10–12]. This segment should be meshed in such a way that an equal number of nodes at its left and right sides and top and bottom sides is obtained. If the periodic lengths L_x and L_y , are small enough, the simplest way to discretise the segment is obtained using just one 4-noded rectangular FE as shown in Figure 3.4. It is worth noting that the element lengths should be neither extremely small in order to avoid rounding-off errors during the computation nor too large in order to avoid dispersion errors. A detailed discussion about the numerical errors involved in the FE discretisation will be given in section 3.5.

With reference to the Figure 3.4, the segment degrees of freedom (DOFs) \mathbf{q}

are given in terms of the nodal DOFs by

$$\mathbf{q} = [\mathbf{q}_1^T \ \mathbf{q}_2^T \ \mathbf{q}_3^T \ \mathbf{q}_4^T]^T, \quad (3.9)$$

where the superscript T denotes the transpose and where \mathbf{q}_j is the vector of the nodal DOFs of all the elements nodes which lie on the j th corner of the segment. Node j is in general a “hypernode” obtained by concatenating all the nodes of the FEs through the thickness. Similarly, the vector of nodal forces is

$$\mathbf{f} = [\mathbf{f}_1^T \ \mathbf{f}_2^T \ \mathbf{f}_3^T \ \mathbf{f}_4^T]^T. \quad (3.10)$$

The vectors \mathbf{q} and \mathbf{f} are then the concatenation of the nodal DOFs and forces. Although free wave motion is considered, and so no external loads are taken into account, the load vector is different from zero since the nodal forces are responsible for transmitting the wave motion from one element to the next.

The equation of motion for the element in Figure 3.4 is

$$(\mathbf{K} + i\omega\mathbf{C} - \omega^2\mathbf{M}) \mathbf{q} = \mathbf{f}, \quad (3.11)$$

where \mathbf{K} , \mathbf{C} and \mathbf{M} are the stiffness, damping and mass matrices. The form of the plane free wave that propagates along the structure can take the form of a Bloch wave [95]. Most famous in photonic crystals, Bloch’s theorem is sometimes called Floquet’s theorem since it represents a generalisation in solid-state physics of the Floquet’s theorem for 1-dimensional problem [67].

Therefore the propagation of a free wave can be obtained from the propagation constants

$$\mu_x = k_x L_x \text{ and } \mu_y = k_y L_y, \quad (3.12)$$

which relate the displacements \mathbf{q} on each side of the periodic element by

$$\mathbf{q}_2 = \lambda_x \mathbf{q}_1; \quad \mathbf{q}_3 = \lambda_y \mathbf{q}_1; \quad \mathbf{q}_4 = \lambda_x \lambda_y \mathbf{q}_1, \quad (3.13)$$

where

$$\lambda_x = e^{-i\mu_x}; \quad \lambda_y = e^{-i\mu_y}. \quad (3.14)$$

The nodal degrees of freedom can be rearranged to give

$$\mathbf{q} = \Lambda_R \mathbf{q}_1, \quad (3.15)$$

where

$$\Lambda_R = [\mathbf{I} \quad \lambda_x \mathbf{I} \quad \lambda_y \mathbf{I} \quad \lambda_x \lambda_y \mathbf{I}]^T. \quad (3.16)$$

In the absence of external excitation, equilibrium at node 1 implies that the sum of the nodal forces of all the elements connected to node 1 is zero. Consequently

$$\Lambda_L \mathbf{f} = \mathbf{0}, \quad (3.17)$$

where

$$\Lambda_L = [\mathbf{I} \quad \lambda_x^{-1} \mathbf{I} \quad \lambda_y^{-1} \mathbf{I} \quad (\lambda_x \lambda_y)^{-1} \mathbf{I}]. \quad (3.18)$$

Substituting equation (3.15) in equation (3.11) and premultiplying both side of equation (3.11) by Λ_L , the equation of free wave motion takes the form

$$[\bar{\mathbf{K}}(\mu_x, \mu_y) + i\omega \bar{\mathbf{C}}(\mu_x, \mu_y) - \omega^2 \bar{\mathbf{M}}(\mu_x, \mu_y)] \mathbf{q}_1 = \mathbf{0}, \quad (3.19)$$

where

$$\bar{\mathbf{K}} = \Lambda_L \mathbf{K} \Lambda_R;$$

$$\bar{\mathbf{C}} = \Lambda_L \mathbf{C} \Lambda_R; \quad (3.20)$$

$$\bar{\mathbf{M}} = \Lambda_L \mathbf{M} \Lambda_R,$$

are the reduced stiffness, damping and mass matrices, i.e. the element matrices projected onto the DOFs of node 1.

The eigenvalue problem of equation (3.19) can also be written as

$$\bar{\mathbf{D}}(\omega, \lambda_x, \lambda_y) = 0, \quad (3.21)$$

where $\bar{\mathbf{D}}$ is the reduced dynamic stiffness matrix (DSM). If there are n DOFs per node, the nodal displacement and force vectors are $n \times 1$, the element mass and stiffness matrices are $4n \times 4n$ while the reduced matrices are $n \times n$.

It can be seen from equation (3.19) that the mathematical formulation of the method is fairly simple. Standard FE packages can be used to obtain the mass and stiffness matrices of the segment of the structure. No new elements or new “spectral” stiffness matrices must be derived on a case-by-case basis and moreover standard FE packages can be used to obtain the mass and stiffness matrices of one period of the structure. This is a great advantage since complicated con-

structions such as sandwich and laminated constructions can be analysed in a systematic and straightforward manner. Moreover if the elements used in the discretisation are brick solid elements, the present method is formulated within the framework of a 3-dimensional approach, that is the stress and displacement assumptions are the one used in the 3-dimensional FE analysis.

3.2.1 Illustrative example

This illustrative example is used throughout the chapter to show some numerical results related to the application of the method. The example deals with flexural vibration of a thin steel plate whose material properties are: Young's modulus $E = 19.2 \cdot 10^{10}$ Pa, Poisson's ratio $\nu = 0.3$, density $\rho = 7800$ kg/m³. The plate thickness is $h = 0.5$ mm. A rectangular element with four nodes is considered. The element has three degrees of freedom at each node: translation in the z direction and rotations about the x and y axes. The shape function assumed for this element is a complete cubic to which the two quartic terms x^3y and xy^3 have been added. For more details see [11] although note typographical errors. The formulation of the mass and stiffness matrices obtained for this example is given in Appendix A. The nondimensional frequency for this example is defined as

$$\Omega = \omega L_x^2 \sqrt{\rho h / D}; \quad (3.22)$$

where

$$D = \frac{Eh^3}{12(1 - \nu^2)},$$

3.3 Application of WFE using other FE implementations

The method can be applied to cases other than 4-noded, rectangular elements straightforwardly, so that the full power of typical element libraries can be exploited.

3.3.1 Mid-side nodes

Mid-side nodes can be accommodated as described by Abdel-Rahman in [79]. Consider the rectangular segment with mid-side nodes shown in Figure 3.5.

Defining the nodal DOFs as

$$\mathbf{q} = [\mathbf{q}_1^T \ \mathbf{q}_2^T \ \mathbf{q}_3^T \ \mathbf{q}_4^T \ \mathbf{q}_L^T \ \mathbf{q}_R^T \ \mathbf{q}_B^T \ \mathbf{q}_T^T]^T, \quad (3.23)$$

the periodicity conditions become

$$\mathbf{q} = \Lambda_R \begin{bmatrix} \mathbf{q}_1 \\ \mathbf{q}_L \\ \mathbf{q}_B \end{bmatrix}, \quad (3.24)$$

where

$$\Lambda_R = \begin{bmatrix} \mathbf{I} & \lambda_x \mathbf{I} & \lambda_y \mathbf{I} & \lambda_x \lambda_y \mathbf{I} & \mathbf{0} & \mathbf{0} & \mathbf{0} & \mathbf{0} \\ \mathbf{0} & \mathbf{0} & \mathbf{0} & \mathbf{0} & \mathbf{I} & \lambda_x \mathbf{I} & \mathbf{0} & \mathbf{0} \\ \mathbf{0} & \mathbf{0} & \mathbf{0} & \mathbf{0} & \mathbf{0} & \mathbf{0} & \mathbf{I} & \lambda_y \mathbf{I} \end{bmatrix}. \quad (3.25)$$

Equilibrium at node 1 gives equation 3.17 while equilibrium at the left and bottom mid-side nodes leads to

$$\begin{aligned} \mathbf{f}_L + \lambda_x^{-1} \mathbf{f}_R &= \mathbf{0}; \\ \mathbf{f}_B + \lambda_y^{-1} \mathbf{f}_T &= \mathbf{0}, \end{aligned} \quad (3.26)$$

and hence

$$\Lambda_L \begin{bmatrix} \mathbf{f}_1 \\ \mathbf{f}_L \\ \mathbf{f}_B \end{bmatrix} = \begin{bmatrix} \mathbf{0} \\ \mathbf{0} \\ \mathbf{0} \end{bmatrix}, \quad (3.27)$$

where

$$\Lambda_L = \begin{bmatrix} \mathbf{I} & \lambda_x^{-1} \mathbf{I} & \lambda_y^{-1} \mathbf{I} & \lambda_x^{-1} \lambda_y^{-1} \mathbf{I} & \mathbf{0} & \mathbf{0} & \mathbf{0} & \mathbf{0} \\ \mathbf{0} & \mathbf{0} & \mathbf{0} & \mathbf{0} & \mathbf{I} & \lambda_x^{-1} \mathbf{I} & \mathbf{0} & \mathbf{0} \\ \mathbf{0} & \mathbf{0} & \mathbf{0} & \mathbf{0} & \mathbf{0} & \mathbf{0} & \mathbf{I} & \lambda_y^{-1} \mathbf{I} \end{bmatrix}. \quad (3.28)$$

The mass and stiffness matrices are again reduced as given by equation (3.20).

An approximation which reduces the size of the resulting eigenproblem is suggested here by enforcing further periodicity conditions between nodes 1, L and B . In this it is assumed that

$$\mathbf{q}_B = \lambda_x^{1/2} \mathbf{q}_1; \quad \mathbf{q}_L = \lambda_y^{1/2} \mathbf{q}_1. \quad (3.29)$$

Hence Λ_L and Λ_R become

$$\begin{aligned}\Lambda_R = & [\mathbf{I} \quad \lambda_x \mathbf{I} \quad \lambda_y \mathbf{I} \quad \lambda_x \lambda_y \mathbf{I} \\ & \lambda_y^{1/2} \mathbf{I} \quad \lambda_x \lambda_y^{1/2} \mathbf{I} \quad \lambda_x^{1/2} \mathbf{I} \quad \lambda_x^{1/2} \lambda_y \mathbf{I}]^T\end{aligned}\tag{3.30}$$

and

$$\begin{aligned}\Lambda_L = & [\mathbf{I} \quad \lambda_x^{-1} \mathbf{I} \quad \lambda_y^{-1} \mathbf{I} \quad \lambda_x^{-1} \lambda_y^{-1} \mathbf{I} \\ & \lambda_y^{-1/2} \mathbf{I} \quad \lambda_x^{-1} \lambda_y^{-1/2} \mathbf{I} \quad \lambda_x^{-1/2} \mathbf{I} \quad \lambda_x^{-1/2} \lambda_y \mathbf{I}]^T.\end{aligned}\tag{3.31}$$

The segment matrices are then projected onto the DOFs of node 1 only. This introduces some errors which seem to be small in most, if not all, cases of interest.

Figure 3.6 shows the WFE wavenumber prediction for flexural waves using the rectangular 4-noded element in section 3.2.1 and an equivalent rectangular 8-noded element. The analytical dispersion curve is also given. The WFE results for the 8-noded element are obtained from the approximated formulation above. It can be noticed that both the numerical results show good accuracy.

3.3.2 Triangular elements

Figure 3.7 shows a triangular element with 3 nodes. The nodal degrees of freedom and the nodal loads are

$$\begin{aligned}\mathbf{q} = & [\mathbf{q}_1^T \quad \mathbf{q}_2^T \quad \mathbf{q}_3^T]^T; \\ \mathbf{f} = & [\mathbf{f}_1^T \quad \mathbf{f}_2^T \quad \mathbf{f}_3^T]^T.\end{aligned}\tag{3.32}$$

A second, identical segment is appended so that together they form a parallelogram with one side parallel to the x axis and another parallel to the direction y' at an angle φ to the y axis. The periodicity conditions are now

$$\mathbf{q}_2 = \lambda_x \mathbf{q}_1; \quad \mathbf{q}_3 = \lambda'_y \mathbf{q}_1; \quad \mathbf{q}_4 = \lambda_x \lambda'_y \mathbf{q}_1,\tag{3.33}$$

where

$$\lambda_{y'} = \lambda_y \lambda_x^{L_y \tan \varphi / L_x}.\tag{3.34}$$

Λ_L and Λ_R are

$$\begin{aligned}\Lambda_L &= [\mathbf{I} \quad \lambda_x \mathbf{I} \quad \lambda'_y \mathbf{I} \quad \lambda_x \lambda'_y \mathbf{I}]^T; \\ \Lambda_R &= [\mathbf{I} \quad \lambda_x^{-1} \mathbf{I} \quad \lambda'_y^{-1} \mathbf{I} \quad (\lambda_x \lambda'_y)^{-1} \mathbf{I}],\end{aligned}\tag{3.35}$$

Once Λ_L and Λ_R are evaluated, the reduced mass, stiffness and damping matrices in equation (3.19) can be obtained by equation (3.20) as shown in the section 3.2.

3.4 Forms of the eigenproblem

By partitioning the dynamic stiffness matrix of the element in equation (3.11) as

$$\mathbf{D} = \begin{bmatrix} \mathbf{D}_{11} & \mathbf{D}_{12} & \mathbf{D}_{13} & \mathbf{D}_{14} \\ \mathbf{D}_{21} & \mathbf{D}_{22} & \mathbf{D}_{23} & \mathbf{D}_{24} \\ \mathbf{D}_{31} & \mathbf{D}_{32} & \mathbf{D}_{33} & \mathbf{D}_{34} \\ \mathbf{D}_{41} & \mathbf{D}_{42} & \mathbf{D}_{43} & \mathbf{D}_{44} \end{bmatrix},\tag{3.36}$$

then the reduced eigenvalue problem is given by

$$\begin{aligned}&[(\mathbf{D}_{11} + \mathbf{D}_{22} + \mathbf{D}_{33} + \mathbf{D}_{44})\lambda_x \lambda_y + (\mathbf{D}_{12} + \mathbf{D}_{34})\lambda_x^2 \lambda_y + \\ &+(\mathbf{D}_{13} + \mathbf{D}_{24})\lambda_x \lambda_y^2 + \mathbf{D}_{32} \lambda_x^2 + \mathbf{D}_{23} \lambda_y^2 + (\mathbf{D}_{21} + \mathbf{D}_{43})\lambda_y + \\ &+(\mathbf{D}_{31} + \mathbf{D}_{42})\lambda_x + \mathbf{D}_{14} \lambda_x^2 \lambda_y^2 + \mathbf{D}_{41}]\mathbf{q} = \mathbf{0}.\end{aligned}\tag{3.37}$$

Since the matrices in equation (3.11) are real, symmetric and positive definite, for the partitions of the dynamic stiffness matrix in (3.36) $D_{ij} = D_{ij}^T$ where T denotes the transpose. Considering the transpose of equation (3.37) divided by $\lambda_x \lambda_y$, it can be proved that the solutions come in pairs involving $\lambda_x, 1/\lambda_x, \lambda_y$ and $1/\lambda_y$ for a given real frequency ω . These of course represent the same disturbance propagating in the four directions $\pm\theta, \pi \pm \theta$.

Equations (3.19) and (3.37) give eigenproblems relating λ_x, λ_y and ω , whose solutions give FE estimates of the wave modes (eigenvectors) and dispersion relations for the continuous structure. Three different algebraic eigenvalue problems follow from formulations (3.19) or (3.37). If μ_x and μ_y are chosen and real, a linear eigenvalue problem results in ω for propagating waves. In the second class of eigenproblem the frequency ω and one wavenumber, say k_x , are given.

This might physically represent the situation where a known wave is incident on a straight boundary so that the (typically real) trace wavenumber along the boundary is given and all possible solutions are sought, real, imaginary or complex. Wave propagation in a closed cylindrical shell is a second example, where the wavenumber around the circumference can only take certain discrete values. In this case, equation (3.37) becomes a quadratic polynomial in λ_y , for which there are $2n$ solutions. When ω and θ are prescribed and k is regarded as the eigenvalue parameter, the resulting problem is either a polynomial eigenvalue problem or a transcendental eigenvalue problem whose solutions for k may be purely real, purely imaginary or complex.

3.4.1 Linear algebraic eigenvalue problem for real propagation constants

To calculate the dispersion relations for free wave propagation, the real propagation constants μ_x and μ_y are given and the corresponding frequencies of propagation ω are to be found. Then

$$|\lambda_x| = 1 \quad \text{and} \quad |\lambda_y| = 1 \tag{3.38}$$

represent free waves that propagate through the structure with a wavenumber $k = \sqrt{k_x^2 + k_y^2}$ in a direction $\theta = \arctan k_y/k_x$. Equation (3.19) then becomes a standard eigenvalue problem in ω .

For real values of μ_x and μ_y it can be proved that the reduced matrices in equation (3.20) are positive definite Hermitian matrices. Therefore, for any given value of the propagation constants, there will be n real positive eigenvalues ω^2 for which wave propagation is possible. The corresponding eigenvectors will define the wave modes at these frequencies. Although there are a certain number of solutions, not all of these represent wave motion in the continuous structure as it will be discussed in section 3.5. Some of them are in fact artifacts of the discretisation by FE of the structure.

3.4.2 Quadratic polynomial eigenvalue problem for complex propagation constant

In the second class of eigenproblem the frequency ω and one wavenumber, say k_x , are given. This might physically represents the situation where a known wave

is incident on a straight boundary so that the (typically real) trace wavenumber along the boundary is given and all possibly solutions for k_y are sought, real, imaginary or complex. Wave propagation in a closed cylindrical shell is a second example, where the wavenumber around the circumference can only take certain discrete values. Hence equation (3.37) becomes a quadratic in λ_y , i.e.

$$[\mathbf{A}_2 \lambda_y^2 + \mathbf{A}_1 \lambda_y + \mathbf{A}_0] \mathbf{q}_1 = \mathbf{0}. \quad (3.39)$$

and a quadratic eigenproblem results, for which there are $2n$ solutions.

Figure 3.8 shows the real and imaginary part of the solutions μ_y as a function of the propagation direction for given μ_x . Solving equation (3.39) for the illustrative example in section 3.2.1, 6 solutions are obtained which correspond to 3 pairs of waves which either decay or propagate in the negative and positive y direction. Since damping is not considered, the solutions for freely propagating waves satisfy the equation $|e^{-i\mu_y}| = 1$. Hence solutions 1 and 2 represent the component in the y direction of the wave that propagates along the $\pm\theta$ direction. Solutions 3 and 4 represent the y components of evanescent waves with amplitudes that decrease in the θ and $-\theta$ directions respectively while solutions 5 and 6 are numerical artifacts. The real part of μ_y shows that adjacent nodes along the y direction vibrate in phase for solution 3 and 4 and in counter phase for solution 5 and 6.

3.4.3 Polynomial eigenvalue problem for complex propagation constants

In the third type of eigenproblem the frequency ω and the direction of propagation θ are specified. Hence λ_x and λ_y are of the form

$$\lambda_x = e^{-i\mu_x}, \quad \lambda_y = e^{-i\mu_y}, \quad \frac{\mu_y}{\mu_x} = \frac{L_y}{L_x} \tan \theta, \quad (3.40)$$

where μ_x and μ_y might be complex, but their ratio is real and given.

If the ratio $\mu_y/\mu_x = m_2/m_1$ is rational, m_2 and m_1 being integers with no common divisor, the propagation constants can be written as $\mu_x = m_1\sigma$ and

$\mu_y = m_2\sigma$. Putting $\gamma = e^{i\sigma}$, the eigenvalue problem (3.37) can be written as

$$\begin{aligned} & [\mathbf{A}_8\gamma^{2m_1+2m_2} + \mathbf{A}_7\gamma^{2m_1+m_2} + \mathbf{A}_6\gamma^{m_1+2m_2} + \mathbf{A}_5\gamma^{m_1+m_2} + \mathbf{A}_4\gamma^{2m_1} + \\ & \quad + \mathbf{A}_3\gamma^{2m_2} + \mathbf{A}_2\gamma^{m_2} + \mathbf{A}_1\gamma^{m_1} + \mathbf{A}_0] \mathbf{q}_1 = \mathbf{0}, \end{aligned} \quad (3.41)$$

or in a more general formulation

$$P(\gamma) = \sum_{j=0}^m \mathbf{A}_j \gamma^j \quad \mathbf{A}_j \in \mathbb{R}, \quad m \in \mathbb{N}, \quad (3.42)$$

where $\mathbf{A}_m \neq 0$. The matrices \mathbf{A} are of order $n \times n$ so that equation (3.41) is a polynomial eigenvalue problem of order $2(m_1 + m_2)$ which has $2n(m_1 + m_2)$ solutions for γ .

As a standard procedure to solve equation (3.42), the regular polynomial form in equation (3.42) is linearised as

$$\left[\begin{pmatrix} \mathbf{A}_{m-1} & \cdots & \mathbf{A}_1 & \mathbf{A}_0 \\ \mathbf{I} & & \vdots & \\ & \ddots & & \\ & & \mathbf{I} & \mathbf{0} \end{pmatrix} - \gamma \begin{pmatrix} -\mathbf{A}_m & & & \\ & \mathbf{I} & & \\ & & \ddots & \\ & & & \mathbf{I} \end{pmatrix} \right] \mathbf{Z} = \mathbf{0}, \quad (3.43)$$

where

$$\mathbf{Z} = \begin{pmatrix} \gamma^{m-1} \mathbf{q} \\ \vdots \\ \gamma \mathbf{q} \\ \mathbf{q} \end{pmatrix}.$$

After multiplying the first row of equation (3.43) by \mathbf{A}_m^{-1} , a standard eigenvalue problem is obtained as

$$[\mathbf{Q} - \gamma \mathbf{I}] \mathbf{Z} = \mathbf{0}, \quad (3.44)$$

where

$$\mathbf{Q} = \begin{pmatrix} -\mathbf{A}_m^{-1} \mathbf{A}_{m-1} & \cdots & -\mathbf{A}_m^{-1} \mathbf{A}_1 & -\mathbf{A}_m^{-1} \mathbf{A}_0 \\ \mathbf{I} & & & \vdots \\ & \ddots & & \\ & & \mathbf{I} & \mathbf{0} \end{pmatrix}. \quad (3.45)$$

The eigenvalues and the eigenvectors of the polynomial eigenproblem in equation 3.42 can be recovered from those of \mathbf{Q} using subroutines for standard eigenproblems. The same procedure for conversion to linear eigenvalue problem can be applied to equation (3.39). An efficient algorithm to order the coefficients and to solve the polynomial eigenproblem in equation (3.42) for any given value of m_1 and m_2 has been realised and is available on request.

Since in numerical computation only finite interval numbers exist, it is interesting evaluate the behaviour of the solutions of equation (3.41) as $m_2/m_1 \rightarrow \tan \theta$ with $\tan \theta$ irrational. As an example $\tan \theta = \sqrt{3}$ is considered. Figure 3.9 shows the roots of equation (3.41) in the complex plane for (m_2, m_1) equal to (17, 10) and (173, 100) as approximations to $\sqrt{3}$ while Figure 3.10 shows the variation of $|\gamma|$ with respect to m_2 and m_1 . Both the Figures show that the absolute value of γ converges to 1 as m_2 and m_1 increase. This behaviour can be inferred considering that, for $m \gg M$, $M \in \mathbb{R}^+$ arbitrarily large, equation (3.42) can be approximated as

$$\sum_{j=1}^m \mathbf{A}_j \gamma^j + \mathbf{A}_0 \approx \mathbf{A}_m \gamma^m + \mathbf{A}_0, \quad (3.46)$$

and therefore when $m \gg M$

$$|\gamma| = |\mathbf{A}_m^{-1} \mathbf{A}_0|^{1/m} \approx 1. \quad (3.47)$$

The order of the eigenvalue problem might be very large and hence there be many solutions, only some of which represent free wave propagation in the continuous structure, the rest being solutions relevant only to the discretised problem. In principle this is not an issue since all but a few solutions lie far enough from the origin in the complex kL plane that the finite element discretisation is known to be inaccurate. However, another approach is given to solve the eigenproblem efficiently when $\tan \theta$ is irrational.

3.4.4 Transcendental eigenvalue problem

In order to consider a general way to solve equation (3.37) for any possible (rational or irrational) value of μ_y/μ_x , equation (3.37) is rewritten in the following general form

$$\mathbf{B}(\lambda_x, \lambda_y) \mathbf{q} = 0. \quad (3.48)$$

To avoid trivial solutions, $|\mathbf{B}|$ must be equal to zero. The function $|\mathbf{B}|$ is a complete polynomial function in the two complex variables λ_x and λ_y

$$|\mathbf{B}| = \sum_{p=0}^{p=2n} \sum_{q=0}^{q=2n} B_{pq} \lambda_x^p \lambda_y^q. \quad (3.49)$$

Since

$$\begin{aligned} \lambda_x &= e^{-i\mu_x} = e^{-ikL_x \cos(\theta)}; \\ \lambda_y &= e^{-i\mu_y} = e^{-ikL_y \sin(\theta)}, \end{aligned} \quad (3.50)$$

equation (3.49) then becomes a transcendental eigenvalue problem in k for given θ , i.e.

$$g(k) = |\mathbf{B}| = \sum_{p=0}^{2n} \sum_{q=0}^{2n} B_{pq} [e^{-ikL_x \cos(\theta)}]^p [e^{-ikL_y \sin(\theta)}]^q. \quad (3.51)$$

The function $g(k)$ in equation (3.51) is a holomorphic function. Holomorphic functions are defined on an open subset of the complex number plane \mathbb{C} and they are complex-differentiable at every point. An equivalent definition for holomorphic functions is the following: a complex function $f(x+iy) = u + iv$ is holomorphic if and only if u and v have continuous first partial derivatives with respect to x and y and they satisfy the *Cauchy–Riemann* conditions, which are

$$\begin{aligned} \frac{\partial u}{\partial x} &= \frac{\partial v}{\partial y}; \\ \frac{\partial u}{\partial y} &= -\frac{\partial v}{\partial x}. \end{aligned} \quad (3.52)$$

For the sake of simplicity a square finite element with sides of length L is considered. The wavenumber k is generally a complex number and it can be split into its real and imaginary parts, say $k = x + iy$. A general term of the polynomial function (3.51) is rewritten as

$$\begin{aligned} B_{pq} [e^{(-ix+y)L \cos(\theta)}]^p [e^{(-ix+y)L \sin(\theta)}]^q &= \\ &= B_{pq} e^{yL(p \cos(\theta) + q \sin(\theta))} e^{-ixL(p \cos(\theta) + q \sin(\theta))}. \end{aligned} \quad (3.53)$$

From this formulation it can be seen that the function $g(k)$ has continuous first partial derivatives with respect to x and y and satisfies the *Cauchy–Riemann* conditions (3.52). It can easily be also shown that the real and imaginary parts

of $g(k)$, which are harmonic functions, satisfy *Laplace's equation*, that is

$$\begin{aligned} \frac{\partial^2 \text{Imag}[g(x, y)]}{\partial x^2} + \frac{\partial^2 \text{Imag}[g(x, y)]}{\partial y^2} &= 0, \\ \frac{\partial^2 \text{Real}[g(x, y)]}{\partial x^2} + \frac{\partial^2 \text{Real}[g(x, y)]}{\partial y^2} &= 0. \end{aligned} \quad (3.54)$$

As expected, $\text{Real}[g(x, y)]$ is an even function while $\text{Imag}[g(x, y)]$ is an odd function. Figures 3.11–3.13 show, as examples, the real and imaginary parts of the function $g(x, y)$ evaluated for $y = 0, 1, -1$, $\theta = \pi/6$ and $\Omega = 0.0837$ for the illustrative example given in section 3.2.1.

The analytical functions involved in equation (3.51), sums and products of exponential functions, are continuous and continuously differentiable with respect to the variable k . Many numerical approaches for finding complex roots of the transcendental equation (3.48) can be found. These include *Interval Newton method* [96–98], *contour integration method* [99], *Powell's Method* [100] or *Muller's method* [101].

However, the most natural technique to solve equation (3.51) is *Newton's method*. A brief summary of how *Newton's method* works for a function of complex variables is given in Appendix B. Sufficient conditions for the existence of the solution and the convergence of *Newton's method* are given by the Kantorovich theorem, [102], which the function $|\mathbf{B}|$ satisfies.

An alternative choice seeks the complex roots of the equation (3.51) using a *Newton's eigenvalue iteration method*, [103, 104]. This method extends *Newton's method* to the matrix $\mathbf{B}(k)$ in the following way. Given

$$\bar{\mathbf{B}} = -\frac{d\mathbf{B}(k)}{dk}, \quad (3.55)$$

then solve for

$$[\mathbf{B}(k_{i-1}) - r_i(\bar{\mathbf{B}}(k_{i-1}))]\mathbf{q}_i = 0, \quad (3.56)$$

$$k_i = k_{i-1} + \min(r_i),$$

where \min means the minimum absolute value of the eigenvalues r_i . The main difference to the method applied to the 1-dimensional case is that the values of r_i are determined by solving an eigenvalue problem for each step in the iteration and that the approach is more general. Although both methods are shown here for first order approximations, higher order approximations can be included by

evaluating higher order terms in the series expansion of either the matrix \mathbf{B} or of the function g .

In the present work, a variant of the *Powell's method*, which is implemented in the function *fsolve* in the Optimization Toolbox of MATLAB, is used to evaluate the complex roots of $g(k)$. The algorithm is similar in nature to the one implemented in [105].

Despite the fact that the solution space seems to be more sensitive to $Real(k)$ than $Imag(k)$, the above algorithms have good guaranteed convergence within the closed interval of interest, that is $-\pi/3 < \mu < \pi/3$ (because the discretisation errors discussed below). The solutions obtained by applying the three different methods have been found to be virtually identical. As an example, Figure 3.14 shows the location of the nondimensional wavenumber $\mu = kL$ obtained by solving equation (3.48) using the function *fsolve* for $\theta = \pi/3$ and $\Omega = 0.0837$.

3.4.5 Bounds of the eigenvalues: an algorithm for the distribution of the roots of the polynomial eigenvalue problem in the complex plane

The generalised eigenvalue problem in equation (3.42) can be solved by a number of eigensolution methods. However, some modes can be missed in the computation and methods to define the exact number of eigenvalues in a given region of the complex plane are therefore often required.

The modified companion linear form (3.44) is considered to define the region in the complex plane in which all possible roots of the eigenproblem (3.42) are defined.

From the *Gershgorin theorem* [99] it can be said that if γ is an eigenvalue of the square matrix $\mathbf{Q} = q_{ij}$, then for some j , $1 \leq j \leq m$, where m is the maximum power in the polynomial equation (3.42), it should be

$$|q_{jj} - \gamma| \leq |q_{j1}| + |q_{j2}| + \cdots + |q_{j,j-1}| + |q_{j,j+1}| + \cdots + |q_{jm}|, \quad (3.57)$$

that is, each of the eigenvalues of \mathbf{Q} lies in one of the disk in the complex plane whose centre is $C = q_{jj}$ and whose radius is given by $R_j = \sum_{i \neq j} |q_{ji}|$.

Another theorem that can be used to obtain bounds for the eigenvalues is *Brauer's theorem* [106]. This theorem states that all the eigenvalues of a square

matrix $\mathbf{Q} = q_{ij}$ lie in the union of the *Cassini ovals*

$$O_{ij} = |\gamma - q_{ii}| |\gamma - q_{jj}| \leq R_i R_j, \quad i \neq j. \quad (3.58)$$

Although the results of *Brauer's theorem* are stronger than those of *Gershgorin's theorem*, in both cases it can be verified that the inclusion is not very sharp.

Another procedure to define the number of eigenvalues in a specified range is the *Sturm sequence*. However, *Sturm's theorem* deals with real roots and disregards their multiplicities. Hence to check the region in the complex plane where all the eigenvalues are distributed a modified *Sturm sequence* is proposed. The method is based on the algorithm proposed by Gleyse et al. in [107], which counts the exact number of complex eigenvalues inside an open unit disk. Here the approach is generalised to an open disk of arbitrary radius. To apply the method the linear eigenvalue problem in (3.44) is represented using its characteristic polynomial form

$$p(\gamma) = \sum_{j=0}^{\bar{m}} a_j \gamma^j, \quad (3.59)$$

where now a_j are real coefficients and $\bar{m} = 2n(m_1 + m_2)$. If the radius of the open disk in which the roots should be counted is R , substitute $\gamma = R\tilde{\gamma}$ in equation (3.42) and hence consider a modified polynomial where the coefficients are $\tilde{a}_j = a_j R^j$. The algorithm states that the number of roots of the polynomial (3.59) inside the open disk of radius R is

$$N = \bar{m} - S[1, \Delta_1, \Delta_2, \dots, \Delta_{\bar{m}}] \quad (3.60)$$

where S is the sign count in the sequence $[1, \Delta_1, \Delta_2, \dots, \Delta_{\bar{m}}]$. Here Δ_i stands for the determinants of the leading principal submatrices in the Schur–Chon matrix [107] of equation (3.59) which is

$$SC_{ij} = \sum_{q=0}^{\min(i,j)} a(\bar{m} - i + q)a(\bar{m} - j + q) - a(i - q)a(j - q). \quad (3.61)$$

For the cases analysed, the method resulted in efficient evaluation of the number of eigenvalues inside some open disk of arbitrary radius. As an example, Table 3.1 shows some results. Here the value $\max|\gamma|$ corresponds to the maximum absolute value of the eigenvalues of the matrix (3.45). The examples show that the

(m_1, m_2)	\bar{m}	$\max \gamma $	R	N
(3, 1)	24	2.69908	2.699	22
			2.7	24
(7, 5)	72	1.32901	1.329	70
			1.33	72
(2, 9)	66	1.62951	1.629	64
			1.63	66

Table 3.1: Number of roots of polynomial (3.59), N , inside an open disk of radius R . The number N is evaluated by equation (3.60).

algorithm predicts with good accuracy the radius R of the disk in the complex plane where all the eigenvalues can be found.

3.5 Numerical issues

In this section some numerical issues related to the application of the WFE method are discussed. Significant issues arise because the original structure is continuous while the WFE model is a lumped, discrete, spring–mass structure which is spatially periodic with periods L_x and L_y in the x and y directions. In particular at high frequencies, or for short wavelengths, there are substantial differences between the behaviour of the continuous structure and the periodic structure [13, 73, 74, 78, 108]. Hence the issue is one of determining which solutions to the eigenvalue problem are artifacts of the spatial discretisation and which are valid estimates of wavenumbers in the continuous structure.

As with conventional FEA, FE discretisation errors become significant if the size of the element is too large [11]. As a rule-of-thumb, there should be at least 6 or so elements per wavelength. These errors also depend on the element aspect ratio and the direction of wave propagation. As in 1-dimensional WFE applications [109], if the size of the element is too small then care must be taken in numerical computations because round-off errors can occur if the dynamic stiffness matrix is to be calculated (i.e. if $\|\omega^2 \bar{\mathbf{M}}\| \ll \|\bar{\mathbf{K}}\|$).

In the first part of this section periodicity conditions are discussed, then numerical errors are investigated. At the end of the section a method is proposed to estimate which solutions represent wave motion in the continuous structure. The method evaluates the sensitivity of the solutions to the dimensions of the element.

3.5.1 Periodicity effects

Equation (3.19) yields the same values of \mathbf{q} and ω for (μ_x, μ_y) or $(\mu_x + 2m_x\pi, \mu_y + 2m_y\pi)$ where m_x and m_y are integers, that is the wave modes and the propagating frequencies are periodic functions of the propagation constants with period 2π because of the spatial periodicity. This aliasing effect is a consequence of considering a discretised structure instead of the continuous one and represents a substantial difference to the analytical approach. Detailed discussion about the periodicity conditions can be found in [13]. The dispersion curves for the illustrative example in section 3.2.1 are shown in Figure 3.15 for $\theta = 0$. It is found by the eigensolution of equation (3.19) considering the example in section 3.2.1, which has 3 solutions for ω^2 for given μ_x . The abscissa represent the nondimensional frequency in equation (3.22) while the ordinate shows the propagation constant $\mu = kL_x$. All solutions are shown, i.e. those for $m_x, m_y = 0, \pm 1, \pm 2, \dots$. From the graph it can be seen that the frequency is a periodic function of μ with period 2π . Also shown is the analytical solution for the continuous plate.

Since a wave propagates in the positive and negative direction in the same way, e.g. $\theta = 0$ and $\theta = \pi$, $\text{Real}(\mu_x) \in [-\pi, \pi]$, $\text{Real}(\mu_y) \in [-\pi, \pi]$ are taken as the most convenient interval in which to examine the variation of ω . This restriction is not arbitrary as it might appear since it contains a complete period of the frequency and avoid ambiguity in the wavenumbers at the same time. As another example, Figure 3.16 shows the plots of the nondimensional (Ω, μ_x, μ_y) surfaces for propagating waves when $\text{Real}(\mu_x) \in [-\pi, \pi]$, $\text{Real}(\mu_y) \in [-\pi, \pi]$. The surfaces in Figure 3.16 show symmetry because the wavenumber is independent of the propagation direction for an isotropic plate.

Periodic structures are known to exhibit *pass-bands* and *stop-bands*, in that disturbances can propagate freely only in certain frequency ranges, otherwise they decay with distance. Since generally the number of propagation surfaces equals the number of degrees of freedom at each node of the structure considered, three *pass bands* are shown in Figures 3.15 and 3.16 for the example considered. The cut-off frequencies are indicated in Figure 3.15. It can be noticed that the model behaves as a *low-pass* filter for all the frequencies below the *cut-off* frequency Ω_a . The frequencies outside the *pass bands*, i.e. $\Omega_a < \Omega < \Omega_b$ and $\Omega > \Omega_c$, do not propagate. However, only the first passing band, sometimes called “acoustic branch” [13] exists for the continuous plate. The second and third *passing bands*, sometimes called “optical branches” [13], are due to the discrete FE model of the plate and the use of the terms “propagating wave” or “wave form” is not

rigorously correct in this case. Although the presence of the *bounding frequencies*, Ω_a , Ω_b and Ω_c , is due to the discretisation of the continuous model, they are characteristics of the discrete periodic structure. The *bounding frequencies* are in fact related to the natural frequencies of the periodic element under various boundary conditions [73, 74, 78, 108]. The WFE results give accurate prediction only for long wavelengths with respect to element size L . For shorter wavelengths, WFE solutions diverge from those of the continuous structure.

3.5.2 Numerical errors

One of the FE approximation error consists in dispersion errors that are caused by the difference between the numerical estimate of the wavenumber and the true value. As a rule-of-thumb, there should be at least 6 or so elements per wavelength. This is an often-used criterion to ensure that there are enough elements per wavelength to accurately characterise the wave. For wavelengths which are long compared to the size of the element, there are no significant consequences of this and the WFE model predicts the wavenumbers with good accuracy as shown in Figure 3.15. The first pass band of the WFE results gives accurate results for μ up to $\pi/3$ or so, which in terms of the wavelength means $L < \lambda/6$. This is illustrated more clearly in Figure 3.17 where propagation in the positive x direction is considered. Analytical solutions are also shown in this figure. Figure 3.17 shows the three WFE solutions for μ as functions of Ω . The first is real in the pass bands and becomes complex in the stop bands. The other two are imaginary, with one accurately representing the evanescent waves while the other is a result of the FE discretisation. The first two eigenvalues are inaccurate for $\mu > \pi/3$ or so due to discretisation errors and break down completely for $\mu > \pi$ because of periodic structure phenomena.

The errors also depend on the element aspect ratio and on the direction of wave propagation. Figure 3.18 and Figure 3.19 show the relative error in the estimated frequencies and the estimated wavenumbers as a function of the direction of propagation. Elements of various aspect ratios are considered. The error in the ordinate axis of Figures 3.18 and 3.19 is calculated as

$$\text{error \%} = \left| \frac{\xi^* - \xi}{\xi^*} \right| \%, \quad (3.62)$$

where ξ^* is the frequency (or the wavenumber) obtained by the analytical formulation while ξ is the corresponding numerical result. The latter are found

by solving the transcendental eigenvalue problem to which there are multiple solutions. The error increases as the size of the element increases and has a maximum for propagation in the direction of the diagonal across the element. The fact that the error shown in Figure 3.19 is piecewise constant is a consequence of the methods used to solve the transcendental equation (3.51), *Powell’s method* or *Newton’s method*. In fact, when these iterative methods are applied to find a root of complex functions, the set of points where the methods converge to the root is a domain of attraction.

For the continuous model it is implicitly assumed that a certain propagation characteristic could be “measured” between particles and that the observable wavelengths will be all the ones included in the interval $0 \leq \lambda \leq \infty$. On the other hand, since the FE model is a discrete model of the structure, if the distances between the nodes along x and y in one element are L_x and L_y , the model will allow any wavelength components along x and y such that $\lambda_x > 2L_x$, $\lambda_y > 2L_y$ [13]. The numerical solutions will approach the theoretical values as the size of the element approaches zero. However the mass and stiffness matrices obtained by the FE model critically depend on L_x and L_y and for decreasing value of the lengths, the stiffness of the element may become predominant with respect to the inertia, resulting in round-off errors if the dynamic stiffness matrix is calculated.

3.5.3 Sensitivity analysis

From the analysis carried out, it is clear that there is a set of WFE solutions which does not correspond to the results for the continuous structure. Thus there is the need for a systematic procedure for enabling results that represent the behaviour of the continuous structure to be evaluated. This means that the eigensolutions that correspond to waves in the continuous model must be identified. Here a proposed criterion is to determine the sensitivities of the estimated solutions to the dimensions of the element: increasing the size of the element both decreases the stiffness and increases the mass, hence reducing the bounding frequencies of the propagating zones. Wavenumber and frequency estimates which are periodic artifacts are thus very sensitive to the dimensions of the element whereas those which provide estimates of wavenumbers and frequencies in the continuum are insensitive to such changes. The sensitivities can be found either analytically or numerically by simple re-meshing. A direct approach to obtain the eigenvalue sensitivities is to differentiate equation (3.19) with respect to the element length L . If the eigenvalues are simple (not multiple) and the eigenvectors are normalised

with respect to the mass matrix, the expression for the derivative of equation (3.19) is

$$\frac{\partial \omega_i^2}{\partial L} = \mathbf{q}_i^T \left(\frac{\partial \bar{\mathbf{K}}}{\partial L} - \omega_i^2 \frac{\partial \bar{\mathbf{M}}}{\partial L} \right) \mathbf{q}_i; \quad i = 1, \dots, n. \quad (3.63)$$

In simple cases the stiffness and mass matrices can be evaluated as functions of the dimension of the element and their derivatives with respect to L can be determined analytically.

For example, for the thin plate in section 3.2.1, the analytical variation of the frequency with respect to the L is:

$$\frac{L}{\omega_1^2} \frac{\partial \omega_1^2}{\partial L} = 3.8780 \cdot 10^{-5}; \quad \frac{L}{\omega_2^2} \frac{\partial \omega_2^2}{\partial L} = -4.1175; \quad \frac{L}{\omega_3^2} \frac{\partial \omega_3^2}{\partial L} = -3.9960. \quad (3.64)$$

Equations (3.64) show clearly that the second and third modes are sensitive to a small change in the element dimension and therefore are numerical artifacts due to the discretisation process.

If any numerical evaluation of the matrices is available, for example the matrices are outputs of commercial FE packages, the derivatives of the element matrices may be approximated by their first order numerical derivatives as

$$\begin{aligned} \frac{\partial \bar{\mathbf{K}}(L)}{\partial L} &\approx \frac{\bar{\mathbf{K}}(L + \Delta L) - \bar{\mathbf{K}}(L)}{\Delta L}, \\ \frac{\partial \bar{\mathbf{M}}(L)}{\partial L} &\approx \frac{\bar{\mathbf{M}}(L + \Delta L) - \bar{\mathbf{M}}(L)}{\Delta L}. \end{aligned} \quad (3.65)$$

Finally it is worth noting that for elements with rigid body modes (i.e. those for which the stiffness matrix is singular), $\omega = 0$ is a cut-off frequency so that at least one wave must propagate from $\omega = 0$ and this wave must represent a wave in the continuous structure.

The FE estimates also depend on the element aspect ratio. This is particularly significant for the higher periodic structure branches while solutions which represent wavemodes in the continuous model are very insensitive to aspect ratio. As an example, the complex values of the nondimensional wavenumbers, kL , are obtained solving the transcendental eigenproblem for $\theta = \pi/3$, $\Omega = 0.0837$ for various element aspect ratios. Figure 3.20 shows the sensitivity of the nondimensional wavenumber location to changes in the element aspect ratio. Only the solutions 1, 2, 3 and 4 indicated in the Figure 3.20 are not affected by changes in the element geometrical parameters. As another example, Figure 3.21 shows the

sensitivity in the estimated wavenumbers as a function of L . The error in the wavenumber is evaluated as $(k(L_0) - k)/k(L_0)\%$ where L_0 is a given initial length. The figure shows that solutions 1, 2, 3 and 4 are insensitive to the variation of L while a change of 1% in the length of the element results in a change of nearly 1% for the other solutions. It can be concluded that, for the case analysed, only solutions 1, 2, 3 and 4 provide good estimates of the wavenumbers in the continuous structure while the rest being solutions relevant only to the discretised problem.

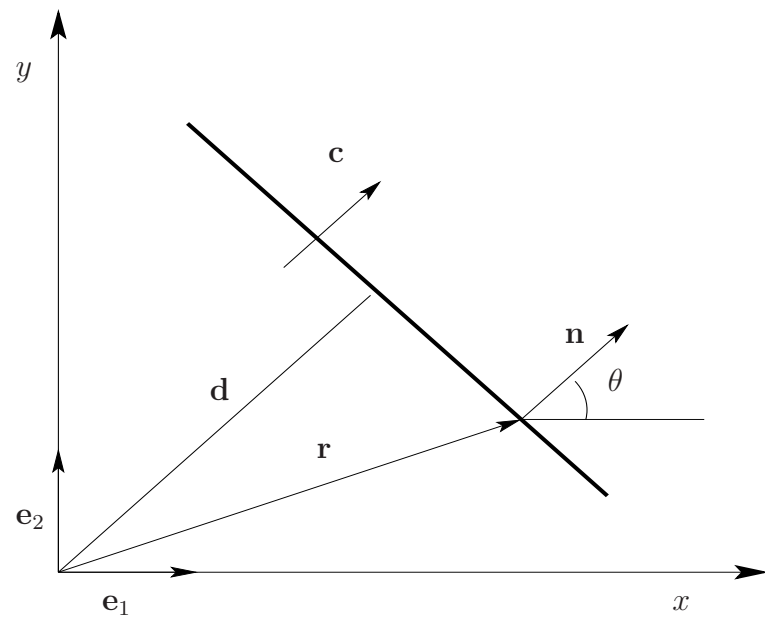


Figure 3.1: Plane wave propagating in the direction \mathbf{n} .

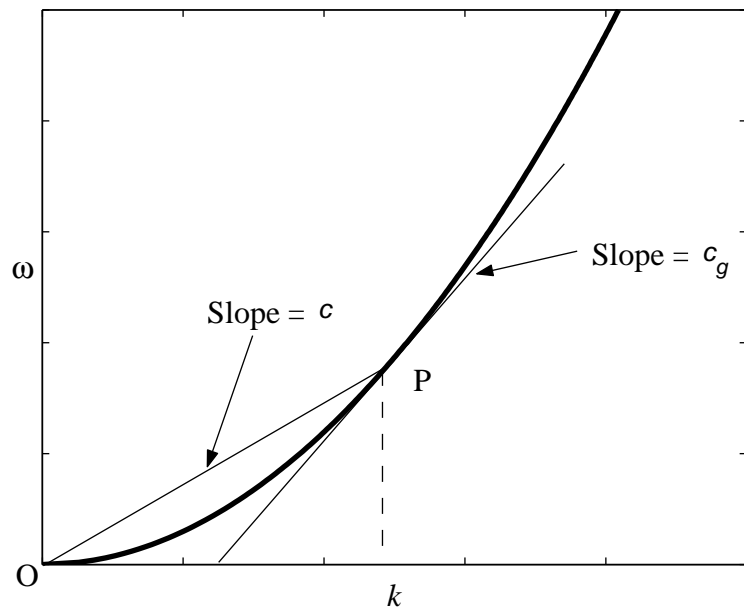


Figure 3.2: Dispersion curve for propagating waves in the positive x -direction for an isotropic thin plate.

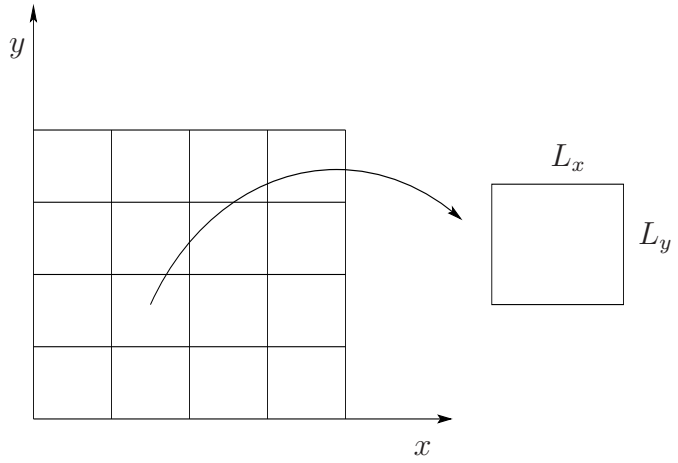


Figure 3.3: Uniform 2–dimensional structure and rectangular segment of dimensions L_x and L_y .

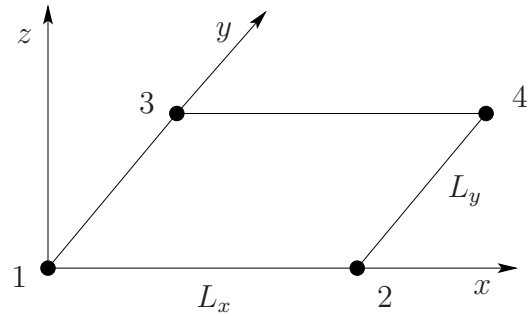


Figure 3.4: FE model of a small rectangular segment meshed with one 4–noded rectangular element.

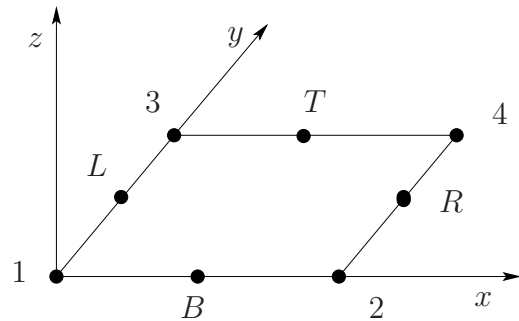


Figure 3.5: Other finite element implementations: element with mid–side nodes.

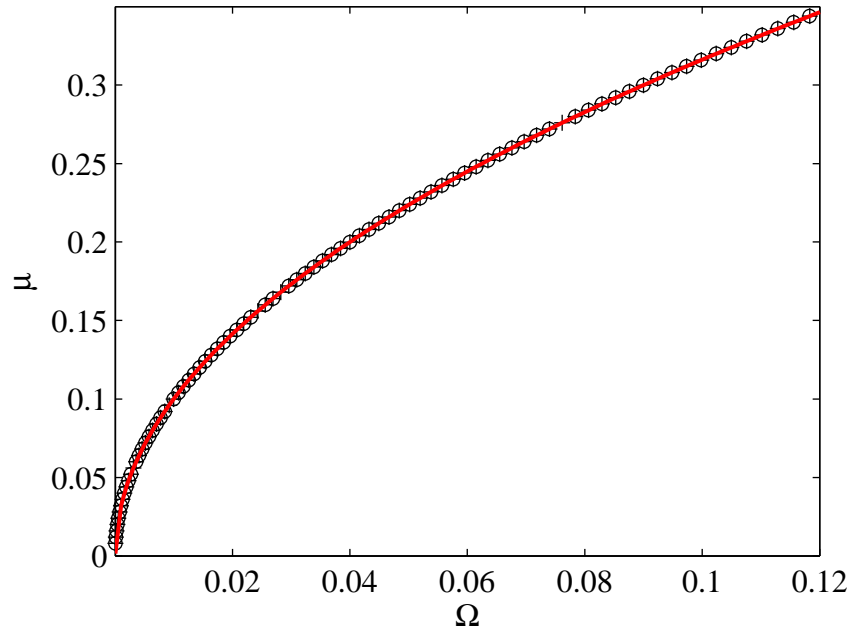


Figure 3.6: WFE and analytical dispersion curves for flexural wave propagation in direction $\theta = 0$: — analytical solution; + + + WFE rectangular 4-noded element; o o o WFE rectangular 8-noded element.

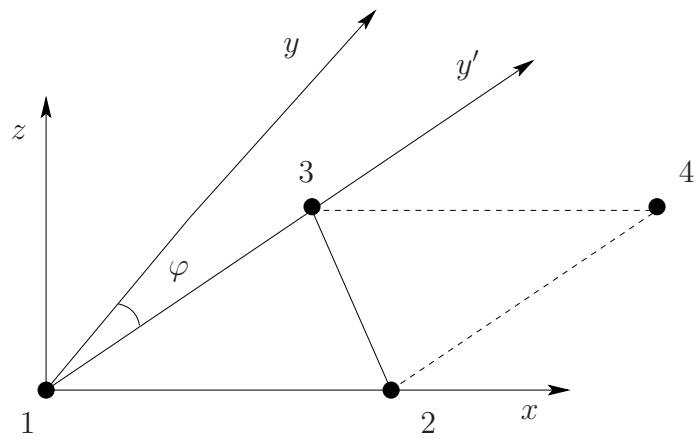
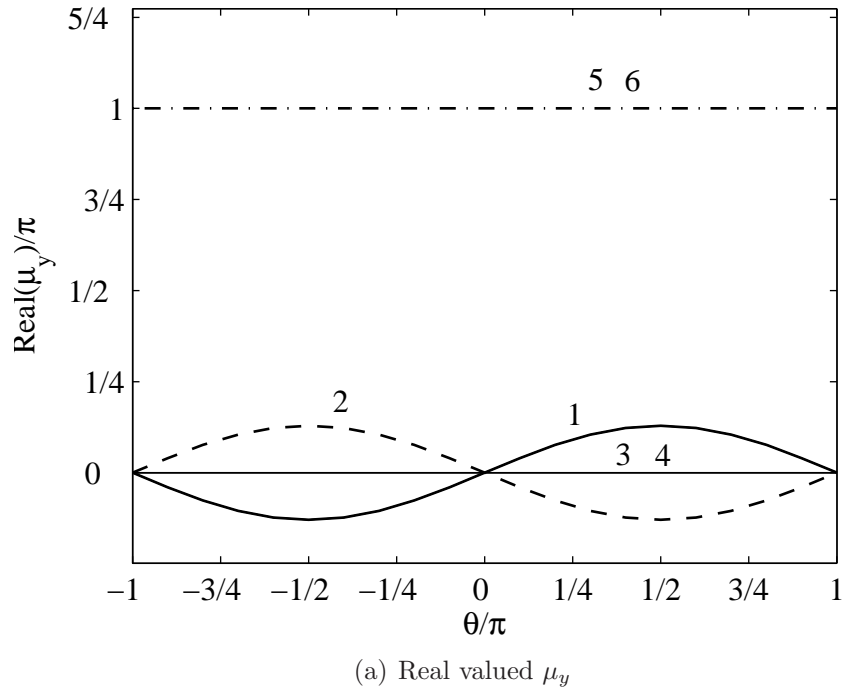
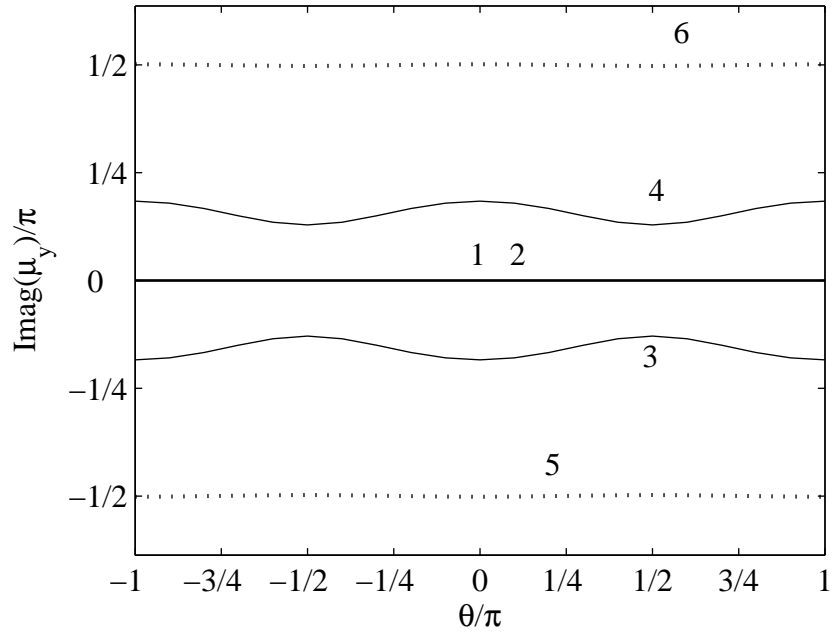


Figure 3.7: Other finite element implementations: triangular element.



(a) Real valued μ_y



(b) Imaginary valued μ_y

Figure 3.8: Real and imaginary part of μ_y as a function of the propagation direction for given μ_x . Isotropic steel plate, $L_x = L_y = 5\text{mm}$, $\Omega = 0.0837$.

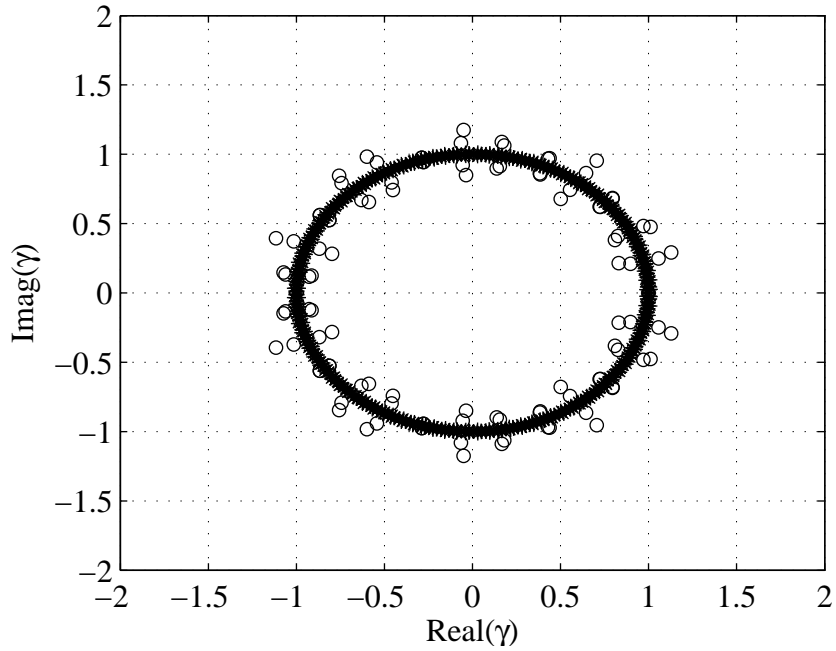


Figure 3.9: Roots of equation (3.41) for $m_2/m_1 \rightarrow \sqrt{3}$: o ($m_2 = 17, m_1 = 10$); * ($m_2 = 173, m_1 = 100$).

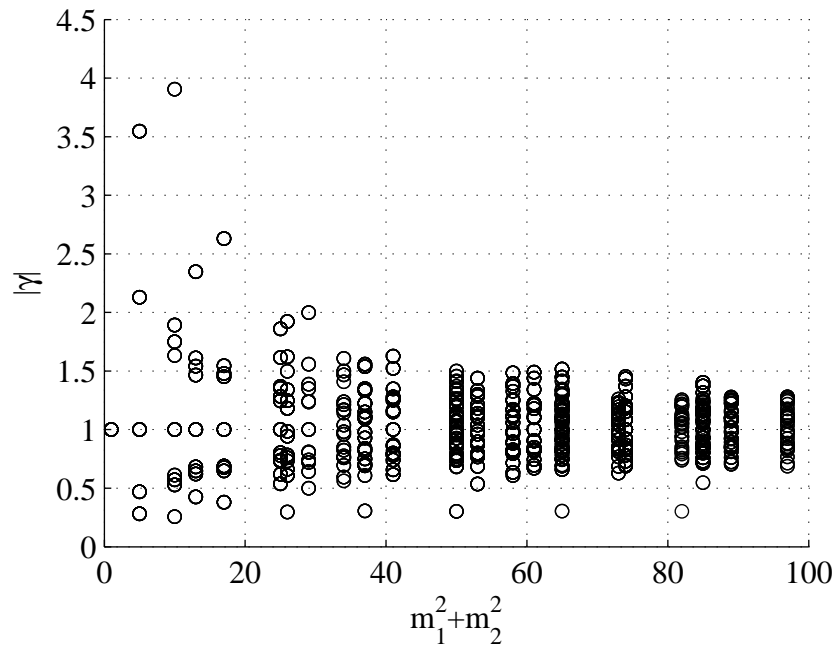


Figure 3.10: Absolute value of the roots of equation (3.41) evaluated for different values of the propagation direction.

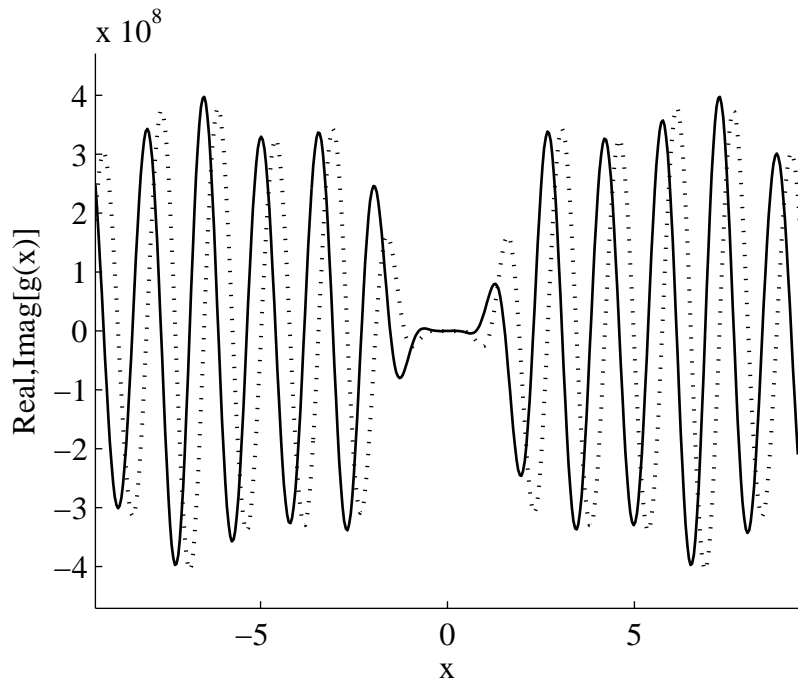


Figure 3.11: Real and imaginary parts of the function $g(x, y)$ evaluated for $y = 0$, $\theta = \pi/6$, $\Omega = 0.0837$: ······ Real[$g(x)$]; — Imag[$g(x)$].

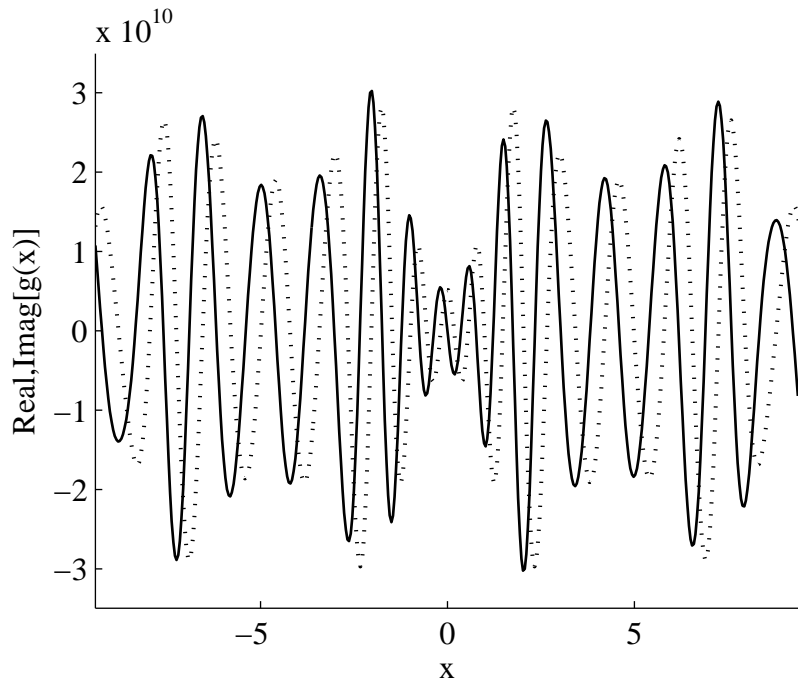


Figure 3.12: Real and imaginary parts of the function $g(x, y)$ evaluated for $y = 1$, $\theta = \pi/6$, $\Omega = 0.0837$: ······ Real[$g(x)$]; — Imag[$g(x)$].

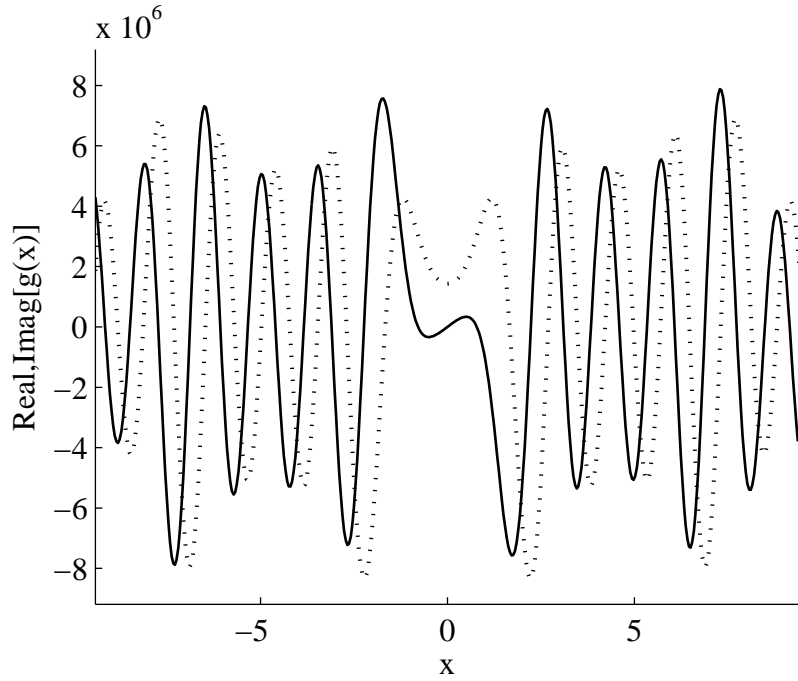


Figure 3.13: Real and imaginary parts of the function $g(x, y)$ evaluated for $y = -1$, $\theta = \pi/6$, $\Omega = 0.0837$: Real[$g(x)$]; — Imag[$g(x)$].

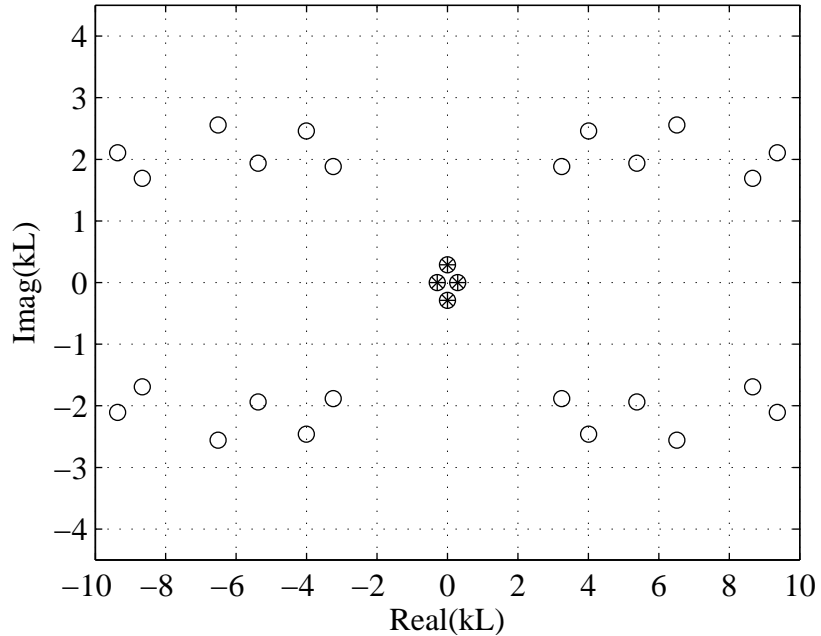


Figure 3.14: Free wave propagation in an isotropic plate in direction $\theta = \pi/3$, $\Omega = 0.0837$, $\mu = 0.289$: + analytical solutions; o numerical solutions to the transcendental eigenvalue problem.

50

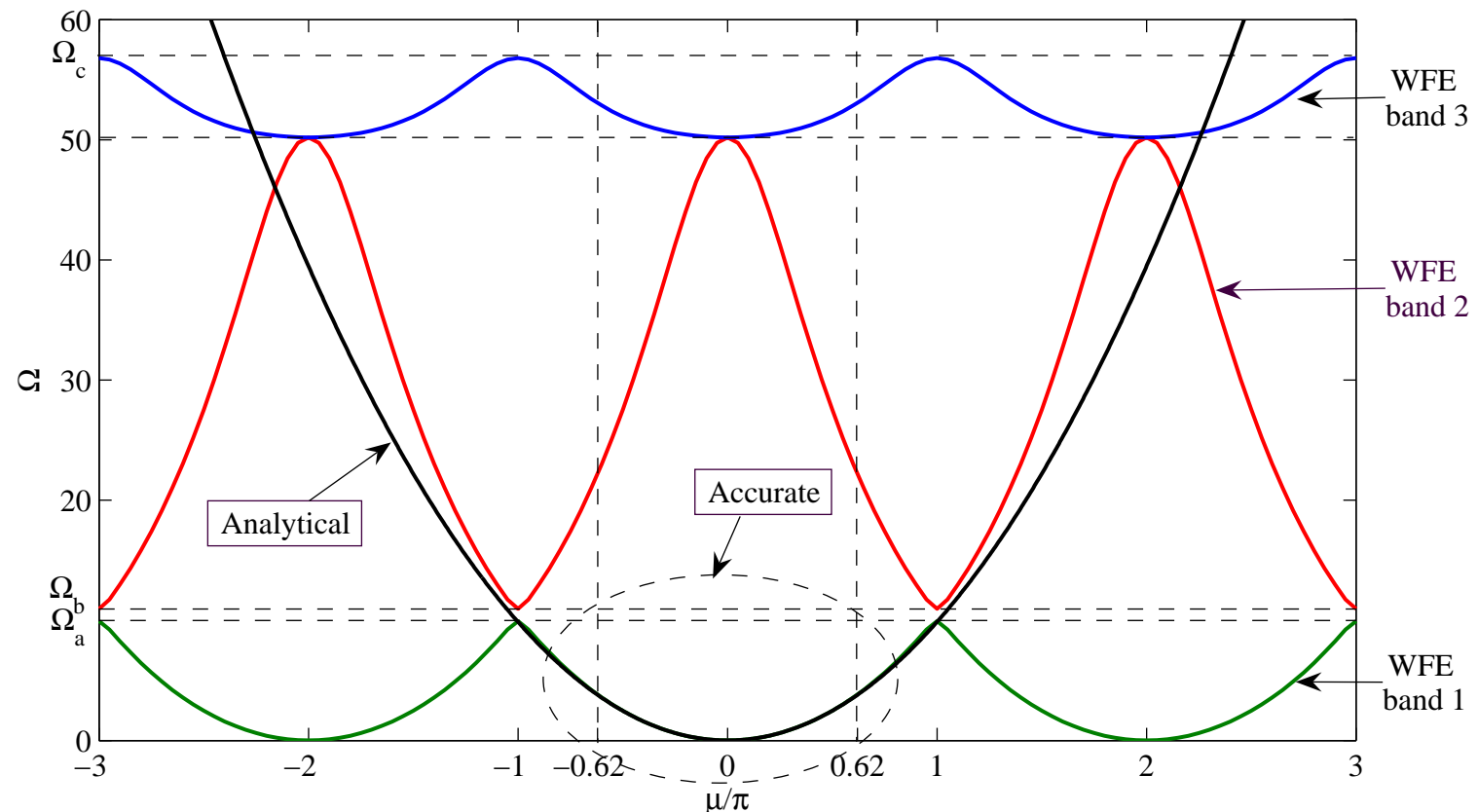


Figure 3.15: Dispersion curves for isotropic plate, propagating waves, $\theta = 0$: WFE dispersion curves and analytical dispersion curve.

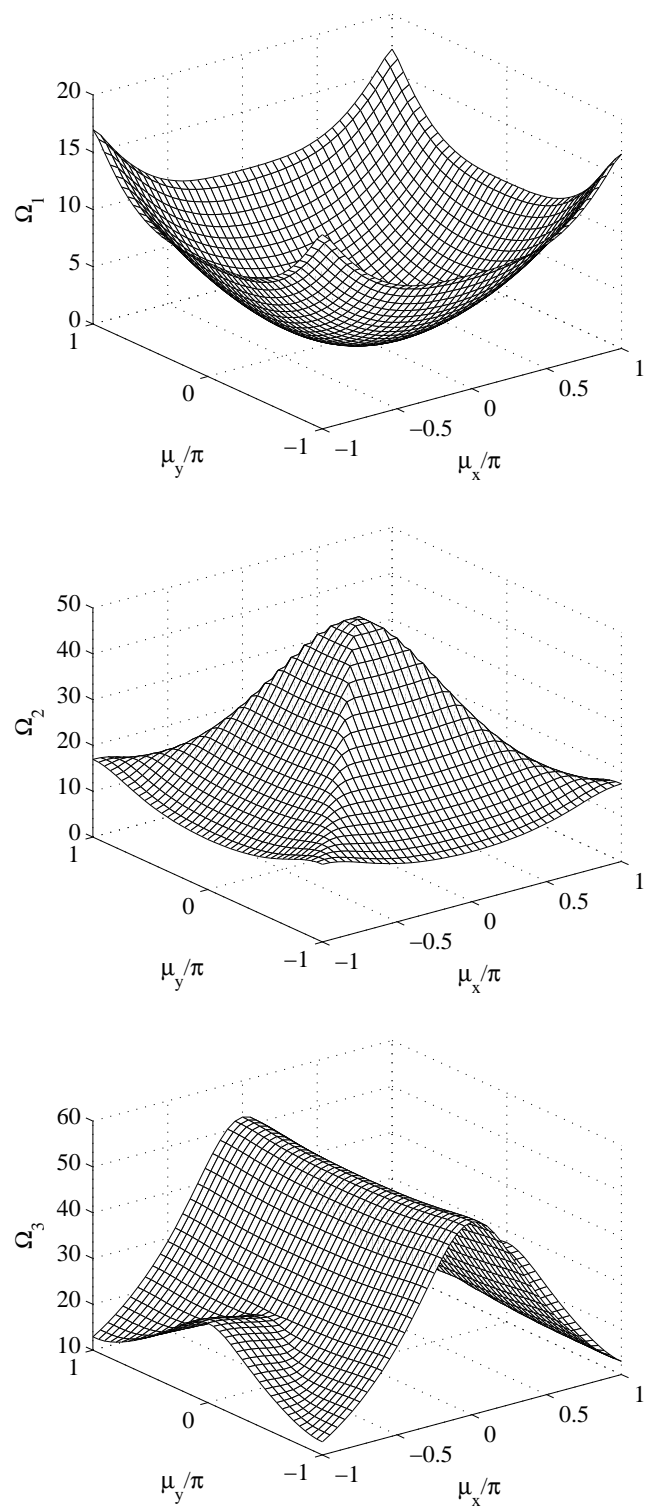
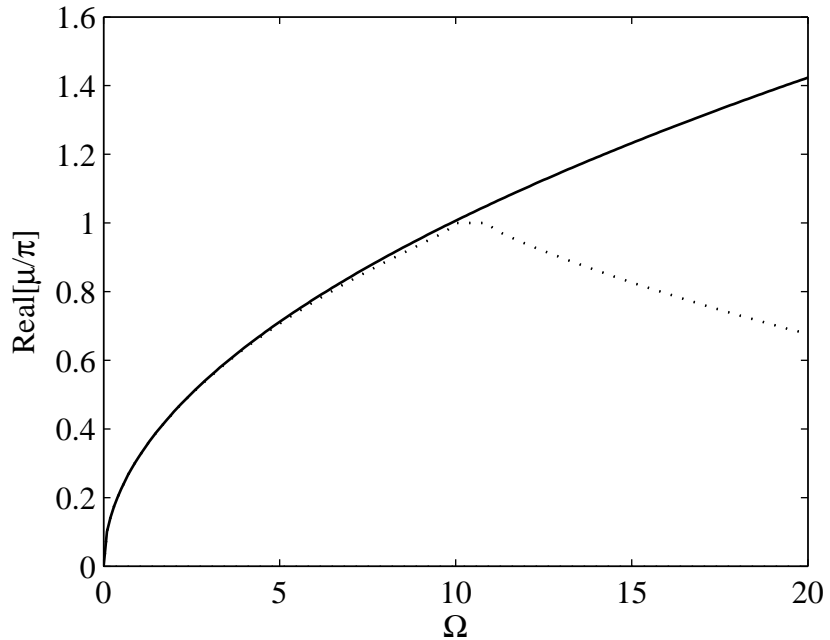
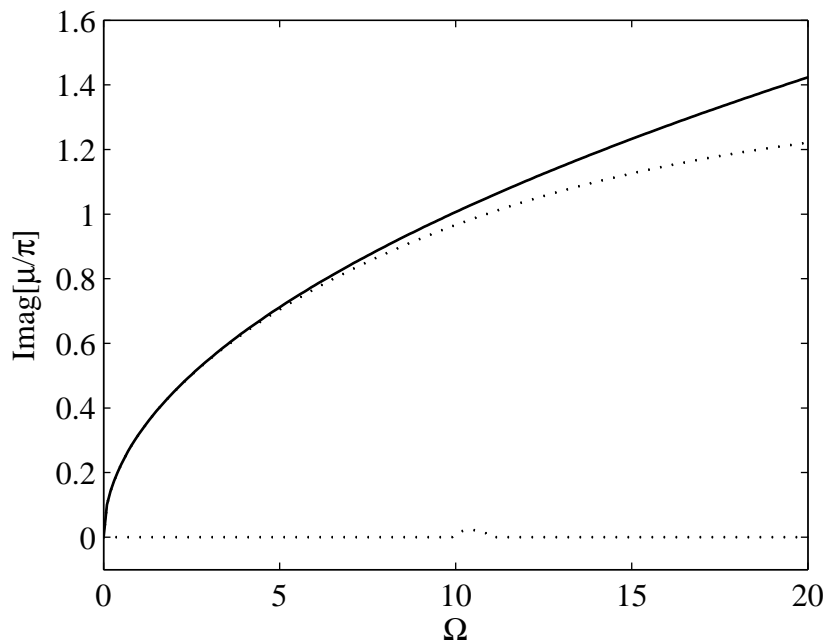


Figure 3.16: Propagation surfaces for an isotropic plate in bending vibration.



(a) Real valued μ



(b) Imaginary valued μ

Figure 3.17: Dispersion curves for isotropic plate, $\theta = 0$: ——— analytic solution; ····· WFE results.

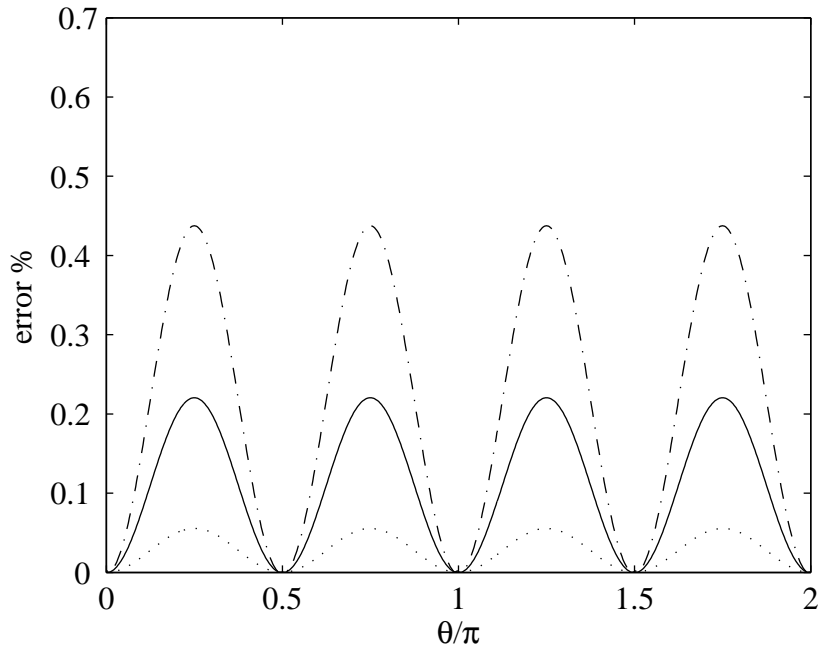


Figure 3.18: Relative error in estimated frequency as a function of θ for propagating waves in an isotropic plate, $\Omega = 0.0837$, $\mu = 0.289$: ——— $L_y = L$; ······ $L_y = L/2$; - - - - - $L_y = \sqrt{2}L$.

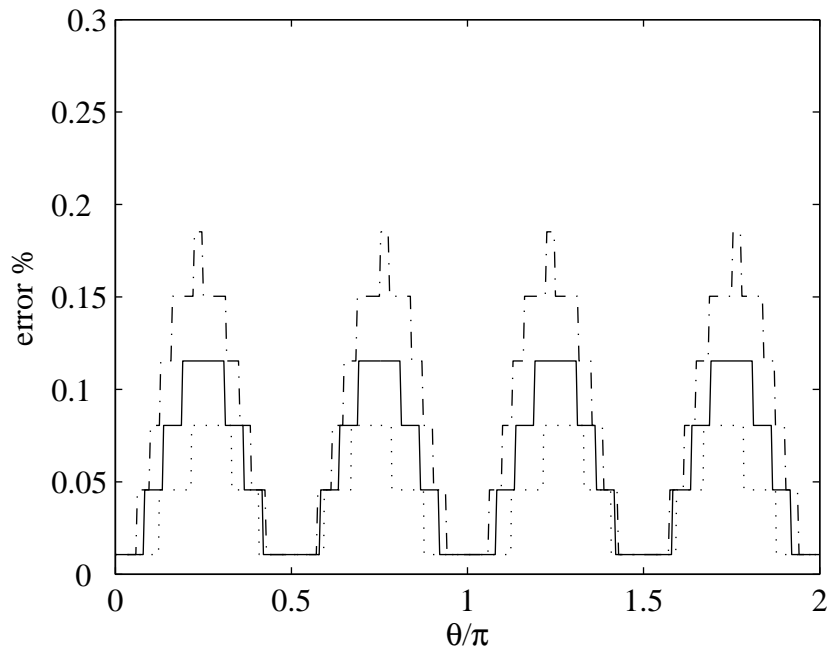


Figure 3.19: Relative error in estimated frequency as a function of θ for propagating waves in an isotropic plate, $\Omega = 0.0837$, $\mu = 0.289$: ——— $L_y = L$; ······ $L_y = L/2$; - - - - - $L_y = \sqrt{2}L$.

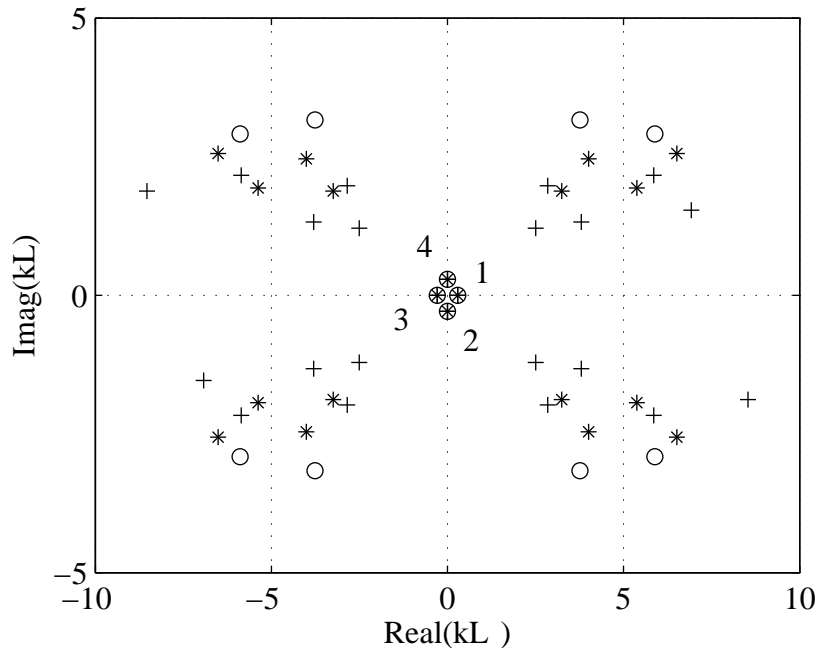


Figure 3.20: Location of the solutions in the complex $(\text{Real}(kL_x), \text{Imag}(kL_x))$ plane, $\theta = \pi/3$, $\Omega = 0.0837$: * $L_y = L$; o $L_y = L/2$; + $L_y = \sqrt{2}L$.

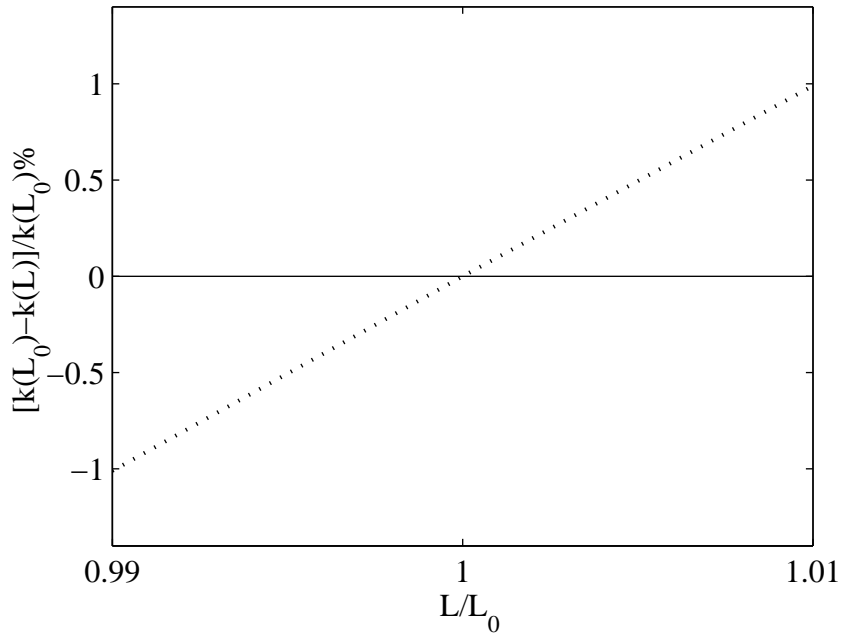


Figure 3.21: Sensitivity of eigensolutions with respect to element length, $\theta = \pi/3$, $\Omega = 0.0837$, $\mu = 0.289$: — numerical solutions to the transcendental eigenvalue problem corresponding to true solutions; ····· other solutions (periodic artifacts).

Chapter 4

Wave Finite Element Method: application to plates

4.1 Introduction

In this chapter the application of the WFE method to plates is illustrated. One aim is to validate the approach in situations for which analytical solutions are well established. Another aim is to apply the method to situations where no analytical solutions are available.

The first part of the chapter concerns plane wave propagation in an isotropic plate. The real and imaginary valued dispersion curves are given and an analysis of the wave characteristics through the study of the mode shapes is provided. Subsequently another example concerning a thick orthotropic plate made of a glass–epoxy composite material is discussed. In the last part of the chapter the wave propagation characteristics in sandwich and layered plates are investigated. These represent the most meaningful case studies in which the method shows its advantages when compared to other semi-analytical techniques. The use of the FEA libraries, in fact, greatly simplifies the analysis and allows one to solve complicated problems of the dispersion relations for high frequency wave propagation in a simple, systematic and straightforward manner.

Two different kinds of FE model can be used to apply the technique. The first can be employed when the plate has a moderate thickness compared to the wavelength. In this case only one rectangular finite element of shell type can be used to discretise the plate as shown in Figure 4.1. In developing the mass and stiffness matrices for this kind of elements various assumptions and approximations are made concerning the stress distribution in the solid, whose

motion is described fully in terms of the displacements of the neutral plane. ANSYS, as other commercial FE softwares, offers a choice of shell elements. In the present work element types SHELL63, SHELL91 and SHELL181 of the ANSYS libraries have been used. All these elements have four nodes and six degrees of freedom at each node: three translations and rotations about the nodal x , y , and z -axes. The accuracy in modelling composite shells is generally governed by the Mindlin-Reissner shell theory in which the effect of the shear deformation and rotary inertia are included. Further details can be found in the ANSYS user's manual.

As the thickness is increased, the approximate theories become less appropriate. The FE model for thick plate is shown in Figure 4.2, where the structure is then meshed by solid elastic elements. Solid elements of the type SOLID45 in ANSYS are used. This element type has eight nodes each having three degrees of freedom: translations in the x , y , and z directions. To apply the WFE method, the nodal DOFs are formed by concatenating those of all the element nodes through the thickness of the segment, although for simplicity the nodes referred to subsequently as nodes. Every node has a number of degrees of freedom equal to a quarter of the total number of the degrees of freedom of the model. Hence, the mass and the stiffness matrices \mathbf{M}_r and \mathbf{K}_r in equation (3.19) are square matrices of order $n \times n$, where n is the number of the total degrees of freedom of the model divided by 4.

For the sake of simplicity, in the following examples the elements used for the FE analysis are square elements in the (x, y) plane. With reference to Figures 4.1 and 4.2, this implies that $L_x = L_y = L$.

In the first part of the chapter the wave behaviour of isotropic and orthotropic plate is studied. The second part concerns laminated and composite sandwich plates.

4.2 Isotropic plate

When a wave propagates in a 2-dimensional uniform isotropic plate-like structure, it is guided by the plate surface. Guided waves propagating at high frequencies along a plate with traction-free boundary conditions at the surfaces are sometimes called *Lamb waves*, named after Lamb's classical analysis in this subject, [23, 110]. More recently, an extensive analysis of wave propagation in plates is due to Mindlin, [9, 53, 111, 112]. In isotropic plates, guided waves are classified

into three types: extensional, flexural and shear waves. The classification can be given according to the direction of the displacement vector for wave propagating in the x direction. The waves involving motion of the medium in the $x - z$ plane, are defined as extensional or flexural. For these kinds of waves, the displacements of the particles are directed primarily along the x and z axes respectively, that is $y = 0$, $x \neq 0$, $z \neq 0$. On the other hand, waves which involve motion of the medium primarily in the y direction, or in other terms $x = z = 0$, $y \neq 0$, are classified as shear waves. The flexural and extensional waves are governed by a plane strain state in the $(x - z)$ plane while shear waves by an antiplane and hence displacement y only. The behaviour of the waves is termed as symmetric or antisymmetric according to the symmetry or antisymmetry of the displacements about the middle plane of the cross section as shown in Figures 4.3 and 4.4.

The isotropic plate studied in this section is an aluminium plate of thickness h whose central plane is located in the (x, y) plane. The material properties are taken to be: Young's modulus $E = 71\text{GPa}$, Poisson's ratio $\nu = 0.329$, density $\rho = 2700\text{kg/m}^3$. As a first case a thin plate is studied and a comparison with the analytical results is given while the second case studied concerns a thick plate.

4.2.1 Thin isotropic plate

If the ratio between the thickness of the plate and the wavelength is roughly less than $1/10$, the classical Love–Kirchoff theory can give accurate results for the wavenumber. The upper frequency limit is approximately

$$\omega \approx \frac{0.04\pi^2}{h^2} \sqrt{\frac{D}{\rho h}},$$

where $D = Eh^3/12(1 - \rho^2)$ is the bending stiffness of the plate. A thin plate of thickness 5mm is considered in order to accurately compare WFE results and analytical results up to 20kHz. The mass and stiffness matrices were found from a single shell element of type SHELL63 in ANSYS. The dispersion curves for real μ , i.e. for free wave propagation, are shown in Figure 4.5 for $\theta = 0$. They are found by the eigensolution of equation (3.19). Analytical solutions are also given. The figure shows very good agreement between the WFE and the analytical results. The three branches in Figure 4.5 correspond respectively to flexural, shear and longitudinal waves [8].

4.2.2 Thick isotropic plate

There are various plate theories, each of which involves various assumptions and approximations concerning the distribution of stresses, strains or displacements across the plate. At higher frequencies these models become inaccurate. An alternative in FEA is to model the structure through the thickness using a number of solid elastic elements. Henceforth, 8-noded elements with 3 displacement DOFs per node are used in the numerical simulations. These were implemented as SOLID45 elements in ANSYS. The thickness of the plate investigated is $h = 15\text{mm}$ while the lengths of the sides of the element are $L_x = L_y = 1\text{mm}$. The FE model of the plate is realised using solid elements as shown in Figure 4.2.

A mesh convergence study has been carried out for this example. The element size across the section is reduced, i.e. the number of element to discretise the cross-section is increased, in order to determine a good element size for accurate prediction. As an example, the dispersion curves and the wavenumber estimates at 130kHz are given in Figures 4.6 and 4.7 respectively for an increasing number of FEs in the model. It can be seen that the wavenumber estimation is affected by the number of elements used in the discretisation, in particular at high frequency. However, Figures 4.6 and 4.7 show that 10 elements suffices to give an accurate estimate of the wavenumber at this frequency.

The complete dispersion curves for plane waves in the thick plate are given in Figure 4.8 for $\theta = 0$. Results are presented in terms of the dimensionless frequency

$$\Omega = \frac{h\omega}{\pi c_T},$$

where

$$c_T = \sqrt{\frac{E}{2\rho(\nu + 1)}}$$

is the shear wave speed. The complex branches are here represented by plotting the real and imaginary parts of the wavenumber separately. The plate is meshed using 20 solid elements with $L_x = L_y = 1\text{mm}$, although as shown in Figures 4.6 and 4.7 fewer elements provide accurate results in the frequency range considered. The term cut-on frequency here refers to the frequency value at which a certain wave starts propagating (the wavenumber becomes pure real) while cut-off frequency indicates the frequency for which the wave stops propagating as the frequency increases. Only those solutions which propagate for $\Omega < 2.5$ are shown in Figure 4.8. There are 3 propagating waves for $\Omega < 1$, which correspond

to primarily flexural, shear and extensional waves. Higher order modes across the thickness cut-on at $\Omega = 1$, these being primarily antisymmetric shear and extensional waves. The cut-on frequencies are here sometimes called *critical frequencies*. Quoting L. M. Brekhovskikh [113]: *at a critical frequency a certain number of longitudinal or transverse half wavelengths fits into the thickness of the plate. At frequency below critical, the phase velocity turns out to be imaginary for a given shape of oscillations of the plate. In this case there is no traveling along the plate, and there are only oscillations of particles with the same phase along the plate, and an amplitude decaying according to an exponential law.*

A pair of complex conjugate wavenumbers bifurcates into a pair of propagating waves with real wavenumbers around $\Omega \approx 1.8$. One of these propagating waves has phase and group velocities of opposite sign.

In order to investigate the characteristics of the propagating waves, in particular the higher order waves, the mode shapes are studied. The mode shapes are the eigenvectors obtained by solving the polynomial eigenproblem in equation (3.19) for a specified frequency. The eigenvectors, representing the displacements that are propagated along the structure, are of primary importance in evaluating the wave behaviours.

According to the number of nodal degrees of freedom of the element used for the mesh, the eigenvectors are decomposed in three different vectors representing respectively the components of the cross-section displacements in the x , y and z directions. In the following, the real part of the eigenvectors are plotted with respect to the thickness of the plate for each of the numbered branches in Figure 4.8(a). These plots represent the deformation of the $(x = 0, y = 0)$ cross-section at the time $t = 0$ in the x , y and z directions respectively.

The displacement of branch 1 in Figure 4.8(a) at $\Omega = 0.5$ is shown in Figure 4.9(a). The dominant displacement of branch 1 is an almost constant displacement in the z direction. Hence this wave represents an antisymmetric flexural wave although note that there is a small component in the x direction due mainly to rotation of the cross-section.

Figures 4.9(b) and 4.9(c) show that the dominant displacements of waves represented by branches 2 and 3 are respectively along y and x directions, both symmetric with respect to the middle plane. They represent symmetric shear and extensional waves. Lateral displacements are due to Poisson contraction. It can be seen from Figure 4.8(a) that the first shear branch, branch 2, represents a non dispersive shear wave while the other higher shear branches represent waves

that propagate dispersively.

At $\Omega = 1$ two higher order waves cut-on. Their behaviour is evaluated at $\Omega = 1.1$. From Figures 4.10(a) and 4.10(b) it can be observed that the principal disturbance propagated is a displacement in the y and x directions respectively. Hence these two waves are primarily antisymmetric shear and extensional waves.

Between $\Omega = 1.3$ and $\Omega = 1.6$, branch 3 and branch 4 cross. In particular the shape of the mode represented by branch 3 changes. To investigate how the characteristics of this branch change, its mode shapes are plotted at $\Omega = 1.3$ in Figure 4.11(a) and at $\Omega = 1.6$ and in Figure 4.11(b). At both frequencies the wave resembles a quasi extensional wave symmetric about the middle plane with some Poisson contraction in the z direction. At $\Omega = 1.6$ the displacement in the z direction becomes more significant.

At $\Omega = 1.98$ branch 6 cuts-on. For frequencies close to and below this critical frequency, the wavenumber appears to be double-valued with phase and group velocities having the same or the opposite sign depending on the wavenumber. In this example, for $\mu = [0, 0.11]$, the phase and group velocities of branch 6 have opposite sign. The mode shapes of branch 6 are evaluated at $\Omega = 1.92$. At this frequency, the wave that corresponds to the lower wavenumber has phase and group velocities of opposite sign. The two waves seem to behave mainly as quasi-extensional symmetric waves as shown in Figure 4.12. It can also be seen in Figure 4.8(a) that a complex branch cuts-off from this second extensional branch at the point in which the branch exhibits a non-zero minimum with respect to the Ω axis. These phenomena were theoretically predicted by several authors. The existence of certain wavemodes having energy transport directions opposite to the phase velocity was noticed by Mindlin [53, 112]. Tolstoy, in [114], tried to physically explain the significance of negative group velocity: “*Clearly, this does not mean that the energy is traveling towards the source, but merely that the phase and group velocities are in opposite directions. In an infinite plate, the situation is entirely symmetrical with respect to the source and the sign of the group velocity is therefore immaterial. But this result does imply that the phase and group velocities are of opposite sign, i.e. that we have negative phase velocity. In other words, given certain optimum conditions of detection and/or excitation one may see some slow wave packets in which the wave troughs and crests will be traveling, at rather high speed, in the opposite direction towards the source.*”. More recently Wolf et al. [115] measured experimentally the existence of Lamb wavemodes having negative group velocity. The experiment was carried

out to investigate the S_1 mode of a thin brass plate and the results were compared with computational predictions. However the authors pointed out that the approach should be applicable to any Lamb wave space mode that is predicted to exhibit negative group velocity. In [116] the higher order Lamb wavemodes and in particular their anomalous behaviours were investigated. It was shown that the S_1 Lamb mode always exhibits phase and group velocities of opposite sign. It was also shown that there are an “infinite” number of such waves for symmetric modes. Marston in [117] reviewed some of the literature concerning higher order symmetric Lamb waves and considered some related applications to scattering of sound by elastic shells in water.

At about $\Omega = 2.3$ branch 6 crosses branch 7. At the crossover point the frequency and the phase velocity are the same for both branch 6 and 7 but the group velocities are different. In particular, the waves represented by this point seem to carry extensional energy faster than the energy related to shear deformation. Branches 7 and 8, which cut-on at $\Omega = 2$, are shown at $\Omega = 2.1$ in Figure 4.13. They correspond to quasi-shear and quasi-extensional waves.

4.3 Orthotropic plate

In this section an orthotropic plate made of a glass–epoxy is considered, whose material properties given in Table 4.1. The plate has uniform thickness $h = 5\text{mm}$.

$E_x = 54\text{GPa}$	$E_y = 54\text{GPa}$	$E_z = 4.8\text{GPa}$
$G_{xy} = 3.16\text{GPa}$	$G_{yz} = 1.78\text{GPa}$	$G_{xz} = 1.78\text{GPa}$
$\nu_{xy} = 0.06$	$\nu_{yz} = \nu_{xz} = 0.313$	$\rho = 2000\text{kg/m}^3$

Table 4.1: Orthotropic plate: material properties.

For such a plate the equation for bending vibrations is

$$D_x \frac{\partial^4 w}{\partial x^4} + 2H \frac{\partial^4 w}{\partial x^2 \partial y^2} + D_y \frac{\partial^4 w}{\partial y^4} = -\rho h \frac{\partial^2 w}{\partial t^2}, \quad (4.1)$$

where h is the plate thickness and $H = D_1 + 2D_{xy}$. The rigidities are defined as

$$\begin{aligned} D_x &= \frac{E_x h^3}{12(1 - \nu \nu_m)}; & D_y &= \frac{E_y h^3}{12(1 - \nu \nu_m)}; \\ D_1 &= \frac{E_y \nu h^3}{12(1 - \nu \nu_m)}; & D_{xy} &= \frac{G_{xy} h^3}{12}, \end{aligned} \quad (4.2)$$

where ν_m is the minor Poisson's ratio. For more details see [118]. Substituting (3.3) into (4.1) and considering that $k_x = k \cos \theta$ and $k_y = k \sin \theta$, the free wavenumber is

$$k = \sqrt{\omega} \sqrt[4]{\frac{\rho h}{D_x \cos \theta^4 + 2H \cos \theta^2 \sin \theta^2 + D_y \sin \theta^4}}. \quad (4.3)$$

Figure 4.14 shows the flexural dispersion curves obtained by equation (4.3) and that predicted by the WFE method. The Figure shows that WFE results gives accurate estimation for μ up to $\pi/3$ or so.

4.4 Sandwich and layered plates

In the present section the WFE method is applied to evaluate the wave propagation characteristic of sandwich and layered panels.

Layered panels consists of different layers of different materials such as fiber reinforced material attached at their interface. Each lamina can be usually treated as equivalent homogenous orthotropic or transversely isotropic. For a layered plate, the repeatedly reflections at the top and the bottom surfaces that guided the waves in isotropic plate are complicated by the reflections and refractions between the layers. As a consequence, the three types of wave, i.e. flexural, shear and extensional, are generally coupled and pure wave modes are lost. A detailed illustration of the theory of wave propagation in layered media can be found in [113].

The approaches to obtain theoretical information about the wave characteristic of layered plate generally involve assumptions to simplify the problem. The majority of the formulations proposed in literature assume the laminate symmetric and each layer modelled by thin plate theory. In reference [119] an exhaustive discussion of approximate theories developed for laminated plate is given.

The term sandwich is here used to refer to structures with thin skins, which

can be made by laminated or isotropic high-strength-materials, that bind a thick lightweight core. The sandwich panels can be classified considering the properties of the core: strong-core or soft-core. For thin laminated and thin sandwiches with a strong core, at low frequencies equivalent orthotropic shells can be assumed and theories for moderately thick shells may be used to obtain the dispersion relations. However, this is not generally true for the case of sandwich plates with soft core or at higher frequencies. For increasing frequencies, in fact, the bending of the sandwich becomes influenced by the shear and rotation in the core and the out-of-plane modes are expected to decrease with increasing frequency as described in [120]. Hence, for sandwich structures, the classical plate theory becomes inadequate and the analytical model increases in complexity since, at least a first order shear deformation theory has to be considered. Moreover, shear correction coefficients are required, which are generally strongly related to the problem considered. The classical model of a three-layer symmetric sandwich plate assumes that the core carries transverse and shear stress primarily while the skins are responsible to carry the bending, tensile and compressive stresses. Di Taranto [121] assumed constant shear stress and negligible in-plane stress in the core while negligible shear strain was considered in the face-plates. The normal stress between laminates and core was ignored. The same assumptions were used by Mead and Markus [18] to evaluate the transverse displacement of a three-layer sandwich beam with viscoelastic core. As another example, Nilsson assumed in [122] that the displacement in the core was described by a combination of longitudinal and shear waves. The equations of motion for each thin layers was set taking shear and normal stress at the surfaces of the laminates. The characteristics equation for wave propagation was then obtained using continuity of the displacements and stresses at the two junctions between laminate and core. Other kind of assumption can be made in order to capture the dynamic properties of the core and special formulation have been proposed for the core dynamics [123].

The WFE method for a moderately thick layered or sandwich panel can be applied using a simple FE model obtained by a single shell element with layer or sandwich capability, e.g. SHELL91, SHELL99 or SHELL181 in ANSYS. If the thickness of the plate increases, the plate should be meshed using solid element in order to evaluate the wave characteristics at high frequencies. The FE mesh made using solid elements is generally preferred for composite structure because it does not involve any assumptions concerning the motion. For sandwich plates,

in order to better evaluate the cross-section deformation, more elements must be generally used to mesh the core. However, the correct number of elements that should be used to mesh the section changes on a case-to-case basis. In particular, if the interest is most in a high frequency range, a convergence analysis is usually required. It is worth pointing out that the latter model is not within the so called thin-wall theory.

In the first part of this section the results for the bending vibrations are compared with those obtained in [18] for a three layered sandwich beam. Then the dispersion curves for the same sandwich panel are given for a frequency range up to 10kHz and the characteristics of the propagating waves are studied. The second case shows the real valued dispersion curves for a layered plate. A comparison with the wavenumber solutions in [19] is given. The real-valued dispersion curves for several propagation directions are also shown. In the third part of this section the complex frequency spectrum for the more complicated cases of an asymmetric sandwich plate is given.

4.4.1 Isotropic sandwich panel

The skins of the sandwich plate considered for this analysis are 5mm thick with material properties as follow: Young modulus $E = 16.7\text{GPa}$, Poisson's ratio $\nu = 0.3$ and density $\rho = 1730\text{kg/m}^3$. The core is a 50mm isotropic with material properties: $E = 0.13\text{GPa}$, $\nu = 0.3$ and $\rho = 130\text{kg/m}^3$. Sixty SOLID45 elements are used to mesh the section: five for each skin and fifty for the core. In this example $L_x = L_y = 1\text{mm}$ and $\theta = \pi/2$.

Figure 4.15 shows the dispersion curve for flexural waves obtained applying the WFE method and the method proposed by Mead and Markus in [18] up to 5.5kHz. The comparison between the two curves shows good agreement. Dispersion curves for the sandwich plate are shown in Figure 4.16. As the figure shows, the complex frequency spectrum is complicated, in particular at high frequency. In order to have a clearer outline of the waves propagating in the plate, only the real valued dispersion curves are given in Figure 4.17. Figure 4.18 shows results in the frequency interval 3.7–4.3kHz. It can be noticed that both branches 3 and 6 exhibit the behaviour already pointed out for the isotropic case in Figure 4.8: a positive phase speed but a negative group velocity with complex cut-off branches. The same behaviours was observed by Waki et al. [84] analysing wave propagation in a vehicle tyre. This phenomenon was seen in [64] and in [76] for a similar sandwich plate. In particular in [76], the loci of the complex valued

wavenumbers was given in a frequency range close to a complex cut-off point in the frequency spectrum.

Some wavemodes for the sandwich plate are now investigated. Only the real parts of the eigenvectors, which represent the displacements in the x , y and z directions of the nodes in the FE model at $(x = 0, y = 0)$, is plotted with respect to the plate thickness.

A description of the wavemodes is here given in terms of their predominant displacements. Although pure wavemodes do not exist in this case, the terms *quasi-flexural*, *quasi-shear* and *quasi-extensional* are here used to refer to the predominant behaviour of the wavemodes. Figures 4.19–4.24 show the mode shapes of branches 1, 2 and 3 at 1.5kHz, branches 4 and 5 at 2.5kHz, branches 3 and 6 at 4.5kHz and branches 7 and 8 at 8kHz. From Figures 4.19 and 4.20 it can be observed that the predominant displacement of the wavemode for branch 1 is along the z direction and it resembles an antisymmetric flexural wave. However, as already pointed out, the mode is not fully described by a flexural wave. As shown in Figure 4.19(b), it is coupled with slightly antisymmetric shear motion where the skins and the core are moving in antiphase. The slightly symmetric extensional displacement may due to rotation of the cross-section. For branch 2, the wave in Figure 4.19(c) seems to be a quasi-symmetric shear wave with Poisson contraction while for branch 3, the wave in Figure 4.20(a), as expected, resembles a symmetric extensional wave with lateral displacement. The small displacements in the z direction of this wave are symmetric. At about 2.278kHz two waves cut-on. The wavemodes of these branches are shown at 2.5kHz in Figure 4.21. At 2.5kHz the wave represented by branch 4 seems to be a quasi-antisymmetric-shear wave while the wave represented by branch 5 resembles a quasi-extensional wave with antisymmetric shear in the core. The skins and core out-of-plane displacements are in phase. Furthermore, Figure 4.17 shows that as the frequency increases, branch 3 veers and changes its behaviour.

At about 4.262kHz a higher order wave starts propagating. The wavemodes that correspond to branches 3 and 6 are studied at 4.5kHz. As shown in Figure 4.22(a) the extensional nature of branch 3 seems to couple with a flexural behaviour at 4.5kHz. Figure 4.23(a) shows that at 4.5kHz branch 6 has characteristics that are similar to an extensional wave with the skins and the core in slightly antiphase. At about 7.9kHz this branch crosses branch 4. At this point the frequency and the phase velocity are the same for the two branches but the group velocities are different. The same phenomenon seems to happen at

about 7.55kHz between branches 7 and 5. The behaviours of the two higher order branches which cut-on at about 7.02kHz are evaluated at 8kHz and their cross-sectional displacements are given in Figure 4.24. The wavemodes in Figure 4.24 can be described as quasi-shear and quasi-extensional wavemodes respectively.

4.4.2 Laminated plate

Consider a laminated plate comprising two 5mm thick layers of composite fiber reinforced material. The ply-stacking of the laminae is an asymmetric [0/90] sequence. The WFE results for the dispersion curves are compared with those obtained by Chackraborty and Gopalakrishnan in [19]. The WFE model has 2 solid elements across the section. The FEs are 3D solid elements of the type SOLID45 in ANSYS. Figure 4.25 shows the real-valued dispersion curves for k_x when $k_y = 50\text{m}^{-1}$ together with the results using the method in [19]. The agreement is good at low frequencies and less good as the frequency increases. This is explained in part because Chackraborty and Gopalakrishnan used a first-order layer-wise laminate theory, which becomes less accurate as frequency increases.

One further advantage of the 2-dimensional WFE approach is that the dispersion curves can be readily evaluated for different directions of propagation. As an example, Figure 4.26 shows the real-valued dispersion curves for various values of θ .

4.4.3 Antisymmetric cross-ply sandwich panel

The WFE approach can be applied equally to laminates of arbitrary complexity, with an arbitrary number of layers. The final example is an asymmetric, cross-ply laminated sandwich panel. The two outer skins of the asymmetric angle-ply laminated sandwich considered in this section comprise 4 sheets of 0.25mm of graphite-epoxy material. The stacking sequence of the bottom and the top skins are [45/ - 45/ - 45/45] and [-45/45/45/ - 45] respectively. The core is a 5mm thick foam core. Material properties for the skins and the core are shown in Table 4.2.

To model the structure 4 SOLID45 elements with $L_x = L_y = 1\text{mm}$ were used for each skin and 5 SOLID45 elements used for the core. The reduced WFE model has therefore 42 DOFs. Figures 4.27 shows the real propagation constant, kL , versus the frequency for $\theta = 0$ and $\theta = \pi/4$. The first three branches in Figures 4.27 represent the first quasi-flexural, quasi-shear and quasi-extensional waves

Graphite–epoxy			Foam core
$E_x = 119\text{GPa}$	$E_y = 8.67\text{GPa}$	$E_z = 8.67\text{GPa}$	$E_x = 0.18\text{GPa}$
$E_z = 8.67\text{GPa}$	$G_{yz} = 3.9\text{GPa}$	$G_{xy} = G_{xz} = 5.18\text{GPa}$	$\rho = 110\text{kg/m}^3$
$\nu_{xy} = \nu_{xz} = 0.31$	$\nu_{yz} = 0.02$	$\rho = 1389\text{kg/m}^3$	$\nu = 0.286$

Table 4.2: Laminated sandwich plate: material properties.

propagating in the laminated sandwich. At higher frequency, further propagating waves cut-on, which involve higher order modes across the thickness of the plate. It can be noticed that the dispersion characteristics are very complicated at high frequency, involving coupling between the various wave modes, veering and so on.

The dispersion curves can be evaluated for different directions of propagation as contour curves for fixed value of the frequency. Considerations about the direction of the group velocity can be obtained analysing these contour curves. The dispersion curves in the (k_x, k_y) plane are in fact obtained as contour curves such that $\omega = f(k_x, k_y)$ and therefore the gradient

$$\nabla\omega = \left[\frac{\partial\omega}{\partial k_x}, \frac{\partial\omega}{\partial k_y} \right]^T \quad (4.4)$$

is in the direction of the normal to the contour curves. Since the group velocity is defined by

$$\mathbf{c}_g = \frac{d\omega}{dk}, \quad (4.5)$$

the direction of \mathbf{c}_g (or the direction of the energy flow) coincides with the direction of the normal to the dispersion curves in the (k_x, k_y) plane. As an example, Figure 4.28 shows the dispersion contours at 5kHz and 10kHz in the (μ_x, μ_y) plane where $\mu_x = k_x L_x$ and $\mu_y = k_y L_y$. It can be noticed in Figure 4.28(b) that the contour curves corresponding to shear waves shows regions in which a particular value of μ_y corresponds to two distinct values of μ_x . These represent two distinctly different propagating waves. In particular the directions of the group velocity are different, with the wave represented by one of these points having a negative group velocity in the x direction. As an example, points A and B are shown in Figure 4.28(b) for $\mu_y = 0.02$ and 10kHz. Figure 4.28(b) shows that the normal vector to the curve at the point B has a positive component with respect to the x direction and therefore it has a positive group velocity in the x direction. On the other hand at point A , the curve has a normal with a negative component along x axis denoting that positive group velocity is in the $-x$ direction with

phase velocity and the group velocity of opposite signs. The curves for lower frequencies have similar shapes. It can be seen that the dispersive behaviour strongly depends on the propagation direction.

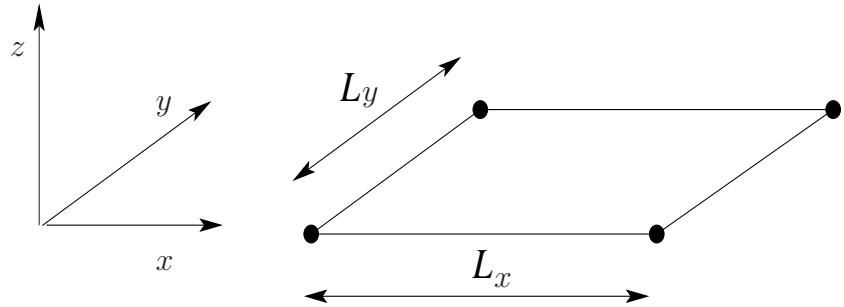


Figure 4.1: FE model of a small rectangular segment of a 2-dimensional homogeneous plate meshed with one shell element.

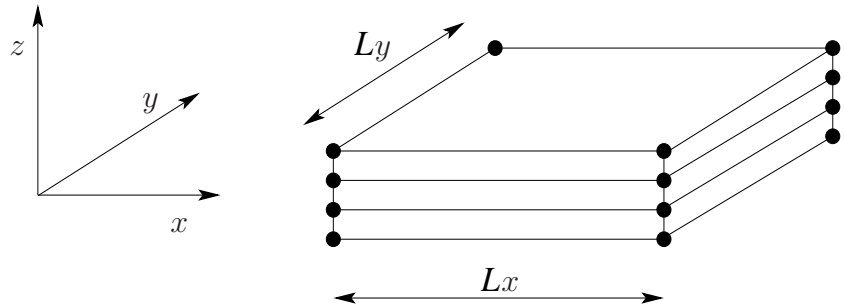


Figure 4.2: FE model of a small rectangular segment of a 2-dimensional homogeneous thick plate meshed with solid elements.

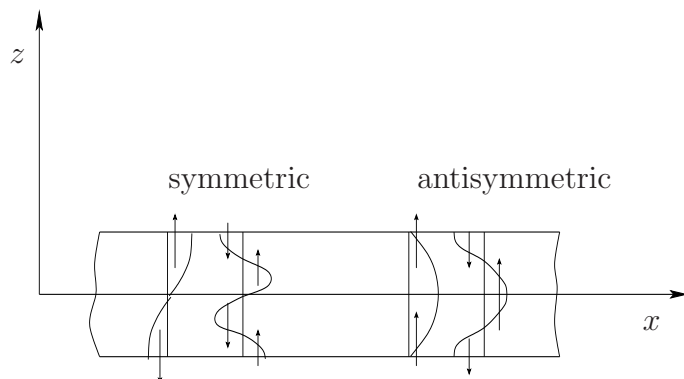


Figure 4.3: Examples of symmetric and antisymmetric components of the displacements in the z direction.

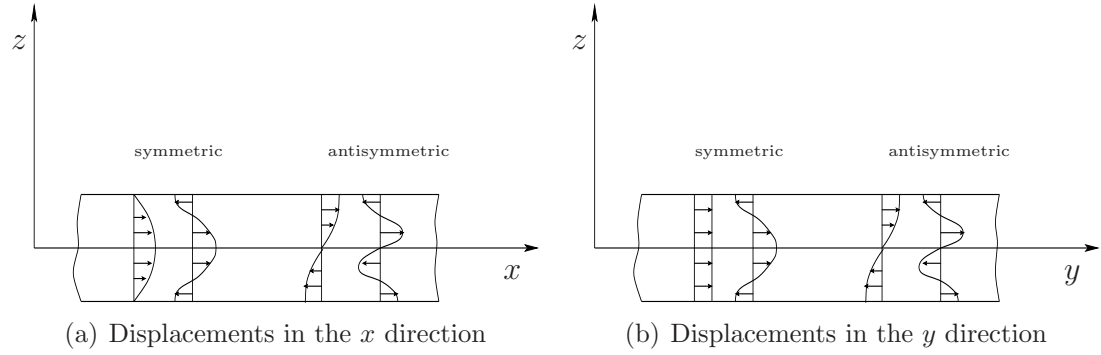


Figure 4.4: Examples of symmetric and antisymmetric components of the displacements in the x and y directions.

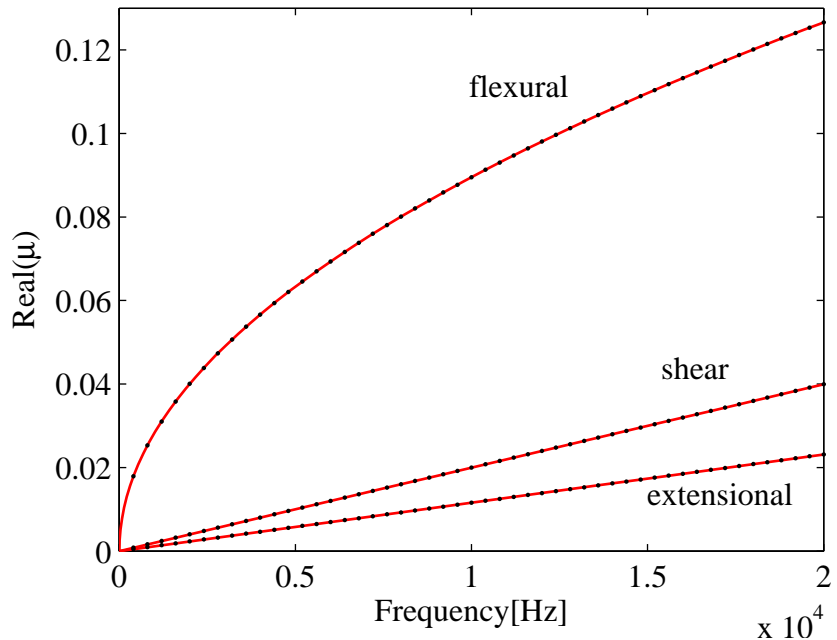


Figure 4.5: Real valued dispersion curves for a thin isotropic plate: —— analytic solution; ······ WFE results

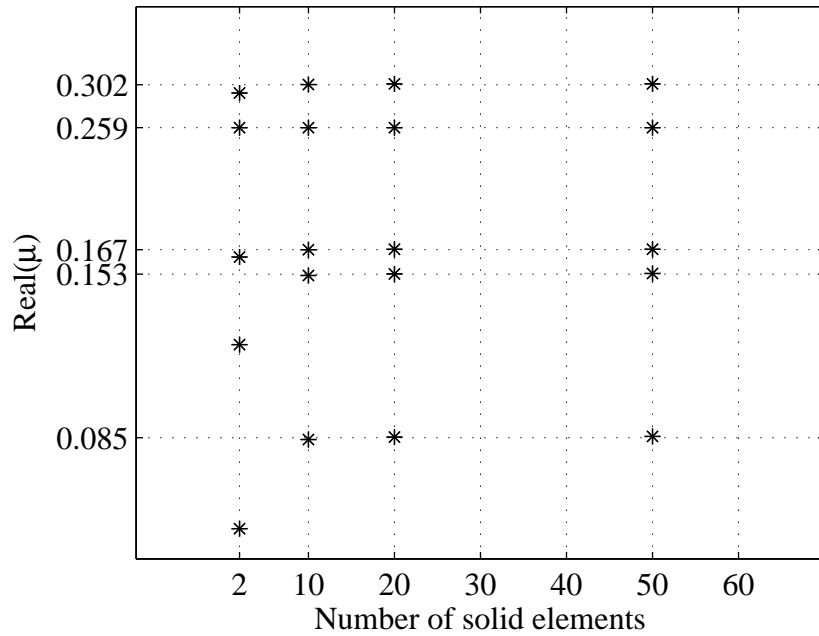


Figure 4.6: Isotropic thick plate: convergence of the nondimensional wavenumber estimates at 130kHz.

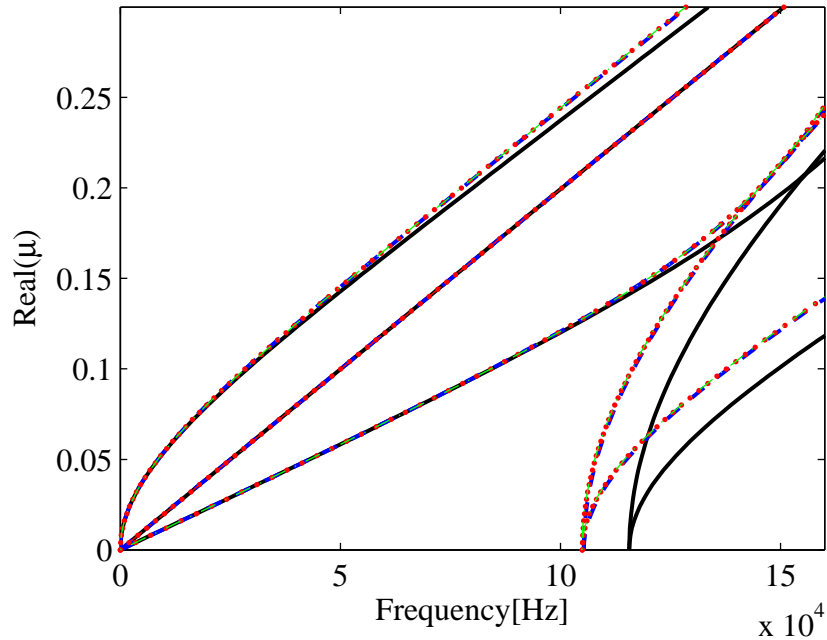
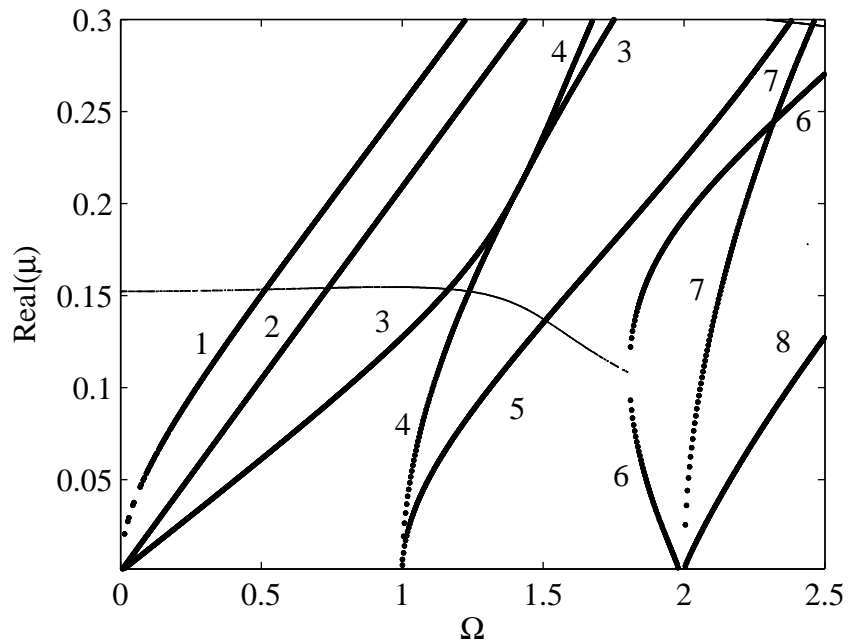
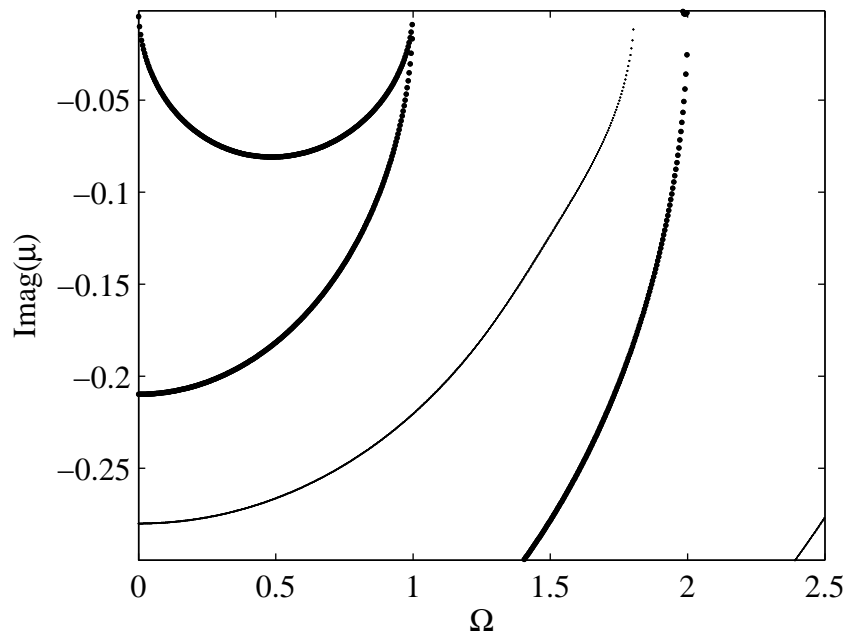


Figure 4.7: Real valued dispersion curves for a thick isotropic plate. Results obtained increasing the number of FEs: — 2; - - - 10; ····· 20 and - ···· 50 solid elements.



(a) Real dispersion curves



(b) Imaginary dispersion curves

Figure 4.8: Thick isotropic plate, $h = 15\text{mm}$, $\theta = 0$ complex valued wavenumbers; pure real and pure imaginary wavenumbers

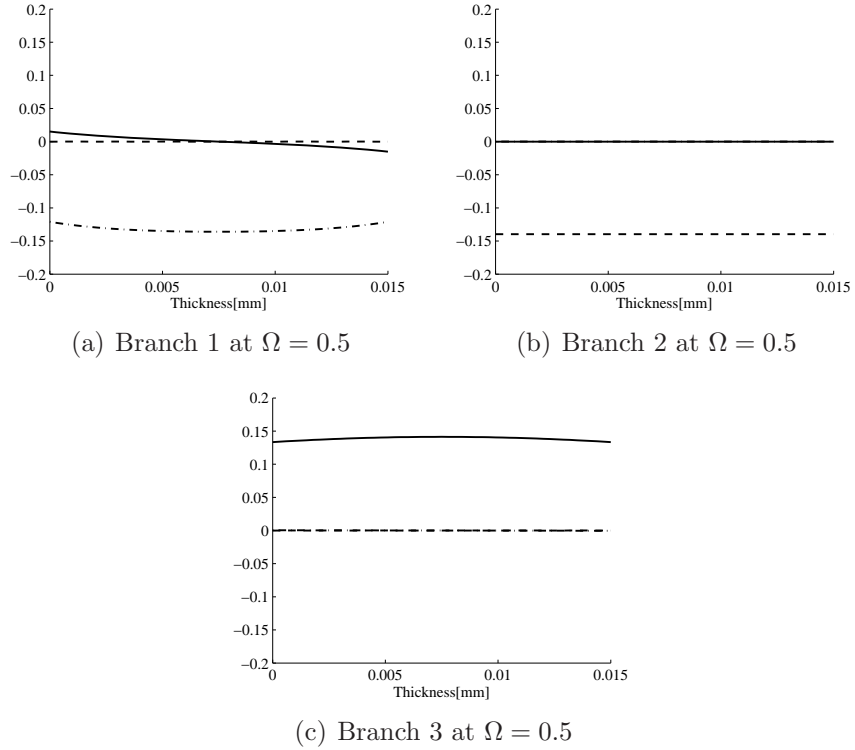


Figure 4.9: Isotropic thick plate. Mode shapes of branches 1, 2 and 3 in Figure 4.8(a) evaluated at $\Omega = 0.5$: ——— x ; - - - - y ; - · - · - z .

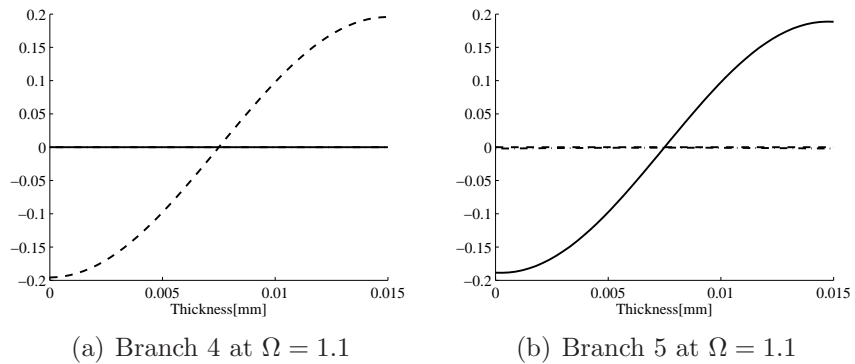


Figure 4.10: Isotropic thick plate. Mode shapes of branch 4 and branch 5 in Figure 4.8(a) evaluated at $\Omega = 1.1$: ——— x ; - - - - y ; - · - · - z .

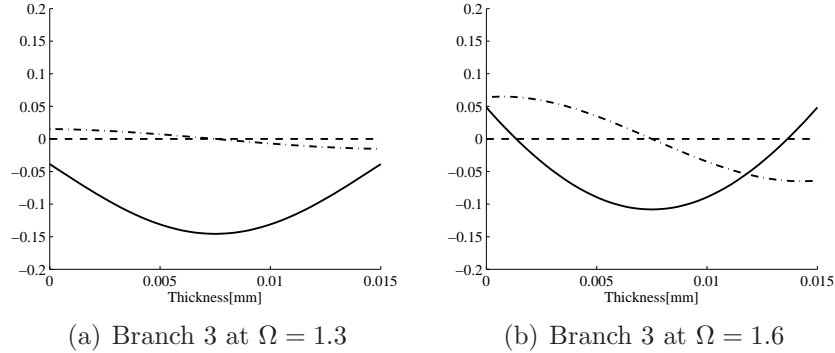


Figure 4.11: Isotropic thick plate. Mode shapes of branch 3 in Figure 4.8(a) evaluated at $\Omega = 1.3$ and $\Omega = 1.6$: ——— x ; - - - - y ; - · - · - z .

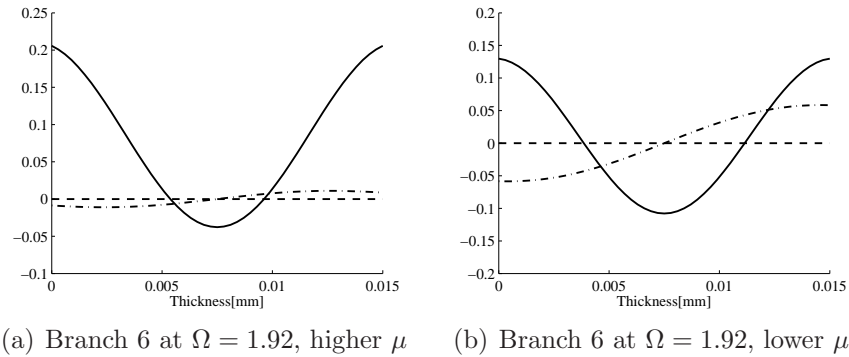


Figure 4.12: Isotropic thick plate. Mode shapes of branch 6 in Figure 4.8(a) evaluated at $\Omega = 1.92$: ——— x ; - - - - y ; - · - · - z .

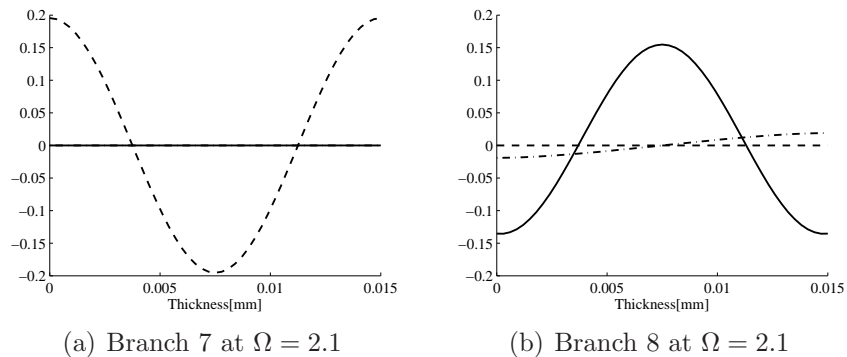


Figure 4.13: Isotropic thick plate. Mode shapes of branch 7 and 8 in Figure 4.8(a) evaluated at $\Omega = 1.92$: ——— x ; - - - - y ; - · - · - z .

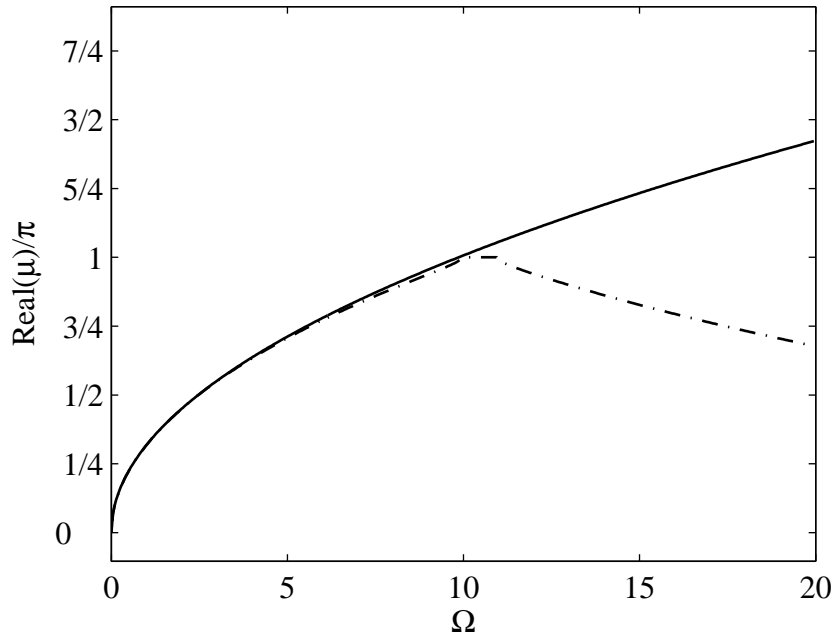


Figure 4.14: Orthotropic plate, dispersion curve for flexural wave propagation, $\theta = 0$: ——— analytic solution; ····· WFE results.

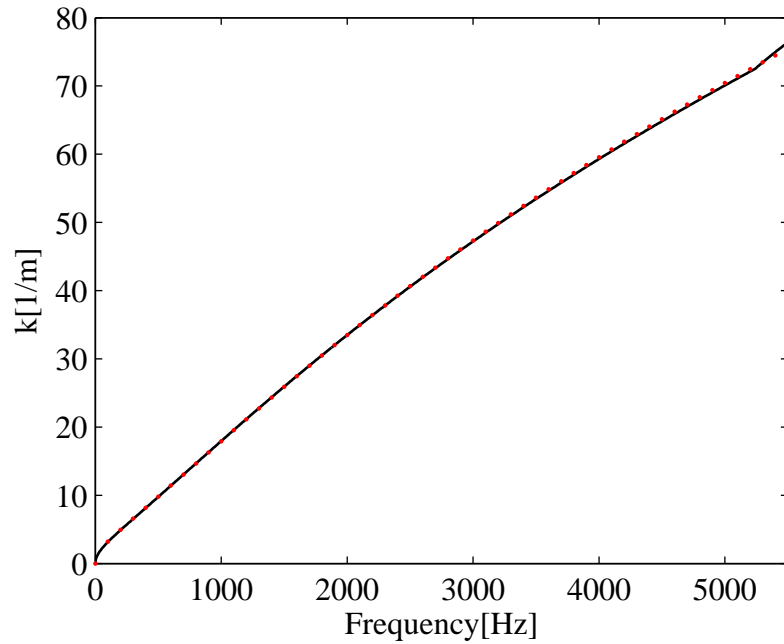
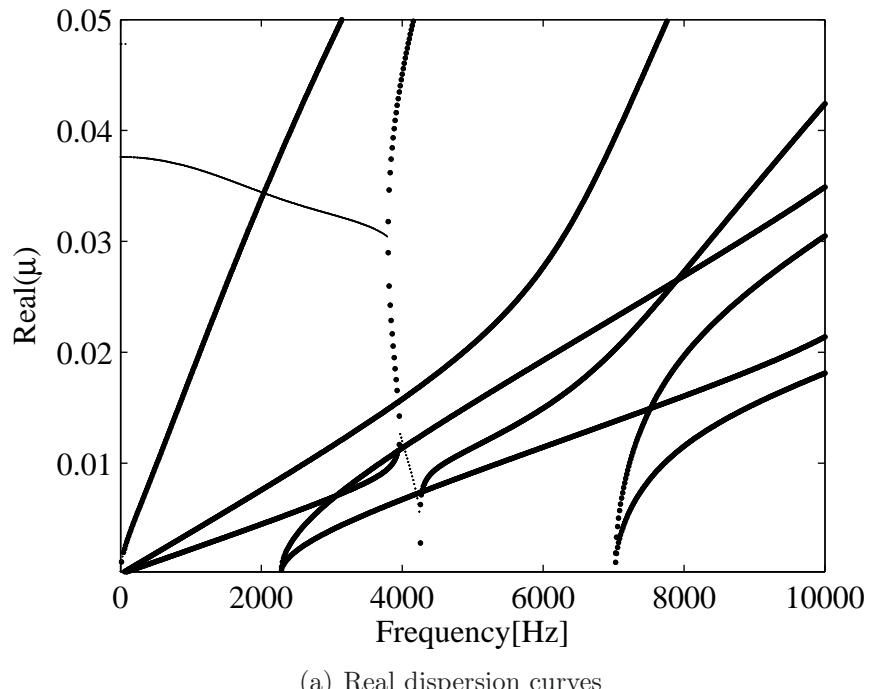
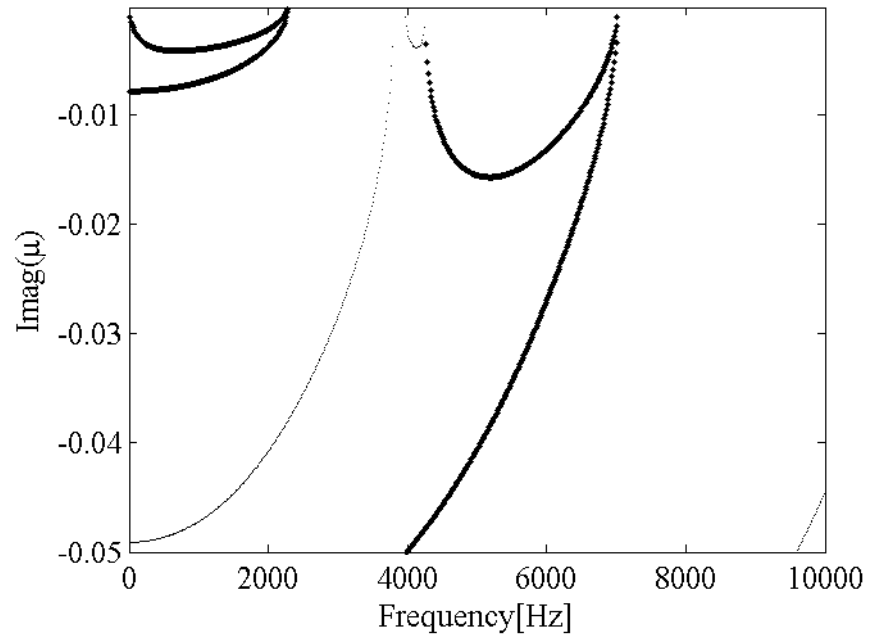


Figure 4.15: Isotropic sandwich panel, dispersion curve for flexural wave propagation: ——— WFE results; ····· theory of [18].



(a) Real dispersion curves



(b) Imaginary dispersion curves

Figure 4.16: Isotropic sandwich panel, $\theta = \pi/2$. Dispersion curves: complex valued wavenumbers; pure real and pure imaginary wavenumbers.

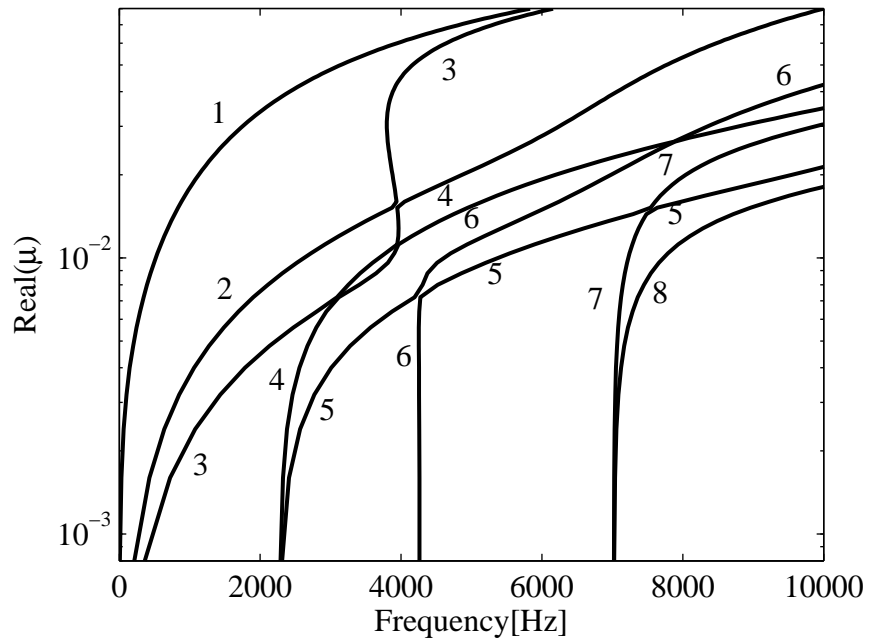


Figure 4.17: Isotropic sandwich panel: real valued dispersion curves.

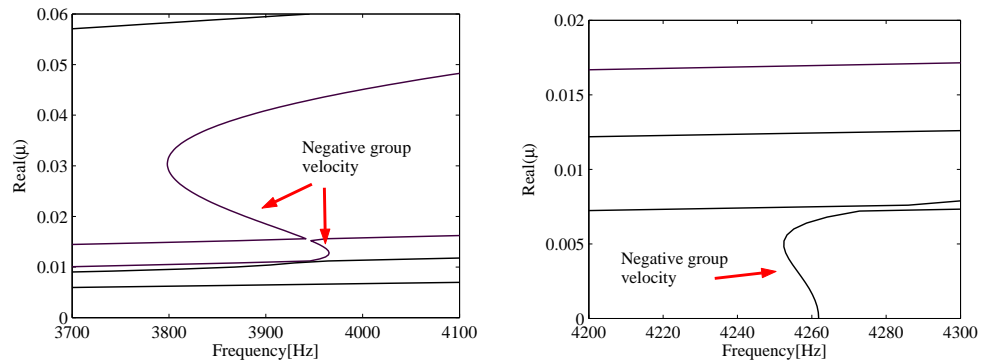


Figure 4.18: Isotropic sandwich panel: real valued dispersion curves in the 3700–4300 Hz band.

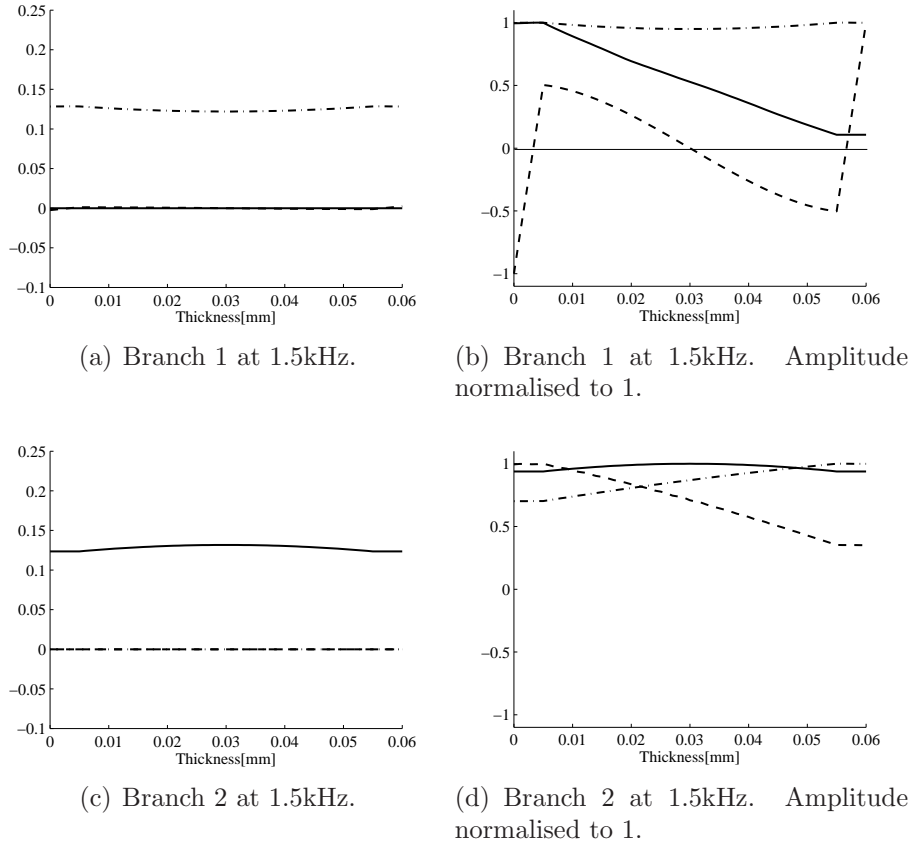


Figure 4.19: Isotropic sandwich plate. Mode shapes of branches 1 and 2 in Figure 4.15 evaluated at 1.5kHz: ——— x ; - - - - y ; - · - · - z .

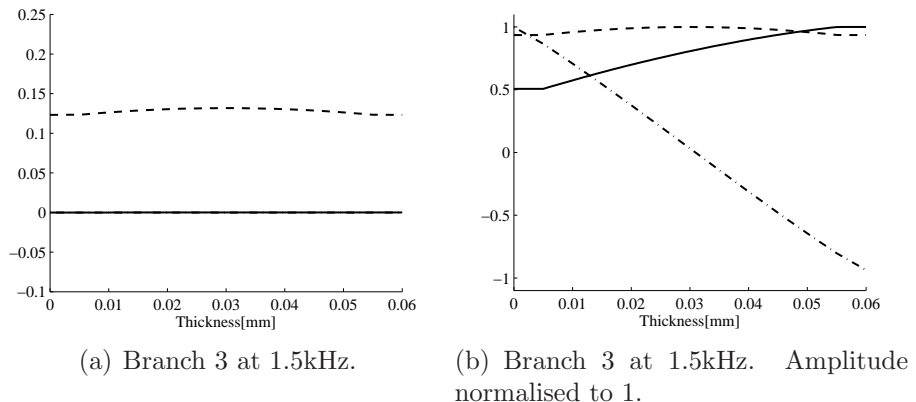


Figure 4.20: Isotropic sandwich plate. Mode shapes of branch 3 in Figure 4.15 evaluated at 1.5kHz: ——— x ; - - - - y ; - · - · - z .

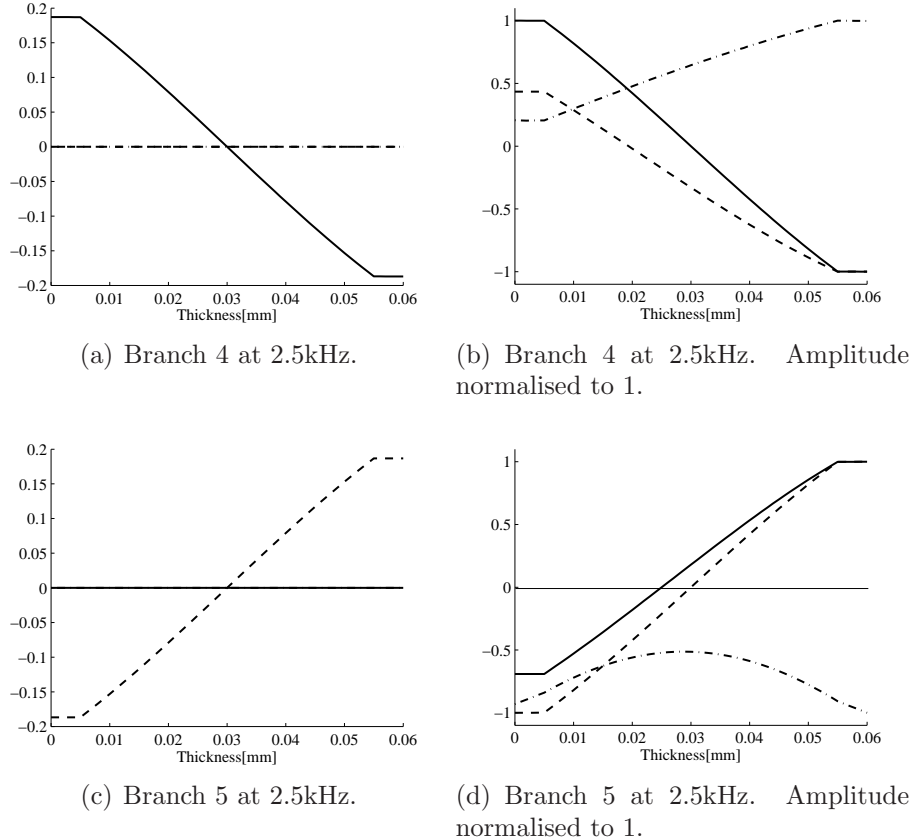


Figure 4.21: Isotropic sandwich plate. Mode shapes of branches 4 and 5 in Figure 4.15 evaluated at 2.5kHz: ——— x ; - - - - y ; - · - · - z .

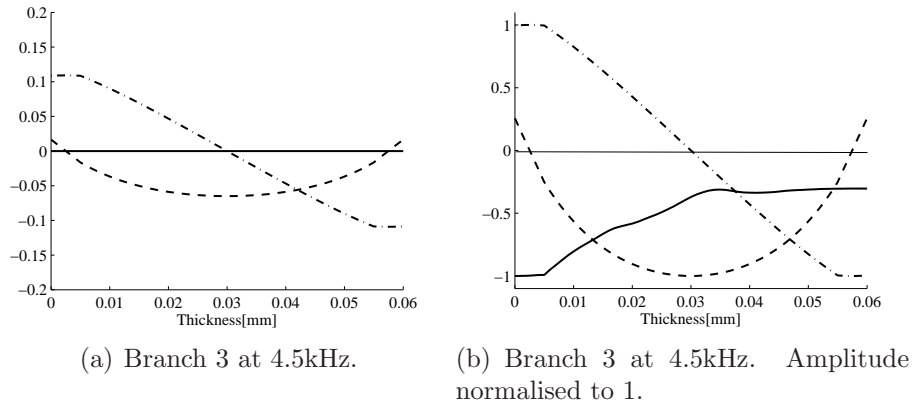


Figure 4.22: Isotropic sandwich plate. Mode shapes of branches 3 in Figure 4.15 evaluated at 4.5kHz: ——— x ; - - - - y ; - · - · - z .

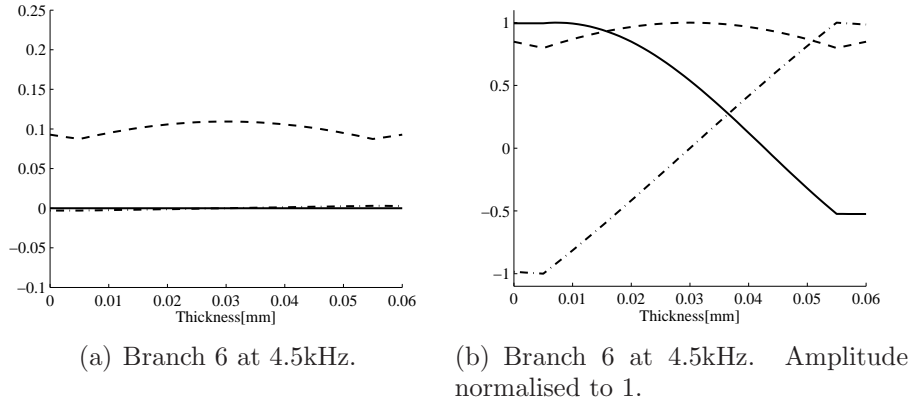


Figure 4.23: Isotropic sandwich plate. Mode shapes of branches 6 in Figure 4.15 evaluated at 4.5kHz: ——— x ; - - - - y ; - · - · - z .

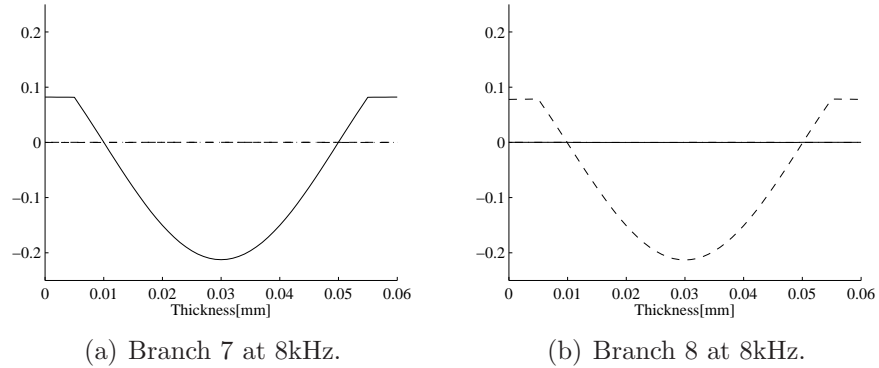


Figure 4.24: Isotropic sandwich plate. Mode shapes of branches 7 and 8 in Figure 4.15 evaluated at 8kHz: ——— x ; - - - - y ; - · - · - z .

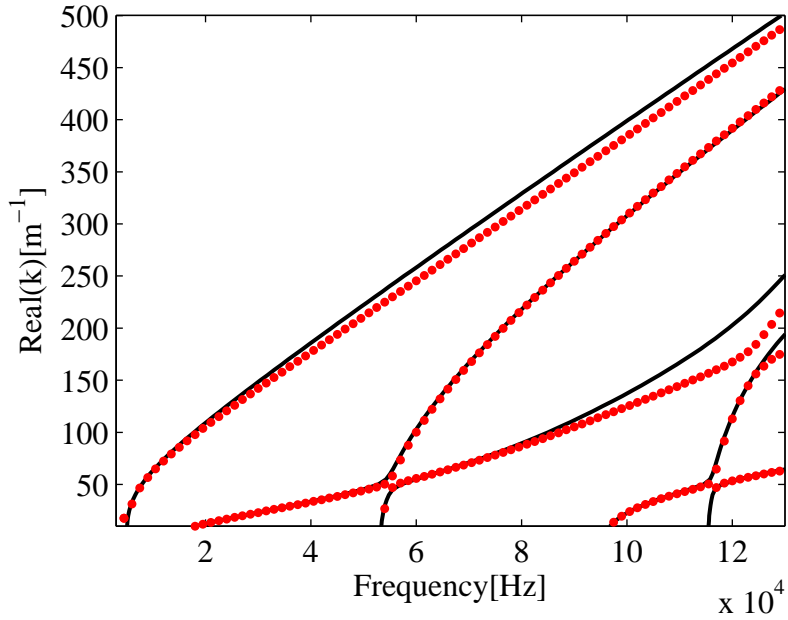


Figure 4.25: Asymmetric cross-ply laminate plate: real valued dispersion curves, $k_y=50\text{m}^{-1}$: — WFE results; ····· theory of [19].

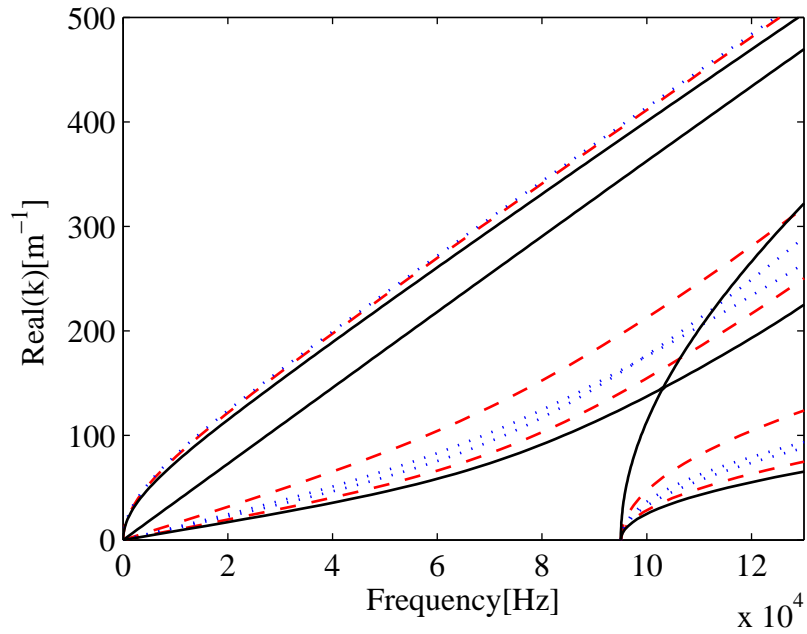
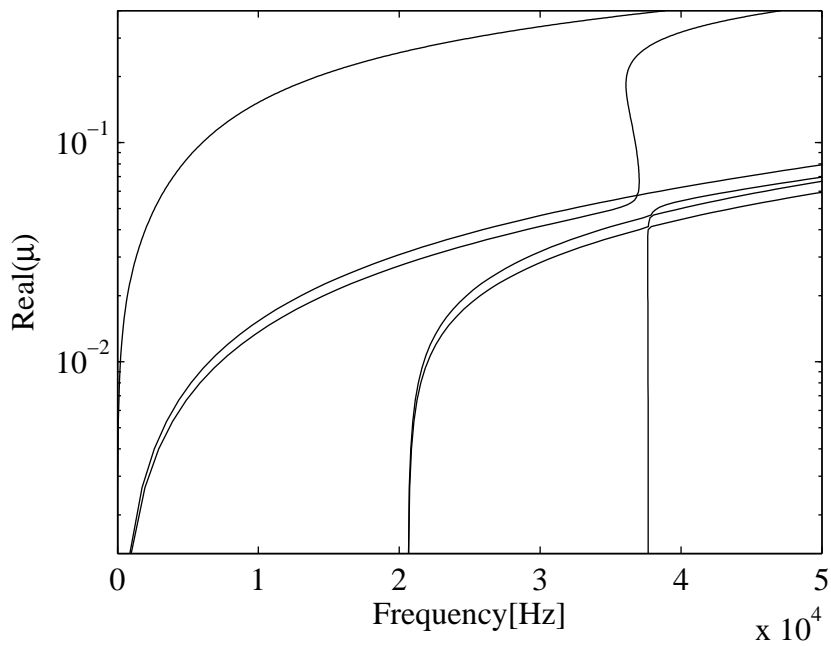
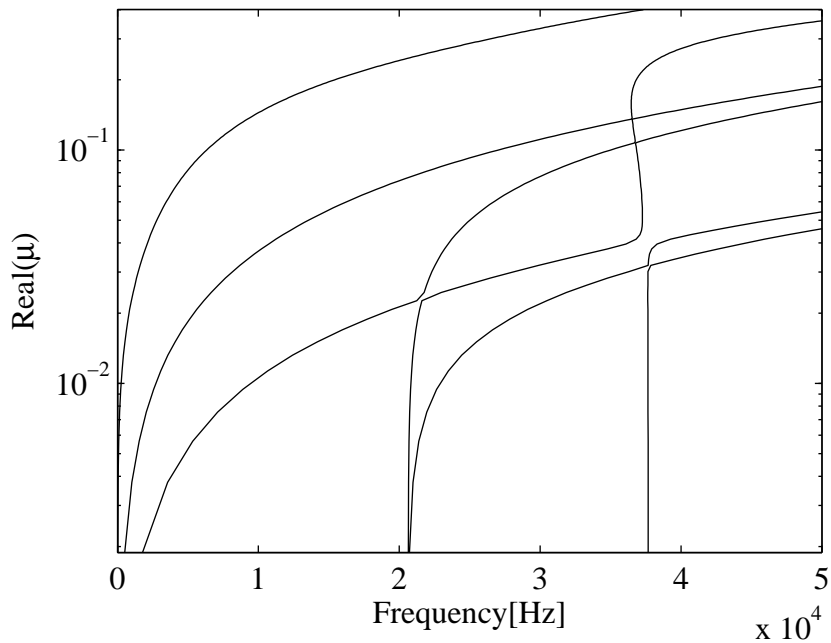


Figure 4.26: Asymmetric cross-ply laminate: real-valued dispersion curves: — $\theta = 0$; ····· $\theta = \pi/4$; - - - - $\theta = \pi/3$.

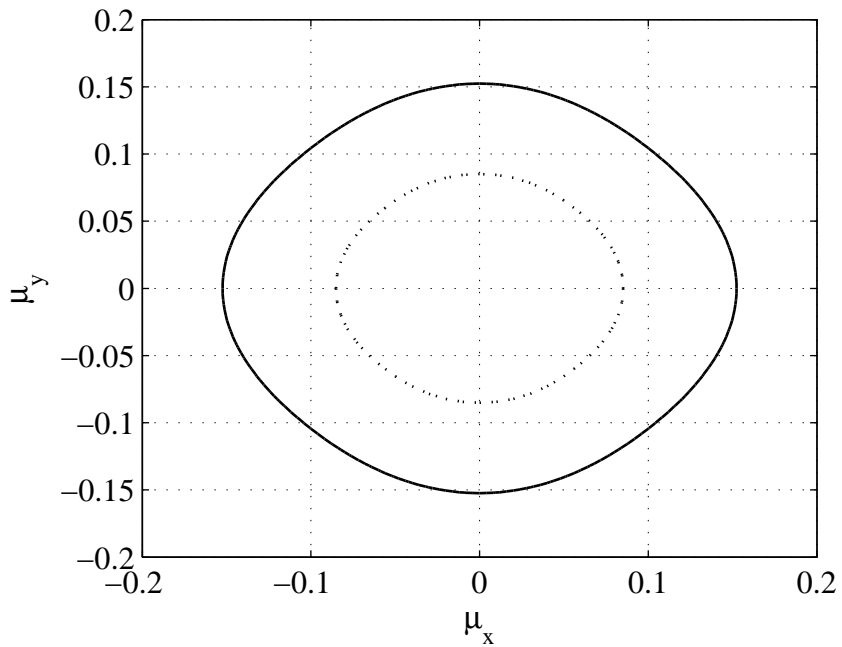


(a) Dispersion curves, $\theta = 0$

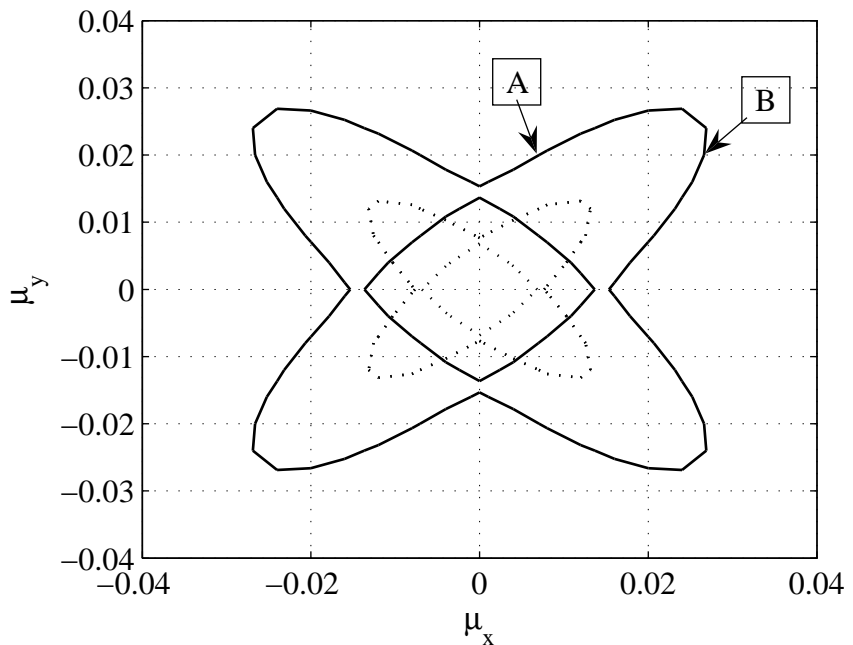


(b) Dispersion curves, $\theta = \pi/4$

Figure 4.27: Asymmetric sandwich plate: real-valued dispersion curves.



(a) Quasi-flexural waves



(b) Quasi-shear and quasi-extensional waves

Figure 4.28: Asymmetric sandwich plate, dispersion contour curves: 5kHz and —— 10kHz.

Chapter 5

Wave Finite Element Method: application to cylinders

5.1 Introduction

Cylindrical panels are used in many engineering applications such as rotorcraft, pipes, acoustic ducts, aerospace structures and so on. Because of the great interest in their vibrational characteristics they have been a subject of many studies. However these studies require a comprehensive development of a mathematical model that is difficult at best. Analytical expressions can be developed for simple cases - e.g. isotropic cylinders - but for more complex structures analytical approaches become very difficult or even impossible. Although some authors have studied the problem of wavepropagation in cylindrical shells in the framework of the exact three-dimensional elasticity theory [124–133], analytical approaches are extremely complicated. This is particularly true for laminated structures due to the massive amount of algebra involved in enforcing interlaminar continuity when a large number of layers is considered. Moreover, there are numerical problems in obtaining the dispersion curves because of convergence difficulties for short wavelengths, large circumferential wavenumbers and especially for complex layered structures. A common approach is to study composite curved structures by making assumptions and approximations concerning the stress distribution and the displacements. However, in any event, the equations lead to a complicated dispersion relation to which numerical solutions are sought.

The free vibration characteristics of isotropic cylindrical shells have been obtained by various approximate theories. A good summary of these theories is given by Leissa in [134]. There have been also a number of previous studies

about wave propagation in thin cylindrical shells and a brief summary of some of them is given here.

D. C. Gazis analysed the propagation of free harmonic waves in a thin long cylinder. He provided the frequency equation for an arbitrary number of waves around the circumference in [126] and he presented the results for free harmonic waves in [127]. Kumar and Stephens [128] studied dispersion of flexural waves in isotropic shells of various wall thickness using the exact three dimensional equations of linear elasticity. In [135], Fuller considered the effect of wall discontinuities on flexural waves in an isotropic cylindrical shell. He also provided the dispersion curves in a semi-infinite thin walled shell for circumferential modal number $n = 1$. More recently Langley [136, 137] extended the analysis to general helical motion in isotropic cylindrical shells and studied the modal density and mode count of the out-of-plane modes for isotropic thin cylinders and curved panels. Tyutekin [138] obtained the dispersion curves in an isotropic cylindrical shell for different angles of propagation of the helical waves. He also evaluated the dispersion characteristics and the eigenfunctions of circumferential waves for Neumann and Dirichlet boundary conditions [139].

The present chapter is devoted to the application of the WFE method to the analysis of wave propagation in homogeneous axisymmetric structures, and in particular cylinders. Several examples are provided to show the accuracy of the method and its applicability. The examples concern homogeneous isotropic and orthotropic thin shells, for which analytical solutions are well established, and composite laminated cylinders for which analytical solution are not available.

5.2 WFE formulation for axisymmetric structures

The application of the WFE method to axisymmetric structures could be considered as a special case of WFE analysis of 2-dimensional structures. Figure 5.1 shows a schematic representation of a cylindrical structure. The cylindrical coordinates are y , r and α while u , v and w are the axial, circumferential and radial displacements respectively. R is the mean radius of the shell and h is the thickness. A time harmonic disturbance at a frequency ω is assumed to propagate through the structure with a helical pattern so that, for example,

$$w(r, \alpha, y, t) = W(r)e^{i(\omega t - k_\alpha \alpha - k_y y)}, \quad (5.1)$$

where k_α and k_y are the projections of the wavenumber in the circumferential and axial directions while $W(r)$ is the complex wave amplitude.

Quite frequently in practice the structure is thin and therefore it is possible to define a mean radius R . Examples include *in vacuo* cylinders. Under this circumstances it is perhaps more convenient to define an axis x around the circumference, for which $x = R\alpha$. This substitution allows the wavenumber k_α to be replaced with $k_x = k_\alpha/R$. Hence k_x , which is related to the linear distance x instead of the angle α , represents the wavenumber of the circumferential component of the wave whose corresponding wave vector is directed along the tangent to the circumference of radius R . Therefore the helical wave in equation (5.1) takes the form

$$w(r, x, y, t) = W(r)e^{i(\omega t - k_x x - k_y y)}. \quad (5.2)$$

Equation (5.2) represents a plane wave propagating along the axisymmetric structure in a manner analogous to a wave propagating in an infinite flat structure in two dimensions. Figures 5.3 and 5.3 depict helical waves in cylindrical coordinates and the equivalent plane waves in Cartesian coordinates respectively.

To apply the WFE method, a small segment of the structure subtending a small angle L_α is taken and modelled using FEs as shown in Figure 5.4. With FEs, curved structures are commonly approximated by piece-wise-flat surfaces. Therefore for the subsequent analysis, the two different kinds of FE models shown in Figures 5.5 and 5.6 are used to apply the technique. For thin structures, a single shell element as shown in Figure 5.5 can be used to obtain good accuracy for a wide range of frequencies while for moderately thick shells, laminated composites, sandwich constructions and so on, an appropriate model consists of several elements across the section as shown in Figure 5.6. Note that for the model in Figure 5.6 any internal DOFs are condensed to obtain a 4-noded hyperelement. From Figure 5.5, the element degrees of freedom \mathbf{q} are

$$\mathbf{q} = [\mathbf{q}_1^T \ \mathbf{q}_2^T \ \mathbf{q}_3^T \ \mathbf{q}_4^T]^T, \quad (5.3)$$

with a similar expression for the nodal forces \mathbf{f} .

The node \mathbf{q}_j are obtained concatenating all the nodes of the FE model through the thickness. When applying the periodicity condition, the local coordinates must be rotated in order to model the desired curvature. For example, the DOFs of node 2 and node 4 (defined in local coordinates) are transformed to global coordinates by a rotation through an angle L_α as shown in Figure 5.7. A trans-

formation matrix \mathbf{R} can be defined as

$$\bar{\mathbf{R}} = \begin{bmatrix} \mathbf{I} & \mathbf{0} & \mathbf{0} & \mathbf{0} \\ \mathbf{0} & \mathbf{R} & \mathbf{0} & \mathbf{0} \\ \mathbf{0} & \mathbf{0} & \mathbf{I} & \mathbf{0} \\ \mathbf{0} & \mathbf{0} & \mathbf{0} & \mathbf{R} \end{bmatrix}, \quad (5.4)$$

so that the mass and stiffness matrices of the “curved” element become

$$\begin{aligned} \mathbf{M} &= \bar{\mathbf{R}}^T \mathbf{M}_{LOC} \bar{\mathbf{R}}; \\ \mathbf{K} &= \bar{\mathbf{R}}^T \mathbf{K}_{LOC} \bar{\mathbf{R}}, \end{aligned} \quad (5.5)$$

where \mathbf{M}_{LOC} and \mathbf{K}_{LOC} are the element’s mass and stiffness matrices in local coordinates, that is the mass and stiffness matrices of the flat FE model obtained by conventional FE methods or FE commercial packages. In equation (5.4) the order of the matrices $\mathbf{0}$, \mathbf{I} and \mathbf{R} equals the number of the nodal degrees of freedom of the FE model.

With reference to Figure 5.5, the nodal rotation matrix \mathbf{R} is

$$\mathbf{R} = \begin{bmatrix} \mathbf{r} & \mathbf{0} \\ \mathbf{0} & \mathbf{r} \end{bmatrix}, \quad (5.6)$$

while for the FE model in Figure 5.6 (solid elements are used to mesh the cross section) the matrix \mathbf{R} takes the form

$$\mathbf{R} = \begin{bmatrix} \mathbf{r} & \mathbf{0} & \cdots & \cdots & \mathbf{0} \\ \mathbf{0} & \mathbf{r} & \mathbf{0} & \cdots & \mathbf{0} \\ \vdots & & \ddots & & \vdots \\ \mathbf{0} & \cdots & & & \mathbf{r} \end{bmatrix}, \quad (5.7)$$

where $\mathbf{0}$ is a 3×3 zero matrix and \mathbf{r} is the affine transformation

$$\mathbf{r} = \begin{bmatrix} \cos(\alpha) & 0 & -\sin(\alpha) \\ 0 & 1 & 0 \\ \sin(\alpha) & 0 & \cos(\alpha) \end{bmatrix}. \quad (5.8)$$

Once the mass and stiffness matrices for the curved element are calculated ac-

cording to equation (5.5), the WFE method reduces to that for the case of flat structures.

5.2.1 The eigenvalue problem for closed axisymmetric structures

Equations 5.1 and 5.2 correspond to the general case of a non closed axisymmetric structures so that k_α can in principle attain any value: real, imaginary or complex denoting propagating, evanescent or decaying waves respectively.

However, in closed structures the phase change of a wave as it propagates around the circumference must be a multiple of 2π . Therefore the circumferential wavenumber can only take the discrete values $k_\alpha = n$, $n = 0, 1, 2, \dots$ which defines the order n of the wave mode. The modes n are independent and can be analysed separately. For cylindrical shells of mean radius R where the x axis is such that $x = R\alpha$, then $k_x = n/R$, $n = 0, 1, 2, \dots$. Under these circumstances

$$\lambda_x = e^{-inL_x/R} \quad (5.9)$$

is known for a given circumferential order n and equation (3.37) becomes either a linear eigenproblem in ω^2 for a given λ_y or a quadratic eigenproblem in λ_y for a given ω . In the latter case, the polynomial eigenvalue problem in equation (3.37) takes the form

$$[\mathbf{A}_2\lambda_y^2 + \mathbf{A}_1\lambda_y + \mathbf{A}_0] \mathbf{q} = 0, \quad (5.10)$$

where $\mathbf{A}_2 \neq 0$. In order to avoid conditioning errors in solving equation 5.10, the following standard linear companion form

$$\mathbf{L}(\lambda_y) = \begin{bmatrix} -\mathbf{A}_2^{-1}\mathbf{A}_1 & -\mathbf{A}_2^{-1}\mathbf{A}_0 \\ \mathbf{I} & \mathbf{0} \end{bmatrix} - \lambda_y \begin{bmatrix} \mathbf{I} & \mathbf{0} \\ \mathbf{0} & \mathbf{I} \end{bmatrix} \quad (5.11)$$

is considered and the eigenvalues and the eigenvectors of equation (5.10) are recovered from those of (5.11) using subroutines for the standard linear eigenproblem. The eigenvalues may be purely real, purely imaginary or complex and therefore the complex frequency spectrum can be determined for any circumferential number.

5.2.2 The ring frequency

For cylindrical shells the ring frequency is usually defined as the frequency at which one longitudinal wavelength wave equals the cylinder perimeter [2], that is

$$\omega_r = \frac{1}{R} \sqrt{\frac{E}{\rho(1-\nu^2)}}. \quad (5.12)$$

This frequency plays an important role in describing the dynamics of cylindrical structures and it is used to indicate the frequency range for which the curvature effects are important. Above the ring frequency the shell behaves more as a flat plate while near and below the ring frequency the effect of the curvature stiffens the structure considerably and results in more complicated behaviour.

In order to investigate how ω_r can be evaluated graphically from the dispersion curves, the analytical wave number solutions are evaluated for an isotropic cylindrical shell. As already pointed out, there are a number of theories regarding the dynamics of cylindrical shells. Here the Flügge equations of motion are used since they provide quite accurate results for moderately thick shells. The partial differential operator for the evaluation of the Flügge equation of motion can be found in [134], Chapter 2. In the following analysis the non dimensional coordinate s defined in [134] is replaced with the axial coordinate y . The displacement solution is assumed to have the form

$$\begin{aligned} u &= Ae^{-iky} \cos n\theta e^{i\omega t}; \\ v &= Be^{-iky} \sin n\theta e^{i\omega t}; \\ w &= Ce^{-iky} \cos n\theta e^{i\omega t}, \end{aligned} \quad (5.13)$$

where A, B, C are the amplitudes of the displacements. Substituting (5.13) into the differential operators given in [134], an eighth order algebraic equation in k is obtained. This means that there are eight admissible axial waves in the cylinder. The characteristic equation can be written as a quartic in k^2

$$D_8(\Omega)(k^2)^4 + D_6(\Omega)(k^2)^3 + D_4(\Omega)(k^2)^2 + D_2(\Omega)k^2 + D_0(\Omega) = 0, \quad (5.14)$$

where $\Omega = \omega/\omega_r$. Equation (5.14) has been directly evaluated and solved in closed-form. The coefficients D_8, D_6, D_4, D_2, D_0 are given in Appendix B. Algebraic expressions for these coefficients and for direct evaluation of the wavenumbers can be found in [140]. The solutions of equation (5.14) are rather complicated

and it is quite difficult to have a clear idea of the dispersion characteristics. Assuming that the thickness of the shell is small compared to the mean radius, a good approximation to the solutions is given in [14] as

$$k_1^2 = \frac{\omega^2 \rho(1 - \nu^2)}{E} - \frac{1}{R^2} - n^2; \quad (5.15)$$

$$k_2^2 = \frac{\omega^2 \rho 2(1 + \nu)}{E} - n^2; \quad (5.16)$$

$$k_3^2 = \frac{1}{2R^2} + \sqrt{\frac{\omega^2 \rho h}{D} + \frac{1}{4R^4} - \frac{n^2}{R^2}} - n^2; \quad (5.17)$$

$$k_4^2 = \frac{3}{2R^2} - \sqrt{\frac{\omega^2 \rho h}{D} + \frac{9}{4R^4} - \frac{n^2}{R^2}} - n^2, \quad (5.18)$$

where $D = Eh^3/(12(1 - \nu^2))$ is the flexural rigidity. It can be noticed from equations (5.15)–(5.18) that the first two solutions for $n = 0$ represent extensional and shear waves respectively while the third and fourth are dispersive flexural waves. However the equation (5.18) does not give pure real wavenumber and therefore it does not represent propagating waves. Solution (5.16) is not affected by the curvature while the influence of the curvature for the solutions (5.15), (5.17) and (5.18) become less significant as the frequency increases. Figure 5.8 shows the dispersion curves for a thin steel plate and a steel cylindrical shell. It can be seen that for frequencies above ω_r the cylinder behaves like a flat plate while in the neighbourhood of and below ω_r the effect of the curvature is to stiffen the structure and results in a more complicated behaviour. The cut-on frequencies for the waves in equations (5.15)–(5.18) are respectively

$$\omega_1 = \frac{\sqrt{1/R^2 - n^2}}{c_L}; \quad (5.19)$$

$$\omega_2 = \frac{n}{c_T}; \quad (5.20)$$

$$\omega_3 = n^2 \sqrt{\frac{D}{\rho h}}; \quad (5.21)$$

$$\omega_4 = \sqrt{n^4 - 2 \frac{n^2}{R^2}} \sqrt{\frac{D}{\rho h}}, \quad (5.22)$$

where

$$c_L = \sqrt{E/\rho(1 - v^2)} \quad (5.23)$$

and

$$c_T = E/2\rho(1 + \nu) \quad (5.24)$$

are the phase velocities of longitudinal and torsional waves. The $n = 0$ waves represented by (5.16) and (5.17) start propagating from values of ω close or equal to zero while wave (5.15), which represents an extensional wave, has a cut-on frequency $\omega = \omega_r$, where ω_r is the ring frequency given by equation (5.12). At the ring frequency ω_r this mode involves only radial displacement along the thickness. Therefore, it can be concluded that the ring frequency can be considered as the first cut-on, or transition frequency, of the dispersion equation. When the assumption of a very thin structure does not hold, as in the Flügge equation of motions, the value of the ring frequency is slightly different from the one in equation (5.12). Solving the Flügge equation of motion for the circumferential mode order $n = 0$ and considering only axial u and radial displacements w , a sixth order algebraic equation, cubic in k^2 , is obtained

$$D_6(\Omega)(k^2)^3 + D_4(\Omega)(k^2)^2 + D_2(\Omega)k^2 + D_0(\Omega) = 0. \quad (5.25)$$

When $D_0(\Omega)$ vanishes, two roots coalesce to zero and therefore the value of the frequency that gives $D_0 = 0$ can be taken as the ring frequency. Given that $D_0 = \Omega^2(1 + b^2) - \Omega^4$, where $b = h/(R\sqrt{12})$, the ring frequency in this case is

$$\omega_r = \sqrt{1 + b^2} \frac{1}{c_L R}. \quad (5.26)$$

The same value can be obtained setting to zero the coefficient D_0 in equation (5.14).

5.3 Isotropic cylinders

In this section an isotropic cylindrical shell is studied by post-processing an ANSYS FE model. The material properties are as follow: Young's modulus $E = 19.2 \cdot 10^{10}$ Pa, Poisson's ratio $\nu = 0.3$ and density $\rho = 7800$ kg/m³. The finite element lengths in the (x, y) plane are taken as $L_y = L_x = 1$ mm. The nondimensional frequency $\Omega = \omega/\omega_r$ is introduced, where ω_r is the shell ring frequency. The dispersion curves of two examples of isotropic cylinders are predicted and

discussed. In order to validate the method, the WFE results are compared with those derived directly from the Flügge equations of motion [141] for the first example.

5.3.1 Isotropic cylindrical shell, $h/R = 0.05$

The ratio of the thickness to mean radius for the cylinder is $\bar{h} = h/R = 0.05$, $R = 1\text{m}$. The rectangular four node element SHELL63 was used to obtain the mass and stiffness matrices resulting in a system with 6 DOFs after the WFE reduction. The real-valued dispersion curves for circumferential modes of order $n = 0, 1, 2, 3$ obtained from the WFE method are given in Figures 5.8–5.11. Figures 5.9–5.11 show also analytical results obtained solving directly the Flügge equation of motions for the cylindrical shell. In applying the WFE method, since the element has 6 DOFs per node, six real *passing bands* are obtained. However, only the first three are shown since they are the ones that correspond to propagating waves in the continuous shell while the other are numerical artifacts due to the discretisation. The three branches shown in Figures 5.9–5.11 broadly correspond to flat-plate flexural, torsional and extensional waves as shown in Figure 5.8 for $n = 0$. This behaviour is particularly clear above the ring frequency. It is seen that the results computed from the WFE method agree extremely well with those obtained by Flügge theory. Figures 5.12–5.15 show the wave speed of the branches 1, 2 and 3 where the nondimensional wave speed c^* is defined as the ratio of the wave speed and the phase velocity of an extensional wave in a thin plate given by equation (5.23). From Figures 5.8 and 5.12 it can be noticed that only waves 1 and 2 exist below the ring frequency. They propagate as in-plane extensional and torsional waves respectively. Hence, for $\Omega < 1$ and $n = 0$ the cylindrical shell seems to behave dynamically as a membrane. For $n = 1$, Figure 5.9 shows that both waves 1 and 2 propagate below the ring frequency. Figure 5.13 shows that these two branches asymptotically resemble a flexural and a shear wave in a plate. However, their behaviour cannot be considered as purely flexural or shear, in particular for small values of k_y as clearly shown Figure 5.13. For increasing values of the circumferential wave number, waves start propagating at certain frequencies different from zero. For $n > 1$, below the ring frequency, only wave 1 exists and its behaviour approaches that of a flexural wave in a plate as the circumferential order n increases.

5.3.2 Isotropic cylinder, $h/R = 0.1$

Consider now a thick cylinder for which the nondimensional thickness is $\bar{h} = h/R = 0.1$, where $R = 0.5\text{m}$. The mass and stiffness matrices were found using 20 SOLID45 elements in ANSYS. Since the elements used are brick solid elements, the present method is formulated within the framework of a three-dimensional approach. Figure 5.16 shows the complex dispersion curves for circumferential modes of orders $n = 0, 1, 2, 3$. At very high frequencies other cross-section waves start propagating but are not shown here for simplicity.

The complex frequency spectrum results are quite complicated, in particular at high frequency. It can be seen that for the breathing and bending modes, $n = 0$ and $n = 1$, only two types of plane waves can propagate below the ring frequency. For $n = 0$ two waves start propagating at $\Omega = 0$: they represent shear and extensional waves. At the ring frequency a third branch cuts-on as an extensional wave while the second branch veers approaching a flexural waves in a flat plate. For $n = 1$ only one wave propagates from $\Omega = 0$ while another one cuts-on below the ring frequency. Waves of orders $n > 1$ can propagate only above a certain frequency and only the first branch propagates below the ring frequency. There are also complex branches of the dispersion curves (representing a pair of complex conjugate wavenumbers) for which the real and the imaginary parts reduce with increasing frequency. At the frequency for which the real part of this complex wavenumber becomes zero, the corresponding imaginary part bifurcates into a pair of evanescent waves with pure imaginary wavenumbers. This phenomenon is here indicated as a complex cut-off, that is the complex wavenumber becomes purely imaginary. It can be seen from Figure 5.16 that complex cut-off appears at the minima of the imaginary branches with respect to the frequency axis. From this frequency to the one at which the next propagating wave cuts-on, the imaginary branches are multi-valued for a single frequency.

It is worth pointing out that the evaluation of the dispersion curves for higher order circumferential modes using the WFE method does not present any differences or numerical difficulties compared to the evaluation of dispersion curves for low order modes.

Figures 5.17–5.19 show the contour curves of various dispersion branches for $\Omega = 0.1, 0.2, 1.5, 2$ and 3 . It can be seen that only the first two branches propagate below $\Omega \approx 1 + b$, where b is defined in section 5.2.2, while for $\Omega = 1.5$ all the three branches appear in the graph. Figure 5.19 shows that at $\Omega = 2$ and $\Omega = 3$ all the three waves propagate. For an isotropic plate the dispersion characteristics

do not depend on the propagation angle θ and therefore the contour curves are circular. However, for the curved shell, the presence of the curvature stiffens the structure resulting in different shapes of the contour curves with respect to circular one. In particular at $\Omega = 1.5$, Figure 5.18, the contour curves show an elliptical shape similar to that of extensional, torsional and flexural waves in an equivalent orthotropic plate.

At low frequencies there exist regions in which a particular value of $k_y R$ corresponds to two distinct values of $k_x R$. As an example, points *A* and *B* are shown in Figure 5.17 for $k_y R = 2$ and $\Omega = 0.5$. As shown in chapter 4, section 4.4.3, the direction of the group velocity is given by the direction of the normal to the contour curves. It can be seen from Figure 5.17 that the normal vector to the curve at the point *A* has a component with respect to the x direction opposite to that at the point *B*, thus showing that the points represent respectively two distinct waves having different directions of the group velocity in the circumferential direction. Figure 5.20 shows the wavemodes of waves *A* and *B*. As expected the predominant displacement is out-of-plane for both the waves.

A discussion about the nature of the waves associated with the dispersion curves can be found in [136]. In [136], Langley analysed the relative contribution of the in-plane and out-of-plane motion to the kinetic energy for waves propagating in an isotropic cylinder at $\Omega = 0.6, 1.1, 1.5$. In particular, for waves similar to waves *A* and *B* in Figure 5.17, it was shown that, although the predominant displacement is out-of-plane, the energy associated with the wave with the smaller circumferential wave number is transmitted mostly through in-plane tractions.

5.4 Orthotropic cylinder

An orthotropic cylinder, whose material properties are shown in Table 5.1 is considered in this section. The cylinder has a thickness-to-mean radius ratio of $\bar{h} = h/R = 0.05$, where $R = 1\text{m}$. The FE model is realised using 20 SOLID45 elements in ANSYS for which $L_x = L_y = 1\text{mm}$.

The effects of changing circumferential order are mostly noticeable at low frequency and low wavenumber, i.e. below or around the ring frequency. The real valued dispersion curves are shown in Figures 5.21 and 5.22 for $n = 0, 1, 2, 3$ up to 8kHz. It can be seen that for large values of the wavenumber, the dispersion curves do not significantly depend on the circumferential order. However, changing the

$E_x = 144.48\text{GPa}$	$E_y = 9.63\text{GPa}$	$E_z = 9.63\text{GPa}$
$G_{xy} = 4.128\text{GPa}$	$G_{yz} = 4.128\text{GPa}$	$G_{xz} = 4.128\text{GPa}$
$\nu_{xy} = \nu_{xz} = 0.02$	$\nu_{yz} = 0.3$	$\rho = 1389\text{kg/m}^3$

Table 5.1: Orthotropic cylinder: material properties.

circumferential order may lead to significant changes in the dispersion curves for low wavenumbers.

Figures 5.23 and 5.24 show the complex dispersion curves for the circumferential modes $n = 0$ and $n = 5$ up to 45kHz. Modes of order $n = 0$ and $n = 5$ are here chosen to illustrate various feature since there are no significant changes in the dispersion curves for other order branches. The sixth high frequency branch indicates the presence of a wave having group and phase velocities of opposite sign. At the cut-on frequency, that is the minimum frequency for which the wave represented by branch 6 propagates, a complex branch bifurcates into a pair of propagating waves with real wavenumbers. One of these propagating waves has phase and group velocities of opposite sign with a behaviour similar to the one already studied for the case of a plate. Branch 6 seems not to be affected by changing the mode order. Branches 3, 5 and 8 in Figure 5.23(a) also do not appear to be very sensitive to a change in the circumferential order.

5.5 Laminated sandwich cylinder

In this section the WFE method is applied to evaluate the wave propagation characteristics of sandwich structures. The real valued dispersion curves and the complete complex dispersion spectra are given. The eigensolutions yield numerical estimates of the dispersion relations in a straightforward and systematic manner. The behaviour is in general very complicated, involving coupling between the various wave modes, complex cut-off phenomena at non-zero wavenumbers, veering and so on.

The sandwich shell comprises two laminated skins sandwiching a foam core. The two skins each comprise 4 orthotropic sheets with a lay-up of $[+45/-45/-45/+45]$ and a total thickness of 4mm. The material properties for the skins are given in the previous chapter in Table 5.1. The core material is a 10mm polymethacrylamide ROHACELL whose material properties are: Young modu-

lus $E = 1.8 \cdot 10^8 \text{ Pa}$, Poisson's ratio $\nu = 0.286$, density $\rho = 110 \text{ Kg/m}^3$. The nondimensional thickness of the sandwich construction is $\bar{h} = 0.018$ with mean radius $R = 1\text{m}$. A very similar construction was considered by Heron [20]. In [20], Heron assumed a classical theory for sandwich structures: a thick core that carries shear stress and thin skins that work in bending and extension. To study the symmetric, single curved sandwich, a discrete layer theory was used accomplishing a 47th order dispersion system, which was subsequently solved numerically to determine the dispersion relations. The WFE model was realised using 18 SOLID45 elements in ANSYS, 4 for each skin and 10 for the core, resulting in 57 DOFs after the reduction.

The choice of a symmetric laminate is due to the fact that this kind of laminate is often used in the aerospace industry. In the analytical approach, material symmetry relative to the coordinate axis allows eigensystems to be simplified. On the contrary, the WFE technique enables any kind of stacking sequence for the composite laminate to be analysed with the same degree of simplicity.

Figures 5.25 and 5.26 show the frequency spectrum for the circumferential orders $n = 0, 1, 2, 3$. Real and imaginary parts of the wavenumber are plotted separately. The ring frequency for the sandwich cylinder, which is the first transition frequency for $n = 0$, is found at $\approx 622.7\text{Hz}$. For $n = 0$ and $n = 1$, only waves represented by branches 1 and 2 propagate below the ring frequency. For $n = 2$, branch 2 propagates for frequencies close to the ring frequency, while for $n = 3$ only the wave represented by branch 1 propagates below the ring frequency. The lowest cut-on frequencies for branches 1 and 2 are $\approx 11.5\text{Hz}$ and $\approx 550.3\text{Hz}$ respectively. As expected, the wave behaviour below the ring frequency is very complex and cannot be described simply in terms of torsional, extensional and flexural waves alone. However some main features can be observed. It can be seen that the frequency spectrum exhibits complex cut-on and cut-off phenomena with non-zero wavenumber. Some branches exhibit phase and group velocities of opposite sign and as a consequence there are regions in which there are two or more possible values of a pure real wavenumber for the same frequency. It can be seen in Figure 5.25(b) that for $n = 0$ there is a bifurcation from a complex wavenumber to two evanescent waves. For one of these two waves, as the frequency increases the wavenumber decreases until the wave starts propagating. For $n = 1$ the propagating branches exhibit complex cut-on and cut-off phenomena. It can be noticed that for branch 1, between 0Hz and 600Hz, there is a bifurcation from a pair of complex conjugate wavenumbers to a pair

of propagating waves, one with phase and group velocities of the same sign and another with phase and group velocities of opposite sign. When the wave with phase and group velocities of opposite sign meet the one having phase and group velocity of same sign there is another bifurcation point. At this point a complex branch links the two stationary points of branches 1 and 2. This complex branch leaves the first propagating branches at a maximum and re-enter as a real at a minimum of the next branch where a “rightward” and a “backward” waves start propagating. For $n = 1$, branches 1 and 2 exhibit more than one possible value of $k_y R$ for the same value of the frequency. For $n = 1$, branch 1, there are three values of $k_y R$ for the same frequency when $384\text{Hz} \lesssim f \lesssim 399\text{Hz}$. The lower and the higher values correspond to waves with positive group velocities in the y direction while the middle value corresponds to a wave which has phase and group velocities of opposite sign. Moreover, for $n = 1$, branch 2 exhibits two values of $k_y R$, which correspond to two different waves travelling in opposite directions in the frequency range $428\text{Hz} \lesssim f \lesssim 550\text{Hz}$. In particular, the wave associated with the lower value of $k_y R$ has a negative group velocity in the y direction. Similar conclusions can be drawn for the dispersion curves in Figure 5.26.

The WFE technique is not limited to either low frequencies or to propagating waves. Figures 5.27 and 5.28 show the complex dispersion curves up to 20kHz for circumferential modes $n = 1, 2$ as an example. The behaviour is again very complicated. Complex cut-on and cut-off phenomena can be observed in both the real and imaginary plane.

Dispersion curves in the $(k_x R, k_y R)$ plane are shown in Figures 5.29 and 5.30. These figures show that there are regions in which distinct values of $k_x R$ correspond to the same value of $k_y R$ and distinct values of $k_y R$ correspond to the same value of $k_x R$. The dispersion curves in Figures 5.29 and 5.30 are almost identical in shape to those obtained by Heron in [20] using an analytical approach.

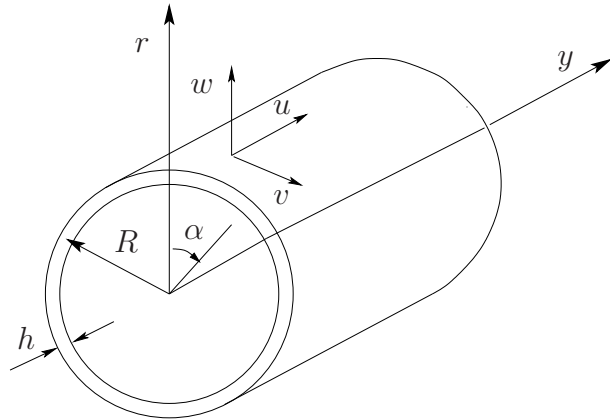


Figure 5.1: Axisymmetric structure. The diagram shows the cylindrical coordinate system, mean radius R and the thickness h .

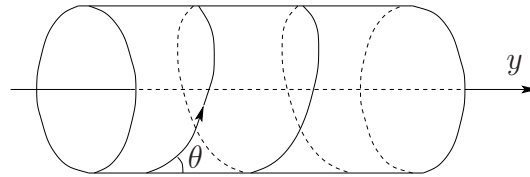


Figure 5.2: Axisymmetric structure: schematic representation of a helical wave in cylindrical coordinates.

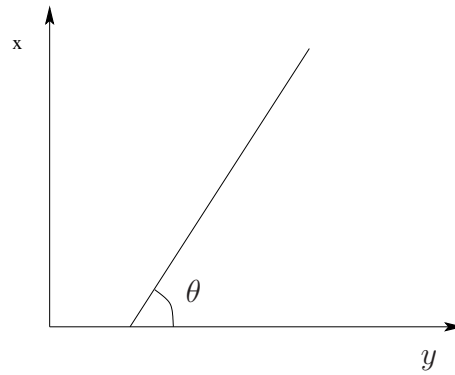


Figure 5.3: Axisymmetric structure: schematic representation of a helical wave in Cartesian coordinates.

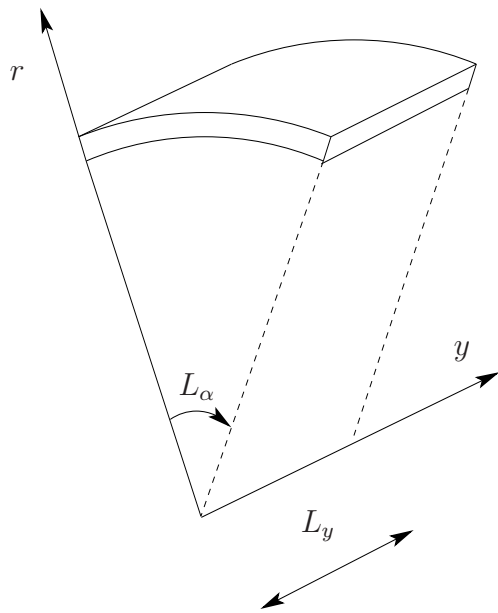


Figure 5.4: Small rectangular segment of the axisymmetric structure.

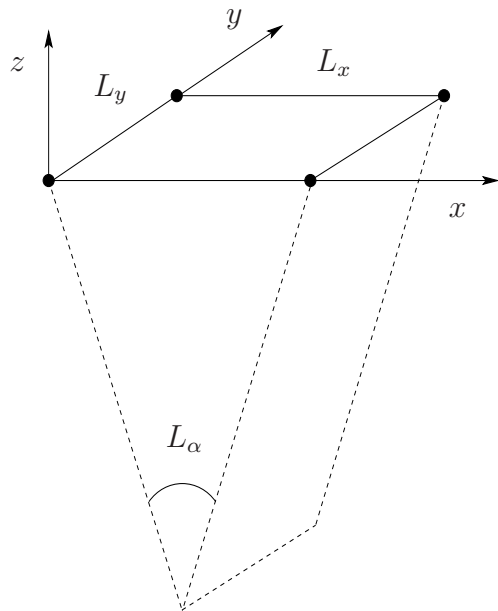


Figure 5.5: FE mesh of a small rectangular segment of a thin axisymmetric structure.

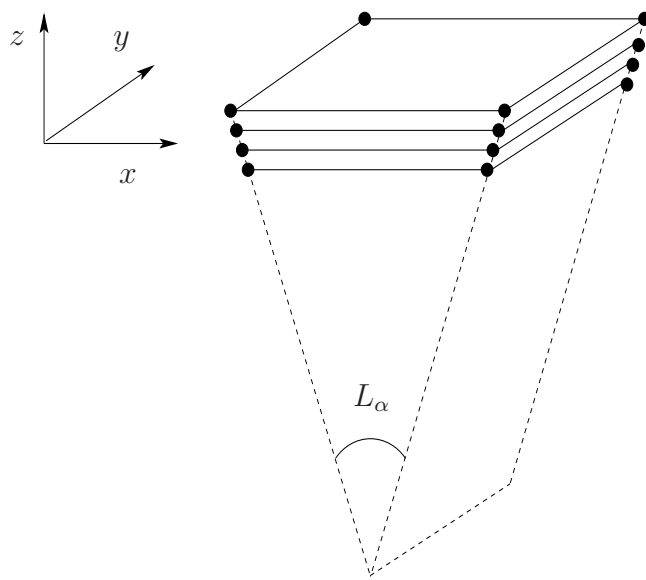


Figure 5.6: FE mesh of a small rectangular segment of a thick axisymmetric structure.

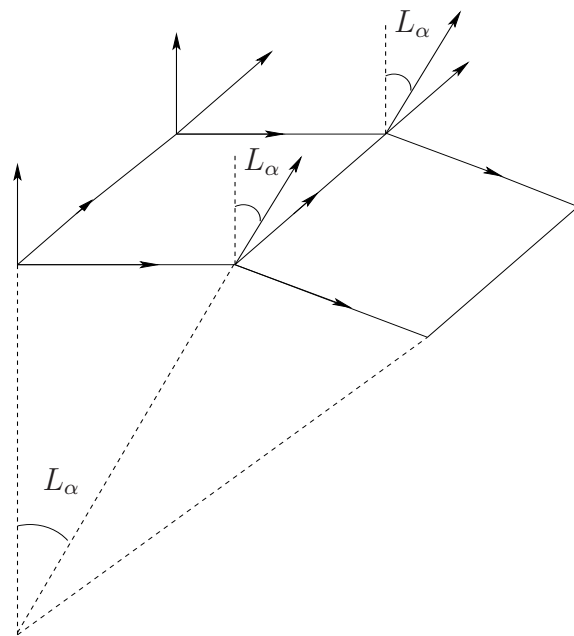


Figure 5.7: Rectangular flat shell elements.

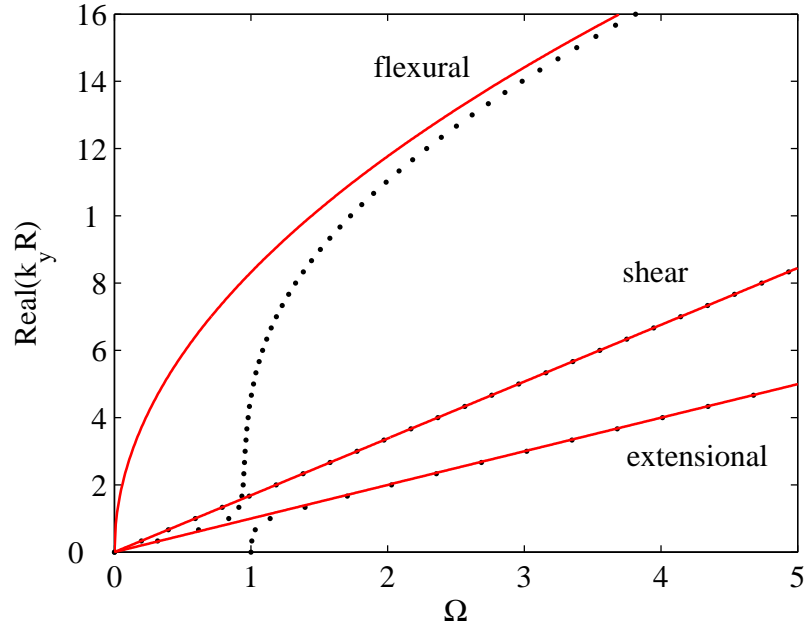


Figure 5.8: Real valued dispersion curves for an isotropic cylindrical shell, $\bar{h} = 0.05$, $R = 1\text{m}$, circumferential mode $n = 0$: WFE results; — flexural, shear and extensional dispersion branches in the equivalent flat thin plate.

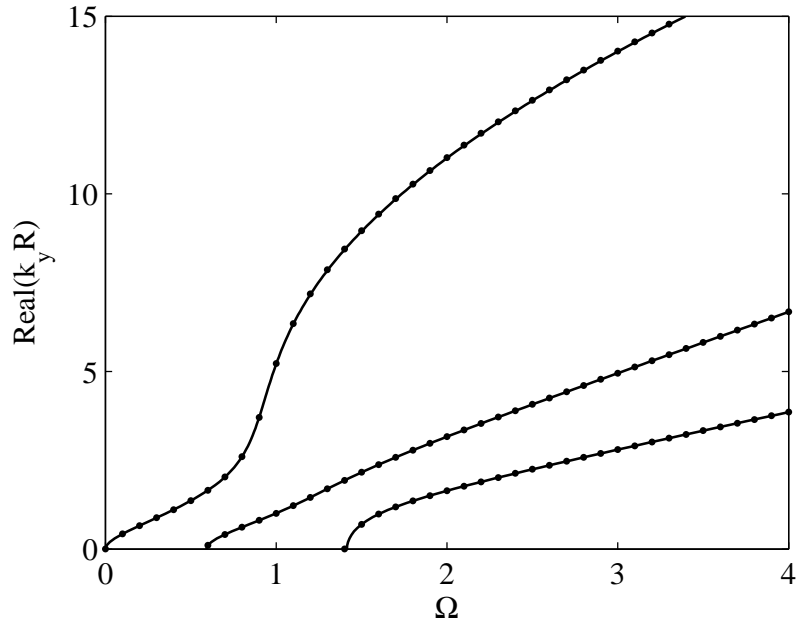


Figure 5.9: Real valued dispersion curves for an isotropic cylindrical shell, $\bar{h} = 0.05$, $R = 1\text{m}$, circumferential mode $n = 1$: WFE results; — analytic solution from the Flügge equations of motion.

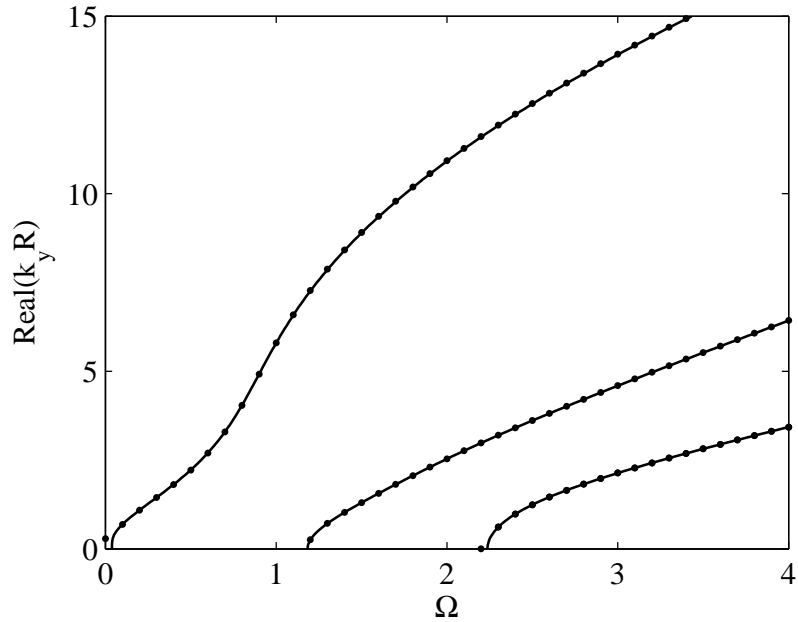


Figure 5.10: Real valued dispersion curves for an isotropic cylindrical shell, $\bar{h} = 0.05$, $R = 1\text{m}$, circumferential mode $n = 2$: WFE results; — analytic solution from the Flügge equations of motion.

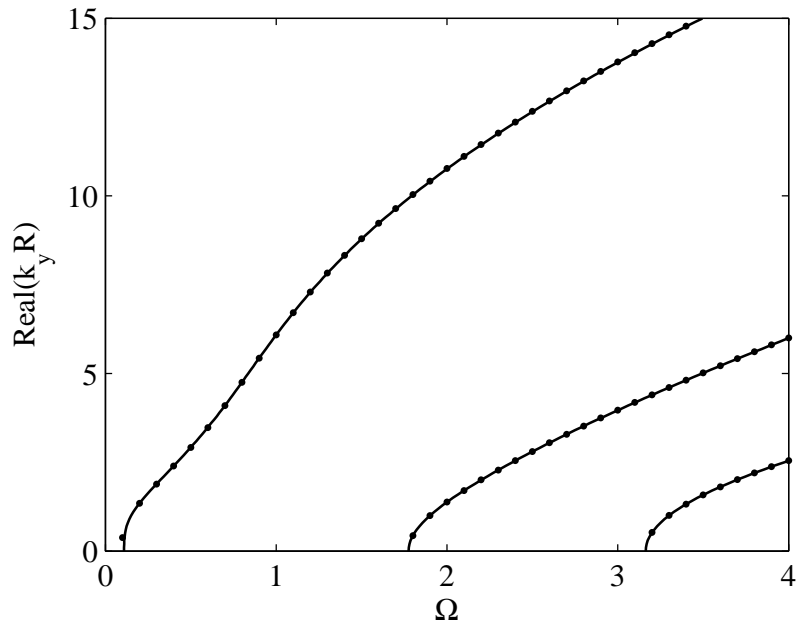


Figure 5.11: Real valued dispersion curves for an isotropic cylindrical shell, $\bar{h} = 0.05$, $R = 1\text{m}$, circumferential mode $n = 2$: WFE results; — analytic solution from the Flügge equations of motion.

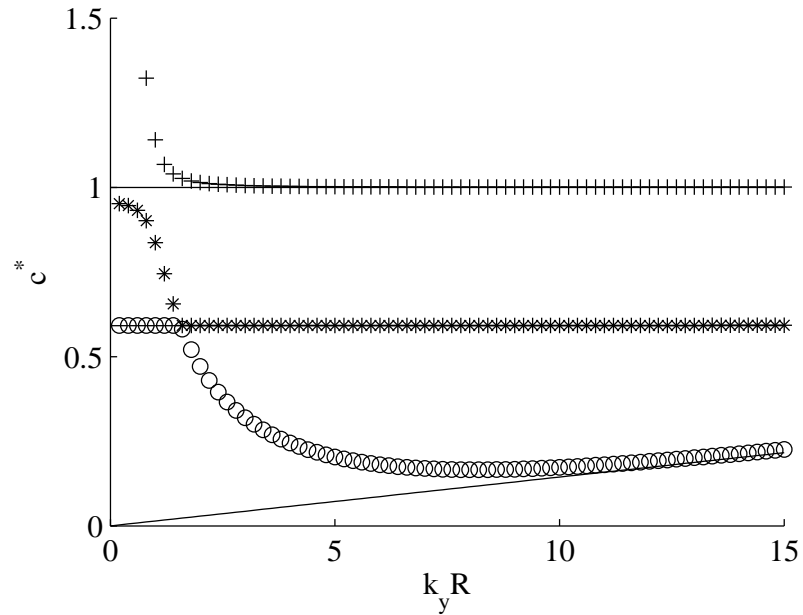


Figure 5.12: Isotropic shell, $\bar{h} = 0.05\text{mm}$, $R = 1\text{m}$. Nondimensional wave speed for circumferential mode $n = 0$: — extensional, torsional and flexural wave speed in the flat shell; + o * wave speeds in the cylindrical shell.

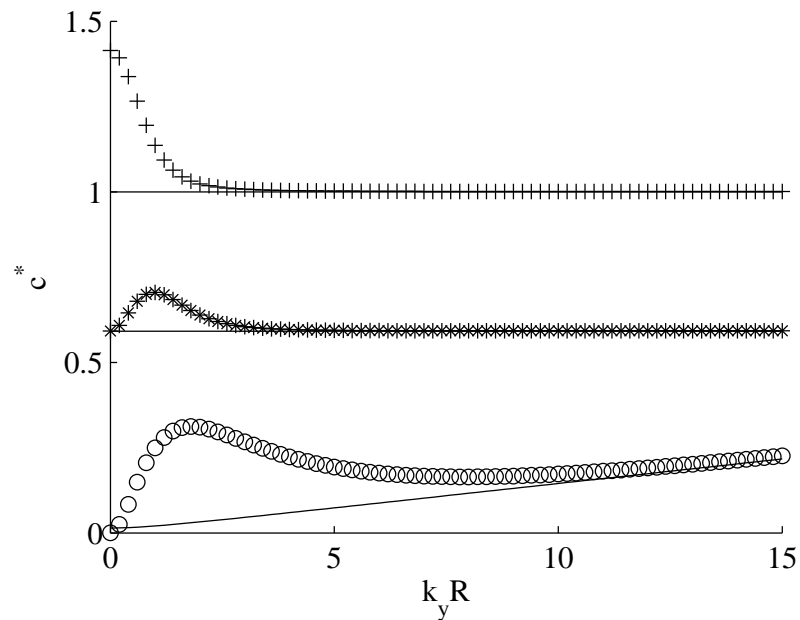


Figure 5.13: Isotropic shell, $\bar{h} = 0.05\text{mm}$, $R = 1\text{m}$. Nondimensional wave speed for circumferential mode $n = 1$: — extensional, torsional and flexural wave speed in the flat shell; + o * wave speeds in the cylindrical shell.

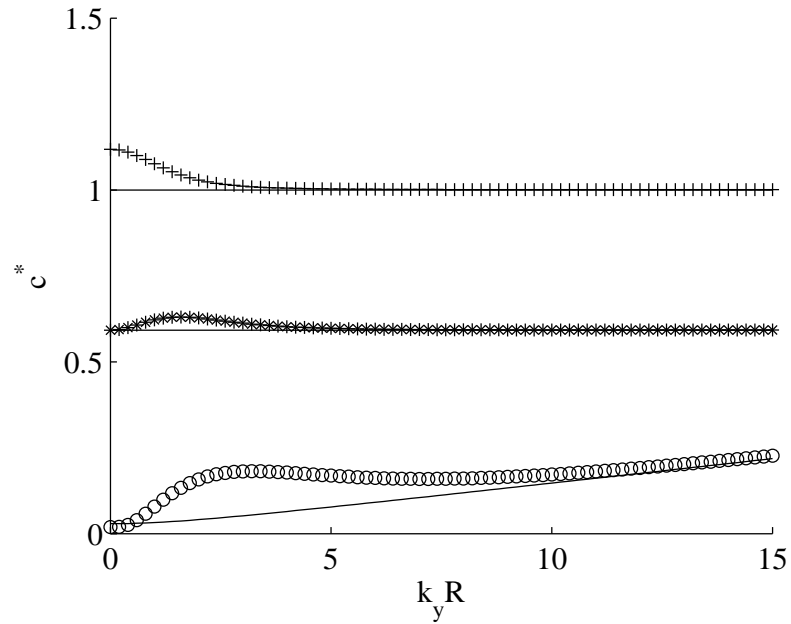


Figure 5.14: Isotropic shell, $\bar{h} = 0.05\text{mm}$, $R = 1\text{m}$. Nondimensional wave speed for circumferential mode $n = 2$: — extensional, torsional and flexural wave speed in the flat shell; + o * wave speeds in the cylindrical shell.

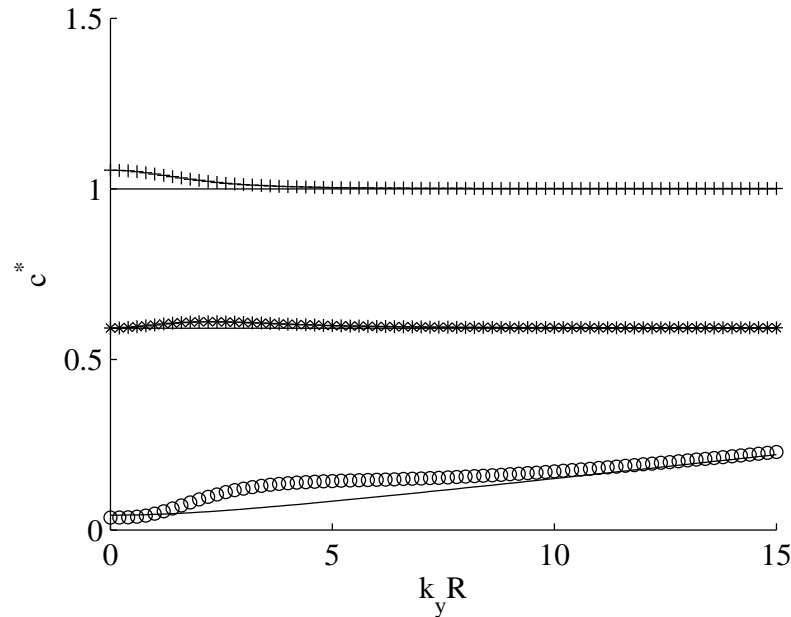
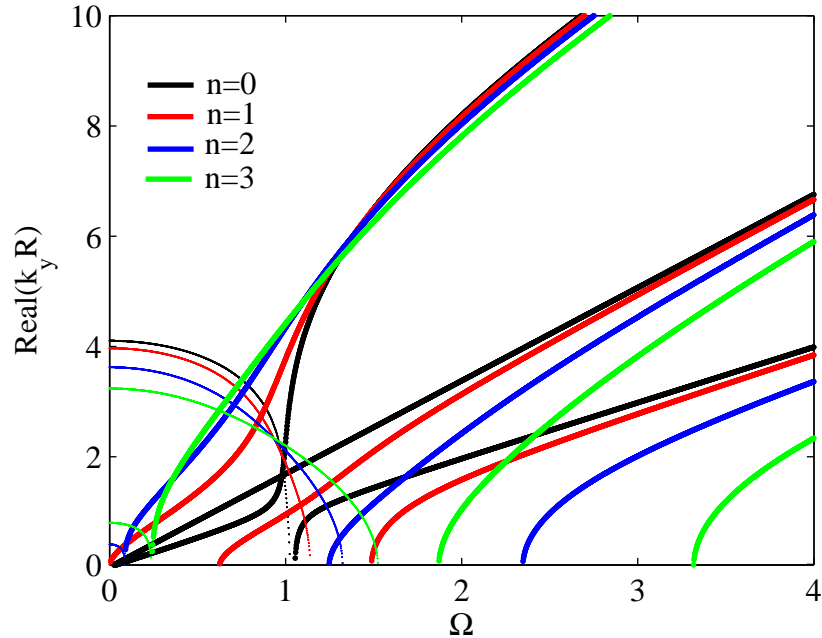
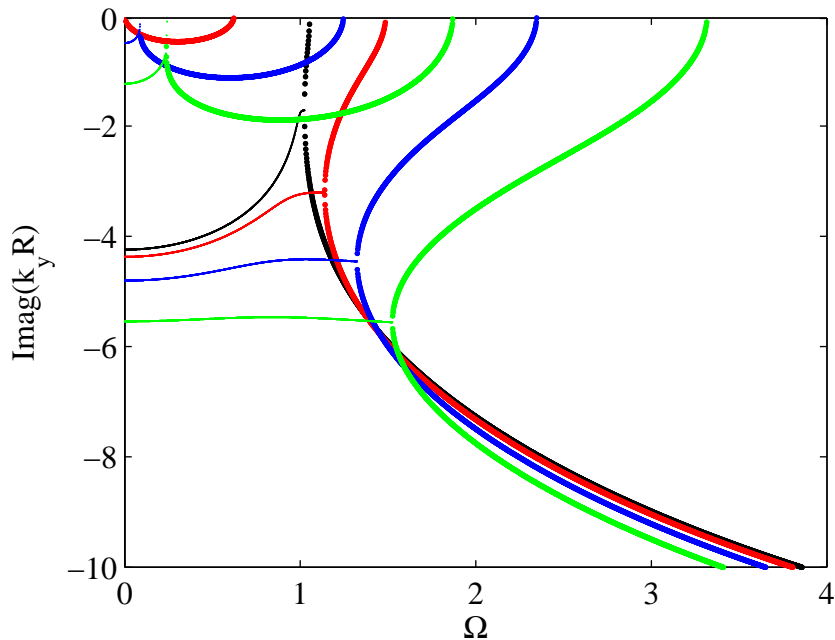


Figure 5.15: Isotropic shell, $\bar{h} = 0.05\text{mm}$, $R = 1\text{m}$. Nondimensional wave speed for circumferential mode $n = 3$: — extensional, torsional and flexural wave speed in the flat shell; + o * wave speeds in the cylindrical shell.

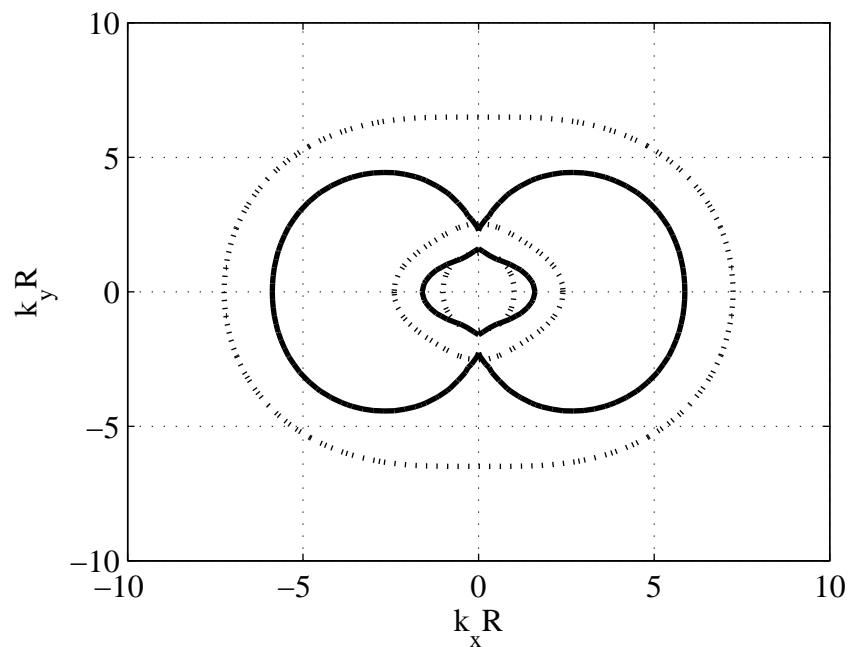
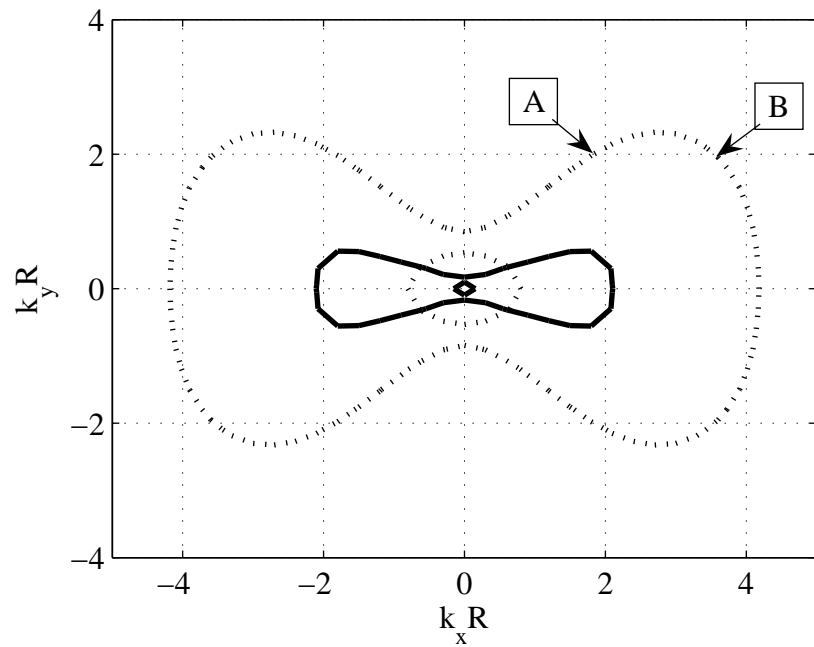


(a) Real dispersion curves



(b) Imaginary dispersion curves

Figure 5.16: Isotropic cylinder, $\bar{h} = 0.1$, $R = 0.5\text{m}$. Dispersion curves for circumferential modes $n = 0, 1, 2, 3$: complex valued wavenumbers; pure real and pure imaginary wavenumbers.



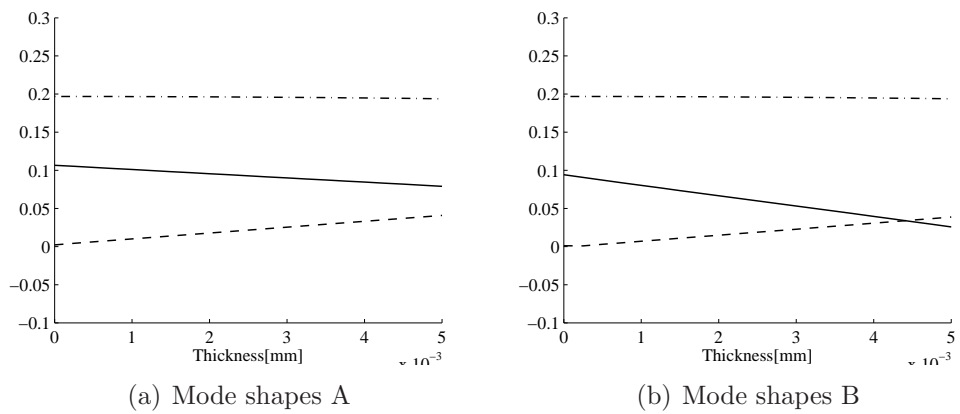
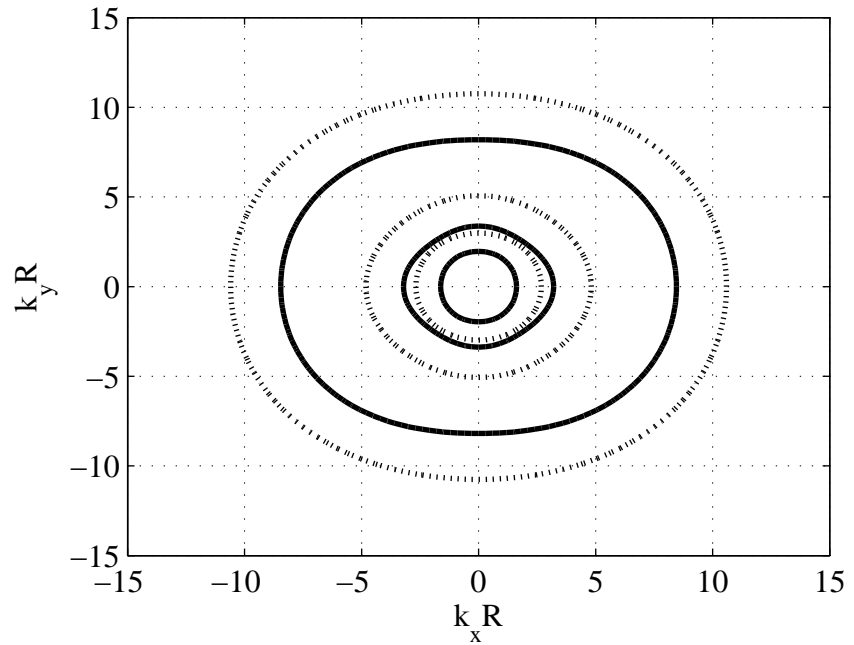


Figure 5.20: Isotropic cylindrical shell. Mode shapes of waves A and B in Figure 5.17: — x ; - - - y ; - · - · - z .

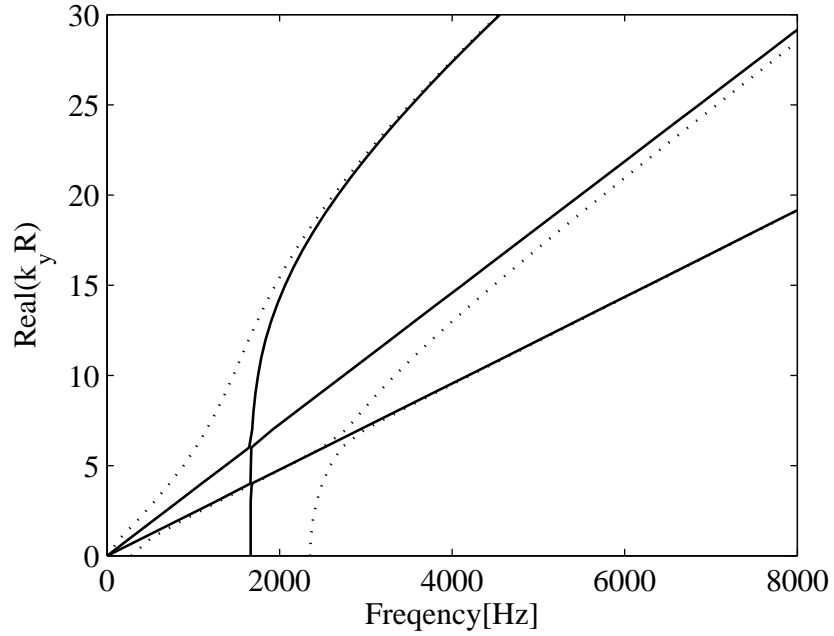


Figure 5.21: Orthotropic cylindrical shell, $\bar{h} = 0.05$, $R = 1\text{m}$. Real valued dispersion curves: ——— circumferential modes $n = 0$; ······ circumferential modes $n = 1$.

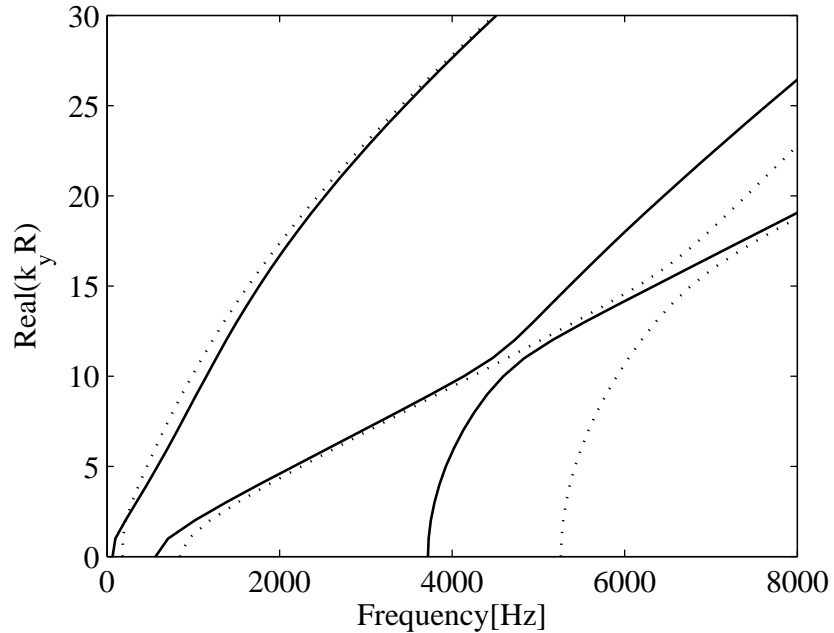
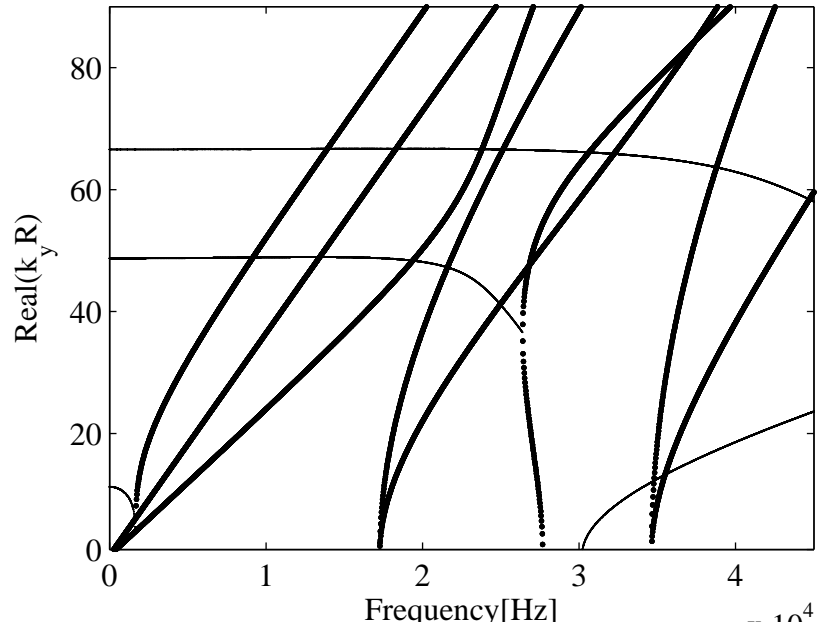
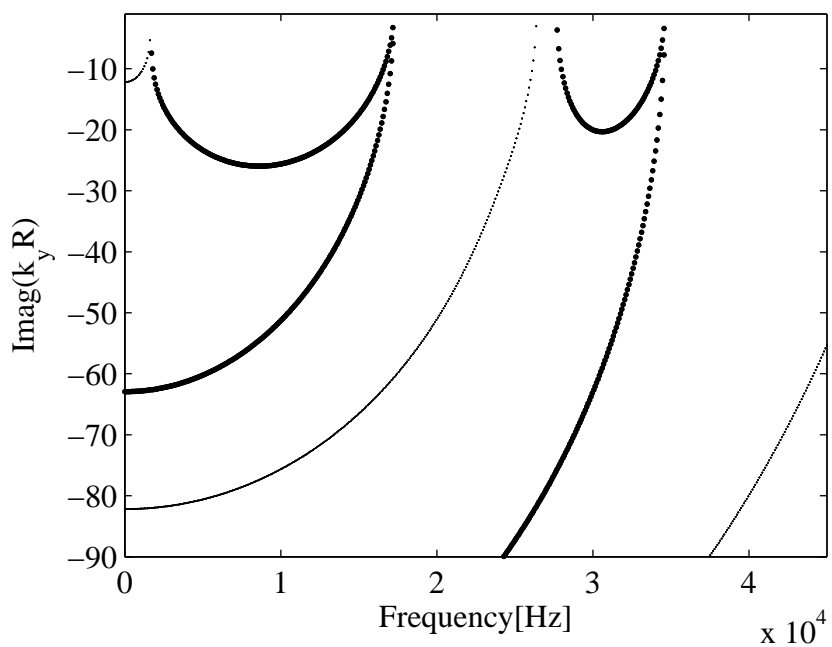


Figure 5.22: Orthotropic cylindrical shell, $\bar{h} = 0.05$, $R = 1\text{m}$. Real valued dispersion curves: ——— circumferential modes $n = 2$; ······ circumferential modes $n = 3$.

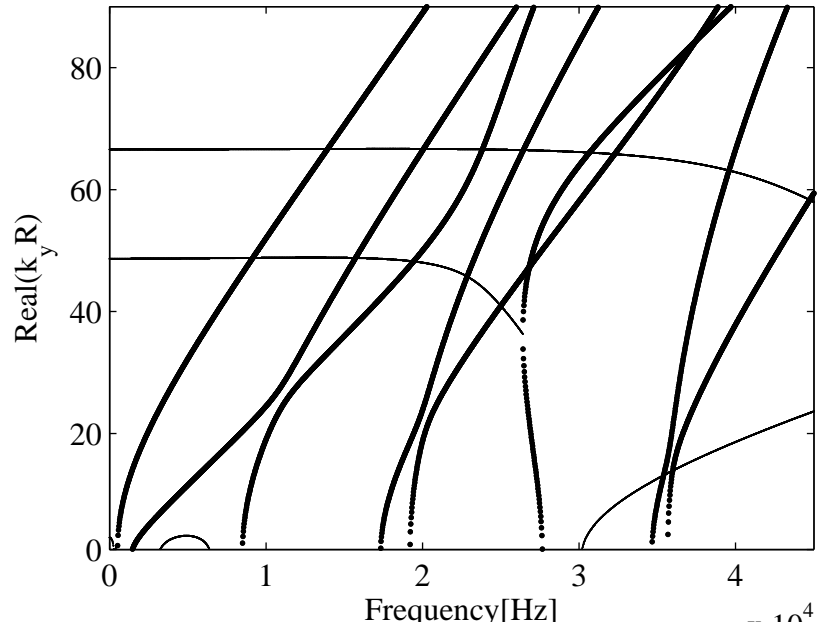


(a) Real dispersion curves

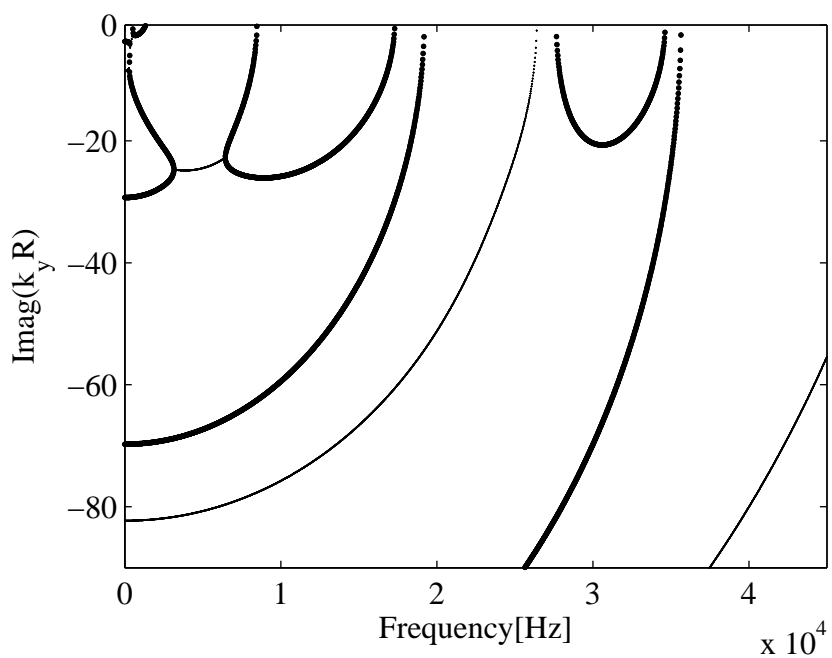


(b) Imaginary dispersion curves

Figure 5.23: Orthotropic cylindrical shell, $\bar{h} = 0.05$, $R = 1\text{m}$. Dispersion curves for circumferential mode $n = 0$: complex valued wavenumbers; pure real and pure imaginary wavenumbers.

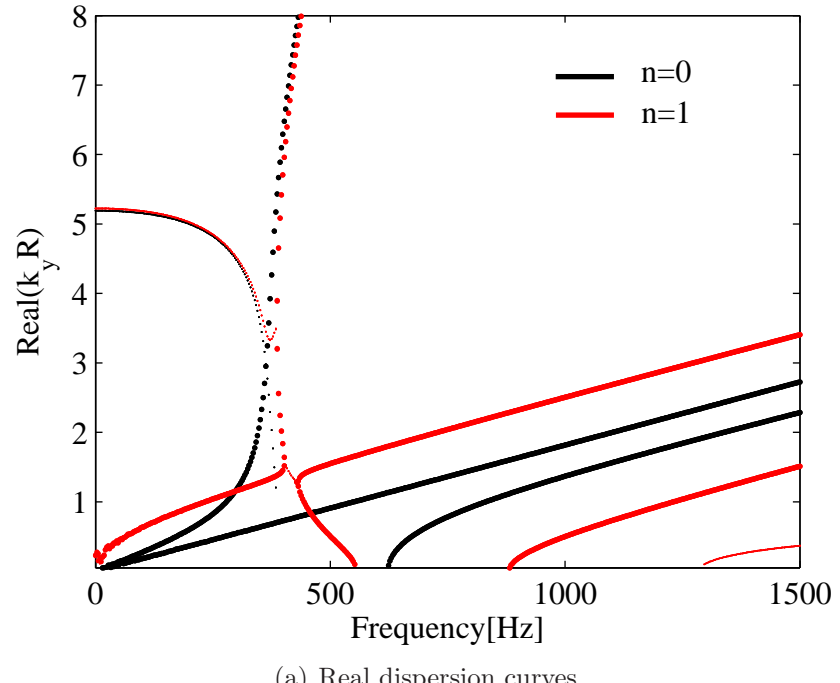


(a) Real dispersion curves

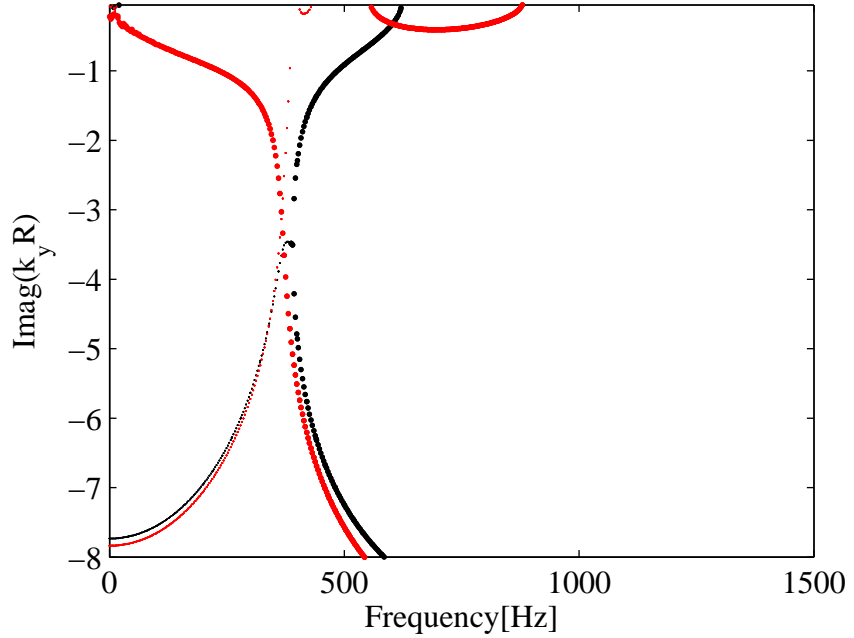


(b) Imaginary dispersion curves

Figure 5.24: Orthotropic cylindrical shell, $\bar{h} = 0.05$, $R = 1\text{m}$. Dispersion curves for circumferential mode $n = 5$: complex valued wavenumbers; pure real and pure imaginary wavenumbers.



(a) Real dispersion curves



(b) Imaginary dispersion curves

Figure 5.25: Sandwich cylindrical shell, $h/R = 0.018$, $R = 1\text{m}$. Dispersion curves for circumferential modes $n = 0$ and $n = 1$: complex valued wavenumbers; pure real and pure imaginary wavenumbers.

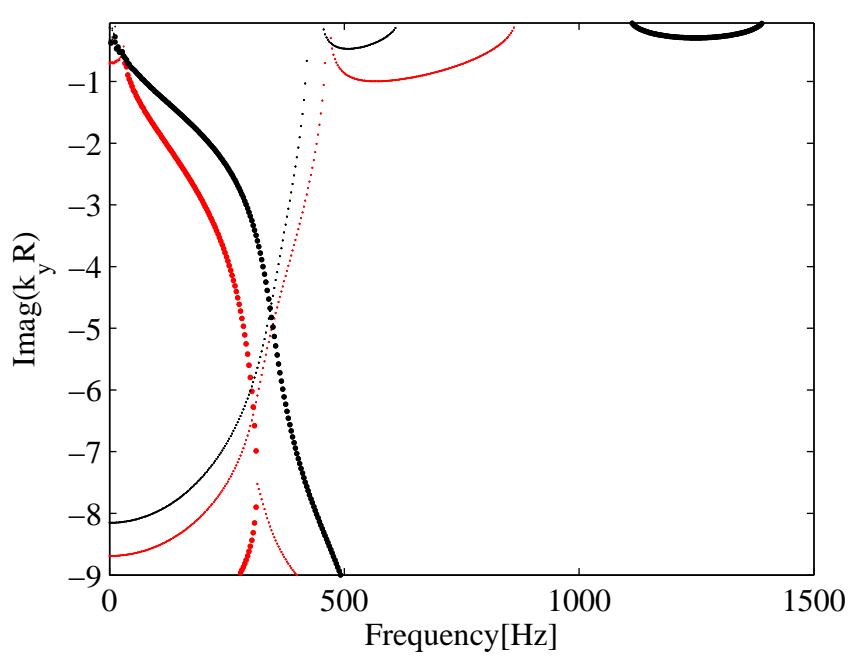
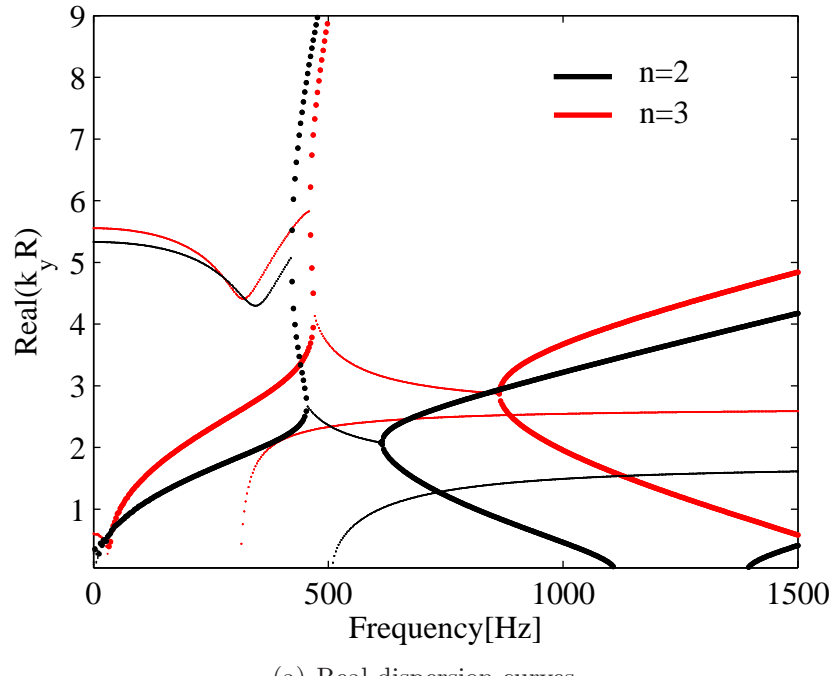
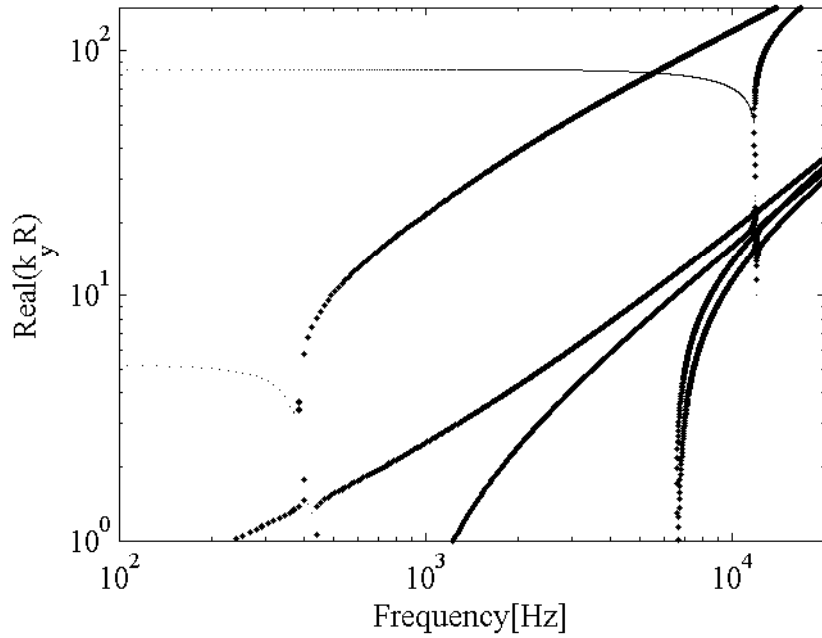
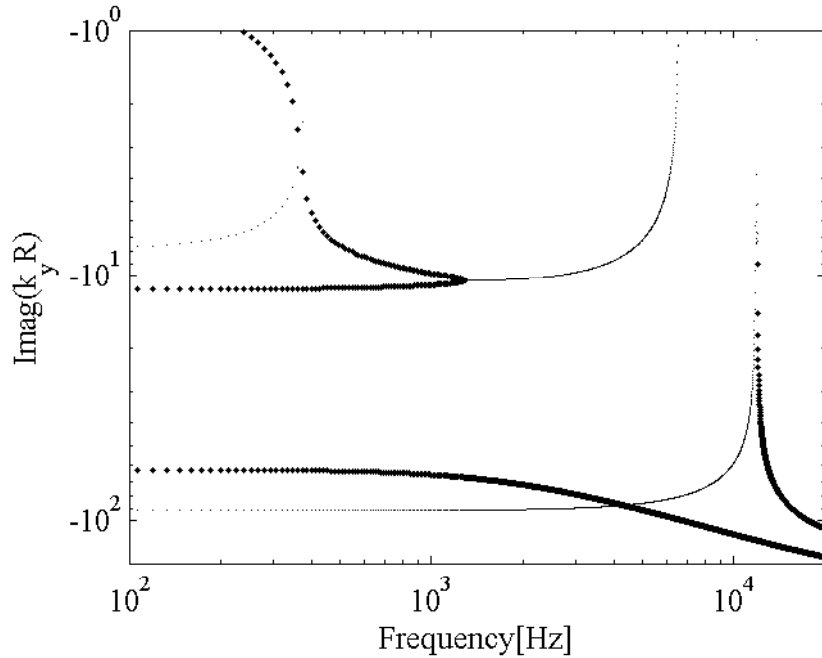


Figure 5.26: Sandwich cylindrical shell, $h/R = 0.018$, $R = 1\text{m}$. Dispersion curves for circumferential modes $n = 2$ and $n = 3$: complex valued wavenumbers; pure real and pure imaginary wavenumbers.

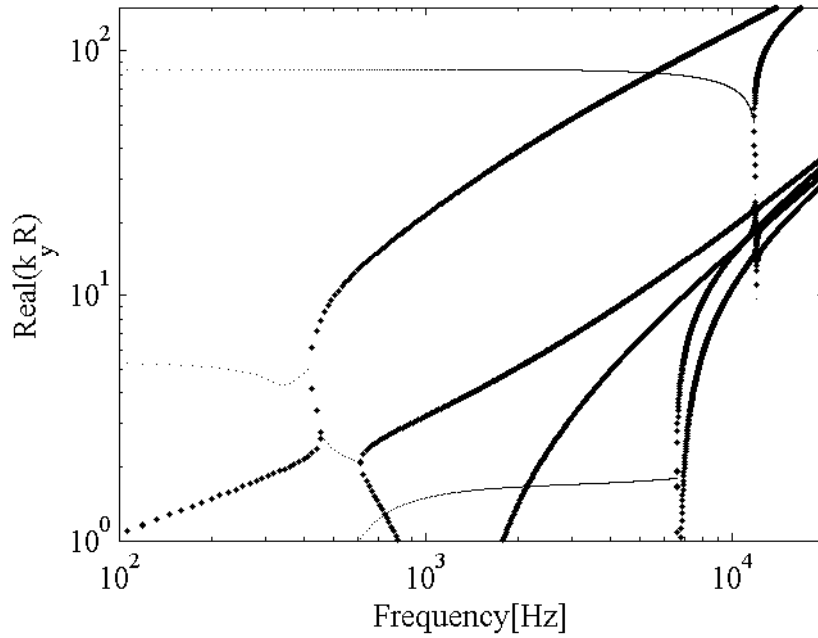


(a) Real dispersion curves

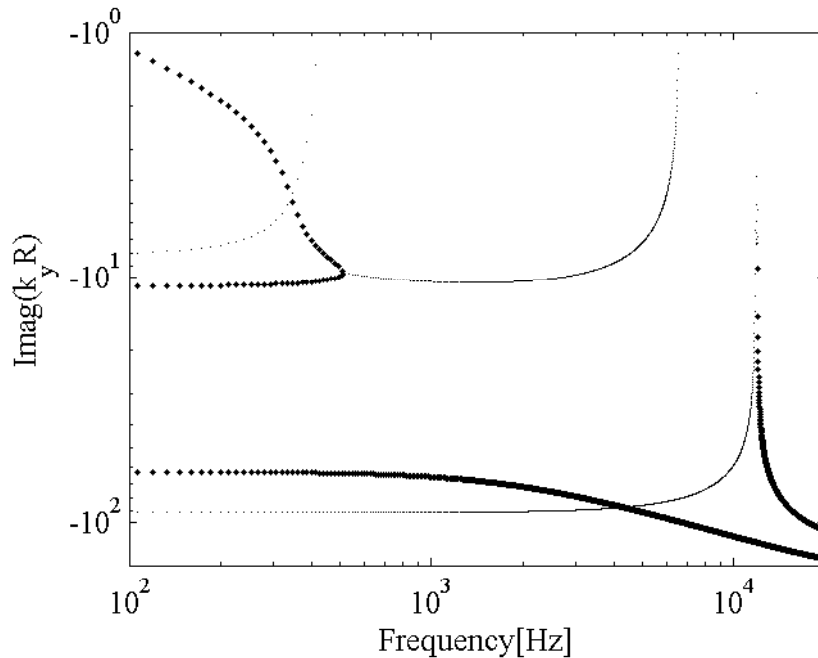


(b) Imaginary dispersion curves

Figure 5.27: Sandwich cylindrical shell, $h/R = 0.018$, $R = 1\text{m}$. Dispersion curves for circumferential modes $n = 1$: complex valued wavenumbers; pure real and pure imaginary wavenumbers.



(a) Real dispersion curves



(b) Imaginary dispersion curves

Figure 5.28: Sandwich cylindrical shell, $h/R = 0.018$, $R = 1\text{m}$. Dispersion curves for circumferential modes $n = 2$: complex valued wavenumbers; pure real and pure imaginary wavenumbers.

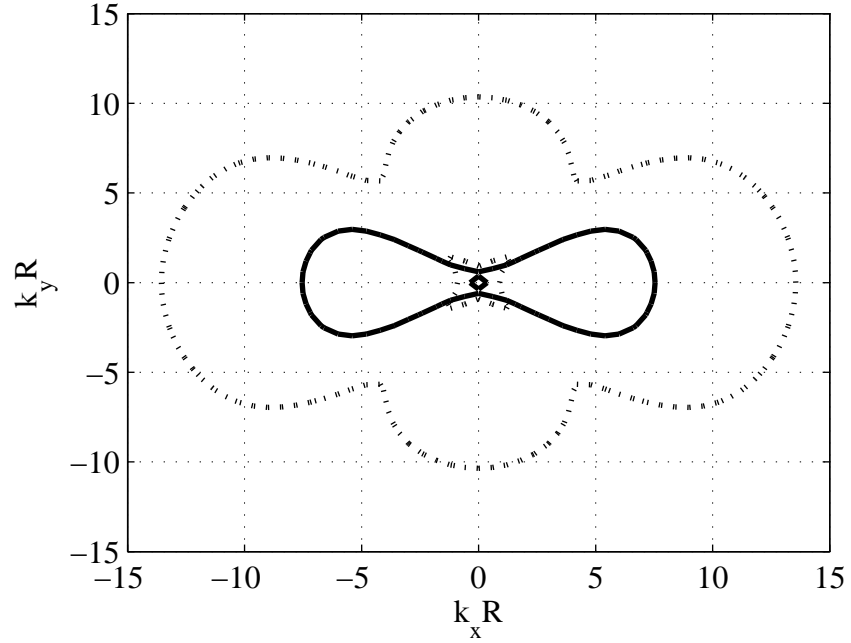


Figure 5.29: Sandwich cylindrical shell, $h/R = 0.018$, $R = 1\text{m}$. Dispersion contour curves: —— 200Hz; ······ 500Hz.

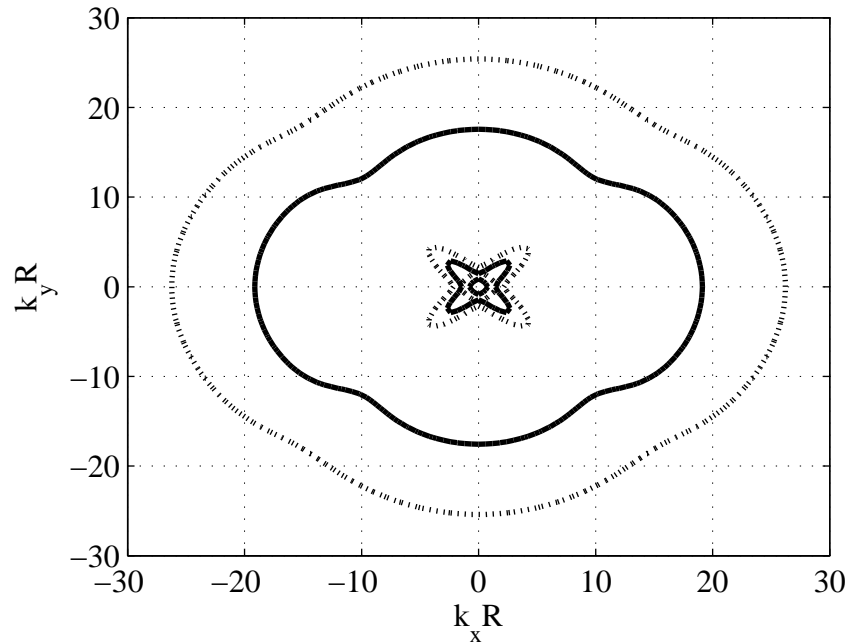


Figure 5.30: Sandwich cylindrical shell, $h/R = 0.018$, $R = 1\text{m}$. Dispersion contour curves: —— 800Hz; ······ 1200Hz.

Chapter 6

Wave Finite Element Method: application to fluid–filled elastic cylindrical shells

6.1 introducion

This chapter addresses prediction of wave propagation in fluid–filled elastic cylindrical shells using the WFE method. In industrial applications piping systems convey vibrational energy from sources, such as compressors pumps or valves, via wave propagation in both the pipe shell and the fluid, resulting in undesired sound radiation and excitation of other equipments. Evaluation of dispersion curves in fluid–filled pipes are of primary importance to evaluate vibration and noise transmission and are extensively exploited in non–destructive tests.

Wave propagation, as well as the control of wave propagation in fluid–filled elastic cylindrical shells, has been analysed in a number of papers [142–146]. Nevertheless, most of the studies available in literature have a high–frequency limit of applicability and attention directed only toward the lowest mode. Therefore the high frequency behaviour of fluid–filled pipes is still a subject of research. Moreover, in many cases of interest, the analysis is very difficult, involving dependence between the parameters and highly transcendental Hankel functions for which explicit solutions for the roots of the dispersion relation do not exist.

6.2 FE formulation for fluid–filled cylindrical shells

The analysis that follows exploits the capability of FE package to model acoustic fluid–structure coupling. To apply the WFE method, as in the previous cases, a small rectangular portion of the structures is meshed using conventional FEs. The FE model for the fluid–filled cylindrical shell is shown in Figure 6.1. Here 8–noded elements are used to mesh the acoustic fluid and the structure respectively. In the FE model realised using solid elements no assumptions such as thin–wall theory might be made in and therefore, depending of the fineness of the FE mesh, the wave behaviour can be predicted for thick pipes and for frequency much higher than the ring frequency. In the analysis it will be assumed that the structure and the fluid are losses and that the fluid is compressible and inviscid. The mean density and pressure are uniform throughout the fluid and no mean flow of the fluid is considered. Under these circumstances, the wave equation for propagation of sound in the fluid is

$$\frac{1}{c^2} \frac{\partial^2 p}{\partial t^2} - \nabla^2 p = 0, \quad (6.1)$$

where c is the speed of sound in the fluid and p is the acoustic pressure. Considering time harmonic varying pressure $p = Pe^{i\omega t}$, equation (6.1) reduces to the well–known Helmholtz equation

$$\frac{\omega^2}{c^2} P - \nabla^2 P = 0. \quad (6.2)$$

At the fluid–structure interface S , the relationship between the normal pressure gradient of the fluid and the normal acceleration of the structure at the surface S is [10]

$$\mathbf{n} \cdot \nabla P = -\rho_f \mathbf{n} \cdot \frac{\partial^2 \mathbf{u}}{\partial t^2}, \quad (6.3)$$

where \mathbf{n} is the unit normal to the interface S , \mathbf{u} is the displacement vector of the structure at the interface and ρ_f is the mean fluid density.

Considering the standard FE discretisation for the spatial variation of the displacement and pressure, equation (6.1) can be written in matrix notation to get the discretised wave equation

$$\mathbf{M}_f \ddot{\mathbf{p}} + \mathbf{K}_f \mathbf{p} + \rho_f \mathbf{C}^T \ddot{\mathbf{q}} = 0. \quad (6.4)$$

In equation (6.5) \mathbf{p} is the vector of nodal pressures, \mathbf{q} the nodal structural DOFs,

\mathbf{M}_f and \mathbf{K}_f are the fluid mass and stiffness matrices while $\rho_f \mathbf{C}^T$ is the coupling mass matrix at the fluid–structure interface. In order to obtain the complete discretised equations of motion for the fluid–structure interaction problem, the fluid pressure load vector \mathbf{F}_p at the interface S is added to the discretised structural equation of motion (3.11)

$$\mathbf{M}\ddot{\mathbf{q}} + \mathbf{K}\mathbf{q} = \mathbf{F} + \mathbf{F}_p, \quad (6.5)$$

where \mathbf{F}_p is obtained by integrating the pressure over the area of the surface S . Since $\mathbf{F}_p = \mathbf{C}\mathbf{p}$, the complete finite element discrete equations of motion of the structural–acoustic problem are

$$\begin{bmatrix} \mathbf{M} & \mathbf{0} \\ \rho_f \mathbf{C}^T & \mathbf{M}_f \end{bmatrix} \begin{bmatrix} \ddot{\mathbf{q}} \\ \ddot{\mathbf{p}} \end{bmatrix} + \begin{bmatrix} \mathbf{K} & -\mathbf{C} \\ \mathbf{0} & \mathbf{K}_f \end{bmatrix} \begin{bmatrix} \mathbf{q} \\ \mathbf{p} \end{bmatrix} = \begin{bmatrix} \mathbf{F} \\ \mathbf{0} \end{bmatrix}. \quad (6.6)$$

6.3 WFE formulation for fluid–filled cylindrical shells

Once the mass and the stiffness matrices for the whole segment of the structure are obtained from the FEA, they are post–processed as explained in chapter 3. In the structural–acoustic interaction models obtained by ANSYS for example, the nodal degrees of freedom are arranged as $[\mathbf{q}, \mathbf{p}]$, that is first the structural degrees of the freedom and then the pressure degrees of freedom. Therefore an algorithm is implemented to partition the DOFs. Since the acoustic duct is axisymmetric, the same assumptions and considerations as depicted in section 5.2 hold. In particular, in order to model the desired curvature, the DOFs must be transformed to global coordinates by a rotation through an opportune angle as shown in section 5.2.

As discussed in the previous chapter concerning in vacuo axisymmetric structures, a time harmonic disturbance at a frequency ω is assumed to propagate as

$$w(r, \alpha, y, t) = W(r)e^{i(\omega t - k_\alpha \alpha - k_y y)}, \quad (6.7)$$

where k_α and k_y are the projections of the wavenumber in the circumferential and axial directions while $W(r)$ is the complex wave amplitude. In closed structures the phase change of a wave as it propagates around the circumference must be a multiple of 2π so that the circumferential wavenumber can only take the discrete

values $k_\alpha = n$, $n = 0, 1, 2, \dots$. The order n defines the circumferential order mode. Under these circumstances $\lambda_\alpha = e^{-ik_\alpha\alpha}$ is known for a given circumferential order n and equation (3.37) becomes either a linear eigenproblem in ω^2 for a given λ_y or a quadratic eigenproblem in λ_y for a given ω . In the latter case, the polynomial eigenvalue problem in equation (3.37) takes the form

$$[\mathbf{A}_2\lambda_y^2 + \mathbf{A}_1\lambda_y + \mathbf{A}_0] \mathbf{q} = 0, \quad (6.8)$$

where $\mathbf{A}_2 \neq 0$. To solve equation (6.8), the standard linear companion form

$$\mathbf{L}(\lambda_y) = \begin{bmatrix} -\mathbf{A}_2^{-1}\mathbf{A}_1 & -\mathbf{A}_2^{-1}\mathbf{A}_0 \\ \mathbf{I} & \mathbf{0} \end{bmatrix} - \lambda_y \begin{bmatrix} \mathbf{I} & \mathbf{0} \\ \mathbf{0} & \mathbf{I} \end{bmatrix} \quad (6.9)$$

is considered.

6.4 Isotropic undamped steel cylindrical shell filled with water

In this section the WFE method is applied to a water-filled steel pipe with thickness-to-mean radius ratio equal to $\bar{h} = 0.1$, $R = 0.4\text{m}$. A similar example was studied by Maess et al. in [87] applying the WFE method for 1-dimensional waveguides according to Mace et al. [76]. In [87], a cross-section segment of a fluid-filled pipe was modelled using FE-code. The dynamic stiffness matrix was rearranged in a transfer matrix form and periodicity conditions were then applied in order to obtain an eigenvalue problem whose solution gave the dispersion characteristics as shown in [76]. In [87] only real-valued dispersion curves were discussed. As the dispersion curves were obtained the circumferential order had to be inferred. On the contrary, the present approach allows the dispersion curves to be evaluated for selected circumferential orders without any further analysis. Moreover, the larger number of DOFs and the potential numerical difficulties implicit in the use of the transfer matrix, makes the WFE method for 2-dimensional applications, as proposed in this thesis, a preferable choice for the analysis of axisymmetric structures compared to its WFE formulation for 1-dimensional waveguides as adopted in [87].

The FE model for the fluid–filled shell is here realised in ANSYS using 2 solid structural brick elements (SOLID45) and 20 fluid elements (FLUID30), resulting

in 30 DOFs after the reduction. The model includes the fluid structure interaction at the interface between the fluid and the structure. The frequency Ω in the numerical examples is the non-dimensional frequency $\Omega = \omega/\omega_r$ where ω_r is the ring frequency for the cylindrical shell *in vacuo* given by equation (5.12).

Figure 6.2 shows the WFE predictions of the dispersion curves for mode orders $n = 0, 1, 2, 3, 4$. The non-dimensional wavenumber $k_y R$ is considered. The various waves can be associated with motion that is predominantly structure or fluid–borne. It can be noticed that the dispersion characteristics when the structure is coupled with acoustical field are more complicated than the *in vacuo* case (Figure 5.16) and coupling between the fluid and the shell affects the vibration even at low frequency. To each circumferential mode there correspond distinct axial wavenumbers, which can be real, imaginary or complex. They represent propagating, evanescent or propagating decaying waves respectively. The complex frequency spectra for the fluid–filled cylindrical shell are given in Figures 6.3–6.5 for circumferential orders $n = 0, 1, 3$. The $n = 0$ “breathing” mode and the $n = 1$ “bending” mode are analysed since they are easily excited by fluid–borne sources and hence they are of major importance for the vibration analysis of pipes. The $n = 3$ mode is chosen as a representative example of a “lobar mode”. Figures 6.3–6.5 show also the *in vacuo* dispersion curves for comparison. The behaviour of the fluid–filled cylindrical shell for modes $n = 0$ and $n = 1$ was analysed in details in [142]. In [142] Fuller and Fahy originally obtained the dispersion relation for a fluid–filled pipe using the Donnell–Mushtari equations of motion. A short description of the dispersion curves is here given following the physical interpretation discussed in [142].

The dispersion curves for the cylindrical shell *in vacuo* and filled with water vibrating in the circumferential mode $n = 0$ are shown in Figure 6.3. As shown in Figure 6.3(a) the *in vacuo* shell exhibits only two propagating waves at low frequency. The first real branch for the *in vacuo* shell is a pure shear wave while the second branch is an extensional wave at low frequency and it changes into a flexural wave around the ring frequency. For the water–filled steel pipe vibrating at $n = 0$, branch 1 in Figure 6.3(a) cuts–on as an acoustically slow wave close in nature to a fluid wave in a rigid–walled while it approaches the *in vacuo* flexural branch as the frequency increases. It can be noticed that the presence of liquid in the pipe has very little effect on the characteristics of this shear wave (branch 2). Branch 2 represents in fact a torsional mode whose motion is a predominantly tangential and is therefore almost unaffected by the contained

fluid. Branch 3 cuts-on as a structure-borne longitudinal wave. At $\Omega = 1$ the shell starts resonating as a ring. Hence, for $\Omega \geq 1$ the motion of the shell and the fluid becomes strongly coupled due to rapid increase in radial vibration. Branch 3 thus turns into a fluid-type mode for $\Omega \geq 1$. At $\Omega = 0.96$ branch 4 cuts-on as a fluid-type mode, at $\Omega \approx 1.5$ it veers, resembling that of the corresponding extensional structural wave, and then veers again sharply to approach a fluid-born wave. At $\Omega = 1.47$ branch 5 cuts-on as a fluid-type mode. The behaviour of higher order branches show similarities. All these branches cut-on as a fluid wave, turn to a structural extensional wave uncoupled from the fluid and then veer to approach a fluid wave. For these higher wave modes, at the point where one branch approaches a structural wave, the previous one changes to a fluid wave. This behaviour can be explained considering that as the frequency is increased the shell becomes less stiff in the radial direction. Hence there is a large coupling between fluid and structure. The imaginary part of the dispersion curves in Figure 6.3(b) also appears quite complicated. At low frequency the branches are very similar to the rigid-walled duct modes. As the frequency increases the shell becomes less stiff in the radial direction and coupling between fluid and shell motion occurs. Complex waves cut-on, and cut-off frequencies appear at the minima and the maxima of the imaginary branches. Fuller and Fahy showed in [142] the existence in the imaginary plane of a complex branch at low frequency which progresses with increasing frequency as a series of complex and imaginary sections.

Figure 6.4 shows the dispersion curves for the $n = 1$ order for the *in vacuo* and the water-filled shell. For higher order branches, the behaviour for mode $n = 1$ is similar to that discussed for the case $n = 0$. However there are some significant differences between Figures 6.3 and 6.4 at low frequency, i.e. $\Omega < 1$. Figure 6.4(a) shows only one propagating wave at low frequency. For the water-filled pipe this first branch behaves like a beam type shell motion. At $\Omega = 0.62$ a second branch cuts-on, which correspond to the first rigid walled mode for $n = 1$. This second branch exhibits a complex cuts-off and there is a wave with phase and group velocities of opposite sign. Higher branches are associated with cross-section modes and start propagating at certain cut-on frequencies: branch 3 cuts-on at $\Omega \approx 0.62$, branch 4 at $\Omega \approx 1.4$ and branch 5 at $\Omega \approx 1.72$. Looking at the imaginary plane in Figure 6.4(b), it can be seen that the second complex branch in Figure 6.4(a) cuts-on from two evanescent waves.

The dispersion curves for circumferential mode order $n = 3$ are given in Figure

6.5. Only one propagating wave exists below $\Omega = 1.5$. For the water–filled pipe this branch resembles that of the *in vacuo* shell. Waves of orders $n > 1$ can propagate only above a certain frequency. The dispersion curves in Figure 6.5 shows similarities to the one for circumferential order $n = 1$ shown in Figure 6.3.

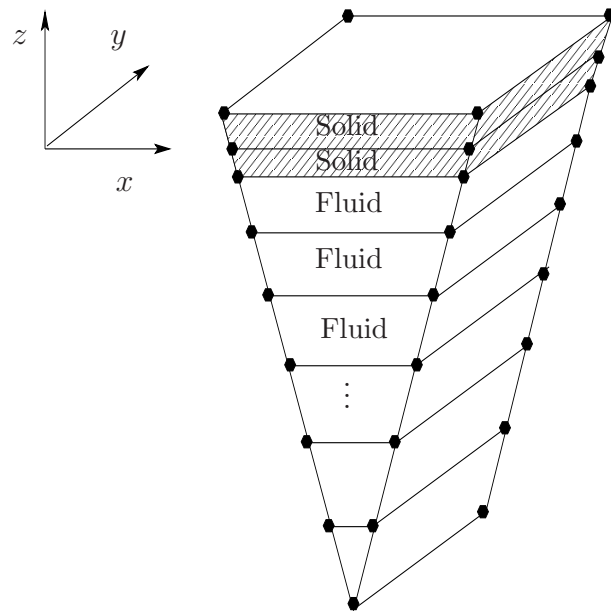


Figure 6.1: FE model of a small rectangular segment of a fluid–filled cylindrical shell.

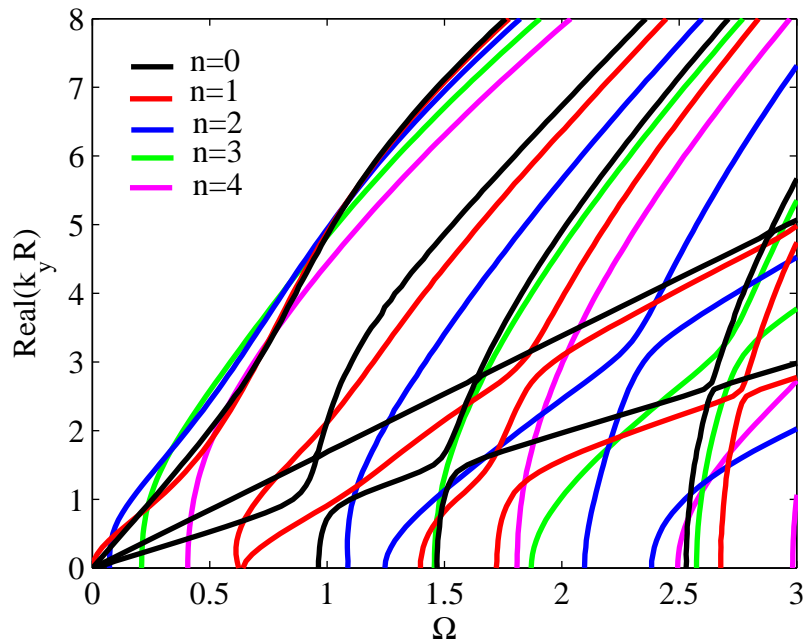
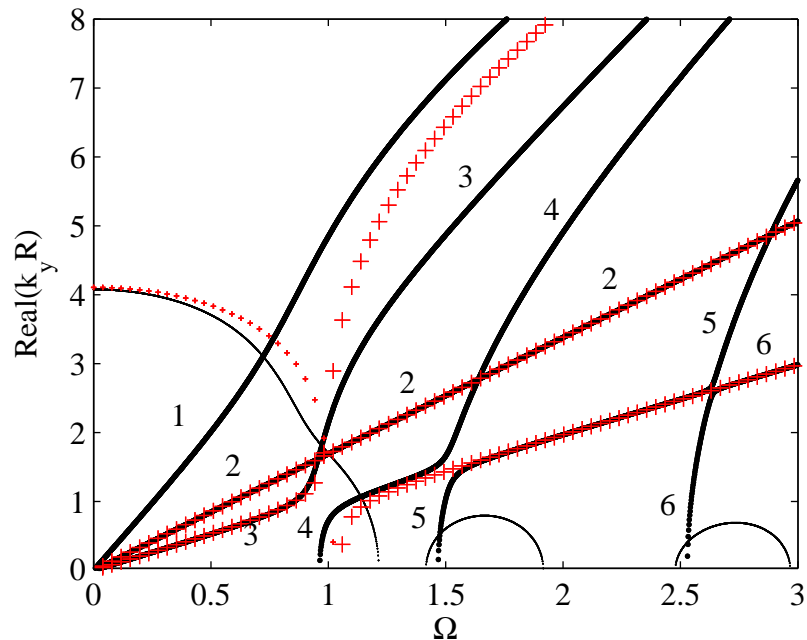
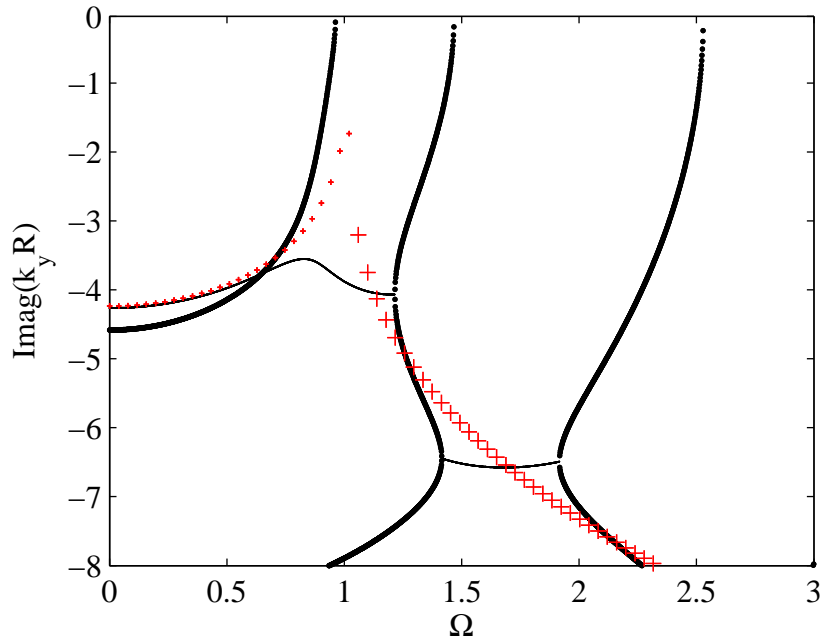


Figure 6.2: Real valued dispersion curves for a water–filled steel pipe, $\bar{h} = 0.1$, $R = 0.4\text{m}$, circumferential mode $n = 0, 1, 2, 3, 4$.

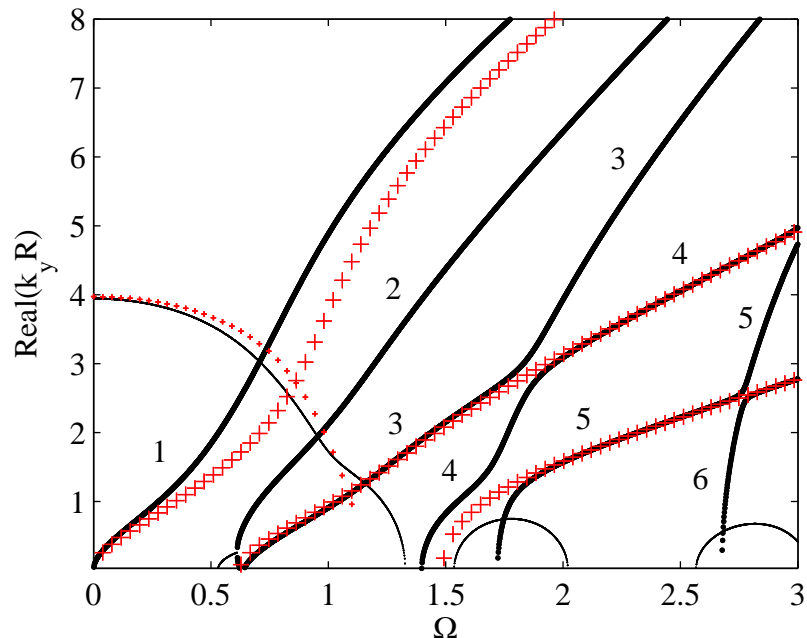


(a) Real dispersion curves

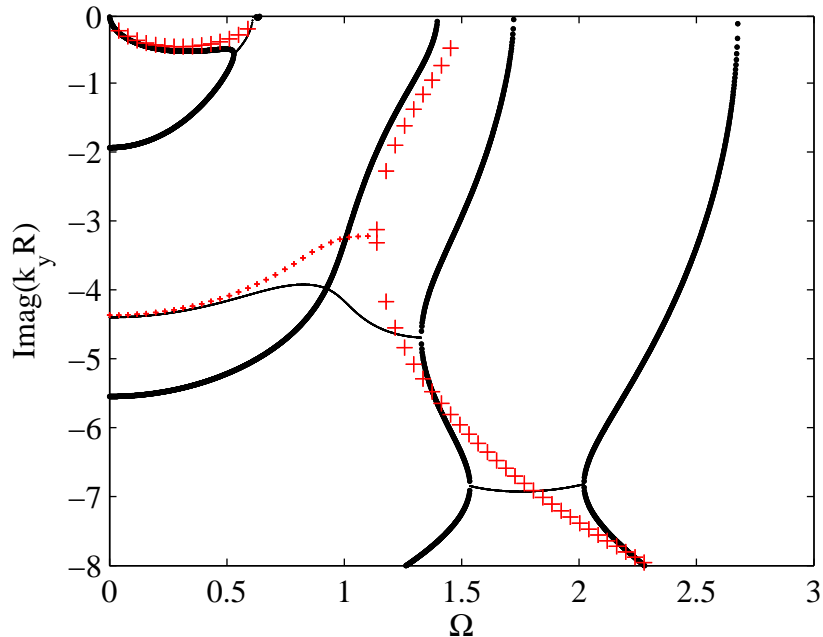


(b) Imaginary dispersion curves

Figure 6.3: Isotropic steel cylinder, $\bar{h} = 0.1$, $R = 0.4\text{m}$. Dispersion curves for circumferential mode $n = 0$: complex valued wavenumbers of the water-filled cylinder; pure real and pure imaginary wavenumbers of the water-filled cylinder; + + + complex valued wavenumbers of the in vacuo cylinder; + + + pure real and pure imaginary wavenumbers of the in vacuo cylinder.

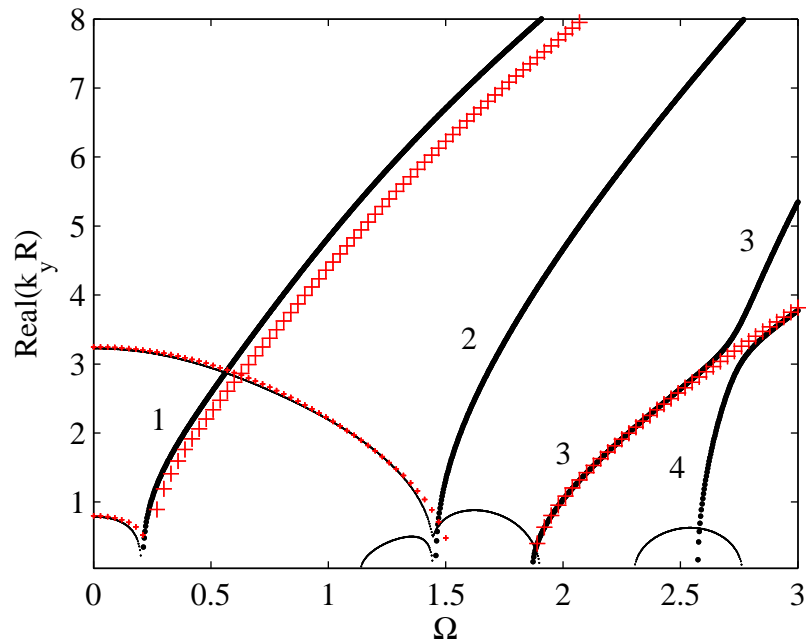


(a) Real dispersion curves

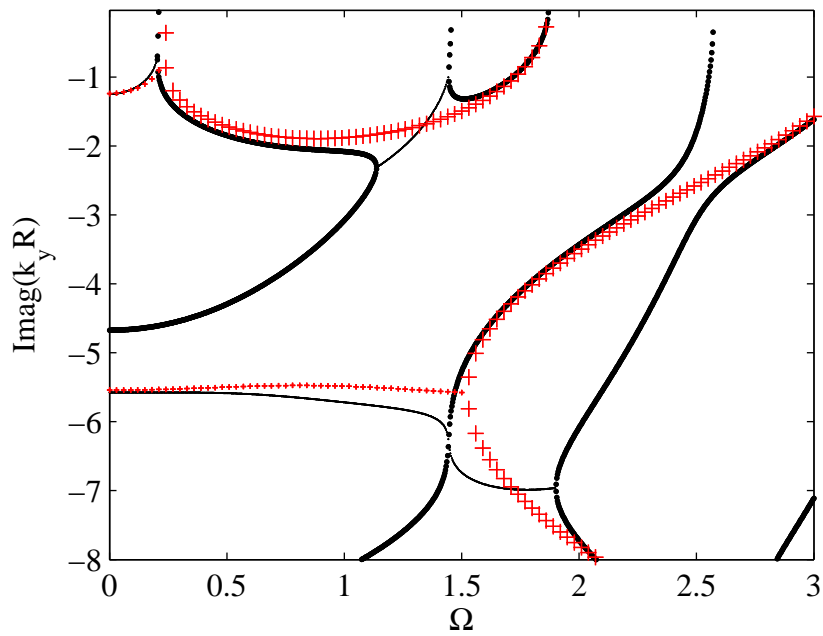


(b) Imaginary dispersion curves

Figure 6.4: Isotropic steel cylinder, $\bar{h} = 0.1$, $R = 0.4\text{m}$. Dispersion curves for circumferential mode $n = 1$: complex valued wavenumbers of the water-filled cylinder; pure real and pure imaginary wavenumbers of the water-filled cylinder; + + + + complex valued wavenumbers of the in vacuo cylinder; + + + + pure real and pure imaginary wavenumbers of the in vacuo cylinder.



(a) Real dispersion curves



(b) Imaginary dispersion curves

Figure 6.5: Isotropic steel cylinder, $\bar{h} = 0.1$, $R = 0.4\text{m}$. Dispersion curves for circumferential mode $n = 3$: complex valued wavenumbers of the water-filled cylinder; pure real and pure imaginary wavenumbers of the water-filled cylinder; + + + complex valued wavenumbers of the in vacuo cylinder; + + + pure real and pure imaginary wavenumbers of the in vacuo cylinder.

Chapter 7

Wave Finite Element Method: application to the estimation of loss factor

7.1 Introduction

In this chapter the WFE method is extended to account for viscoelastic materials, enabling the prediction of dispersion, attenuation and damping behaviour when inherent material damping is not negligible. In particular the WFE method is applied to predict the loss factor of composite structures with constrained layer damping (CLD) treatments. The method can be used to estimate quickly and easily the wavenumbers and loss factors given the design parameters of composite viscoelastic structures.

A brief literature review about the loss factor of CLD treatments is given first. Section 7.3 introduces some characteristics of viscoelastic materials and gives definitions of the modal loss factor. The last section concerns some numerical examples, which include isotropic and laminated plate with CLD and an asymmetric angle ply–laminated sandwich plate.

7.2 Constrained layer damping

Constrained viscoelastic layers are widely used as passive damping treatments to reduce vibration and the noise radiated from the structures. They are realised by bonding a layer of viscoelastic material between two other layers, which can be metallic or fibre reinforced layered sheets.

A classical analysis of CLD was carried out more than 40 years ago by Kerwin [21]. After this work, Ungar and Kerwin, gave in [147] a formulation for the loss factor in terms of energy, which has became the basis for the evaluation of the loss factor and the parametric design of damped structures. Since then, a number of works have been published to predict damping and to improve the performance of passive constrained layer treatments applied to beams and plates, e.g. [18, 121, 148, 149]. Most of the classical works about three-layer sandwich beams and plates use the same basic assumptions about the shear-stress distribution in the structure. These assumptions are clearly pointed out in [150], where Mead compared some of the classical theories proposed for the study of the flexural vibration of damped sandwich beams. In some cases these assumptions result in inaccurate predictions and more detailed models are required. In particular, transverse shear and rotational inertia could significantly influence the dynamics of the structure at higher frequency. For example, in [151] vibrations of unsymmetrical sandwich beams and plates with viscoelastic cores were studied including the effect of longitudinal inertia and shear deformation in the skins while in [152] there is an extension of the well-known sixth order Mead and Markus theory to include thickness deformation in the viscoelastic layer.

The level of damping that a structure with CLD treatment can achieve strongly depends on the choice of the cross-section characteristics and a design strategy can greatly improve the damping capability of structures with viscoelastic damping treatments [153, 154]. A proper choice of the viscoelastic material type, its location and its thickness, the material characteristics of the constraining layers, the laminate stacking sequence and the use of multi-layer damping configuration can optimise the damping capability with respect to frequency and temperature without penalising the stiffness or mass of the structure. However, since viscoelastic material properties are frequency and temperature dependent, parametric optimisation requires iterative algorithms and therefore simple methods for fast numerical evaluation of the global damping.

Passive treatments are more efficient at higher frequencies, while semi-active or active control methods might also be used to improve the damping properties at low frequency. These include, in particular, active constrained layer damping, ACLD, treatments which consists of a layer of viscoelastic material constrained by the host structure and a smart material, such as piezoelectric material. There have been many studies to investigate the energy dissipation mechanisms, control mechanisms and optimisation performances of ACLD, e.g.

[155–157]. However, the high cost and complexity in implementation of ACLD have made passive damping using viscoelastic layers the preferred choice in many applications, ranging from aerospace, vehicle and marine structures to civil constructions. Moreover, these kinds of treatments are quite easy to apply and are effective in dissipating energy with little influence on the structural stiffness and strength.

Fibre reinforced materials are used extensively in many practical applications because of their high strength-to-weight ratio compared to metallic materials. In addition, fibre reinforced polymers exhibit better fatigue and corrosion performance compared to steel or aluminium. Many structures are therefore realised by alternating uniaxial plies in two or more directions of fibre reinforced material, i.e. laminate structures. The damping in these structures derive mainly from the resin matrix, which is often a polymer. The introduction of a viscoelastic core layer is also widely used to improve their damping performance. In many cases, e.g. detection of damage, noise transmission and so on, it is of importance to be able to predict dispersion, attenuation and damping of laminated composites.

7.3 The loss factor

7.3.1 Definition of the loss factor

Viscoelastic materials are so called because they combine the properties of an elastic material, for which all the energy stored during loading is returned as the load is removed, and a viscous material, which does not return any of the energy stored during loading. The physical mechanisms that describe the damping of viscoelastic materials are quite a complicated subject and it is not the aim of this study to explain it. However, for our purposes, it can be modelled considering that, for pure elastic materials under a harmonic loading, the cyclic stress and strain curves are in phase; the stress is proportional to the strain and their ratio gives the elastic modulus. On the other hand, for a purely viscous material the cyclic stress and strain are out of phase by $\pi/2$ and the stress/strain ratio is defined as the loss modulus of the material. For viscoelastic materials the stress and strain induced by a harmonic loading are out of phase by an angle between 0 and $\pi/2$ and therefore the modulus can be represented by a complex quantity. The absolute value is given by the ratio of the amplitudes of the stress and strain gives the elastic modulus while the phase angle between these two gives

the material damping capacity. The complex elastic modulus is then

$$E^* = E' + iE'' = E'(1 + i\eta), \quad (7.1)$$

where E' is the dynamic modulus of elasticity called the storage modulus (Young's modulus) while E'' , the loss modulus, measures the internal losses. The material loss factor is defined as

$$\eta = E''/E', \quad (7.2)$$

where $0 \leq \arctan \eta \leq \pi/2$ is the phase angle between stress and strain. A short overview on the nature of damping materials related to their applications for passive damping control can be found in [158].

The loss factor is a suitable quantity to characterise the dissipated energy of a structure treated with viscoelastic materials. Ungar and Kerwin in [147] defined the loss factor of a viscoelastic system under harmonic excitation as

$$\eta = \frac{1}{2\pi} \frac{\text{Energy dissipated in the system per cycle}}{\text{Maximum amount of energy stored per cycle}}. \quad (7.3)$$

7.3.2 Definition of the loss factor for a structure including viscoelastic components

Consider a general laminated plate, where each layer of the structure, including the viscoelastic layers, is denoted with the subscript q . The material properties, including the material loss factor, are assumed to be uniform in each layer. Moreover, the loss factor is assumed to be small. For motion in mode j , equation (7.3) can be obtained in terms of “modal” strain energy, [158], to give

$$\eta_j = \frac{\sum_{q=1}^N \eta_q U_{j,q}}{U_j} \quad (7.4)$$

where N is the total number of layers, η_q is the material loss factor of the q th layer while $U_{j,q}$ is the maximum strain energy stored in each layer for one cycle of mode j . Equation (7.4) provides exact values only if the damping is uniformly distributed along the the whole structure, that is when η_q is the same for each layer. When the damping is not uniform, the loss factor evaluated by equation (7.4) is only approximated since the modes of vibration are generally coupled. However, the approximation has generally been found to be satisfactory [158].

7.3.3 Modelling the loss factor using FEA

A hysteretic damping model is assumed to represent material damping. The material properties are therefore modelled by considering complex components in the material stiffness matrix. If the laminate is discretised using FEs, where each FE is defined by the subscript q , the stiffness matrix for the whole laminated structure is

$$\mathbf{K} = \sum_{q=1}^N \mathbf{K}'_q + i\mathbf{K}''_q = \mathbf{K}' + i\mathbf{K}'', \quad (7.5)$$

where N is the total number of solid elements used in the FE discretisation while \mathbf{K}'_q and \mathbf{K}''_q are the real and imaginary stiffness matrix contributions of the q th finite element to the global matrices \mathbf{K}' and \mathbf{K}'' . Assuming time harmonic solutions, the discretised equation of motion gives the complex eigenvalue problem

$$\mathbf{K}\mathbf{Q} = \lambda\mathbf{M}\mathbf{Q} \quad (7.6)$$

where λ is the diagonal matrix of generalised eigenvalues and \mathbf{Q} is a matrix whose columns are the corresponding eigenvectors. It is worth noting that the stiffness matrix \mathbf{K} is symmetric but not Hermitian while the mass matrix is positive definite, symmetric and real. The eigenvectors \mathbf{Q} in (7.6) are therefore generally complex and not orthogonal with respect to the mass matrix \mathbf{M} and the stiffness matrix \mathbf{K}' , that is $\mathbf{Q}^*\mathbf{K}'\mathbf{Q}$ and $\mathbf{Q}^*\mathbf{M}\mathbf{Q}$ are not diagonal matrices. This physically means that there are energy exchanges between the modes and it is not possible define a proper modal energy. However, an approximate formulation for the modal loss factor can be obtained as shown in [159]. Consider the right and left eigenvector matrices for the eigenvalue problem in equation (7.6), where the left eigenvector matrix in this case is nothing else than the transpose of the right one. For mode j and mode k

$$\mathbf{K}\mathbf{Q}_j = \lambda_j \mathbf{M}\mathbf{Q}_j; \quad (7.7)$$

$$\mathbf{K}\mathbf{Q}_k = \lambda_k \mathbf{M}\mathbf{Q}_k. \quad (7.8)$$

Transposing equation (7.8) gives

$$\mathbf{Q}_k^T \mathbf{K} = \lambda_k \mathbf{Q}_k^T \mathbf{M}. \quad (7.9)$$

Premultiplying equation (7.7) by \mathbf{Q}_k^T and postmultiplying equation (7.9) by \mathbf{Q}_j gives

$$\mathbf{Q}_k^T \mathbf{K} \mathbf{Q}_j = \lambda_j \mathbf{Q}_k^T \mathbf{M} \mathbf{Q}_j; \quad (7.10)$$

$$\mathbf{Q}_k^T \mathbf{K} \mathbf{Q}_j = \lambda_k \mathbf{Q}_k^T \mathbf{M} \mathbf{Q}_j. \quad (7.11)$$

Subtracting equation (7.10) and (7.11), one finds

$$(\lambda_j - \lambda_k) \mathbf{Q}_k^T \mathbf{M} \mathbf{Q}_j = 0. \quad (7.12)$$

Hence, when $j \neq k$

$$\mathbf{Q}_k^T \mathbf{M} \mathbf{Q}_j = \mathbf{Q}_k^T \mathbf{K} \mathbf{Q}_j = 0. \quad (7.13)$$

$\mathbf{Q}^T \mathbf{K} \mathbf{Q}$ and $\mathbf{Q}^T \mathbf{M} \mathbf{Q}$ are now diagonal and the left and right eigenvectors are said to be biorthogonal. In practise, the complex eigenvectors \mathbf{Q}_j are often approximated by the real eigenvectors \mathbf{V}_j obtained for the equivalent conservative system, that is when $\mathbf{K}'' = \mathbf{0}$ and the stiffness matrix is purely real, i.e. the eigensolutions of

$$\mathbf{K}' \mathbf{V}_j = \omega_{nj}^2 \mathbf{M} \mathbf{V}_j. \quad (7.14)$$

The approximation is acceptable if \mathbf{K}'' is small. The complex eigenvalues λ_j of equation (7.6) can be written as

$$\lambda_j = \omega_{nj}^2 (1 + i\eta_j), \quad (7.15)$$

where η_j is the modal loss factor of mode j . Using equation (7.5) for the complex stiffness matrix, equation (7.6) can be rewritten as

$$\omega_j^2 (1 + i\eta_j) = \frac{\mathbf{V}_j^T \mathbf{K}' \mathbf{V}_j}{\mathbf{V}_j^T \mathbf{M} \mathbf{V}_j} + i \frac{\mathbf{V}_j^T \mathbf{K}'' \mathbf{V}_j}{\mathbf{V}_j^T \mathbf{M} \mathbf{V}_j}. \quad (7.16)$$

The real and imaginary part of equation (7.16) can be separated such that

$$\begin{aligned} \omega_j^2 &= \frac{\mathbf{V}_j^T \mathbf{K}' \mathbf{V}_j}{\mathbf{V}_j^T \mathbf{M} \mathbf{V}_j}; \\ \omega_j^2 \eta_j &= \frac{\mathbf{V}_j^T \mathbf{K}'' \mathbf{V}_j}{\mathbf{V}_j^T \mathbf{M} \mathbf{V}_j}, \end{aligned} \quad (7.17)$$

where the first equation in (7.17) is the well known Rayleigh quotient. Eliminating ω_j^2 from equations (7.17) gives

$$\eta_j = \frac{\mathbf{V}_j^T \mathbf{K}'' \mathbf{V}_j}{\mathbf{V}_j^T \mathbf{K}' \mathbf{V}_j} \quad (7.18)$$

or equivalently

$$\eta_j = \frac{\sum_{q=1}^N \mathbf{V}_j^T \mathbf{K}_q'' \mathbf{V}_j}{\sum_{q=1}^N \mathbf{V}_j^T \mathbf{K}_q' \mathbf{V}_j}, \quad (7.19)$$

where \mathbf{V}_j is the eigenvector associated at the j th undamped mode. The sum over q in equation (7.19) gives the sum of the dissipated and stored energies. Equation (7.19) has been frequently used to evaluate the global loss factor of structures with components having different material properties such as laminated structures or sandwich structures. It has been seen to predict the loss factor with satisfactory approximation and to be simple in application.

7.3.4 Estimation of the loss factor using WFE

To apply the WFE method a small segment of the structure is taken and discretised using solid FE. The viscoelastic characteristics of the composites are taken into account by considering complex components in the material's stiffness matrix as in equation (7.5). Therefore the WFE formulation given in the section 3.2 applies where $\mathbf{C} = 0$ and the stiffness matrix in equation (3.11) is complex as shown in equation (7.5).

Wave propagation in viscoelastic media gives rise to frequencies and wavenumbers that can be real or complex. Forced wave propagation in the viscoelastic structure leads to real frequencies and propagating, nearfield and oscillating but highly decaying waves. All the wavenumbers, including those for propagating waves, are complex. For the remainder of the chapter, however, complex nearfield and oscillating but highly decaying waves are not considered. For propagating waves, the imaginary part of the wavenumber describes the decay of the wave due to damping. The dispersion curves for propagating waves are predicted by the WFE method by solving the polynomial eigenvalue problem in equation (3.44) when the (real) frequency and the propagation direction are specified. On the other hand free vibrations give rise to complex frequencies and real wavenumbers.

The real part of the frequency is the frequency of oscillation while the imaginary part describes the decay of free vibration with time. Complex frequencies are predicted by the solutions to the eigenproblem in equation (3.19) for free waves with no applied tractions.

In the present chapter the loss factor can be obtained by WFE from equation (7.19) and also considering the eigenproblem in equation (3.19) modified as

$$[(\bar{\mathbf{K}} - \omega_r^2 \bar{\mathbf{M}}) - \lambda \bar{\mathbf{M}}] \mathbf{q}_1 = \mathbf{0}, \quad (7.20)$$

where the real propagation constant μ_x and $\mu_y = \tan \theta \mu_x$ and ω_r , the real part of the frequency, are prescribed. If ω_i^2 is neglected, the eigenvalues λ in equation (7.20) are $\lambda = i2\omega_r\omega_i$, where ω_i is the imaginary part of the frequency. Once the eigenproblem in equation (7.20) is solved, the loss factor η can be approximated as

$$\eta = 2 \frac{\omega_i}{\omega_r}. \quad (7.21)$$

7.3.5 Estimation of the loss factor using WFE: inclusion of frequency dependent material properties

The properties of viscoelastic materials are influenced by many parameters. They include frequency, temperature, static pre-load, aging and so on. The most important of these are the temperature and frequency. Hence the stiffness matrix, and consequently the material loss factor, is given as a function of the frequency and temperature, i.e.

$$\mathbf{K}(\omega, T) = \sum_{q=1}^N \mathbf{K}'_q(\omega, T) + i \mathbf{K}''_q(\omega, T). \quad (7.22)$$

Suppose now that only the constrained viscoelastic layer has material properties that are frequency dependent for a fixed temperature T_0 . The viscoelastic material is considered isotropic with constant Poisson's ratio ν and density ρ at T_0 . Let \bar{q} be the constrained viscoelastic layer. Since the stiffness matrix is proportional to the Young's modulus E (for constant ν), the contribution to the global stiffness matrix $\mathbf{K}(\omega, T)$ of the viscoelastic layer \bar{q} at a frequency ω will be given by [84]

$$\mathbf{K}_{\bar{q}}(\omega, T_0) = \frac{E(\omega)}{E(\omega_0)} \mathbf{K}'_{\bar{q}}(\omega_0, T_0) [1 + i\eta_{\bar{q}}(\omega, T_0)] \quad (7.23)$$

where $\eta_{\bar{q}}(\omega, T_0)$ is the frequency dependent loss factor and $\mathbf{K}'_{\bar{q}}(\omega_0, T_0)$ is the stiffness matrix of the viscoelastic layer \bar{q} evaluated at ω_0 and neglecting damping.

For layers $q \neq \bar{q}$ we suppose material that are generally orthotropic and whose properties are frequency and temperature independent; hence

$$\begin{aligned} E_{II} &= E_{II}(1 + i\eta_{II}); \quad I = 1, 2, 3; \\ G_{12} &= G_{12}(1 + i\eta_{12}); \\ G_{23} &= G_{23}(1 + i\eta_{23}); \\ G_{13} &= G_{13}(1 + i\eta_{13}). \end{aligned}$$

The contribution to the global stiffness matrix of the q th layer is then

$$\mathbf{K}_q = \mathbf{K}'_q + i\mathbf{K}''_q \quad q \neq \bar{q}. \quad (7.24)$$

From equations (7.23) and (7.24), the global stiffness matrix in equation (7.22) can be rewritten in its real and imaginary parts as

$$\begin{aligned} \bar{\mathbf{K}}'(\omega, T_0) &= \sum_{q=1, q \neq \bar{q}}^N \mathbf{K}'_q + \frac{E(\omega)}{E(\omega_0)} \mathbf{K}_{\bar{q}}(\omega_0, T_0) \\ (7.25) \end{aligned}$$

$$\bar{\mathbf{K}}''(\omega, T_0) = \sum_{q=1, q \neq \bar{q}}^N \mathbf{K}''_q + \eta(\omega, T_0)_{\bar{q}} \frac{E(\omega, T_0)}{E(\omega_0, T_0)} \mathbf{K}_{\bar{q}}(\omega_0, T_0)$$

and the global loss factor (7.19) at frequency ω , is

$$\eta_j(\omega, T_0) = \frac{\mathbf{V}_j^T \bar{\mathbf{K}}''(\omega, T_0) \mathbf{V}_j}{\mathbf{V}_j^T \bar{\mathbf{K}}'(\omega, T_0) \mathbf{V}_j} \quad (7.26)$$

7.4 Numerical examples

In this section some numerical examples are presented to illustrate the application of the WFE method for damping prediction of composite structures.

7.4.1 Aluminum beam with CLD treatment

As a first example, the WFE results are compared with those obtained by Kerwin [21], and by Ghinet and Atalla [22], for the flexural loss factor of an aluminium beam with an attached constrained layer damping treatment. A schematic representation of the cross section of the beam is given in Figure 7.1.

It can be assumed that the mechanism of energy dissipation in the viscoelastic layer is predominantly due to the shear strain that it undergoes during the vibration of the whole structure. That is, according to [149], the energy dissipated per cycle per unit length and width is

$$E_d = \pi h_2 G'' \gamma_2^2, \quad (7.27)$$

where G'' is the imaginary part of the shear modulus of the viscoelastic material while γ_2 is the amplitude of the induced shear strain in the viscoelastic layer. The analytical expression for γ_2 can be quite complicated, however following [18], under some assumptions (the shear strain is negligible in the skins, which experience pure bending; small displacement; longitudinal stress negligible in the core; the viscoelastic layer thickness remains constant) it can be approximated by

$$\gamma = \frac{u_{tc} - u_{bc}}{h_2} + \frac{\partial w}{\partial x}, \quad (7.28)$$

where the meaning of symbols is given in Figure 7.2. Since

$$u_{tc} = u_t + \frac{h_1}{2} \frac{\partial w}{\partial x}$$

$$u_{bc} = u_b - \frac{h_3}{2} \frac{\partial w}{\partial x},$$

it follows that

$$\gamma = \frac{u_t - u_b}{h_2} + \frac{1 + (h_1 + h_3)/2}{h_2} \frac{\partial w}{\partial x}. \quad (7.29)$$

The global damping loss factor was estimated by Kerwin in [21] assuming the approximations given above. Other simplifying assumptions were also made in [21] to obtain an approximate analytical formulation for the loss factor of bending waves. In particular equation (IV-5) in [21], is accurate only for a thin constrained layer damping treatment, that is $h_3/h_1 \leq 0.2$. The data for the elastic properties of the damping layer in the numerical examples are extrapolated from the frequency dependent real and imaginary part of the shear modulus given in [21]. Three cases are studied. In each, the thickness of the constraining layer is changed as shown in Table 7.1, while the bottom layer and the core thicknesses are $h_1 = 3.175\text{mm}$ $h_2 = 0.254\text{mm}$ respectively. The FE model is realised using five SOLID45 elements to discretise the bottom layer, one SOLID45 element to discretise the viscoelastic core and one SOLID45 element to discretise the upper layer, resulting in a model with 24 DOFs after the WFE reduction. The

Bar	W	X	Y
h_3	0.1524 mm	0.254 mm	0.508 mm

Table 7.1: Thickness of the constraining layer for the three-layer aluminum beam configuration

convergence of the WFE method has been checked for this example. Figure 7.3 shows a comparison between the loss factor obtained by the WFE method, the loss factor obtained by Kerwin, equation (IV–5) in [21] and by Ghinet and Atalla (data provided by Ghinet) [22]. To evaluate the loss factor Ghinet and Atalla used a discrete laminate method where the displacement field of any discrete layer was described by the Reissner–Mindlin theory. It can be seen that the WFE results are in good agreement with other results. The slight differences can be explained in part considering the a priori assumptions, which concern the variation of stress and strain through the thickness in [21] and [22].

The influence of the thickness of the outer layers is now analysed. With reference to Figure 7.4 several configurations are considered for which the distance from the middle plane of the composite plate and the middle plane of the damping layer d is increased. The thickness of the top and bottom layers vary, but $h_1 + h_3$ remains constant. The material properties of the plate are the same as that used in the previous example. When $d = 0$, the thicknesses are $h_1 = h_3 = 1\text{mm}$ and $h_2 = 0.1\text{mm}$. The flexural loss factor is shown in Figure 7.5 for four different configurations: $d = 0\text{mm}$, $d = 0.25\text{mm}$, $d = 0.5\text{mm}$ and $d = 0.75\text{mm}$. It can be seen that the loss factor decreases as the offset d increases. When the two skins have the same thickness, the shear deformation in the viscoelastic core is maximised and therefore the loss factor is a maximum with respect to the other configurations.

7.4.2 Laminated plate with CLD treatment

The WFE approach can be applied equally to laminates of arbitrary complexity, with an arbitrary number of layers. In this example a laminated plate with a CLD treatment is considered. The skin material material properties are given in Table 7.2. The plate cross section configuration is shown in Figure 7.1. The global damping performance of the laminate is basically affected by two causes: the fibre orientation with respect to the direction of propagation and the shear strain in the viscoelastic layer induced by the relative strain of the top and bottom

$E_x = 119\text{GPa}$	$E_y = 8.67\text{GPa}$	$E_z = 8.67\text{GPa}$
$E_z = 8.67\text{GPa}$	$G_{yz} = 3.9\text{GPa}$	$G_{xy} = G_{xz} = 5.18\text{GPa}$
$\nu_{xy} = \nu_{xz} = 0.31$	$\nu_{yz} = 0.02$	$\rho = 1389\text{kg/m}^3$
$\eta_{xy} = \eta_{xz} = \eta_x = 0.118\%$	$\eta_{yz} = 0.846\%$	$\eta_y = \eta_z = 0.620\%$

Table 7.2: Laminated plate: material properties

constraining layers. The first cause is explained because the damping of the fibre reinforced material derives essentially from the resin matrix while the second is due to the mechanism we assume of energy dissipation in the viscoelastic layer, equation (7.27). Since the relative stress-strain distribution in the skins influences the shear strain in the core, it is expected that a proper choice of the fibre orientation, stacking sequence and viscoelastic material can optimise the loss factor. As a first case the effect of the viscoelastic material properties and the influence of the fibre orientation on the flexural loss factor are analysed assuming the configuration [0/d/0], where d refers here to the damping layer. Two viscoelastic materials are considered, named material N.1 and material N.2. The material properties for material N.1 are obtained from Figure 6 in [21] at a temperature of 25°C. For material N.2, the curves for the frequency dependence of the shear modulus and the loss factor are given in Figures 7.6 and 7.7. The geometrical parameters of the sandwich construction are $h_1 = 1\text{mm}$, $h_2 = 0.1\text{mm}$ and $h_3 = 1\text{mm}$. Figures 7.8 and 7.9 show the flexural loss factors for propagation directions $\theta = 0$, $\theta = \pi/4$ and $\theta = \pi/2$ using the viscoelastic materials N.1 and N.2 respectively. It can be observed that the loss-factor behaviour is influenced by the fibre orientation and by the choice of the viscoelastic material. Suppose we are interested in the case in which the propagation direction is primarily in the $\theta = 0$ direction and the frequency range of interest is between 500Hz and 1kHz. This simplified case study is here considered in order to do an early stage study and to show how the WFE method can be applied to optimise the damping characteristic of laminated constructions. Considering the frequency of range of interest, Figures 7.8 and 7.9 show that the loss factor is maximised when material N.1 is used and the propagation direction is $\theta = \pi/2$. Equivalently, if the propagation direction that we are considering is $\theta = 0$, the lay-up [90/d/90] is here taken as optimised with respect to the global loss factor.

As a further analysis, the flexural loss factor for laminates with lay-ups [0/90/d/90/0], [45/90/d/90/45] and [-45/90/d/90/-45], is compared with the

flexural loss factor for the case [90/ d /90] in Figure 7.10. It can be noticed that between 500Hz and 1kHz, a slight improvement in the loss factor is obtained if the configuration [0/90/ d /90/0] is used.

The influence of symmetric and antisymmetric ply–stacking configuration on the loss factor is also evaluated. Figure 7.11 and 7.12 show the global loss factor versus frequency for [0/90/ d /90/0], [0/90/ d /0/90] and [45/90/ d /90/45], [45/90/ d /45/90] laminated configuration. From Figures 7.11 and 7.12 it is seen that the symmetric laminate has higher damping for the cases investigated.

7.4.3 Asymmetric angle–ply laminated sandwich plate

The two outer skins of the asymmetric angle–ply laminated sandwich considered in this section comprise 4 sheets of 0.25mm thickness of glass–epoxy material. The stacking sequence of the bottom and the top skins are [45/ – 45/ – 45/45] and [–45/45/45/ – 45] respectively. The core is a 5mm thick foam core. Material properties for the skins are given in Table 7.2 while the core material properties are: $E = 0.18\text{GPa}$, $\rho = 110\text{kg/m}^3$, $\nu = 0.286$ and $\eta = 10\%$. The FE model for the structure is realised using 4 SOLID45 elements for each skin and 5 SOLID45 elements to discretise the core, resulting in 13 elements. The reduced WFE model therefore has 42 DOFs. Figure 7.13 shows the real and imaginary parts of the propagation constant, kL , versus the frequency for propagating waves (i.e. those waves which would be true propagating waves if the damping were zero). The first three branches in Figure 7.13(a) represent the first quasi–flexural, quasi–shear and quasi–extensional waves propagating in the laminated sandwich. At higher frequency, further propagating waves cut–off, which involve higher order modes across the thickness of the plate. It can be noticed that the dispersion characteristics are very complicated at high frequency, involving coupling between the various wave modes, veering and so on. Comparison with the results obtained by solving the eigenproblem in equation (3.19) for the undamped case has shown that the material damping has a negligible effect on the real dispersion curves.

The loss factor for the first quasi–flexural wave in the laminated sandwich plate is evaluated using both the formulation in equation (7.26) and the eigenvalues obtained from (7.20). Propagations direction $\theta = 0^\circ$ and $\theta = 45^\circ$ are considered. The results are given in Figure 7.14. It can be noticed that there is good agreement between the results found using the two methods of estimating the loss factor.

In Figure 7.15, the loss factor of the laminated sandwich plate is given as

function of the propagation direction θ at 5kHz and 10kHz. The results are obtained solving equation (7.20). It can be observed that the damping is affected by the direction of propagation but not by a great deal.

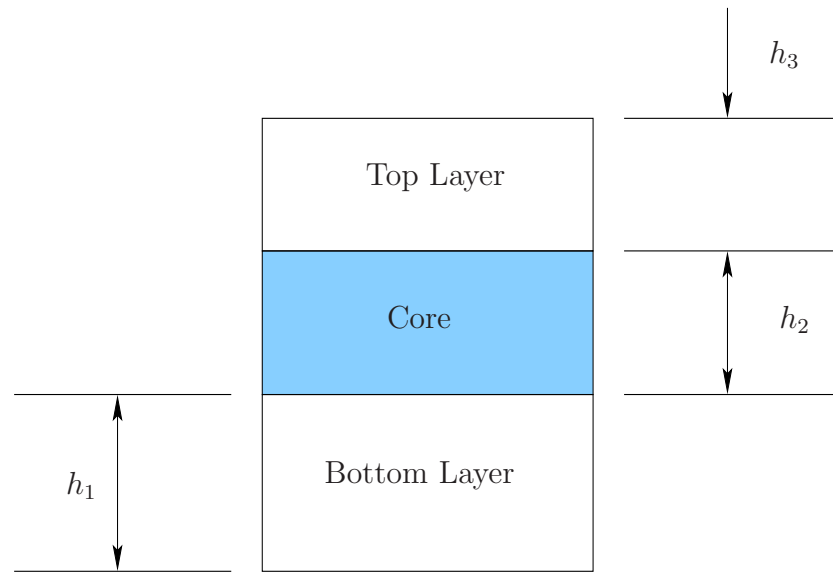


Figure 7.1: Schematic representation of the cross section of a three-layer sandwich structure.

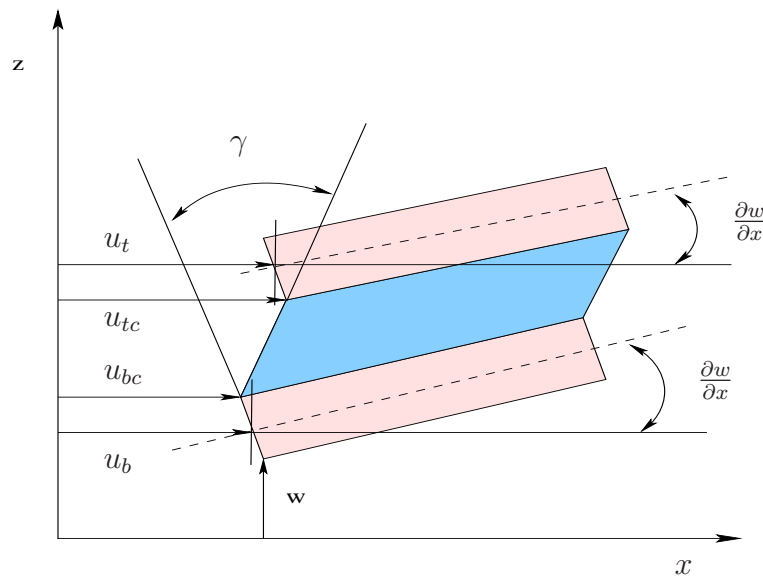


Figure 7.2: Deformation of the three layer sandwich structure with no shear deformation in the top and bottom layers.

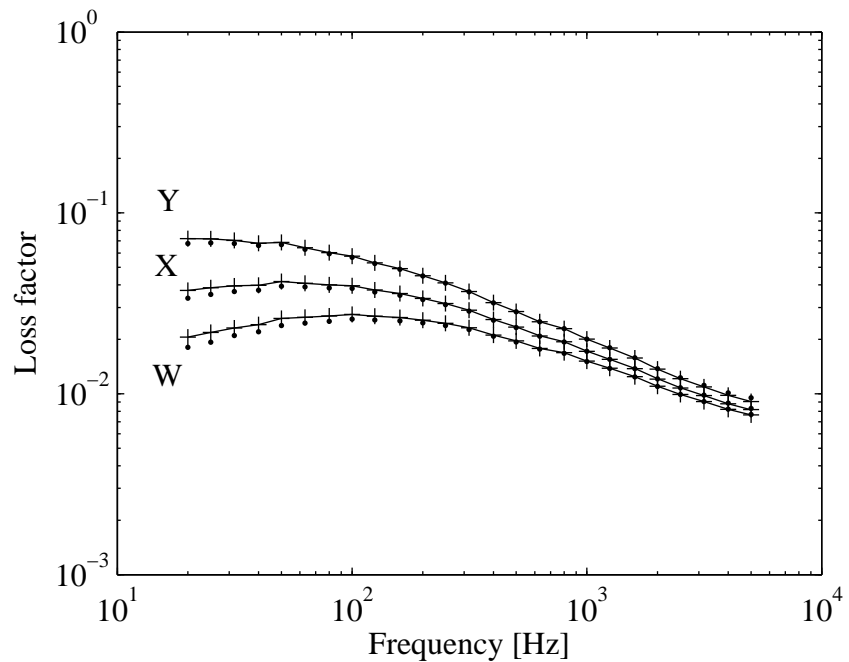


Figure 7.3: Loss factor for the first flexural wave in the aluminum beam with CLD treatment: WFE results; — theory of [22]; +++++ theory of [21].

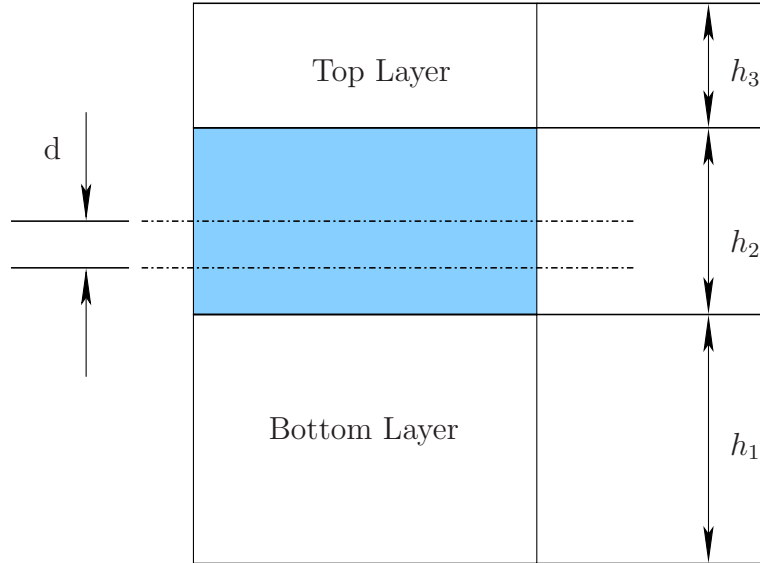


Figure 7.4: Schematic representation of the cross section of a three-layer non-symmetric sandwich structure.

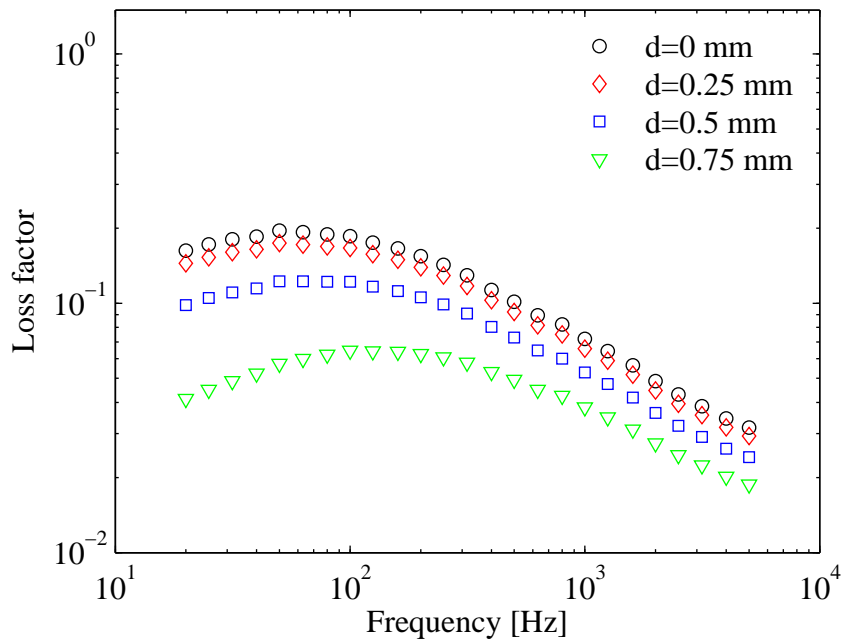


Figure 7.5: Flexural loss factor of an aluminum plate with constrained layer damping treatment: effect of the thickness of the outer layers.

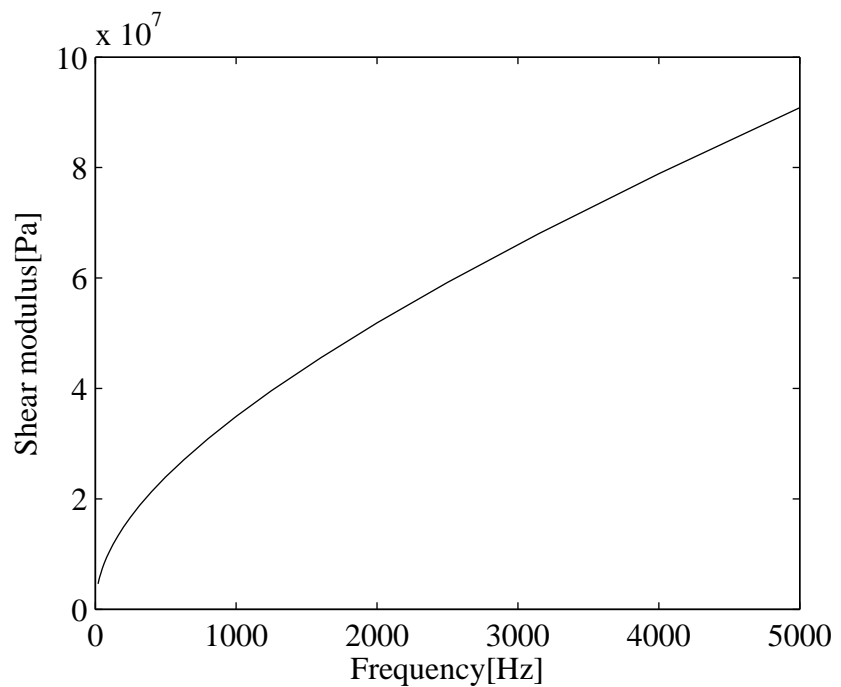


Figure 7.6: Viscoelastic material N.2: shear modulus as a function of frequency.

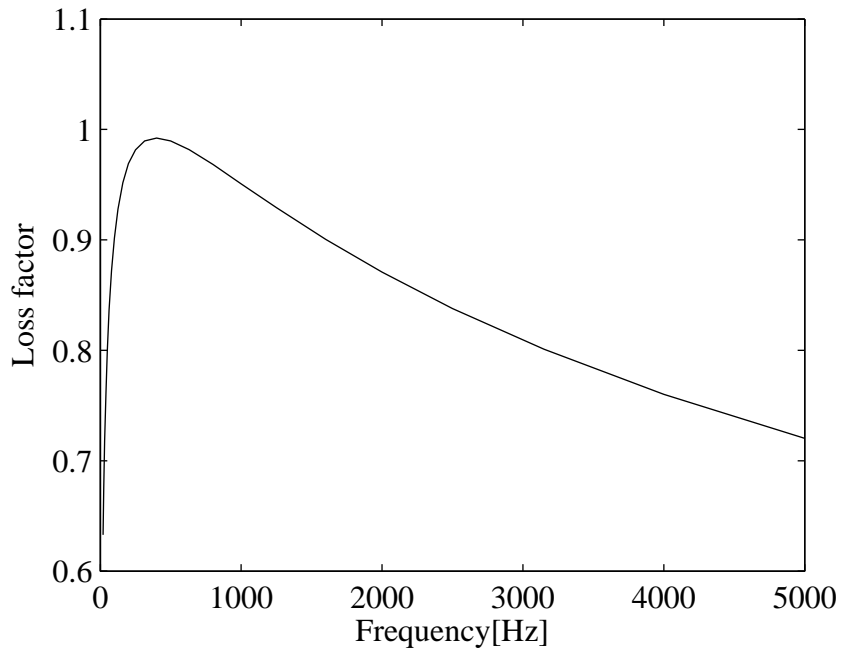


Figure 7.7: Viscoelastic material N.2: loss factor as a function of frequency.

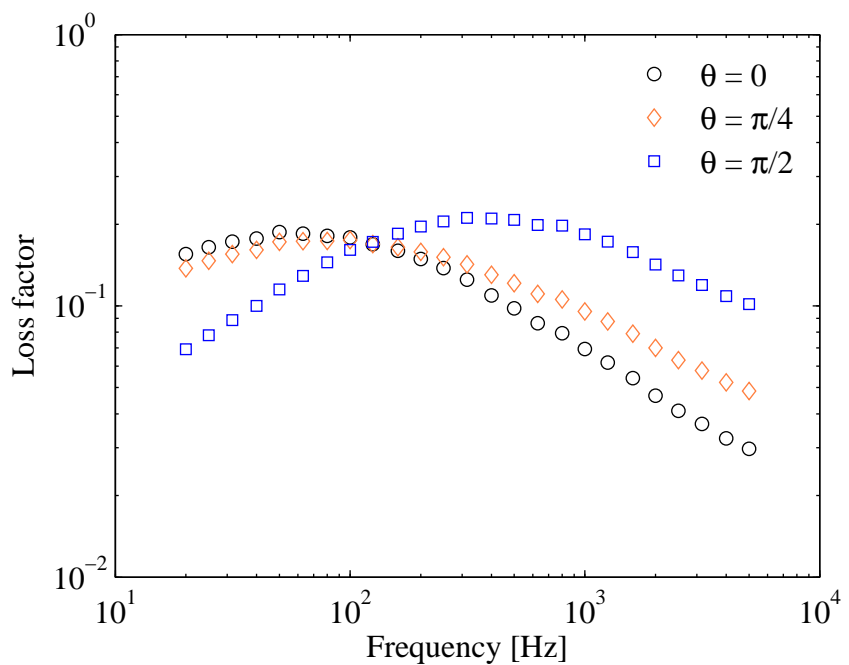


Figure 7.8: Influence of the propagation direction on the flexural loss factor: laminated plate [0/d/0], material N.1.

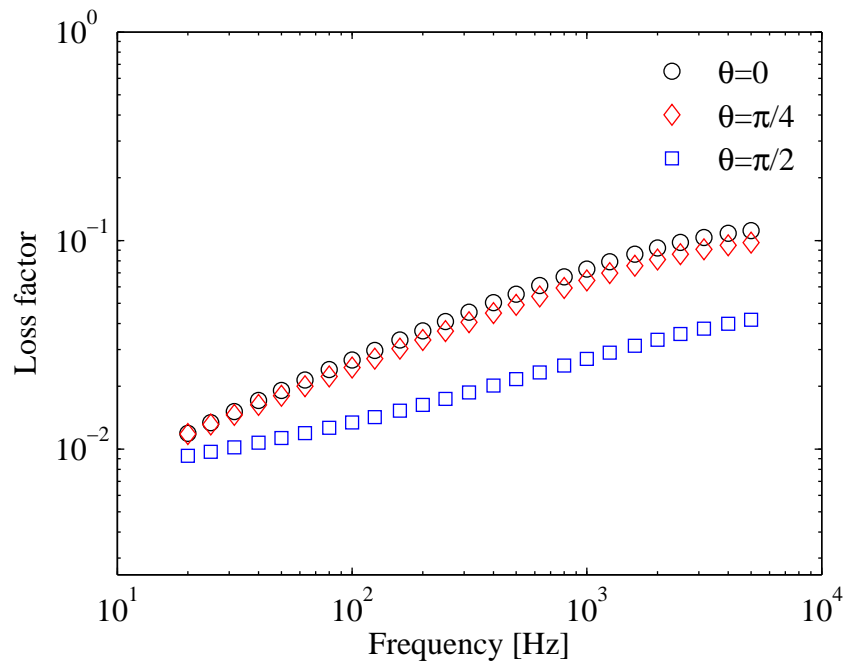


Figure 7.9: Influence of the propagation direction on the flexural loss factor: laminated plate [0/d/0], material N.2.

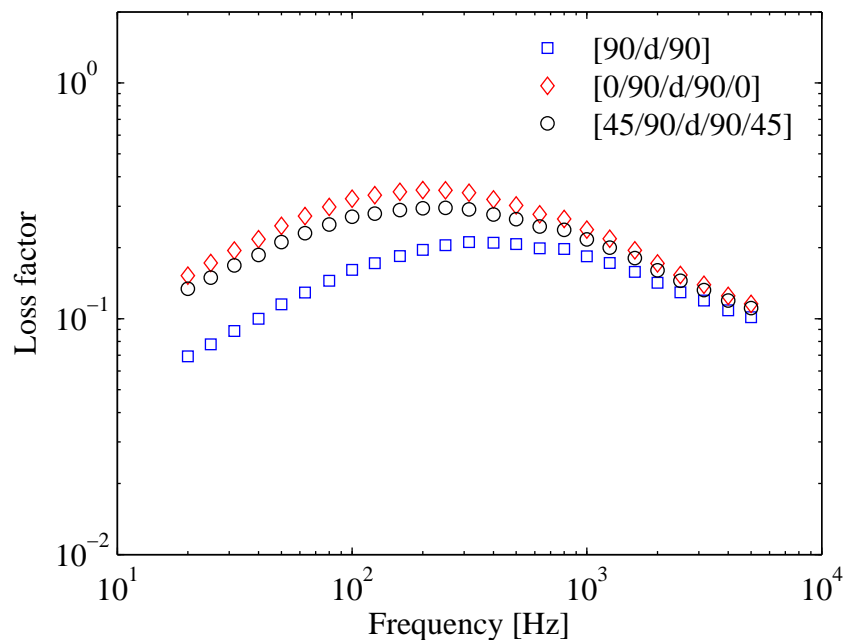


Figure 7.10: Influence of different laminate lay-up on the flexural loss factor: laminated plate [90/d/90], [0/90/d/90/0], [45/90/d/90/45]. Propagation direction $\theta = 0$. Material N.1.

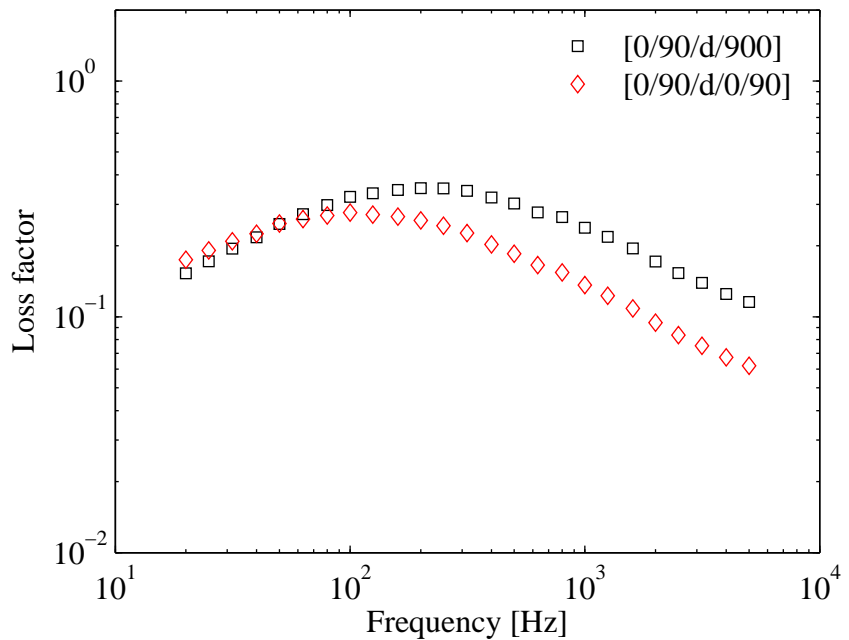


Figure 7.11: Influence of the symmetric $[0/90/d/90/0]$ and antisymmetric $[0/90/d/0/90]$ lay-up on the flexural loss factor, $\theta = 0$. Material N.1.

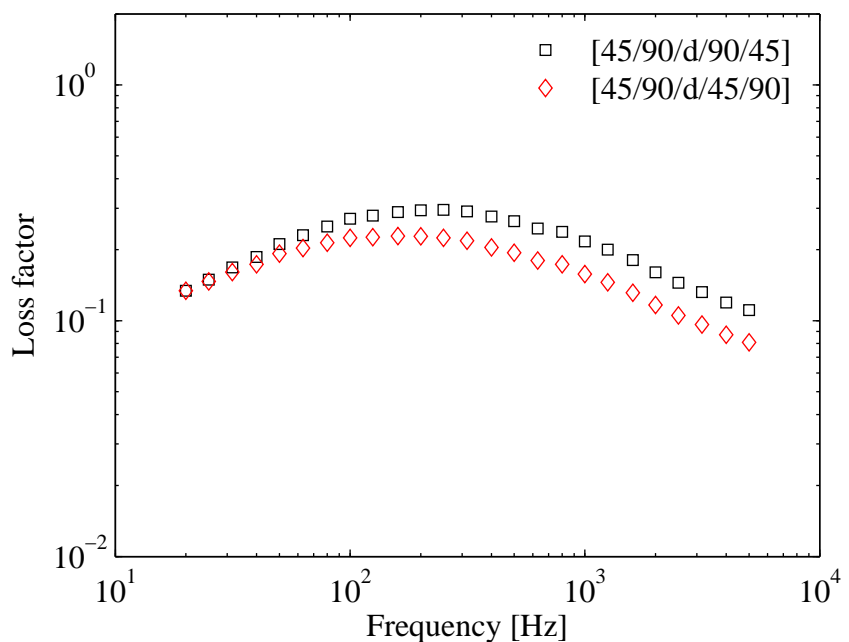
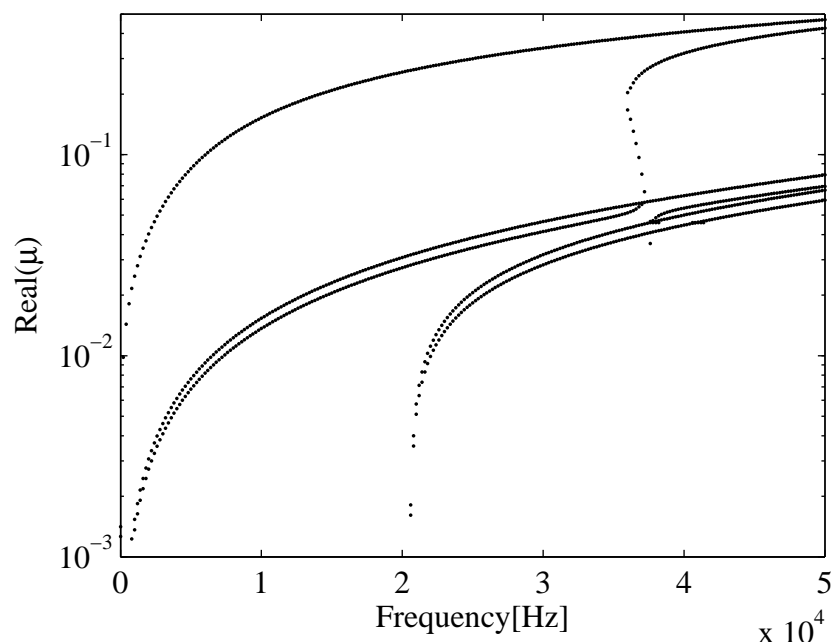
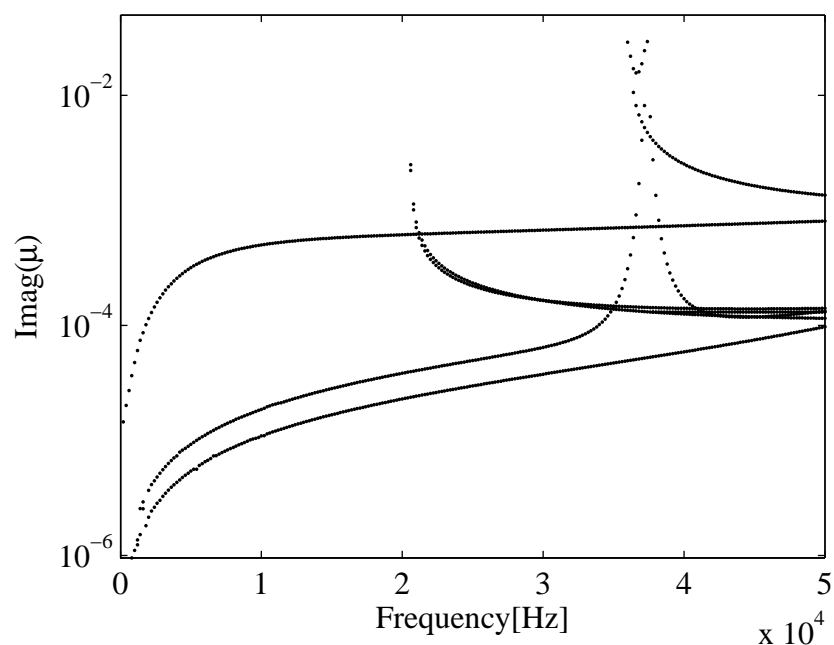


Figure 7.12: Influence of a symmetric $[45/90/d/90/45]$ and antisymmetric $[45/90/d/45/90]$ lay-up on the flexural loss factor, $\theta = 0$. Material N.1.



(a) Real part of the wavenumber



(b) Imaginary part of the wavenumber

Figure 7.13: Dispersion curves for the laminated sandwich plate, $\theta = 0$.

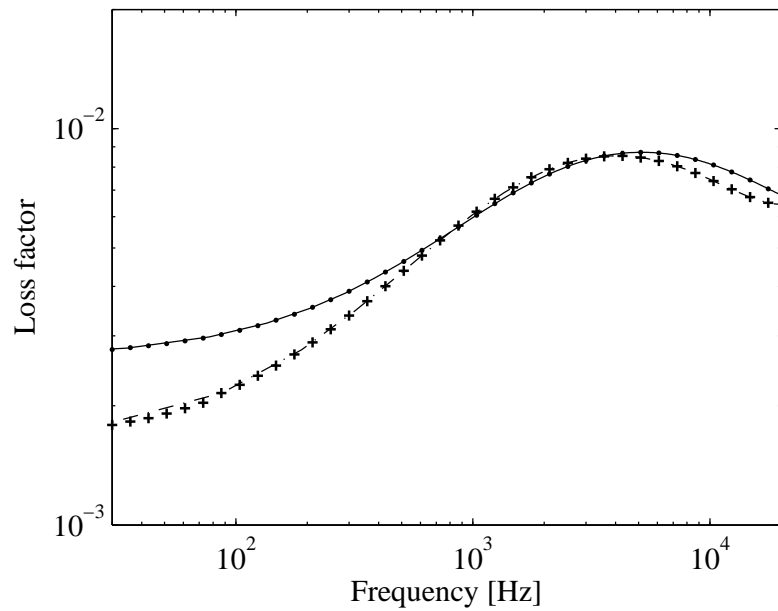


Figure 7.14: Loss factor for the first flexural wave in the laminated sandwich plate as a function of frequency: $\theta = 0$ and +++++ $\theta = \pi/4$, results obtained from equation (7.19); ——— $\theta = 0$ and - - - - - $\theta = \pi/4$, results obtained by solving equation (7.20).

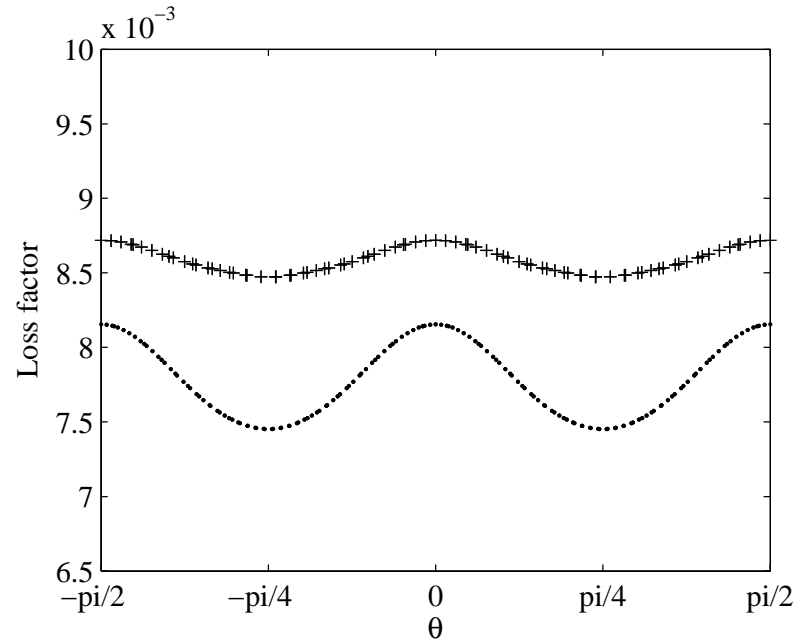


Figure 7.15: Loss factor for the first flexural wave in the laminated sandwich plate as a function of the propagation direction: +++++ 5kHz and 10kHz

Chapter 8

Concluding remarks

In this thesis a method for the numerical prediction of wave characteristics of 2-dimensional structures using standard FE analysis has been presented. The structures are homogeneous in 2 dimensions but the properties might vary through the thickness. The method involves post-processing the mass and stiffness matrices of a small segment of the structure, produced using conventional FE methods. Emphasis was placed on a 4-noded rectangular segment, although other element types can be used. Periodicity conditions were then applied using the approach developed by Abdel-Rahman [79] in the context of FE analysis of periodic structures. Eigenproblems of various forms then arise, the form depending on the nature of the problem at hand. These eigenproblems are the kernel of the method and might be linear, quadratic, polynomial or transcendental eigenproblems. The solutions sought provide the frequency evolution of the wavenumber (dispersion curves) and the wavemodes, which are related to the cross-section motion. Although not analysed in this thesis, the forced response can be determined from these eigensolutions. Further technical details can be found in [77] for the forced response. An alternative approach to the forced response is described in [84].

Numerical issues were discussed. It has been found that issues arise because the original structure is continuous while the WFE model is a lumped, discrete, spring-mass structure which is spatially periodic. First, there is the issue of spatial discretisation and consequent aliasing effects: the frequency of propagation is a periodic function of the real propagation constant μ . In practical applications this is not important since $Real(\mu) \in [-\pi, \pi]$ is taken as the most convenient interval in which to examine the variation of the frequency. This restriction is not as arbitrary as it might appear since it contains a complete period of the frequency and avoids ambiguity in the wavenumbers at the same time. Moreover,

in common with conventional FEA, FE discretisation errors become significant if the size of the element is too large [11]. As a rule-of-thumb, there should be at least 6 or so elements per wavelength. Hence the FE discretisation is known to be inaccurate for $\mu > \pi/3$ or thereabouts. It has also been observed that the WFE model exhibits pass- and stop-bands structure, in which disturbances can propagate freely only within certain frequency ranges, otherwise they decay with distance. For a 2-dimensional element with n DOFs per node there will be n propagation surfaces. The issue is to determine which ones are artifacts of the spatial periodicity rather than being representative of wave motion in the continuum. Which of these is the case was determined by sensitivity analysis.

The method has been applied to several examples including isotropic, orthotropic, laminated and sandwich plates and cylindrical shells, fluid-filled cylindrical shells and plates with constrained layer damping treatments. The FE software ANSYS was used to obtain the mass and stiffness matrices of a small segment of the structure. One aim was to validate the approach in situations for which analytical solutions are well established. Another aim was to apply the method to situations where no analytical solutions are available. Of particular interest was the case of either asymmetric or symmetric angle-ply laminate sandwiches since the analytical approach for these types of panels is extremely complicated. Various interesting wave propagation phenomena have been observed, particularly concerning cut-off and bifurcations between various wave modes at high frequencies. Accurate predictions of the dispersion relations have been found at negligible computational cost. The application of the method has been seen to be straightforward even in complicated cases. In the analytical approach, material symmetry relative to the coordinate axis allows eigensystems to be simplified. On the contrary, the WFE technique enables any kind of stacking sequence for the composite laminate to be analysed with the same degree of simplicity. The dispersion curves have been readily evaluated for high frequencies and for different propagation directions. Mesh convergence studies, carried out for the examples analysed, have shown the number of elements required to discretise the cross-section is generally small.

In summary, the WFE approach involves the systematic post-processing of element matrices typically found using a commercial FE package, in this case ANSYS. The size of the numerical model is very small - laminates typically involve about 3 degrees of freedom per layer. This method is particularly appealing at mid to high frequencies, when the size of the structure is large compared to

the wavelength.

The main advantages of the technique can be thus summarised as follows:

- ◊ the computational cost becomes independent of the size of the structure since the method requires the treatment of a small FE model whose size is related to the cross-section dynamic within the frequency band of interest;
- ◊ the meshing capabilities and the wealth of existing element libraries of commercial FE packages can be exploited. Hence complicated constructions can be analysed in a straightforward and systematic manner;
- ◊ making use of wave content, the WFE approach enables the wave characteristics to be evaluated up to high frequencies;
- ◊ the formulation is general and can be applied to any kind of homogeneous structure. In particular the WFE approach can be applied equally to composite laminates of arbitrary complexity with the same degree of simplicity;
- ◊ the technique is particularly appealing for free wave analysis.

Current and future work concerns issues such as:

- ◊ transmission loss calculation;
- ◊ optimisation of constrained layer damping treatments;
- ◊ wave propagation in fluid-filled cylindrical shell with internal mean flow;
- ◊ calculation of reflection and transmission coefficients for complicated joints in structures;
- ◊ evaluation of the response to external loads such as point forces or random pressure fields.

Appendix A

Mass and stiffness matrices of a thin rectangular isotropic plate bending element

A rectangular element with four node points is considered. The nodes are numbered as in Figure 3.4. Each node has three degrees of freedom: displacement normal to the plane of the plate and two rotations in the x and y directions. The polynomial displacement function is a complete cubic to which two quartic terms are added. More details can be found in [11]. The mass and stiffness matrices are here shown since typographical errors have been found in [11]. E , ρ , and ν are the Young's modulus, density and Poisson's ratio, h is the plate thickness and L_x , L_y are the element dimensions in the x and y directions. In the following $a_x = L_x/2$, $a_y = L_y/2$, $A = a_x/a_y$ and $B = a_y/a_x$.

The mass matrix is

$$\mathbf{M} \left(\frac{\rho a_x a_y h}{6300} \right) \begin{bmatrix} \mathbf{M}_{11} & \mathbf{M}_{21}^T \\ \mathbf{M}_{21} & \mathbf{M}_{22} \end{bmatrix}$$

where

$$\mathbf{M}_{11} = \begin{bmatrix} 3454 & 922 a_y & -922 a_x & 1226 & 398 a_y & 548 a_x \\ 922 a_y & 320 a_y^2 & -252 a_x a_y & 398 a_y & 160 a_y^2 & 168 a_x a_y \\ -922 a_x & -252 a_x a_y & 320 a_x^2 & -548 a_x & -168 a_x a_y & -240 a_x^2 \\ 1226 & 398 a_y & -548 a_x & 3454 & 922 a_y & 922 a_x \\ 398 a_y & 160 a_y^2 & -168 a_x a_y & 922 a_y & 320 a_y^2 & 252 a_x a_y \\ 548 a_x & 168 a_x a_y & -240 a_x^2 & 922 a_x & 252 a_x a_y & 320 a_x^2 \end{bmatrix};$$

$$\mathbf{M}_{21} = \begin{bmatrix} 394 & 232 a_y & -232 a_x & 1226 & 548 a_y & 398 a_x \\ -232 a_y & -120 a_y^2 & 112 a_x a_y & -548 a_y & -240 a_y^2 & -168 a_x a_y \\ 232 a_x & 112 a_x a_y & -120 a_x^2 & 398 a_x & 168 a_x a_y & 160 a_x^2 \\ 1226 & 548 a_y & -398 a_x & 394 & 232 a_y & 232 a_x \\ -548 a_y & -240 a_y^2 & 168 a_x a_y & -232 a_y & -120 a_y^2 & -112 a_x a_y \\ -398 a_x & -168 a_x a_y & 160 a_x^2 & -232 a_x & -112 a_x a_y & -120 a_x^2 \end{bmatrix};$$

$$\mathbf{M}_{22} = \begin{bmatrix} 3454 & -922 a_y & 922 a_x & 1226 & -398 a_y & -548 a_x \\ -922 a_y & 320 a_y^2 & -252 a_x a_y & -398 a_y & 160 a_y^2 & 168 a_x a_y \\ 922 a_x & -252 a_x a_y & 320 a_x^2 & 548 a_x & -168 a_x a_y & -240 a_x^2 \\ 1226 & -398 a_y & 548 a_x & 3454 & -922 a_y & -922 a_x \\ -398 a_y & 160 a_y^2 & -168 a_x a_y & -922 a_y & 320 a_y^2 & 252 a_x a_y \\ -548 a_x & 168 a_x a_y & -240 a_x^2 & -922 a_x & 252 a_x a_y & 320 a_x^2 \end{bmatrix}.$$

The stiffness matrix is

$$\mathbf{K} = \frac{Eh^3}{48(1-\nu^2)a_x a_y} \begin{bmatrix} \mathbf{K}_{11} & \mathbf{K}_{21}^T & \mathbf{K}_{31}^T & \mathbf{K}_{41}^T \\ \mathbf{K}_{21} & \mathbf{K}_{22} & \mathbf{K}_{32}^T & \mathbf{K}_{42}^T \\ \mathbf{K}_{31} & \mathbf{K}_{32} & \mathbf{K}_{33} & \mathbf{K}_{43}^T \\ \mathbf{K}_{41} & \mathbf{K}_{42} & \mathbf{K}_{43} & \mathbf{K}_{44} \end{bmatrix}$$

where

$$\mathbf{K}_{11} = \begin{bmatrix} 4B^2 + 4A^2 + \frac{14}{5} - \frac{4}{5}\nu & (4A^2 + \frac{2}{5} + \frac{8}{5}\nu) a_y & (-4B^2 - \frac{2}{5} - \frac{8}{5}\nu) a_x \\ (4A^2 + \frac{2}{5} + \frac{8}{5}\nu) a_y & (\frac{16}{3}A^2 + \frac{16}{15} - \frac{16}{15}\nu) a_y^2 & -4\nu a_x a_y \\ (-4B^2 - \frac{2}{5} - \frac{8}{5}\nu) a_x & -4\nu a_x a_y & (\frac{16}{3}B^2 + \frac{16}{15} - \frac{16}{15}\nu) a_x^2 \end{bmatrix};$$

Appendix

$$\mathbf{K}_{21} = \begin{bmatrix} -4B^2 + 2A^2 - \frac{14}{5} + \frac{4}{5}\nu & (2A^2 - \frac{2}{5} - \frac{8}{5}\nu) a_y & (4B^2 + \frac{2}{5} - \frac{2}{5}\nu) a_x \\ (2A^2 - \frac{2}{5} - \frac{8}{5}\nu) a_y & (\frac{8}{3}A^2 - \frac{16}{15} + \frac{16}{15}\nu) a_y^2 & 0 \\ (-4B^2 - \frac{2}{5} + \frac{2}{5}\nu) a_x & 0 & (\frac{8}{3}B^2 - \frac{4}{15} + \frac{4}{15}\nu) a_x^2 \end{bmatrix};$$

$$\mathbf{K}_{31} = \begin{bmatrix} -2B^2 - 2A^2 + \frac{14}{5} - \frac{4}{5}\nu & (-2A^2 + \frac{2}{5} - \frac{2}{5}\nu) a_y & (2B^2 - \frac{2}{5} + \frac{2}{5}\nu) a_x \\ (2A^2 - \frac{2}{5} + \frac{2}{5}\nu) a_y & (\frac{4}{3}A^2 + \frac{4}{15} - \frac{4}{15}\nu) a_y^2 & 0 \\ (-2B^2 + \frac{2}{5} - \frac{2}{5}\nu) a_x & 0 & (\frac{4}{3}B^2 + \frac{4}{15} - \frac{4}{15}\nu) a_x^2 \end{bmatrix};$$

$$\mathbf{K}_{41} = \begin{bmatrix} 2B^2 - 4A^2 - \frac{14}{5} + \frac{4}{5}\nu & (-4A^2 - \frac{2}{5} + \frac{2}{5}\nu) a_y & (-2B^2 + \frac{2}{5} + \frac{8}{5}\nu) a_x \\ (4A^2 + \frac{2}{5} - \frac{2}{5}\nu) a_y & (\frac{8}{3}A^2 - \frac{4}{15} + \frac{4}{15}\nu) a_y^2 & 0 \\ (-2B^2 + \frac{2}{5} + \frac{8}{5}\nu) a_x & 0 & (\frac{8}{3}B^2 - \frac{16}{15} + \frac{16}{15}\nu) a_x^2 \end{bmatrix};$$

$$\mathbf{K}_{22} = \mathbf{I}_3^T \mathbf{K}_{11} \mathbf{I}_3; \quad \mathbf{K}_{32} = \mathbf{I}_3^T \mathbf{K}_{41} \mathbf{I}_3; \quad \mathbf{K}_{33} = \mathbf{I}_1^T \mathbf{K}_{11} \mathbf{I}_1;$$

$$\mathbf{K}_{42} = \mathbf{I}_3^T \mathbf{K}_{31} \mathbf{I}_3; \quad \mathbf{K}_{43} = \mathbf{I}_1^T \mathbf{K}_{21} \mathbf{I}_1; \quad \mathbf{k}_{44} = \mathbf{I}_2^T \mathbf{K}_{11} \mathbf{I}_2;$$

$$\mathbf{I}_1 = \begin{bmatrix} -1 & 0 & 0 \\ 0 & 1 & 0 \\ 0 & 0 & 1 \end{bmatrix}; \quad \mathbf{I}_2 = \begin{bmatrix} 1 & 0 & 0 \\ 0 & -1 & 0 \\ 0 & 0 & 1 \end{bmatrix}; \quad \mathbf{I}_3 = \begin{bmatrix} 1 & 0 & 0 \\ 0 & 1 & 0 \\ 0 & 0 & -1 \end{bmatrix}.$$

Appendix B

Newton's method for functions of complex variables

Consider a function $f(z) = u(x, y) + iv(x, y)$ where $z = x + iy \in \mathbb{C}$ with $(x, y) \in \mathbb{R}^2$. To apply the *Newton method* one need to calculate $f(z)/f'(z)$. Considering the *Cauchy-Riemann equations* ($u_x = v_y$ and $u_y = -v_x$) we can write:

$$\begin{aligned} \frac{f(z)}{f'(z)} &= \frac{u + iv}{u_x + iv_x} = \frac{(uu_x + vv_x) + i(uu_y + vv_y)}{u_x^2 + v_x^2} \rightarrow \\ &\rightarrow \frac{1}{u_x^2 + v_x^2} \begin{pmatrix} uu_x + vu_x \\ uu_y + vv_y \end{pmatrix}. \end{aligned} \quad (8.1)$$

Therefore the “next iteration” of the Newton method is:

$$z_{k+1} = z_k - \frac{f(z_k)}{f'(z_k)} \rightarrow z_k - \frac{1}{u_x^2 + v_x^2} \begin{pmatrix} uu_x + vu_x \\ uu_y + vv_y \end{pmatrix}. \quad (8.2)$$

Since the absolute value of f is $F(x, y) = |f(x + iy)| = \sqrt{u^2 + v^2}$, differentiable except where $f(z) = 0$, and the gradient of F is

$$\nabla F = \frac{1}{\sqrt{u^2 + v^2}} \begin{pmatrix} uu_x + vu_x \\ uu_y + vv_y \end{pmatrix}, \quad (8.3)$$

the Newton method for function of complex variable can be explained as a gradient method for the absolute value of the function f .

The geometrical interpretation is analogous to the real case: the “next iteration point” in the method is in fact the intersection between the (x, y) plane, the tangent plane of $|f|$ at the point $(z_k, |f(z_k)|)$ and the vertical plane passing through z_k which contain $\nabla|f|(z_k)$.

Sufficient conditions for the existence of the solution and the convergence of the Newton's process are given by the Kantorovich theorem, see [102].

Appendix C

Coefficients of the dispersion relation in equation (5.14) obtained from the Flügge equations of motions for a cylindrical shell

Coefficients of the dispersion relation in equation (5.14) are obtained for a cylindrical shell of thickness h , mean radius R , Poisson's ratio ν . In the following Ω is the nondimensional frequency $\Omega = \omega/\omega_r$ where ω_r is the ring frequency in equation (5.12), n is the circumferential mode order and $\bar{h} = h/(R\sqrt{12})$ is a non dimensional thickness.

$$D_8(\Omega) = \frac{1 - \nu}{2} (\bar{h}^2 + 2\bar{h}^4 - 3\bar{h}^6)$$

$$\begin{aligned} D_6(\Omega) = & 2\bar{h}^2\nu\frac{1-\nu}{2} + 6\bar{h}^4\nu\frac{1-\nu}{2} + \bar{h}^2n^2(-1 - 2\frac{1-\nu}{2} - \frac{1-\nu^2}{2} + \frac{1+\nu^2}{2}) + \\ & + \bar{h}^4n^2(1 - 6\frac{1-\nu}{2} - 6\frac{1-\nu^2}{2} - 2\frac{1+\nu}{2}\frac{3-\nu}{2} + \frac{3-\nu^2}{2}) - 9\bar{h}^6n^2\frac{1-\nu^2}{2} + \\ & + \Omega^2\bar{h}^2(1 - \bar{h}^2 + \frac{1-\nu}{2} + 3\frac{1-\nu}{2}\bar{h}^2); \end{aligned}$$

$$\begin{aligned} D_4(\Omega) = & \frac{1-\nu}{2} + 4\frac{1-\nu}{2}\bar{h}^2 + 3\frac{1-\nu}{2}\bar{h}^4 - \nu^2\frac{1-\nu}{2} - 3\bar{h}^2\nu^2\frac{1-\nu}{2} + \bar{h}^2n^2(-2\nu - 2\frac{1-\nu}{2} + \\ & + 2\nu\frac{1-\nu^2}{2} + 2\frac{1+\nu}{2} - 2\frac{3-\nu}{2} + 2\nu\frac{1+\nu}{2}\frac{3-\nu}{2}) + \bar{h}^4n^4(2 + 2\frac{1-\nu}{2} + 2\frac{1-\nu^2}{2} - 2\frac{1+\nu^2}{2}) + \\ & + \bar{h}^4n^2(-6\frac{1-\nu}{2} + 6\nu\frac{1-\nu^2}{2}) + \bar{h}^4n^4(6\frac{1-\nu}{2} + 8\frac{1-\nu^2}{2} - \frac{1-\nu^3}{2} - 2\frac{1-\nu}{2}\frac{1+\nu}{2}\frac{3-\nu}{2} + \\ & - \frac{1-\nu}{2}\frac{3-\nu^2}{2}) + \bar{h}^6n^4(6\frac{1-\nu^2}{2} - 3\frac{1-\nu^3}{2} - \frac{1-\nu}{2}\frac{3-\nu^2}{2}) + \Omega^2(2\bar{h}^2\nu - \frac{1-\nu}{2} + \\ & - 3\frac{1-\nu}{2}\bar{h}^2 + \bar{h}^2n^2(-3 - 3\frac{1-\nu}{2}) + \bar{h}^4n^2(-9\frac{1-\nu}{2} + \frac{3-\nu^2}{2})) + \Omega^4\bar{h}^2; \end{aligned}$$

$$\begin{aligned} D_2(\Omega) = & n^2\nu^2 - n^2\frac{1-\nu^2}{2} - 2n^2\nu\frac{1+\nu}{2} + n^2\frac{1+\nu^2}{2} + \bar{h}^2n^2(-1 - 5\frac{1-\nu^2}{2} + \frac{1+\nu^2}{2}) + \\ & + \bar{h}^2n^4(2 - 2\nu\frac{1-\nu}{2} + 2\frac{1-\nu^2}{2} + 2\frac{1-\nu}{2}\frac{1+\nu}{2} - 2\frac{1+\nu^2}{2} + 2\frac{1-\nu}{2}\frac{3-\nu}{2}) + \\ & + \bar{h}^2n^6(-1 - 2\frac{1-\nu}{2} - \frac{1-\nu^2}{2} + \frac{1+\nu^2}{2}) - 7\bar{h}^4n^2\frac{1-\nu^2}{2} + \bar{h}^4n^4(8\frac{1-\nu^2}{2} + 2\frac{1-\nu}{2}\frac{3-\nu}{2}) + \\ & + \bar{h}^4n^6(-2\frac{1-\nu}{2} - 3\frac{1-\nu^2}{2}) - 3\bar{h}^6n^2\frac{1-\nu^2}{2} + 6\bar{h}^6n^4\frac{1-\nu^2}{2} - 3\bar{h}^6n^6\frac{1-\nu^2}{2} + \\ & + \Omega^2(1 + \bar{h}^2 + n^2 - \nu^2 + \frac{1-\nu}{2} + 4\frac{1-\nu}{2}\bar{h}^2 + 3\frac{1-\nu}{2}\bar{h}^4 + n^2\frac{1-\nu^2}{2} - n^2\frac{1+\nu^2}{2} + \\ & + \bar{h}^2n^2(-2 - 2\frac{1-\nu}{2} + 2\nu\frac{1-\nu}{2} + 4\frac{1-\nu^2}{2} - 2\frac{3-\nu}{2}) + \bar{h}^2n^4(3 + 3\frac{1-\nu}{2}) + \bar{h}^4n^2(-6\frac{1-\nu}{2} + \\ & + 3\frac{1-\nu^2}{2}) + \bar{h}^4n^4(5\frac{1-\nu}{2} - \frac{1-\nu^2}{2})) + \Omega^4(-1 - \frac{1-\nu}{2} - 3\frac{1-\nu}{2}\bar{h}^2 - 2\bar{h}^2n^2); \end{aligned}$$

Appendix

$$\begin{aligned} D_0(\Omega) = & \frac{1-\nu}{2} (\bar{h}^2 n^4 - 2 \bar{h}^2 n^6 + \bar{h}^2 n^8 + \bar{h}^4 n^4 - 2 \bar{h}^4 n^6 + \bar{h}^4 n^8) + \\ & + \Omega^2 (-n^2 \frac{1-\nu}{2} - n^4 \frac{1-\nu}{2} - \bar{h}^2 n^2 - 2 \frac{1-\nu}{2} \bar{h}^2 n^2 + 2 \bar{h}^2 n^4 + \frac{1-\nu}{2} \bar{h}^2 n^4 - \\ & - \bar{h}^2 n^6 - \frac{1-\nu}{2} \bar{h}^2 n^6 - \frac{1-\nu}{2} \bar{h}^4 n^2 + 2 \frac{1-\nu}{2} \bar{h}^4 n^4 - \frac{1-\nu}{2} \bar{h}^{10}) + \\ & + \Omega^4 (1 + \bar{h}^2 + n^2 + n^2 \frac{1-\nu}{2} - 2 \bar{h}^2 n^2 + \frac{1-\nu}{2} \bar{h}^2 n^2 + \bar{h}^2 n^4) - \Omega^6 \end{aligned}$$

Bibliography

- [1] R. Ruotolo. A spectral element for laminated composite beams: theory and application to pyroshock analysis. *Journal of Sound and Vibration*, 270:149–169, 2004.
- [2] L. Cremer, M. Heckl, and B. A. T Petersson. *Structure-borne sound*. Springer-Verlag, 2005.
- [3] S. S. Tavallaey. Wave propagation in sandwich structures. Technical report, PhD thesis, The Marcus Wallenberg Laboratory for Sound and Vibration Research, Stockholm, Sweden, 2001.
- [4] J. J. Diftri. Plate wave acoustic emission. *Journal of Acoustical Society of America*, 90:358–364, 1991.
- [5] J. J. Diftri. On the determination of the elastic moduli of anisotropic media from limited acoustical data. *Journal of Acoustical Society of America*, 95:1761–1767, 1994.
- [6] D. E. Chimenti. Guided waves in plates and their use in material characterisation. *Applied Mechanics Reviews*, 50:247–284, 1997.
- [7] R.H. Lyon and R.G. De Jong. *Theory and Application of Statistical Energy Analysis*. Butterworth-Heinemann, 1995.
- [8] K. Graff. *Wave motion in elastic solids*. Dover Publications, 1991.
- [9] R. D. Mindlin. Influence of rotatory inertia and shear on flexural motions of isotropic, elastic plates. *Journal of Applied Mechanics*, 18:31, 1951.
- [10] O. C. Zienkiewicz and R. L. Taylor. *The finite element method. Vol I*. Butterworth-Heinemann, 2000.

Bibliography

- [11] M. Petyt. *Introduction to finite element vibration analysis*. Cambridge University Press, 1990.
- [12] O. C. Zienkiewicz and R. L. Taylor. *The finite element method. Vol II*. Butterworth–Heinemann, 2000.
- [13] L. Brillouin. *Wave propagation in periodic structures*. Dover Publications, 1953.
- [14] J. F. Doyle. *Wave Propagation in Structures*. Springer–Verlag, 1997.
- [15] S. Finnveden. Evaluation of the modal density and group velocity by a finite element method. *Journal of Sound and Vibration*, 273:51–75, 2004.
- [16] J. C. Duke. *Acousto-Ultrasonics: Theory and Application*. Plenum Press, 1988.
- [17] S. Ghinet, N. Atalla, and H. Osman. The transmission loss of curved laminates and sandwich composite panels. *Journal of Acoustical Society of America*, 118:774–790, 2005.
- [18] D. J. Mead and S. Markus. The forced vibration of a three-layer, damped sandwich beam with arbitrary boundary conditions. *Journal of Sound and Vibration*, 10:163–175, 1969.
- [19] A. Chackraborty and S. Gopalakrishnan. A spectrally finite element model for wave propagation analysis in laminated composite plate. *Journal of Vibration and Acoustics*, 128:477–488, 2006.
- [20] K. Heron. Curved laminates and sandwich panels within predictive SEA. *Proceedings of the Second International AutoSEA Users Conference, Troy, Michigan, USA*, 2002.
- [21] E. M. Kerwin. Damping of flexural waves by constrained viscoelastic layer. *Journal of the Acoustical Society of America*, 31:952–962, 1959.
- [22] S. Ghinet and N. Atalla. Wave approach modeling of sandwich and laminate composite structures with viscoelastic layers. *9th International Congress on Acoustics, ICA 2007, Madrid, Spain*, 2007.
- [23] H. Lamb. On waves in an elastic plate. *Proceedings of the Royal Society of London, Series A*, 93:114–120, 1917.

Bibliography

- [24] J. R. Banerjee. Dynamic stiffness formulation for structural elements: a general approach. *Computers and Structures*, 63:101–103, 1997.
- [25] J. Lee and D. J. Thompson. Dynamic stiffness formulation, free vibration and wave motion of helical springs. *Journal of Sound and Vibration*, 239:297–320, 2001.
- [26] R. S. Langley. Application of the dynamic stiffness method to the free and forced vibrations of aircraft panels. *Journal of Sound and Vibration*, 135:319–331, 1989.
- [27] D. R. Mahapatra and S. Gopalakrishnan. A spectral finite element for analysis of axial–flexural–shear coupled wave propagation in laminated composite beams. *Composite Structures*, 59:67–88, 2003.
- [28] J. R. Banerjee and H. Su. Development of a dynamic stiffness matrix for free vibration analysis of spinning beams. *Computers and Structures*, 82:2189–2197, 2004.
- [29] J. R. Banerjee. Development of an exact dynamic stiffness matrix for free vibration analysis of a twisted Timoshenko beam. *Journal of Sound and Vibration*, 270:379–401, 2004.
- [30] W. P. Howson and A. Zare. Exact dynamic stiffness matrix for flexural vibration of three-layered sandwich beams. *Journal of Sound and Vibration*, 282:753–767, 2005.
- [31] J. R. Banerjee and A. J. Sobey. Dynamic stiffness formulation and free vibration analysis of a three-layer sandwich beam. *International Journal of Solids and Structures*, 42:2181–2197, 2005.
- [32] W. H. Wittrick and F. W. Williams. A general algorithm for computing natural frequencies of elastic structures. *Quarterly Journal of Mechanics and Applied Mathematics*, 24:263–284, 1971.
- [33] U. Lee and J. Kim. Dynamics of elastic–piezoelectric two-layer beams using spectral element method. *International Journal of Solids and Structures*, 37:4403–4417, 2000.
- [34] U. Lee and J. Kim. Spectral element modeling for the beams treated with active constrained layer damping. *International Journal of Solids and Structures*, 38:5679–5702, 2001.

Bibliography

- [35] D. R. Mahapatra and S. Gopalakrishnan. A spectral finite element for analysis of wave propagation in uniform composite tubes. *Journal of Sound and Vibration*, 268:429–463, 2003.
- [36] N. Kim and M. Kim. Exact dynamic stiffness matrix of non-symmetric thin-walled curved beams subjected to initial axial force. *Journal of Sound and Vibration*, 284:851–878, 2005.
- [37] M. Ruzzene. Vibration and sound radiation of sandwich beams with honeycomb truss core. *Journal of Sound and Vibration*, 277:741–763, 2004.
- [38] U. Lee and H. Oh. The spectral element model for pipelines conveying internal steady flow. *Engineering Structures*, 25:1045–1055, 2005.
- [39] N. Hu, H. Fukunaga, M. Kameyama, D. R. Mahapatra, and S. Gopalakrishnan. Analysis of wave propagation in beams with transverse and lateral cracks using a weakly formulated spectral method. *Journal of Applied Mechanics*, 74:119–127, 2007.
- [40] J. B. Casimir, S. Kevorkian, and T. Vinh. The dynamic stiffness matrix of two-dimensional elements: application to Kirchhoff’s plate continuous element. *Journal of Sound and Vibration*, 287:571–589, 2005.
- [41] A. Chackraborty and S. Gopalakrishnan. A spectrally formulated finite element for wave propagation analysis in layered composite media. *International Journal of Solid and Structures*, 41:5155–5183, 2004.
- [42] W. T. Thompson. Transmission of elastic waves through a stratified solid medium. *Journal of Applied Physic*, 21:89, 1950.
- [43] H. Nayfeh. The general problem of elastic wave propoagation in multilayered anisotropic media. *Journal of Acoustical Society of America*, 89:1521–1531, 1991.
- [44] B. Brouard, D. Lafrage, and J. F. Allard. A general method of modelling sound propagation in layered media. *Journal of Vibration and Acoustics*, 183:129–142, 1995.
- [45] J. Chen, E. Pan, and H. Chem. Wave propagation in magneto-electro-elastic multilayered plates. 44:1073–1085, 2007.

Bibliography

- [46] L. Wang and S. I. Rokhlin. Stable reformulation of transfer matrix method for propagation in layered anisotropic media. *Ultrasonics*, 39:413–424, 2001.
- [47] L. Knopoff. A matrix method for elastic wave problems. *Bulletin of the Seismological Society of America*, 54:431–438, 1964.
- [48] J. Park and E. Kausel. Numerical dispersion in the thin-layer method. *Computers and Structures*, 82:607–625, 2004.
- [49] E. Kausel. Wave propagation in anisotropic layered media. *International Journal for Numerical Methods in Engineering*, 23:1567–1578, 1986.
- [50] L. Gavrić. Computation of propagative waves in free rail using a finite element technique. *Journal of Sound and Vibration*, 185:531–543, 1995.
- [51] B. Aalami. Waves in prismatic guides of arbitrary cross section. *Journal of Applied Mechanics*, 40:1067–1072, 1973.
- [52] S. K. Datta, A. H. Shah, R. L. Bratton, and T. Chakraborty. Wave propagation in laminated composite plates. *Journal of the Acoustical Society of America*, 81:2020–2026, 1988.
- [53] R. D. Mindlin and H. D. McNiven. Axially symmetric waves in elastic rods. *Journal of Applied Mechanics*, 27:145–151, 1960.
- [54] S. B. Dong and K. H. Huang. Edge vibrations in laminated composite plates. *Journal of Applied Mechanics*, 52:433–438, 1985.
- [55] O. M. Mukdadi, Y. M. Desai, S. K. Datta, A. H. Shah, and A. J. Niklasson. Elastic guided waves in a layered plate with rectangular cross section. *Journal of the Acoustical Society of America*, 112:1766–1779, 2002.
- [56] O. M. Mukdadi and S. K. Datta. Transient ultrasonic guided waves in layered plate with rectangular cross section. *Journal of Applied Physics*, 93:9360–9370, 2003.
- [57] L. Gavrić. Finite element computation of dispersion properties of thin-walled waveguides. *Journal of Sound and Vibration*, 173:113–124, 1994.
- [58] O. Jr. Onipede and S. B. Dong. Propagating waves and end modes in pretwisted beams. *Journal of Sound and Vibration*, 195:313–330, 1996.

Bibliography

- [59] S. Y. Lee, K. K. Tae, Y. J. Kang, J. S. Kim, J.S Bolton, and Y. J. Kim. Eigenvalue analysis of sound propagation characteristics in a circular duct lined with poroelastic foam. *International Congress and Exposition on Noise Control Engineering, INTER-NOISE 2004, Prague, Czech Republic*, 2004.
- [60] U. Orrenius and S. Finnveden. Calculation of wave propagation in rib-stiffened plate structures. *Journal of Sound and Vibration*, 198:203–204, 1996.
- [61] S. Finnveden. Spectral finite element analysis of the vibration of straight fluid-filled pipes with flanges. *Journal of Sound and Vibration*, 199:125–154, 1997.
- [62] F. Birgersson, S. Finnveden, and G G. Robert. Modelling turbulence-induced vibration of pipes with a spectral finite element method. *Journal of Sound and Vibration*, 278:749–772, 2004.
- [63] L. L. Tassoulas and E. Kausel. Elements for the numerical analysis of wave motion in layered strata. *International Journal for Numerical Methods in Engineering*, 19:1005–1032, 1983.
- [64] P. J. Shorter. Wave propagation and damping in linear viscoelastic laminates. *Journal of the Acoustical Society of America*, 115:1917–1925, 2004.
- [65] C. M. Nilsson and S. Finnveden. Waves in thin-walled fluid-filled ducts with arbitrary cross-sections. *Journal of Sound and Vibration*, 310:58–76, 2008.
- [66] D. J. Mead. Wave propagation in continuous periodic structures: research contribution from Southampton, 1964–1995. *Journal of Sound and Vibration*, 190:495–524, 1996.
- [67] G. Floquet. Sur les équations différentielles linéaires à coefficients périodiques. *Annales scientifiques de l'École Normale Supérieure*, 12:47–88, 1883.
- [68] Y. K. Lin and T. J. McDaniel. Dynamics of beam-type periodic structures. *Journal of Engineering for Industry*, 91:1133–1141, 1969.

Bibliography

- [69] W. X. Zhong and F. W. Williams. On the direct solution of wave propagation for repetitive structures. *Journal of Sound and Vibration*, 181:485–501, 1995.
- [70] R. S. Langley. A transfer matrix analysis of the energetics of structural wave motion and harmonic vibration. *Proceedings of the Royal Society of London, Series A*, 452:1631–1648, 1996.
- [71] N. G. Stephen. Transfer matrix analysis of the elastostatics of one-dimensional repetitive structures. *Proceedings of the Royal Society of London, Series A*, 462:2245–2270, 2006.
- [72] D. J. Mead. A general theory of harmonic wave propagation in linear periodic systems with multiple coupling. *Journal of Sound and Vibration*, 27:235–260, 1973.
- [73] D. J. Mead. Wave propagation and natural modes in periodic systems: I. Mono-coupled systems. *Journal of Sound and Vibration*, 40:1–18, 1975.
- [74] D. J. Mead. Wave propagation and natural modes in periodic systems: II. Multi-coupled systems, with and without damping. *Journal of Sound and Vibration*, 40:19–39, 1975.
- [75] D. J. Mead and S. Markus. Coupled flexural-longitudinal wave motion in a periodic beam. *Journal of Sound and Vibration*, 90:1–24, 1983.
- [76] B. R. Mace, D. Duhamel, M. J. Brennan, and L. Hinke. Finite element prediction of wave motion in structural waveguides. *Journal of the Acoustical Society of America*, 117:2835–2843, 2005.
- [77] D. Duhamel, B. R. Mace, and M. J. Brennan. Finite element analysis of the vibration of waveguides and periodic structures. *Journal of Sound and Vibration*, 294:205–220, 2006.
- [78] R. M. Orris and M. Petyt. A finite element study of harmonic wave propagation in periodic structures. *Journal of Sound and Vibration*, 33:223–236, 1974.
- [79] A. Abdel-Rahman. Matrix analysis of wave propagation in periodic systems. Technical report, PhD thesis, University of Southampton, 1979.

Bibliography

- [80] D. J. Thompson. Wheel–rail noise generation, part III: rail vibration. *Journal of Sound and Vibration*, 161:421–446, 1993.
- [81] L. Gry. Dynamic modelling of railway track based on wave propagation. *Journal of Sound and Vibration*, 195:477–505, 1996.
- [82] J. M. Mencik and M. N. Ichchou. Multi-mode propagation and diffusion in structures through finite elements. *European Journal of Mechanics, A - Solids*, 24:877–898, 2005.
- [83] Y. Waki, B. R. Mace, and M. J. Brennan. Flexural wave propagation in a plate strip with free boundaries using a Wave Finite Element method. *International Congress and Exposition on Noise Control Engineering, INTER-NOISE 2007, Instabul, Turkey*, 2007.
- [84] Y. Waki, B. R. Mace, and M. J. Brennan. Vibration analysis of a tyre using the Wave Finite Element method. *International Congress and Exposition on Noise Control Engineering, INTER-NOISE 2007, Instabul, Turkey*, 2007.
- [85] L. Houillon, M. N. Ichchou, and L. Jezequel. Wave motion in thin-walled structures. *Journal of Sound and Vibration*, 281:483–507, 2005.
- [86] F. Tressède. Numerical investigation of elastic modes of propagation in helical waveguides. *Journal of the Acoustical Society of America*, 121:3398–3408, 2007.
- [87] M. Maess, N. Wagner, and L. Gaul. Dispersion curves of fluid filled elastic pipes by standard FE models and eigenpath analysis. *Journal of Sound and Vibration*, 296:264–276, 2006.
- [88] J. M. Mencik and M. N. Ichchou. Wave finite elements in guided elastodynamics with internal fluid. *International Journal of Solids and Structures*, 44:2148–2167, 2007.
- [89] M. Ruzzene, F. Scarpa, and F. Soranna. Wave beaming effects in two-dimensional cellular structures. *Smart Materials and Structures*, 12:363–372, 2003.
- [90] D. Duhamel. Finite element computation of Green’s functions. *Engineering Analysis with Boundary Elements*, 11:919–930, 2007.

Bibliography

- [91] B. R. Mace and E. Manconi. Modelling wave propagation in two-dimensional structures using a Wave/Finite Element tecnique. *Thematic Conference on Computational Methods in Structural Dynamics and Earthquake Engineering, COMPDYN 2007, Rethymno, Crete, Greece*, 2007.
- [92] E. Manconi and B. R. Mace. Modelling wave propagation in cylinders using a wave finite element technique. *9th International Congress on Acoustics, ICA 2007, Madrid, Spain*, 2007.
- [93] E. Manconi and B. R. Mace. Modelling wave propagation in two-dimensional structures using a Wave/Finite Element technique. *ISVR Technical Memorandum*, 966, 2007.
- [94] L. Brillouin. *Wave propagation and group velocity*. Academic press, 1960.
- [95] F. Bloch. Über die quantenmechanik der elektronen in kristallgittern. *Z. Physik*, 52:555–600, 1928.
- [96] L. E. Bateson, M. A. Kelamanson, and C. Knudsen. Solution of a transcendental eigenvalue problem via interval analysis. *Computers and Mathematics with Applications*, 38:133–142, 1999.
- [97] R. E. Moore. *Interval Analysis*. Prentice-Hall, Englewood Cliff, N. J., 1966.
- [98] E. Hansen. *Global optimization using interval analysis*. Pure and Applied Mathematics, USA, 1992.
- [99] E. Kreyszig. *Advanced Engineering Mathematics*. John Wiley & Son, 1999.
- [100] M. J. D. Powell. A fortran subroutine for solving systems of nonlinear algebraic equations. *Numerical Methods for Nonlinear Algebraic Equations*, P. Rabinowitz, Ch.7, 1970.
- [101] C. F. Gerald. *Applied Numerical Analysis*. Addison-Wesley, 1999.
- [102] R. A. Tapia. The Kantorovich Theorem for Newton’s Method. *The American Mathematical Monthly*, 78:389–392, 1971.
- [103] K. V. Singh and Y. M. Ram. Transcendental eigenvalue problem and its applications. *AIAA Journal*, 40:1402–1407, 2002.
- [104] W. H. Yang. A method for eigenvalues of sparse λ -matrices. *International Journal for Numerical Methods in Engineering*, 19:943–948, 1983.

Bibliography

- [105] J. J. Morè, B. S. Garbow, and K. E. Hillstrom. User guide for minpack 1. *Rept. ANL-80-74*, 1980.
- [106] R. Brauer. A note on systems of homogeneous algebraic equations. *Bulletin of the American Mathematical Society*, 51:749–755, 1945.
- [107] B. Gleyse and M. Moflih. The exact computation of the number of zeros of a real polynomial in the open unit disk: an algebraic approach. *Computers and Mathematics with Applications*, 39:209–214, 2000.
- [108] D. J. Mead and S. Parthan. Free wave propagation in two-dimensional periodic plates. *Journal of Sound and Vibration*, 64:325–348, 1979.
- [109] Y. Waki, B. R. Mace, and M. J. Brennan. Waveguide finite element modelling: numerical issues and application to simple waveguide. *International Conference on Noise and Vibration Engineering, ISMA 2006, Leuven, Belgium*, 2006.
- [110] H. Lamb. On the propagation of tremors over the surface of elastic solid. *Philosophical Transaction of the Royal Society*, A203:1–42, 1904.
- [111] R. D. Mindlin. The thickness shear and flexural vibrations of crystal plates. *Journal of Applied Physics*, 22:316, 1951.
- [112] R. D. Mindlin and M. A. Medick. Extensional vibrations of elastic plates. *Journal of Applied Mechanics*, 26:561–569, 1959.
- [113] L. M. Brekoviskikh. *Waves in layered media*. Academic Press, 1980.
- [114] I. Tolstoy and E. Usdin. Wave propagation in elastic plates: low and high mode dispersion. *Journal of Acoustical Society of America*, 29:37–42, 1957.
- [115] J. Wolf, T. D. K. Ngoc, R. Kille, and W. G. Mayer. Investigation of lamb waves having a negative group velocity. *Journal of Acoustical Society of America*, 83:122–126, 1988.
- [116] M. F. Werby and H. Überall. The analysis and interpretation of some special properties of higher order symmetric lamb waves: the case for plate. *Journal of Acoustical Society of America*, 111:2686–2691, 2002.
- [117] P. L. Marston. Negative group velocity Lamb waves on plates and applications to the scattering of sound by shells. *Journal of Acoustical Society of America*, 113:2659–2662, 2003.

Bibliography

- [118] S. P. Timoshenko and S. Woinowsky-Krieger. *Theory of plates and shells*. McGraw-Hill, 1959.
- [119] J. N. Reddy. *Mechanics of Laminated Composite Plates Theory and Analysis*. CRC Press, 1997.
- [120] G. Kurtze and B. Watters. New wall design for high transmission loss or high damping. *Journal of the Acoustical Society of America*, 31:739–748, 1959.
- [121] R. A. Di Taranto. Theory of vibratory bending for elastic and viscoelastic layered finite-length beams. *Journal of Applied Mechanics*, 32:881–886, 1965.
- [122] A. C. Nilsson. Wave propagation in and sound transmission through sandwich plates. *Journal of Sound and Vibration*, 138:73–94, 1990.
- [123] L. Librescu. *Elastostatics and kinetics of anisotropic and heterogeneous shell-type structures*. Noordhoff, Leyden, The Netherlands, 1975.
- [124] A. E. Armenàkas. Propagation of harmonic waves in composite cylindrical shells. I. Theoretical investigation. *AIAA Journal*, 5:740–744, 1967.
- [125] A. E. Armenàkas. Propagation of harmonic waves in composite cylindrical shells. II. Numerical analysis. *AIAA Journal*, 9:599–605, 1971.
- [126] D. C. Gazis. Three dimensional investigation of the propagation of waves in hollow circular cylinders. i. analytical foundation. *Journal of Acoustical Society of America*, 31:568–573, 1959.
- [127] D. C. Gazis. Three-dimensional investigation of the propagation of waves in hollow circular cylinders. ii. numerical result. *Journal of Acoustical Society of America*, 31:573–578, 1959.
- [128] R. Kumar and R. W. B. Stephens. Dispersion of flexural waves in circular cylindrical shells. *Proceedings of the Royal Society of London, Series A*, 329:283–297, 1972.
- [129] S. Markus and D. J. Mead. Axisymmetric and asymmetric wave motion in orthotropic cylinders. *Journal of Sound and Vibration*, 181:127–147, 1995.

Bibliography

- [130] S. Markus and D. J. Mead. Wave motion in a three-layered, orthotropic-isotropic-orthotropic, composite shell. *Journal of Sound and Vibration*, 181:149–167, 1995.
- [131] I. Mirsky. Wave propagation in transversely isotropic circular cylinders. Part I. Theory. *Journal of Acoustical Society of America*, 37:1016–1021, 1965.
- [132] I. Mirsky. Wave propagation in transversely isotropic circular cylinders. Part II. Numerical results. *Journal of Acoustical Society of America*, 37:1022–1026, 1965.
- [133] F. G. Yuan and C. C. Hsieh. Three-dimensional wave propagation in composite cylindrical shells. *Composite Structures*, 42:153–167, 1998.
- [134] A. W. Leissa. *Vibration of shells*. NASA SP-288, 1973.
- [135] C. R. Fuller. The effects of wall discontinuities on the propagation of flexural waves in cylindrical shells. *Journal of Sound and Vibration*, 75:207–228, 1981.
- [136] R. S. Langley. Wave motion and energy flow in cylindrical shells. *Journal of Sound and Vibration*, 169:29–42, 1994.
- [137] R. S. Langley. The modal density and mode count of thin cylinders and curved panels. *Journal of Sound and Vibration*, 169:43–53, 1994.
- [138] V. V. Tyutekin. Helical waves of an elastic cylindrical shell. *Acoustical Physics*, 50:273–277, 2004.
- [139] V. V. Tyutekin. Circumferential and helical normal waves of a cylindrical waveguide: helical waves in a free space. *Acoustical Physics*, 52:471–476, 2006.
- [140] D. G. Karczub. Expression for direct evaluation of wave number in cylindrical shell vibration studies using Flügge equations of motion. *Journal of Acoustical Society of America*, 119:3553–3557, 2006.
- [141] W. Flügge. *Stresses in Shells*. Springer-Verlag, 1973.
- [142] C. R. Fuller and F. J. Fahy. Characteristics of wave propagation and energy distributions in cylindrical elastic shells filled with fluid. *Journal of Sound and Vibration*, 81:501–518, 1982.

Bibliography

- [143] C. R. Fuller. The input mobility of an infinite circular cylindrical shell filled with fluid. *Journal of Sound and Vibration*, 87:409–427, 1983.
- [144] G. Pavic. Vibro-acoustical energy flow through straight pipes. *Journal of Sound and Vibration*, 154:411–429, 1992.
- [145] B. J. Brèveart and C. Fuller. Active control of coupled wave propagation in fluid-filled elastic cylindrical shells. *Journal of the Acoustical Society of America*, 94:1467–1473, 1993.
- [146] S. Sorokin. Control of wave propagation in compound fluid-filled elastic pipes. *IX International Conference on Recent Advances in Structural Dynamics, Southampton, UK, July 2006*, 2006.
- [147] E. E. Ungar and E. M. Kerwin. Loss factors of viscoelastic systems in terms of energy concepts. *Journal of the Acoustical Society of America*, 34:954–957, 1962.
- [148] D. K. Rao. Frequency and loss factors of sandwich beams under various boundary conditions. *Journal of Mechanical Engineering Science*, 20:271–282, 1978.
- [149] R. Plunkett and C. T. Lee. Length optimization for constrained viscoelastic layer damping. *Journal of the Acoustical Society of America*, 48:150–161, 1970.
- [150] D. J. Mead. A comparison of some equations for the flexural vibration of damped sandwich beams. *Journal of Sound and Vibration*, 83:363–377, 1982.
- [151] Y. V. K. Sadasiva Rao and B.C. Nakra. Vibrations of unsymmetrical sandwich beams and plates with viscoelastic cores. *Journal of Sound and Vibration*, 34:309–326, 1974.
- [152] R. N. Miles and P. G. Reinhard. An analytical model for the vibration of laminated beams including the effects of both shear and thickness deformation in the adhesive layer. *Journal of Vibration and Acoustics*, 108:56–64, 1986.
- [153] Y. Chen and S. Huang. An optimal placement of cld treatment for vibration suppression of plates. *Journal of Mechanical Sciences*, 44:1801–1821, 2002.

Bibliography

- [154] M. Alvelid. Optimal position and shape of applied damping material. *Journal of Sound and Vibration*, In Press, Corrected Proof, Available online, 2007.
- [155] H. Illaire, W. Kropp, and B. Mace. A phenomenological model of active constrained layers. *Journal of Sound and Vibration*, 285:281–302, 2005.
- [156] A. Baz. Optimization of energy dissipation characteristics of active constrained layer damping. *Smart Materials and Structure*, 6:360–368, 1997.
- [157] W. H. Liao and K. W. Wang. On the analysis of viscoelastic materials for active constrained layer damping treatments. *Journal of Sound and Vibration*, 207:319–334, 1997.
- [158] D. J. Mead. *Passive vibration control*. John Wiley & Sons, 1998.
- [159] C. D. Johnson and D. A. Kienholz. Finite element prediction of damping in structures with constrained viscoelastic layers. *AIAA Journal*, 20:1284–1290, 1982.